Lars Tandle Kyllingstad

Aspects of QCD thermodynamics through scalar field theory and NJL models

Thesis for the degree of Philosophiae Doctor

Trondheim, July 2011

Norwegian University of Science and Technology
Faculty of Natural Sciences and Technology
Department of Physics

NTNU – Trondheim
Norwegian University of
Science and Technology

NTNU
Norwegian University of Science and Technology

Thesis for the degree of Philosophiae Doctor

Faculty of Natural Sciences and Technology
Department of Physics

ISBN 978-82-471-2926-5 (printed ver.)
ISBN 978-82-471-2927-2 (electronic ver.)
ISSN 1503-8181

Doctoral theses at NTNU, 2011:188

Printed by NTNU-trykk

Preface

This thesis is submitted to the Norwegian University of Science and Technology (NTNU) for partial fulfilment of the requirements for the degree of Philosophiae Doctor (PhD). The thesis is based on four papers, all of which have been published in peer-reviewed scientific journals. The doctoral work has been performed at the Department of Physics, NTNU, Trondheim, supervised by Professor Jens O. Andersen.

For a full understanding of the material in this thesis, the reader should be familiar with the path integral formulation of quantum field theory, as well as basic statistical mechanics and thermodynamics. However, it is my sincere hope that parts of it will be accessible—interesting, even—to non-experts. Particularly in the first chapter (aptly named "Introduction"), I have tried to keep the technical jargon at an absolute minimum. There, I attempt to confer an intuitive understanding of how the fundamental building blocks of nature behave in extreme conditions, placing my work within the "bigger picture" of things. Readers who are familiar with physics and science in general may also find Chapter 2 interesting. In that chapter I discuss *quantum chromodynamics*, the theory of the strong interaction, in some detail. After that, however, it goes rapidly downhill.

Trondheim, 19 April 2011

Lars Tandle Kyllingstad

Acknowledgements

First, I would like to express my deep gratitude towards Professor Jens O. Andersen, who has been my supervisor not only for my PhD, but also for my master's degree. Constantly providing me with new challenges, always ready to answer questions (even the silly ones), and ever enthusiastic about our work, he deserves most of the credit for turning me from a student into a scientist. I thank him, as well as the Faculty of Natural Sciences and Technology at NTNU, for giving me the opportunity to pursue a PhD in physics.

I would also like to thank Dr. Kim Splittorff for initiating the collaboration which resulted in Paper IV. I found that to be an extremely interesting and fun project. The Niels Bohr Institute, Copenhagen, deserve warm thanks for their hospitality during my two stays there.

I could not have asked for a better office mate than Lars Erlend Leganger. During these four years he has been excellent company at work, at conferences and workshops, and at various social events. I have thoroughly enjoyed our many discussions about life, the Universe, and everything. He and our fellow PhD students Severin Sadjina, Håvard Haugen, Rashid Khan, Arturo Amador Cruz and Lars Husdal, have, through countless coffee breaks, lunch breaks and payday beers, made the Division of Theoretical Physics a very enjoyable workplace.

Sometimes one needs to get away from the office for a bit, and I thank Birgit Ryningen, Magne Brekke Rabben and Jarle Ladstein for many opportunities to do so. I have really appreciated our many coffee breaks and lunch breaks at "Stripa".

Birgit and Jarle, together with the rest of the judo group at NTNUI also deserve warm thanks for keeping my body as fit as my brain. I am as much a *judoka* as I am a physicist, and I count myself lucky to be part of what I truly believe to be the best judo club in Norway.

I would not be where I am today if not for my family. My parents raised me to think for myself, they taught me the value of a good education, and they have always encouraged me to pursue my interests. For these things I am truly grateful.

Last, but by no means least, I wish to thank my wife, Frida, whom I married during the course of my PhD, and who has been a never ending source of love, care and support. After long hours at the office, coming home to her welcoming smile (and a warm dinner) is the high point of my day. Frida, I look forward to a lifetime together with you.

Papers in this thesis

Paper I

Jens O. Andersen and Lars Kyllingstad:
"Four-loop screened perturbation theory",
Phys. Rev. **D78** (2008), 076008.

We study the thermodynamics of massless ϕ^4-theory using screened perturbation theory. In this method, the perturbative expansion is reorganized by adding and subtracting a thermal mass term in the Lagrangian. We calculate the free energy through four loops expanding in a double power expansion in m/T and g^2, where m is the thermal mass and g is the coupling constant. The expansion is truncated at order g^7 and the loop expansion is shown to have better convergence properties than the weak-coupling expansion. The free energy at order g^6 involves the four-loop triangle sum-integral evaluated by Gynther, Laine, Schröder, Torrero, and Vuorinen using the methods developed by Arnold and Zhai. The evaluation of the free energy at order g^7 requires the evaluation of a nontrivial three-loop sum-integral, which we calculate by the same methods. [1]

Paper II

Jens O. Andersen, Lars T. Kyllingstad and Lars E. Leganger:
"Pressure to order $g^8 \log g$ of massless ϕ^4 theory at weak coupling",
JHEP **0908** (2009), 066.

We calculate the pressure of massless ϕ^4-theory to order $g^8\log(g)$ at weak coupling. The contributions to the pressure arise from the hard momentum scale of order T and the soft momentum scale of order gT. Effective field theory methods and dimensional reduction are used to separate the contributions from the two momentum scales: The hard contribution can be calculated as a power series in g^2 using naive perturbation theory with bare propagators. The soft contribution can be calculated using an effective theory in three dimensions, whose coefficients are power series in g^2. This contribution is a power series in g starting at order g^3. The calculation of the hard part to order g^6 involves a complicated four-loop sum-integral that was recently calculated by Gynther, Laine, Schröder, Torrero, and Vuorinen. The calculation of the soft part requires calculating the mass parameter in the effective theory to order g^6 and the evaluation of five-loop vacuum diagrams in three dimensions. This gives the free energy correct up to order g^7. The coefficients of the effective theory satisfy a set of renormalization

group equations that can be used to sum up leading and subleading logarithms of T/gT. We use the solutions to these equations to obtain a result for the free energy which is correct to order $g^8\log(g)$. Finally, we investigate the convergence of the perturbative series. [2]

Paper III

Jens O. Andersen and Lars T. Kyllingstad:
"Pion condensation in a two-flavour NJL model: the role of charge neutrality",
J. Phys. G **37** (2009), 015003.

We study pion condensation and the phase structure in a two-flavour Nambu–Jona-Lasinio model in the presence of baryon chemical potential μ and isospin chemical potential μ_I at zero and finite temperature. There is a competition between the chiral condensate and a Bose–Einstein condensate of charged pions. In the chiral limit, the chiral condensate vanishes for any finite value of the isospin chemical potential, while there is a charged pion condensate that depends on the chemical potentials and the temperature. At the physical point, the chiral condensate is always nonzero, while the charged pion condensate depends on μ_I and T. For $T=\mu=0$, the critical isospin chemical potential μ_I^c for the onset of Bose–Einstein condensation is always equal to the pion mass. For $\mu=0$, we compare our results with chiral perturbation theory, sigma-model calculations, and lattice simulations. Finally, we examine the effects of imposing electric charge neutrality and weak equilibrium on the phase structure of the model. In the chiral limit, there is a window of baryon chemical potential and temperature where the charged pions condense. At the physical point, the charged pions do not condense. [3]

Paper IV

Jens O. Andersen, Lars T. Kyllingstad and Kim Splittorff:
"The sign problem across the QCD phase transition",
JHEP **1001** (2010), 055.

The average phase factor of the QCD fermion determinant signals the strength of the QCD sign problem. We compute the average phase factor as a function of temperature and baryon chemical potential using a two-flavor NJL model. This allows us to study the strength of the sign problem at and above the chiral transition. It is discussed how the $\mathrm{U}(1)_A$ anomaly affects the sign problem. Finally, we study the interplay between the sign problem and the endpoint of the chiral transition. [4]

Notation and conventions

- Unless otherwise is stated we always work in natural units, that is, we set $\hbar = c = k_B = 1$ in all equations. This means that all quantities are measured in units of energy, specifically, in powers of *electronvolts* (eV). Some examples of conversion formulae between natural units and SI units are:

Mass:	$m_{\mathrm{eV}} = m_{\mathrm{kg}} c^2$
Temperature:	$T_{\mathrm{eV}} = k_B T_{\mathrm{K}}$
Length:	$x_{\mathrm{eV}^{-1}} = x_{\mathrm{m}} / \hbar c$

- Three-vectors are written in boldface or with Roman indices. Repeated indices are summed over unless otherwise is specified.

$$\begin{aligned} \mathbf{p} &= (p_1, p_2, p_3), \\ p_i q_i &= p_1 q_1 + p_2 q_2 + p_3 q_3. \end{aligned}$$

- Four-vectors are written with Greek indices: γ^μ, P_μ, ...

- Minkowskian four-vectors are denoted by lower-case letters and we use the signature $(+,-,-,-)$ for the metric:

$$\begin{aligned} p &= (p_0, \mathbf{p}), \\ pq = p_\mu q^\mu &= p_0 q_0 - p_i q_i. \end{aligned}$$

- Euclidean four-vectors are denoted by capital letters:

$$\begin{aligned} P &= (P_0, \mathbf{p}), \\ PQ = P_\mu Q_\mu &= P_0 Q_0 + p_i q_i. \end{aligned}$$

- The Dirac gamma matrices are defined by the anticommutation and Hermiticity relations

$$\{\gamma^\mu, \gamma^\nu\} = 2g^{\mu\nu}, \qquad (\gamma^\mu)^\dagger = \gamma^0 \gamma^\mu \gamma^0.$$

  A fifth anticommuting gamma matrix, γ^5, is defined by

$$\gamma^5 \equiv i\gamma^0\gamma^1\gamma^2\gamma^3$$

  and has the properties that

$$\{\gamma^\mu, \gamma^5\} = 0, \qquad (\gamma^5)^2 = 1, \qquad (\gamma^5)^\dagger = \gamma^5.$$

- The Euclidean gamma matrices are denoted by $\tilde{\gamma}_\mu$. They are related to the gamma matrices in Minkowski space by

$$\tilde{\gamma}_0 = \gamma^0, \qquad \tilde{\gamma}_i = i\gamma^i,$$

  and satisfy the anticommutation relation

$$\{\tilde{\gamma}_\mu, \tilde{\gamma}_\nu\} = 2\delta_{\mu\nu}.$$

  The fifth Euclidean gamma matrix is defined by

$$\tilde{\gamma}_5 \equiv -\tilde{\gamma}_0\tilde{\gamma}_1\tilde{\gamma}_2\tilde{\gamma}_3 = \gamma^5.$$

- The Pauli matrices are denoted by τ_i. They are defined as

$$\tau_1 = \begin{pmatrix} 0 & 1 \\ 1 & 0 \end{pmatrix}, \qquad \tau_2 = \begin{pmatrix} 0 & -i \\ i & 0 \end{pmatrix}, \qquad \tau_3 = \begin{pmatrix} 1 & 0 \\ 0 & -1 \end{pmatrix}.$$

Contents

Part I.

Quantum field theory at finite temperature and density

1. Introduction

What happens to matter when it is heated to extreme temperatures? What if it is put under extreme pressure? And what, exactly, do we mean by "extreme"?

Let us answer the last question first: According to the scientifically accepted theory of the beginning of the Universe, the *Big Bang theory*, the Universe started off in a very hot and dense state and has since expanded and cooled to the dilute state in which we find it today. In the early Universe, a few microseconds after the Big Bang, the temperature was on the order of terrakelvins—that is, trillions of degrees, or 100 000 times the core temperature of the Sun.

Moving from the extremely hot to the cold and dense parts of the Universe, we find another extreme. A *neutron star* is the remnant of a massive star that has gone supernova and collapsed under the gravitational pressure of its own weight. The predicted density of a neutron star is on the order of 10^{17} kg/m^3. If the Earth were compressed to this density, it would have a diameter of about 300 meters—roughly the height of the Eiffel Tower.

Under such extreme conditions it is only to be expected that matter behaves quite differently from what we are used to. Understanding this behaviour will help us understand the evolution of the Universe, it will give us a better foundation on which to analyse astrophysical data, and it will provide us with new insights into the fundamental laws that govern nature.

In recent years there have been huge efforts, both theoretical and experimental, to study, classify and map out the various states of matter under extreme conditions. This thesis, and the papers on which it is based, is a contribution to the theoretical side of this effort.

In this chapter we shall start by introducing the concept of a *phase diagram*, which will be used extensively throughout the thesis. Thereafter we discuss the *strong interaction*, which is one of nature's four fundamental forces, and the role it plays in hot and dense matter.

1.1. Phase diagrams

We are accustomed to thinking that matter comes in three forms, or *phases*: the solid phase, the liquid phase and the vapour phase. The classic example is of course H_2O. At temperatures below 0 °C it is solid ice, at temperatures between 0 °C and 100 °C it is liquid water, and at 100 °C it starts boiling and evaporates into steam.

While this picture is certainly correct, it is very incomplete. For instance, it only takes into account changes in temperature, and not changes in pressure. Specif-

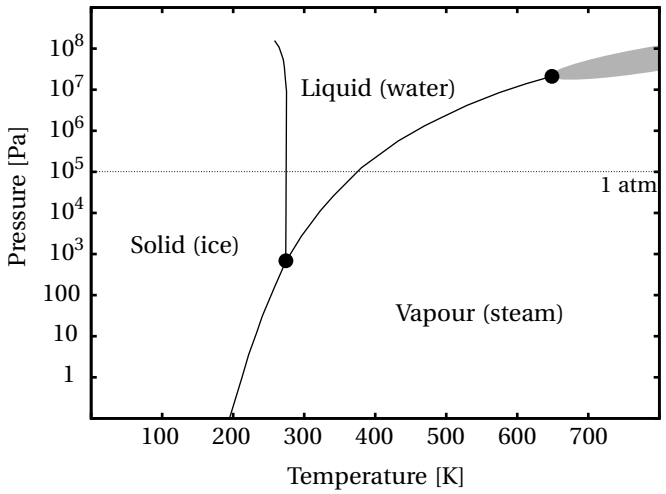

Figure 1.1.: The phase diagram of H_2O. Note that the vertical axis is logarithmic.

ically, it is only valid at a pressure of roughly 100 kPa, the atmospheric pressure at sea level. For example, at the top of Mount Everest (8 848 meters above sea level) where the pressure is a fourth of that, water boils at 69 °C. If you tried to hard-boil an egg up there, you would be in for a rather long wait.

A more complete diagram of the phases of H_2O is shown in Fig. 1.1. Note the thin line drawn straight across the diagram at 100 kPa. Following this line, we see that the transition from the solid phase to the liquid phase happens at 273 K, or 0 °C, and that the transition from the liquid phase to the vapour phase happens at 373 K, or 100 °C—just as expected.

If we lower the pressure a bit, down to just above 600 Pa, we get to a point where the three phases can coexist. This is known as the *triple point*. Below this, there is no liquid phase anymore. These conditions can be found, for instance, on Mars, where the mean surface pressure *is* in fact roughly 600 Pa. If you tried to heat a block of ice on Mars, it wouldn't melt, it would just evaporate. (More precisely, it would *sublime*, which is the correct term for what happens in a solid–gas transition.)

The transition lines drawn in this diagram all represent *first-order phase transitions*, which is the technical term for *discontinuous* phase transitions. When we boil water, the density does not decrease steadily, it makes a "jump" from the high-density liquid phase to the low-density vapour phase. This is why it is so easy for us to distinguish water from steam—there are no intermediate stages between the two.

However, if we follow the liquid–vapour phase transition line in the direction of increasing temperature, we get to a point where the line ends. A point where a phase transition ends is called a *critical point*. Beyond this point the clear dis-

tinction between water and steam ceases to exist, and there is a smooth, continuous transition between the two phases. This kind of phase transition is called a *crossover*, and we illustrate it with the grey area seen to the right of the critical point.

The phase diagram of H_2O is actually a lot more complex even than what is shown in Fig. 1.1. For instance, water has 15 known crystalline phases, all grouped under the general term "ice". We will, however, not go into any more detail as that would take us too far off track. The point of this section was to give an idea of what a phase diagram is, one that will be useful to keep in mind when we get to our main topic: The phase diagram of the strong interaction.

1.2. The strong interaction

Traditionally, it is said that nature has four *fundamental forces*, or *interactions*: electromagnetism, gravity, the weak interaction and the strong interaction.

Most people are only familiar with electromagnetism and gravity, and the reason for this is clear: They are responsible for practically *all* phenomena we observe in our day-to-day lives. But why is this the case? Could it be that the strong interaction—despite its name—and the weak interaction are actually a lot weaker than the two others?

Not so. There are a few of the elementary particles which participate in all four interactions and which thus can be used to compare the forces' relative strengths. As it turns out, the strong interaction *is* the strongest one—and by a good margin at that: It is 10^{38} times stronger[1] than gravity, which is actually the weakest force by far.

Then why don't we see things interacting strongly around us all the time? After all, anyone can measure gravity with a simple kitchen weight, so why can't you go to your local hardware store and ask for a strong-interaction-o-meter?

The reason is that the strong and weak interactions are *short-range* interactions. The range of the strong interaction is only a femtometer—that is, a millionth-billionth of a meter—roughly the size of an atomic nucleus. The range of the weak interaction is again a thousandth of that. This means that if we are to understand the role of these interactions, we have to look inside the very cores of atoms.

As we know, an an atom consists of a positively charged nucleus surrounded by a cloud of negatively charged electrons held in place by the electromagnetic interaction. In-between, there is—well, nothing; most of an atom's volume is just a whole lot of empty space. (Take hydrogen as an example: If the nucleus of a hydrogen atom were the size of an apple, its electron would be a grain of sand tens of kilometres away.)

The nucleus is built up of protons and neutrons, collectively grouped under the term *nucleons*. Neutrons are, as the name implies, electrically neutral. Pro-

[1] Yes, that is a one followed by 38 zeroes.

tons, on the other hand, are positively charged, which means that there is a repulsive electromagnetic force between them. However, they are held in place by the strong interaction, which is roughly a thousand times stronger than electromagnetism. Each nucleon again consists of three *quarks*, also held together by the strong interaction. Quarks, like electrons, are believed to be truly fundamental particles.

A peculiar feature of quarks is that they are never, ever, observed alone. They are only found in pairs, or, as in the case of nucleons, in groups of three. This is believed to be a fundamental property of the strong interaction, and it is called *confinement* because the interaction "confines" the quarks to their composite particles. It begs the question, though: Just because we have never *seen* a lone quark, does that mean they do not exist, and that they never have?

1.2.1. Deconfinement at extreme density

Imagine that we take a lump of matter and start squeezing it. The material of the lump is unimportant; it could be hydrogen, it it could be water, it could be iron—it doesn't matter. What happens to the lump when we apply pressure is of course that its density increases, meaning that its atoms are pushed closer and closer together and the empty space inside and between them becomes smaller and smaller.

At some point the atomic nuclei come within range of the strong interaction which, due to its superior strength, completely dwarfs the electromagnetic interaction. This kind of matter is called *nuclear matter*. In a sense, "ordinary" matter can be seen as a gas, in that the particles (the atoms) are far apart and interact relatively weakly (through electromagnetism). In this picture, nuclear matter is a liquid, because it is dense and the particles interact strongly.

If we apply enough pressure, at some point we reach a density where the atomic nuclei bump into each other. This is called *nuclear density*, because the overall density of the lump is now the same as the density of each individual nucleus. The nuclear density is, on average, $n_{\text{nucl}} = 4 \times 10^{17}$ kg/m^3. Note that n_{nucl} is of the same order of magnitude as the density of a neutron star, and this is no coincidence. What we have described here is in fact exactly what has taken place in a neutron star. The enormous pressure which is needed to make it happen is provided by the gravitational force from the star's own mass. At this point, most of the electrons will have been forced into the nuclei where they combine with protons to form neutrons. In other words, a neutron star mainly consists of neutrons, hence the name.

Continue squeezing. The nuclei are already as close as they can be, so what happens next is that they start to merge with each other. Squeeze some more, and soon even the neutrons and protons will bump into each other and start to overlap. Since there is no longer any clear boundary between the nucleons, the quarks are in effect free of their prisons. That is, they are *deconfined*. We have entered yet another exotic state of matter, one which is called *dense quark*

matter.

We mentioned above that neutron stars consist of nuclear matter. In the same way that the pressure increases as you dive to greater and greater depths when you're out swimming, so does the pressure increase as you "dive" into the depths of a neutron star. It is quite possible that the cores of the heaviest neutron stars are so dense that they consist of quark matter. If such stars do exist, they should be distinguishable from other neutron stars based on various observable properties such as speed of rotation, cooling rate, magnetic field and so on. Currently, no conclusive evidence has been found for the existence of such objects.

There are actually several distinct quark matter phases, and they all behave very differently from the kind of matter we are used to. For instance, it has been hypothesised that there are phases which exhibit a kind of superconductivity, but where the charge being transported is the charge of the strong interaction, and not electric charge. We will return to these parts of the phase diagram in Sec. 2.5, but for now, let us travel back down the density axis and start climbing the temperature axis instead.

1.2.2. Deconfinement at extreme temperature

Suppose that we, instead of squeezing the aforementioned lump of matter, start heating it. If we start from absolute zero, it will be a solid at first, which upon heating will melt into a liquid, and then boil into a gas. A gas is made up of more or less free—that is, noninteracting—atoms and molecules.

Essentially, the temperature of a substance is a measure of the mean kinetic energy of the particles it contains, relative to the substance as a whole. Simply put, all atoms and molecules vibrate, and the hotter they are, the more they vibrate.

If we keep on heating our now-evaporated lump, its constituent particles will eventually become so energetic, and vibrate so violently, that the electromagnetic force is no longer able to hold the electrons in place around their respective nuclei. This phase is called a *plasma*. Plasmas are found in very hot places such as in the Sun and in lightning, but also in less extreme environments such as neon signs and plasma TVs.

But let us not stop here; let us add even more heat. What happens next is that the nuclei are ripped apart by the thermal energies. We now have a plasma of free neutrons, protons and electrons. Finally, if we crank the thermostat up yet another notch, to a temperature of nearly two trillion degrees, the neutrons and protons will disintegrate into free quarks. This is called a *quark–gluon plasma* and is another example of deconfined matter.

Aside from imparting a slight "wow!" factor it is rather meaningless to use the normal units of temperature here, be they kelvins, degrees Celsius or degrees Fahrenheit. Particle physicists prefer to use energy units instead, specifically the *electronvolt*, abbreviated eV. One electronvolt is, by definition, equal to the kinetic energy gained by an electron as it is accelerated through an electric poten-

tial difference of one volt. When used as a temperature unit, it is related to the temperature in kelvins by $T_{\mathrm{eV}} = k_{\mathrm{B}} T_{\mathrm{K}}$, where k_{B} is Boltzmann's constant[2]. On this scale, deconfinement happens at roughly 160 MeV.

It is believed that quark–gluon plasma filled the Universe in its early stages, and thus understanding the properties of this kind of matter is crucial to understanding the evolution of the Universe. There have been attempts to create quark–gluon plasma in the laboratory since the 1980s, first in CERN's Super Proton Synchrotron (SPS) and later in the Relativistic Heavy Ion Collider (RHIC) at Brookhaven National Laboratory. In the case of RHIC, the attempts appear to have been successful. The newly-built Large Hadron Collider (LHC) at CERN aims to continue this effort, primarily within its ALICE experiment.

1.3. Overview of the thesis

This thesis is organised as follows. In Chapter 2 we introduce *quantum chromodynamics* (QCD), the quantum field theory of the strong interaction. We discuss the model on a conceptual as well as a mathematical level. Our current knowledge of the phase diagram of QCD is reviewed, as are the methods which have been employed to gain this knowledge. Next, in Chapter 3 we give a brief introduction to the theoretical tools and techniques which are used to study relativistic quantum fields at high temperature and density. It is assumed that the reader is already familiar with the path integral formulation of quantum field theory, as well as basic statistical mechanics. In Chapter 4 we discuss problems which arise in high-temperature field theory as well as a few methods one can use to mitigate these issues. This chapter sets the stage for the calculations and results of Papers I and II. In Chapter 5 the NJL model is used to study features of the phase diagram of QCD; specifically, chiral symmetry breaking, pion condensation and the sign problem. The chapter complements the discussion in Papers III and IV. Chapter 5 is followed by Papers I, II, III and IV, in which we present our results, summarise and discuss possible future extensions of the work.

[2] $k_{\mathrm{B}} = 8.617343 \times 10^{-5}$ eV/K

2. Quantum chromodynamics

Quantum chromodynamics, or QCD for short, is generally regarded as a correct mathematical model for the strong interaction. Together with the Glashow–Weinberg–Salam (GWS) model, which describes the electroweak[1] interaction, it is part of the *standard model* of particle physics. In this chapter we will introduce QCD and discuss some difficulties one encounters upon using the model, along with the methods that have been developed to deal with them. Finally, we present the phase diagram that has emerged from several years of theoretical, experimental and computational studies. But first, let us briefly recount some history.

2.1. A bit of history

By the end of the 1940s physicists had discovered a number of particles which were at the time believed to be the fundamental building blocks of nature: The electron and its antiparticle the positron, the proton and the neutron, the π meson, the muon and the neutrino. Quoting Griffiths [5],

> For a brief period in 1947 it was possible to believe that the major problems of elementary particle physics were solved. [...] But this comfortable state did not last long.

During the 1950s experimentalists discovered a large number of particles called *hadrons*—so many, in fact, that it became hard to believe that these were nature's most fundamental constituents. The hadrons were classified according to various quantum numbers such as electric charge, baryon number, isospin and strangeness[2], but explanations for these properties had yet to be found.

In the early 1960s Gell-Mann and Ne'eman independently invented the *eightfold way*, a scheme for sorting the hadrons into groups with similar properties and masses [6]. To explain this structure Gell-Mann and Zweig proposed that the hadrons consisted of smaller particles which they called *quarks*, and that the quarks had to come in three types, or *flavours*—the up, down and strange quarks (abbreviated u, d and s). Furthermore, for each type of quark there had to be a

[1] The electroweak interaction is a unification of electromagnetism and the weak interaction. Although they appear to be different forces at the low energies we observe in our everyday lives, the GWS theory describes them as two aspects of the same interaction.

[2] The name "strangeness" is testament to the surprise with which the new particles were met by the physics community.

corresponding antiquark ($\bar{u}$, $\bar{d}$ and $\bar{s}$) with equal mass but otherwise completely opposite quantum numbers.

With this model the properties of the hadrons could now be explained. For instance, the baryon number is a measure of the number of quarks in a hadron relative to the number of antiquarks. More precisely, a baryon number of $+1/3$ was ascribed to each quark and a baryon number of $-1/3$ was ascribed to each antiquark, making the total baryon number for a hadron

$$B = \frac{1}{3}(n_u + n_d + n_s - n_{\bar{u}} - n_{\bar{d}} - n_{\bar{s}}), \tag{2.1}$$

where n_u is the number of up quarks, n_d is the number of down quarks, and so on. Similarly, the strange quark was assigned a strangeness of -1, the strange antiquark was assigned a strangeness of $+1$, while all other quarks had zero strangeness. Thus, strangeness is a measure of the strange quark content of a hadron:

$$S = -(n_s - n_{\bar{s}}). \tag{2.2}$$

Electric charge and isospin could also, along with other quantum numbers, now be expressed simply in terms of quark content.

There was, however, one particle which could not be explained by this simple model: the Δ^{++}, consisting of three up quarks with parallel spins. Quarks are fermions, and as such, this combination should be forbidden by the Pauli exclusion principle, which states that no two fermions of the same type can occupy the same quantum state. To resolve this problem Han and Nambu, Greenberg, and Gell-Mann proposed that quarks carry an additional degree of freedom, an unobserved quantum number which was named *colour*.

At the time, it was unclear whether the quarks were actual, physical entities—particles, as it were—or whether they were merely a convenient mathematical abstraction. The breakthrough came in 1968, when experimentalists at the Stanford Linear Accelerator Center (SLAC) discovered that the proton contained smaller, point-like particles. It became clear that these were the up and down quarks proposed by Gell-Mann and Zweig.

As years went by, theoretical predictions were made for the existence of three more quark flavours, and all were discovered in turn: *charm* in 1974, *bottom* in 1977, and finally *top* in 1995. At the time of writing, theoretical studies have shown it to be highly unlikely that there exist more quark flavours than the six already discovered, but experimental searches are nonetheless ongoing [7].

Table 2.1 shows a listing of the quark flavours along with some of their properties. Looking at this table we understand why the top quark was discovered so much later than the others. It is significantly more massive and therefore requires a lot more energy to produce. As we can see, the top quark is 40 times heavier than the second most massive, the bottom quark, and more than 70 000 times(!) heavier than the up quark, the lightest.

Flavour	Symbol	Mass	Electric charge
down	d	5 MeV	-1/3
up	u	3 MeV	+2/3
strange	s	101 MeV	-1/3
charm	c	1.27 GeV	+2/3
bottom	b	4.19 GeV	-1/3
top	t	172 GeV	+2/3

Table 2.1.: Quark properties [7]. Electric charge is given in units of the elementary charge e.

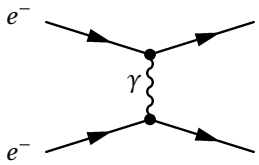

Figure 2.1.: Single photon exchange

2.2. Introduction to QCD

In many ways the prototype for quantum chromodynamics is *quantum electrodynamics* (QED), the quantum theory of electromagnetism. QED describes the interaction between two electrically charged particles as the exchange of one or more *photons*. Photons are the quanta of the electromagnetic field, and they are massless, electrically neutral spin-1 particles. In the nonrelativistic limit, one can show that the force between two charges q_1 and q_2 that arises from the single photon exchange shown in Fig. 2.1 is described by a potential

$$V(r) = \frac{A}{r}, \tag{2.3}$$

where $A \propto q_1 q_2$ and r is the distance between the charges. This is the well-known Coulomb potential which was known as early as the 18th century—150 years before the formulation of QED.

In QCD the strong interaction between quarks is described as an exchange of *gluons* which, like photons, are massless spin-1 particles. Unlike photons, however, gluons carry the charge of the interaction and therefore interact amongst themselves. Because of this the single gluon exchange depicted in Fig. 2.2a only gives a good description of the interaction at short distances. At larger distances ($\gtrsim 0.5$ fm) gluon self-interactions such as the one shown in Fig. 2.2b become important. Unfortunately, these interactions are nonlinear and therefore extremely difficult to deal with mathematically, and to date no exact methods have been found. Our best source of quantitative information about the quark–gluon interaction at large length scales is *lattice QCD*—numerical simulations of QCD using some of the world's most powerful computers.

Lattice calculations have revealed that the static potential between a quark and

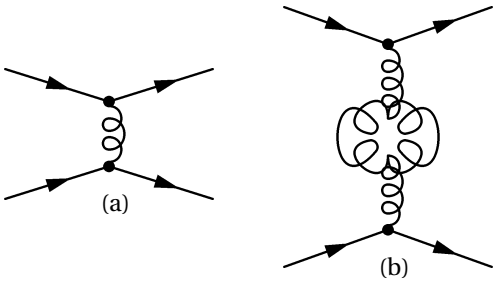

Figure 2.2.: (a) Single gluon exchange between two quarks. (b) Gluon exchange with self-interaction.

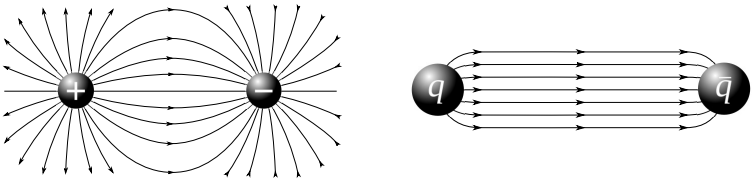

Figure 2.3.: (a) Flux lines of the electric field between two particles with opposite charge. (b) Flux lines of the chromoelectric field between a quark and an antiquark.

an antiquark is compatible with the *Cornell potential*,

$$V(r) = -\frac{A(r)}{r} + Kr. \tag{2.4}$$

At short distances, i.e. when r is small, the first term dominates. This term describes an attractive, Coulomb-like interaction. However, the factor $A(r)$ encodes a scale dependence which causes the interaction to become *weaker* at short distances—that is, at high energies. In the limit $r \to 0$ the quarks are essentially non-interacting, a phenomenon known as *asymptotic freedom*.

When r is large, the second term in Eq. (2.4) dominates. It is linear in r, which means that the energy stored in the *chromoelectric field* between the charges is proportional to the distance between them. In other words, the strong force between the quarks does not decrease as we pull them apart; rather, being the derivative of V with respect to r, it approaches a constant. This means that the flux lines of the field become straight lines that are more or less confined to a narrow region of diameter ~ 0.7 fm. This is called a *flux tube*, and is shown in Fig. 2.3b. For comparison, the familiar pattern of the flux lines of the electric field between two point charges is shown in Fig. 2.3a.

It would seem impossible to tear the quarks completely free of each other, because it requires an infinite amount of energy to be injected into the system. This is true, in a sense, but it misses an important detail: According to special relativity, when the energy stored in the field is greater than twice the rest energy of a

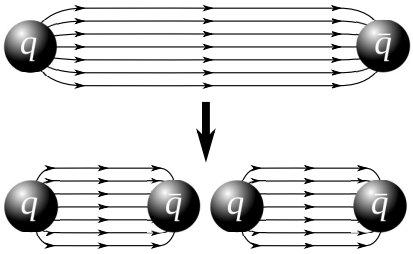

Figure 2.4.: When the energy in the chromoelectric field becomes large enough, a new quark–antiquark pair is created.

quark it becomes possible to create a new quark–antiquark pair in the middle of the tube, so it is split in two (see Fig. 2.4). We briefly discussed the phenomenon of *confinement* in Sec. 1.2.1, and this is an example of how it works at a fundamental level.

The charge of the strong interaction is called *colour*. While there is only one kind of electromagnetic charge, colour charge comes in three types: "red", "green" and "blue". The corresponding negative charges are called "antired", "antigreen" and "antiblue", respectively. Every quark carries a colour while every antiquark carries an anticolour. A gluon carries one colour and one anticolour. If you mix all three colours, or if you mix a colour and its corresponding anticolour, you get "white", or neutral. Confinement can be stated as the fact that one only observes colour neutral states in nature.

The particles that have been observed thus fall into two groups: *mesons* and *baryons*. A meson is a bound state of a quark and an antiquark having opposite colours. The most well-known examples are the three *pions*: π^+, π^- and π^0. For example, π^+ is a combination of an up quark and a down antiquark ($\pi^+ = u\bar{d}$). A baryon, on the other hand, is a bound state of three quarks, each with a different colour. Examples of baryons include the proton ($p = uud$) and the neutron ($n = udd$). Mesons and baryons are collectively known as *hadrons*.

2.3. An SU(3) gauge theory

We will now look at QCD from a more technical perspective, and again, QED will serve as our blueprint. The classical description of electromagnetism is provided by the Maxwell equations, which can be written in covariant form as

$$\partial_\mu F^{\mu\nu} = j^\nu. \tag{2.5}$$

Here, $j = (\rho, \mathbf{j})$ is the electromagnetic four-current, where ρ is the charge density and $\mathbf{j}$ is the current density. The *field strength tensor* is defined as

$$F_{\mu\nu} \equiv \partial_\nu A_\mu - \partial_\mu A_\nu, \tag{2.6}$$

where A_μ is the four-potential of the electromagnetic field.

Eq. (2.5) can be interpreted as a set of Euler–Lagrange equations of motion for A_μ, and the corresponding Lagrangian density is

$$\mathscr{L}_{\text{Maxwell}} = -\frac{1}{4}F_{\mu\nu}F^{\mu\nu} + j^\mu A_\mu. \tag{2.7}$$

If we describe j^μ as a current of Dirac fermions with charge q, i.e. $j^\mu = -q\bar{\psi}\gamma^\mu\psi$, and also include the Dirac Lagrangian to describe their propagation, we arrive at the QED Lagrangian:

$$\mathscr{L}_{\text{QED}} = \mathscr{L}_{\text{Dirac}} + \mathscr{L}_{\text{Maxwell}} = \bar{\psi}(i\gamma^\mu\partial_\mu - m - q\gamma^\mu A_\mu)\psi - \frac{1}{4}F_{\mu\nu}F^{\mu\nu}. \tag{2.8}$$

This Lagrangian has a U(1) gauge symmetry. That is, $\mathscr{L}_{\text{QED}}$ is invariant under local phase transformations on the form

$$\psi \to e^{i\alpha(x)}\psi, \tag{2.9}$$

where $\alpha(x)$ is an arbitrary function of spacetime, provided the electromagnetic field is simultaneously transformed as

$$A_\mu \to A_\mu - \frac{1}{q}\partial_\mu\alpha. \tag{2.10}$$

As it turns out, one can do the procedure in the exact opposite order: If we start with the Dirac Lagrangian for fermions with mass m,

$$\mathscr{L}_{\text{Dirac}} = \bar{\psi}(i\gamma^\mu\partial_\mu - m)\psi, \tag{2.11}$$

and *impose* invariance under the transformation (2.9), then we are forced to replace the derivative ∂_μ with the covariant derivative

$$D_\mu = \partial_\mu + i\,q\,A_\mu, \tag{2.12}$$

where A_μ transforms according to Eq. (2.10). From there it is only a matter of identifying q with the coupling strength—that is, the charge—and adding a term to describe the propagation of the field A_μ, and we arrive once again at Eq. (2.8).

This is the procedure we shall use to derive the QCD Lagrangian. Again, we start with a theory of free fermions, in this case the quarks:

$$\mathscr{L}_{\text{q}} = \bar{\psi}(i\gamma^\mu\partial_\mu - m_q)\psi. \tag{2.13}$$

Here, ψ is the quark field and m_q is the quark mass matrix. We then write ψ as a 3-spinor in colour space,

$$\psi = \begin{pmatrix} \psi_r \\ \psi_g \\ \psi_b \end{pmatrix}, \tag{2.14}$$

and require that the Lagrangian be invariant under local SU(3) transformations:

$$\psi \to e^{iT^a\alpha^a(x)}\psi. \tag{2.15}$$

Here, $\alpha^a(x)$, with $a = 1,2,\ldots,8$, are arbitrary functions of spacetime, while T^a are the eight generators of SU(3). Essentially, Eq. (2.15) is a rotation in colour space.

The generators satisfy the commutation relation

$$[T^a, T^b] = if^{abc}T^c, \tag{2.16}$$

where f^{abc} are the *structure constants* of SU(3). The most common representation of the generators is $T^a = \lambda^a/2$, where λ^a are the Gell-Mann matrices:

$$\lambda^1 = \begin{pmatrix} 0 & 1 & 0 \\ 1 & 0 & 0 \\ 0 & 0 & 0 \end{pmatrix}, \qquad \lambda^2 = \begin{pmatrix} 0 & -i & 0 \\ i & 0 & 0 \\ 0 & 0 & 0 \end{pmatrix}, \qquad \lambda^3 = \begin{pmatrix} 1 & 0 & 0 \\ 0 & -1 & 0 \\ 0 & 0 & 0 \end{pmatrix},$$

$$\lambda^4 = \begin{pmatrix} 0 & 0 & 1 \\ 0 & 0 & 0 \\ 1 & 0 & 0 \end{pmatrix}, \qquad \lambda^5 = \begin{pmatrix} 0 & 0 & -i \\ 0 & 0 & 0 \\ i & 0 & 0 \end{pmatrix}, \qquad \lambda^6 = \begin{pmatrix} 0 & 0 & 0 \\ 0 & 0 & 1 \\ 0 & 1 & 0 \end{pmatrix},$$

$$\lambda^7 = \begin{pmatrix} 0 & 0 & 0 \\ 0 & 0 & -i \\ 0 & i & 0 \end{pmatrix}, \qquad \lambda^8 = \frac{1}{\sqrt{3}}\begin{pmatrix} 1 & 0 & 0 \\ 0 & 1 & 0 \\ 0 & 0 & -2 \end{pmatrix}.$$

In order to make the Lagrangian invariant under the SU(3) transformation we have to replace the derivative by the gauge covariant derivative

$$D_\mu = \partial_\mu + ig_sT^aA^a_\mu, \tag{2.17}$$

where A^a_μ transforms under (2.15) as

$$A^a_\mu \to A^a_\mu - \frac{1}{g_s}\partial_\mu\alpha^a. \tag{2.18}$$

We identify g_s as the strong coupling constant, while the fields A^a_μ are massless vector fields that represent the eight gluons.

Finally, we need an SU(3) gauge invariant term that describes the gluon dynamics:

$$\mathscr{L}_\mathrm{g} = -\frac{1}{4}F^a_{\mu\nu}F^{\mu\nu\,a}. \tag{2.19}$$

Here, $F^a_{\mu\nu}$ is the gluon field strength tensor, defined as

$$F^a_{\mu\nu} \equiv \partial_\nu A^a_\mu - \partial_\mu A^a_\nu - g_sf^{abc}A^b_\mu A^c_\nu. \tag{2.20}$$

The full QCD Lagrangian is thus given by $\mathscr{L}_\mathrm{q} + \mathscr{L}_\mathrm{int.} + \mathscr{L}_\mathrm{g}$, or

$$\mathscr{L}_\mathrm{QCD} = \bar\psi(i\gamma^\mu\partial_\mu - m - ig_s\gamma^\mu T^aA^a_\mu)\psi - \frac{1}{4}F^a_{\mu\nu}F^{\mu\nu\,a}, \tag{2.21}$$

and we immediately see the similarity with Eq. (2.8). The most obvious difference between QED and QCD is the fact that the former has only one gauge field, the photon, whereas the latter has eight. However, a slightly more subtle difference becomes apparent when we compare Eqs. (2.6) and (2.20). If we write out last term in Eq. (2.8), we only find terms which are quadratic in A_μ, i.e. terms that describe photon propagation. Writing out the last term of Eq. (2.21), on the other hand, we also find terms which are cubic and quartic in the fields: three- and four-gluon interactions, the cause of grey hair in many a physicist.

2.4. Other symmetries

Symmetries play a very important role in physics, and in particle physics in particular. Emmy Noether showed in a seminal paper [8, 9] that any differentiable (i.e. smooth) symmetry of the action of a physical system corresponds to a conservation law. For instance, if the Lagrangian of a system is invariant under spatial rotations, Noether's theorem states that the angular momentum of the system is conserved. By the same token, the SU(3) colour symmetry of QCD implies conservation of colour charge.

SU(3) is unarguably the most important symmetry group of QCD. In fact, as we have seen, local SU(3) invariance is what *defines* QCD. However, we have also seen that this symmetry is what makes the theory so difficult to deal with on a mathematical level. Most attempts to approximate QCD with simpler models therefore dispense with the local symmetry and keep it only as a global symmetry, if at all. We therefore turn now to the other symmetries of quantum chromodynamics, as they will become very important when we discuss such "QCD-like" models later.

Let us for a moment pretend that there are only two quark flavours, u and d. Their masses are very similar (see Table 2.1), and to simplify calculations they are often taken to be equal. The QCD Lagrangian is then symmetric under SU(2) transformations in flavour space,

$$\psi \to e^{i\tau_i \alpha_i}\psi, \tag{2.22}$$

where τ_1, τ_2 and τ_3 are the Pauli matrices and α_i are constants.

Furthermore, the u and d masses are so small that in many cases they are simply neglected. The limit $m_q \to 0$ is called the *chiral limit*, because the flavour symmetry is then extended to an $\mathrm{SU}(2)_L \times \mathrm{SU}(2)_R$ chiral symmetry where the left- and right-handed components[3] of the fermion fields can be transformed separately under transformations like Eq. (2.22).

[3] A particle is *right-handed* if its spin points in the direction of its momentum, and *left-handed* if the directions of spin and momentum are opposite. The direction of momentum for a massive particle can always be altered by boosting into a different Lorentz frame, and a massive field therefore has both left- and right-handed components. For a Dirac field, these components can be projected out as $\psi_L = \frac{1}{2}(1-\gamma^5)\psi$ and $\psi_R = \frac{1}{2}(1+\gamma^5)\psi$, respectively.

In QCD, chiral symmetry is broken spontaneously at low temperature by the formation of a *chiral condensate*, given by a nonzero expectation value of $\langle\bar{\psi}\psi\rangle$. The chiral condensate acts as an effective quark mass and partly explains the large mass of the baryons. Goldstone's theorem [10, 11] says, in the context of Lorentz invariant field theories [12], that for each generator of a spontaneously broken continuous symmetry, there will be a massless mode in the spectrum. These are the *Goldstone bosons*. If the symmetry is explicitly broken as well, the Goldstone bosons acquire mass and are called *pseudo-Goldstone bosons*. The mass depends on the severity of the symmetry breaking, and if the symmetry is broken softly, the pseudo-Goldstone bosons will be very light.

SU(2) has three generators, the Pauli matrices, so we expect three Goldstone bosons due to the spontaneous chiral symmetry breaking. As the quark masses are in reality small but nonzero, chiral symmetry is broken softly as well. The Goldstone bosons should therefore have a mass, albeit a small one. It turns out that there are three particles that fit the bill nicely: the pions.

The pions have masses roughly equal to 140 MeV and are thus the lightest of the mesons. They are bound states of up quarks, down quarks and their antiparticles:

$$\begin{aligned} \pi^+ &= u\bar{d} \\ \pi^- &= d\bar{u} \\ \pi^0 &= \frac{u\bar{u} - d\bar{d}}{\sqrt{2}} \end{aligned}$$

Note that the "effective mass" of a quark inside a pion is only ~ 70 MeV, whereas in a proton it is more than 300 MeV. The fact that the pions are so light seems to indicate that nature does in fact have an approximate chiral symmetry, and furthermore that two-flavour QCD is a valid simplification. For this reason it is an extremely common approximation, one which we shall use almost exclusively throughout this thesis.

QCD also has a global U(1) symmetry, that is, the QCD Lagrangian is symmetric under global phase transformations of the quark fields. By Noether's theorem, this symmetry is related to conservation of baryon number, and is therefore often denoted by $\mathrm{U}(1)_B$.

Finally, in the chiral limit, the QCD Lagrangian has a global $\mathrm{U}(1)_A$ axial symmetry. In other words, it is symmetric under transformations of the form

$$\psi \to e^{i\gamma^5\theta}, \tag{2.23}$$

where θ is some constant. This symmetry, however, is broken by the *axial anomaly*, which is due to instanton effects. For a review of instantons in QCD, see Ref. [13]. The axial anomaly is known to have a strong influence on the QCD phase diagram [14], and we will return to it in Sec. 5.4.

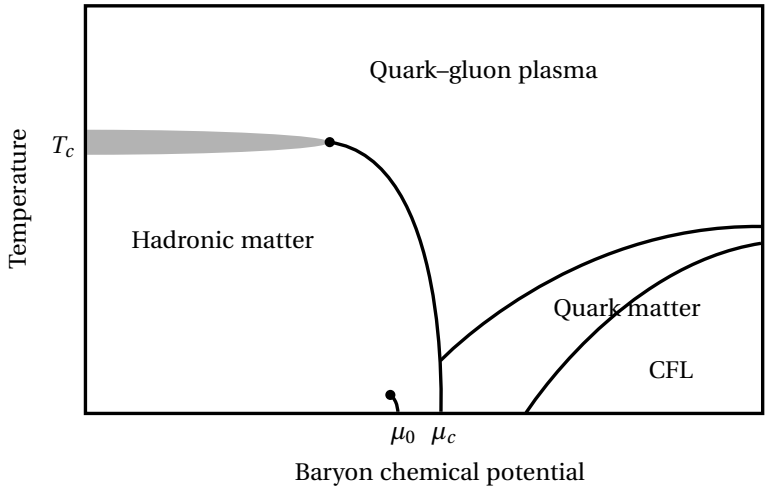

Figure 2.5.: The phase diagram of QCD.

2.5. The phase diagram of QCD

Fig. 2.5 shows, qualitatively, our current understanding of the phase diagram of QCD in the $T-\mu_B$ plane. Here, T is the temperature and μ_B is the *baryon number chemical potential*. Chemical potentials will be discussed in more detail in Sec. 3.6, so for now, suffice to say that the baryon number chemical potential is related to the quark density: A higher μ_B means more quarks and zero μ_B means that there are, on average, no quarks[4].

One can distinguish between three main regions of the phase diagram: The hadronic phase, the quark–gluon plasma phase and the quark matter phase. We will give a rather superficial description of each, and refer to [15] and [16] for more detailed reviews.

The hadronic phase is located in the lower left corner of the phase diagram, that is, at low temperature and low density. In this phase the quarks are confined inside hadrons and chiral symmetry is spontaneously broken. This is the phase in which we find ourselves, together with most of the Universe.

Inside the hadronic phase there is a line of first-order phase transitions starting at $T = 0$ and a critical chemical potential of $\mu_0 \simeq 922$ MeV, and terminating in a critical endpoint at $T \sim 10$ MeV [15]. This is the nuclear liquid–gas phase transition we mentioned briefly in Sec. 1.2.1, and on the right-hand side of it we find nuclear matter. Above the critical endpoint there is no distinction between the two phases.

Moving a bit further out along the μ_B axis, we find another first-order phase transition—the deconfinement phase transition. It starts at $T = 0$ and $\mu_B = \mu_c \simeq 1050$ MeV, and ends in a critical endpoint at $(T, \mu_B) \simeq (160, 720)$ MeV. After the

[4] More precisely: $\mu_B = 0$ means that there are, on average, equally many quarks and antiquarks.

critical endpoint it turns into a crossover, meaning that there is a smooth, gradual transition from the confined phase to the deconfined phase. Lattice calculations indicate that the crossover temperature at $\mu_B = 0$ is somewhere in the range $150 \lesssim T_c \lesssim 200$ MeV depending on the number and masses of the quarks used in the simulation.

At this temperature it is mostly safe to neglect the three heaviest quarks. The strange quark, however, has a mass of roughly 100 MeV, and so we should expect it to have a large impact on the physics near T_c. In fact, if we pretend that the three lightest quarks are massless, one can show that the phase transition is first order all the way down to $\mu_B = 0$ [14, 17]. This means that if we start from the physical strange quark mass and slowly dial it down towards zero, the critical endpoint must move in towards the T axis as well. If we, on the other hand, ignore the strange quark completely (in effect taking the limit $m_s \to \infty$), and only consider two flavours of massless quarks, the phase transition is of second order.

Note that we have drawn only one transition line, and not separate lines for deconfinement and chiral symmetry restoration. This is because calculations indicate that the two transitions coincide. (In fact, it can be shown that confinement implies chiral symmetry breaking [18, 19].) The exact connection between them is still an open question, however, and it is a topic of active research.

At high temperature, deconfined matter is expected to be in the quark–gluon plasma (QGP) phase, where chiral symmetry is restored. There aren't too many places such extreme temperatures can be found. The two candidates are the early Universe, which is believed to have been filled with QGP in the first 10^{-6} seconds after the Big Bang, and in high energy particle collisions. The Relativistic Heavy Ion Collider (RHIC) at Brookhaven National Laboratory, New York, for instance, has started to probe into the QGP phase. In 2005 physicists at RHIC reported the discovery of a new phase of matter which could not be described in terms of ordinary colour neutral hadrons [20, 21, 22, 23], and which may therefore be a quark–gluon plasma. The search for QGP continues at even higher temperatures in the ALICE experiment at CERN's Large Hadron Collider (LHC), which started operation in 2010.

Finally, we get to the lower right part of the phase diagram, where we find cold and very dense quark matter. In the *colour–flavour locked* (CFL) phase it is believed that quarks pair up to form Cooper pairs, much like the Cooper pairs of electrons in the Bardeen–Cooper–Schrieffer (BCS) theory of superconductivity. In the CFL phase, however, the charge being transported is colour charge and not electromagnetic charge. This is called *colour superconductivity*. It is likely that there are several other quark matter phases as well, some of which exhibit colour superconductivity and some which don't. For a review, see Ref. [24].

2.6. QCD from first principles

Due to asymptotic freedom, the QCD coupling constant becomes small at short distances—that is, at high energies. One may therefore expect that this allows for

the use of perturbation theory at high temperature. Indeed, the weak-coupling expansion has been used to calculate the thermodynamic functions of QCD, and the free energy, for instance, is known up to order $g_s^6 \log g_s$ [25, 26, 27, 28, 29, 30, 31, 32, 33]. Unfortunately, it turns out that the expansion has very poor convergence properties and a strong dependence on the renormalisation scale unless the coupling is very small. For example, in the case of three-flavour QCD, the g_s^3 contribution only becomes smaller than the g_s^2 term when $g_s \leq 0.07$. This corresponds to a temperature of $T \sim 10^5$ GeV [34], six orders of magnitude beyond the temperature at which deconfinement is expected to happen.

A nonperturbative approach to the thermodynamics of QCD is offered by lattice gauge theory. *Lattice QCD* is a computational simulation of the strong interaction, in which spacetime is modelled as a grid of discrete points on which the quarks live. The gluons live on the links between lattice points. The partition function is then calculated by using Monte Carlo methods to sample the most important gauge field configurations. (For a thorough introduction to lattice QCD, see Ref. [35].)

Lattice QCD is currently the only way to obtain reliable, quantitative information about the QCD phase diagram from first principles. Unfortunately, the method is severely hampered by the *sign problem*: When the baryon number chemical potential is nonzero the weighting function used in the Monte Carlo importance sampling becomes complex—a rather unfortunate property for a statistical weight.

Several methods have been developed to sidestep the sign problem for small μ_B. Examples include reweighting techniques, Taylor expansions in μ_B around $\mu_B = 0$, and the use of imaginary chemical potentials. For a review, see Ref. [36]. However, these methods only work for $\mu_B \lesssim T$, that is, at low density, and a general solution to the sign problem for all values of the baryon number chemical potential has yet to be found. We will return to the sign problem in Sec. 5.4.

2.7. QCD-like models

Due to the sign problem a large part of the QCD phase diagram is inaccessible to lattice calculations. A complementary approach that works even at nonzero μ_B is offered by *QCD-like models*—models which are simpler than QCD yet share some of its defining properties.

We distinguish between two types of QCD-like models: *low-energy effective field theories* and *toy models* [37]. An effective field theory is an approximate model that includes the symmetries and degrees of freedom of the original theory that are relevant up to a certain energy scale or, equivalently, down to a certain length scale. Physics at higher energy scales, i.e. at shorter length scales, is not described by the model but rather gets encoded in the model parameters. The definition of a toy model, on the other hand, is much less strict. Basically, the term encompasses any model that has some feature in common with QCD and which can therefore be used to study the properties of QCD that are related to

said feature.

In this thesis we use ϕ^4 theory and the NJL model, which both fall into the "toy model" category, to describe various aspects of QCD. These models are properly introduced in Chapters 4 and 5, respectively. In the following, we briefly mention a few other theories and models which are, or have been, commonly used to approximate QCD.

2.7.1. Bag model

The famous *MIT bag model* was proposed in the 1970s as a model for hadrons [38, 39, 40]. In the bag model, hadrons are modelled as a group of free or weakly interacting quarks confined to a finite region of space—the "bag"—by a vacuum pressure $P_{\text{vac}} = B$. B is called the *bag constant*. Confinement and asymptotic freedom are thus put in by hand and are not dynamical results of the theory. Stability of the hadrons results from balancing the pressure of the vacuum outside the bag with the pressure from the quarks inside. The theory says nothing about the origin of this vacuum pressure and just treats B as a free parameter.

2.7.2. Linear sigma model

The *linear sigma model* (LSM) is perhaps the most widely studied effective theory for QCD, mainly due to its simplicity. It is a theory of N real scalar fields with an O(N)-symmetric quartic interaction:

$$\mathscr{L} = \frac{1}{2}(\partial_\mu \phi_i)(\partial^\mu \phi_i) - \frac{1}{2}m^2 \phi_i \phi_i - \frac{\lambda}{4!}(\phi_i \phi_i)^2. \tag{2.24}$$

When $N = 1$ the LSM reduces to ϕ^4 theory, the simplest interacting field theory. When $N = 4$, however, the Lagrangian has an O(4) symmetry which is spontaneously broken down to O(3) by a nonzero vacuum expectation value for one of the fields—ϕ_1, say. After the symmetry has been broken, the fields ϕ_2, ϕ_3 and ϕ_4 describe massless excitations—Goldstone bosons.

As it happens, the group O(4) is homomorphic[5] to the group SU(2) × SU(2), the chiral symmetry group of two-flavour QCD. Moreover, O(3) is homomorphic to SU(2), which is the flavour symmetry group of QCD after chiral symmetry has been broken. The massless fields of the LSM can then be taken to represent the lightest excitations of QCD in the broken phase, the pions, while the expectation value $\langle \phi_1 \rangle$ represents the chiral condensate. (The interpretation of ϕ_1, which is referred to as the *sigma* mode, is less clear. It is commonly associated with the $f_0(600)$ meson, although recent studies seem to indicate that this may be a suboptimal choice [41].) The LSM can thus be used as a low-energy effective theory for QCD in the regime where mesons are the relevant degrees of freedom—that is, for very small values of the baryon chemical potential and for temperatures

[5] When two groups are homomorphic, they have the same structure. More precisely, given two groups G and H, a *group homomorphism* is a mapping $h : G \to H$ such that for all u and v in G, it is true that $h(uv) = h(u)h(v)$.

up to the deconfinement phase transition. Since it doesn't have quark degrees of freedom, there is literally no way it can describe the physics of QCD in the deconfined phase.

It is worth mentioning that the Goldstone modes of the LSM need not necessarily represent the pions. In the CFL phase the lightest excitations are the *kaons*, and the LSM has been used to model this situation as well [42, 43].

Over the years, the O(N) linear sigma model has been studied extensively, using a variety of techniques. Important examples include the $1/N$ expansion [44, 45, 46, 47, 48, 49], the 2PI formalism [50, 51, 52, 53, 54, 55, 56] and optimised perturbation theory [57, 58].

2.7.3. Linear sigma model with quarks

The degrees of freedom in the deconfined phase are the quarks, and as we have seen, this is not accounted for in the linear sigma model. But what if we put them in by hand? That is, say we take the Lagrangian of the linear sigma model and add Dirac terms that describe the quarks, together with Yukawa interactions between the fermions and the scalars. We then obtain what is called the *linear sigma model with quarks* (LSMq), also known as the *quark–meson model* or the *chiral quark model*:

$$\begin{aligned}\mathscr{L} &= \frac{1}{2}(\partial_\mu\phi_i)(\partial^\mu\phi_i) - \frac{1}{2}m^2\phi_i\phi_i - \frac{\lambda}{4!}(\phi_i\phi_i)^2 \\ &\quad + \bar{\psi}i\gamma^\mu\partial_\mu\psi + g\bar{\psi}\Gamma_i\psi\phi_i. \end{aligned} \tag{2.25}$$

Here, we have defined $\Gamma \equiv (1, i\gamma^5\boldsymbol{\tau})$, where $\boldsymbol{\tau} = (\tau_1, \tau_2, \tau_3)$ are the Pauli matrices acting on the flavour space components of ψ. The Lagrangian is O(4) invariant in the scalar sector, while the quark part is symmetric under $\mathrm{SU}(2)_L \times \mathrm{SU}(2)_R$ transformations. Neither symmetry applies to the Yukawa interaction, but any rotation of ϕ can be countered by a flavour transformation of ψ, keeping the last term invariant as well.

Chiral symmetry is spontaneously broken in the LSMq in exactly the same way as in the linear sigma model. Interestingly, here we see how the chiral condensate gives rise to an effective mass for the quarks. If we expand ϕ_1 around its vacuum expectation value,

$$\phi_1 \to \langle\phi_1\rangle + \phi_1, \tag{2.26}$$

we see that the first term in the interaction can be written

$$g\bar{\psi}\psi\phi_1 \to m_q\bar{\psi}\psi + g\bar{\psi}\psi\phi_1, \qquad m_q \equiv g\langle\phi_1\rangle. \tag{2.27}$$

The first term has the exact same form as the mass term of a Dirac field with mass m_q.

The major benefit from adding quarks to the linear sigma model is that it becomes possible to include a chemical potential for baryon number (or, equivalently, quark number). As such, the LSMq has been used extensively to study the phase diagram of QCD in the μ_B–T plane [59, 60, 61, 62, 63, 64, 65, 66].

It should be stressed that, unlike the LSM, the LSMq is not a low-energy effective theory for QCD, because it describes *both* free quarks and mesons even in the regions of the phase diagram where quarks are in reality confined.

3. Thermal field theory

Thermodynamics is the branch of physics that describes a macroscopic system in terms of properties such as temperature, pressure, density, and so on. These properties are determined by the underlying microscopic physics. For example, the temperature of a gas is a measure of the kinetic energy of its constituent atoms and molecules. The link between the microscopic description of the behaviour of individual particles and the macroscopic description in terms of thermodynamical variables is provided by *statistical mechanics*. In statistical mechanics one applies the mathematical tools of probability theory and statistics in order to describe the collective behaviour of large numbers of particles.

The physics of particles at atomic and subatomic scales are described by *quantum mechanics*. If the particles are so energetic that they move at a significant fraction of the speed of light, one also needs to take into account *special relativity*, and the combination of quantum mechanics and special relativity is known as *quantum field theory*.

Finally, in order to obtain a thermodynamical description of a system of relativistic, quantum mechanical particles—a quark–gluon plasma, say—we must combine statistical mechanics and quantum field theory. This is called *thermal field theory*.

In this section we give a brief introduction to thermal field theory. It is assumed that the reader is already familiar with the path integral formalism of quantum field theory, as well as with classical statistical mechanics and thermodynamics. For more complete treatments of thermal field theory, see e.g. Refs. [67, 68, 69].

3.1. Path integrals

Consider the case of a field theory with a single scalar field $\phi(t,\mathbf{x})$, described by the Lagrangian $\mathscr{L}$, where the field is known to be in a certain state ϕ_1 at the time t_1. The probability amplitude for the field to be in the state ϕ_2 at time t_2 can then be expressed as the *path integral*

$$\langle\phi_2|e^{-i(t_2-t_1)\hat{H}}|\phi_1\rangle = \int_{\substack{\phi(t_1,\mathbf{x})=\phi_1(\mathbf{x})\\ \phi(t_2,\mathbf{x})=\phi_2(\mathbf{x})}} \mathscr{D}\phi\, e^{iS}. \tag{3.1}$$

Here, $\hat{H}$ is the system's Hamiltonian operator, while S is the *action*, defined by

$$S = \int_{t_1}^{t_2} \mathrm{d}t \int \mathrm{d}^3x\, \mathscr{L}. \tag{3.2}$$

One way to think of Eq. (3.1) is as follows: Imagine a "path" from ϕ_1 to ϕ_2, i.e. a certain combination of intermediate field configurations that connect one to the other, and let us denote this path by $\phi(t,\mathbf{x})$. In other words, pick some function ϕ that satisfies

$$\phi(t_1,\mathbf{x}) = \phi_1(\mathbf{x}), \tag{3.3}$$
$$\phi(t_2,\mathbf{x}) = \phi_2(\mathbf{x}). \tag{3.4}$$

Now, assign a factor e^{iS} to this path, where S is the action one finds when plugging the function ϕ into the Lagrangian. This is the contribution to the probability amplitude from this single path.

Now, the total amplitude, the path integral, is simply the sum over the amplitudes of each and every such path. In other words, we integrate over *all possible functions* that satisfy the constraints (3.3) and (3.4). Path integrals belong to the class of integrals known as *functional integrals*.

Path integrals are both a convenient and extremely powerful tool in quantum physics. An in-depth review of the subject is, however, beyond the scope of this thesis, and we refer instead to the available literature. See for example Ref. [70] for details on the derivation of Eq. (3.1).

3.2. The partition function

A central concept in statistical mechanics is the *partition function* of a system. This function encodes the statistical properties of the system, and most of the usual thermodynamical quantities, such as pressure, density and free energy, can be derived from it.

In quantum field theory the numbers of different particles are never fixed. Due to the various interactions between the fields, a particle may decay into other types of particles, two or more particles may annihilate against each other—particles are even spontaneously created out of the vacuum. A system with a fluctuating particle number is described in statistical mechanics by the *grand canonical ensemble*.

In the grand canonical ensemble the (grand) partition function Z of a quantum mechanical system is defined as the trace of the operator $e^{-\beta(\hat{H}-\mu_i\hat{N}_i)}$ over the state space,

$$Z = \mathrm{tr}\,(e^{-\beta(\hat{H}-\mu_i\hat{N}_i)}), \tag{3.5}$$

where the sum over i runs over the various particle types in the system. Here, β is the inverse temperature, $\beta = 1/T$, $\hat{H}$ is the system's Hamiltonian operator, $\hat{N}_i$ is the number operator for particles of type i and μ_i is the corresponding chemical potential[1].

[1] Basically, μ_i is defined as the change in the energy of the system upon adding a particle of type i.

More generally, we can associate a chemical potential μ_i with *each conserved quantity*, or *charge*, in the system. Conserved charges arise from the global continuous symmetries of the system and can indeed be particle numbers, but they can also be electric charge, isospin, etc. In QED, for instance, the number of electrons is not conserved because electrons may annihilate against positrons. The conserved quantity in this case is the number of electrons *minus* the number of positrons, which is proportional to the electric charge. Suppose we have a set of independently conserved charges Q_i; the partition function is then

$$Z = \mathrm{tr}\,(e^{-\beta(\hat{H}-\mu_i\hat{Q}_i)}), \tag{3.6}$$

where $\hat{Q}_i$ are the charge operators.

In quantum field theory the "sum over all states" implied by the trace operation means that we have to integrate over all possible field configurations. Thus, the partition function can be expressed as a path integral,

$$Z = \int \mathscr{D}\varphi\, \langle\varphi|e^{-\beta(\hat{H}-\mu_i\hat{Q}_i)}|\varphi\rangle. \tag{3.7}$$

Now, look closer at the integrand in Eq. (3.7) and compare it to the left-hand side of Eq. (3.1). If we perform a Wick rotation to imaginary time, $t = -i\tau$, integrate τ from 0 to β and make the substitution

$$H \to H' = H - \mu_i Q_i, \tag{3.8}$$

we can insert Eq. (3.1) directly into the expression for the partition function provided the initial and final states are the same. That is, we demand that

$$|\phi(0,\mathbf{x})\rangle = |\phi(\tau,\mathbf{x})\rangle = |\varphi(\mathbf{x})\rangle. \tag{3.9}$$

One may think this requirement translates into a periodicity condition on the fields,

$$\phi(0,\mathbf{x}) = \phi(\beta,\mathbf{x}), \tag{3.10}$$

but this is not necessarily true. A field's overall sign is inobservable, so ϕ and $-\phi$ both correspond to the same quantum state. As it turns out, the condition (3.10) is the correct one for bosons, whereas the requirement for fermions is that they are *antiperiodic* in imaginary time [69]:

$$\psi(0,\mathbf{x}) = -\psi(\beta,\mathbf{x}). \tag{3.11}$$

Using bosons as an example we find that the grand partition function can be written as

$$\begin{aligned} Z &= \int \mathscr{D}\varphi \int_{\phi(0,\mathbf{x})=\phi(\beta,\mathbf{x})=\varphi(\mathbf{x})} \mathscr{D}\phi\; e^{i(-i)\int_0^\beta \mathrm{d}\tau \int \mathrm{d}^3x\, \mathscr{L}(t=-i\tau)} \\ &= \int_{\phi(0,\mathbf{x})=\phi(\beta,\mathbf{x})} \mathscr{D}\phi\; e^{\int_0^\beta \mathrm{d}\tau \int \mathrm{d}^3x\, \mathscr{L}(t=-i\tau)} \\ &= \int_{\phi(0,\mathbf{x})=\phi(\beta,\mathbf{x})} \mathscr{D}\phi\; e^{-S_E}, \end{aligned} \tag{3.12}$$

where $\mathscr{L}$ is now the Lagrangian density obtained by a Legendre transform of the Hamiltonian density corresponding to H':

$$\mathscr{L} = \pi\partial_0\phi - \mathscr{H}'. \tag{3.13}$$

Here, π is the conjugate momentum density corresponding to the field ϕ. Suppose the Hamiltonian density of the vacuum field theory is $\mathscr{H}$, then

$$H' = \int \mathrm{d}^3x\, \mathscr{H}' = \int \mathrm{d}^3x\, (\mathscr{H} - \mu_i\rho_i), \tag{3.14}$$

where ρ_i are the charge densities:

$$Q_i = \int \mathrm{d}^3x\, \rho_i. \tag{3.15}$$

A Wick rotation is a transformation from Minkowski space to Euclidean space. S_E is therefore called the *Euclidean action*, and is defined as

$$S_E \equiv \int_0^\beta \mathrm{d}\tau \int \mathrm{d}^3x\, \mathscr{L}_E, \tag{3.16}$$

where $\mathscr{L}_E$ is the Euclidean Lagrangian,

$$\mathscr{L}_E \equiv -\mathscr{L}(t = -i\tau). \tag{3.17}$$

We will henceforth drop the subscript E on $\mathscr{L}$ and S whenever there is no chance of confusion.

3.3. Thermodynamical quantities

In statistical mechanics the *grand (canonical) potential* Φ is defined as

$$\Phi = -T\log Z. \tag{3.18}$$

The grand potential is a very useful quantity from which a number of thermodynamical variables can be calculated. Unfortunately, Φ is an extensive quantity—that is, it is proportional to the volume of the system—and in quantum field theory one usually assumes the volume to be infinite. Therefore, in thermal field theory we use the grand potential *density* instead,

$$\Omega \equiv \frac{\Phi}{V} = -\frac{1}{\beta V}\log Z. \tag{3.19}$$

From this point onwards, whenever an explicit factor of V appears in calculations it is always to be understood in this way—as a formal parameter that always cancels out in the final result.

The grand potential density is equal to minus the pressure,

$$\Omega = -P, \tag{3.20}$$

and it is related to the *Helmholtz free energy density* by

$$\Omega = \mathscr{F} - \mu_i \langle \rho_i \rangle, \tag{3.21}$$

where $\langle \rho_i \rangle$ is the average density of charge i. When all chemical potentials are zero, Ω and $\mathscr{F}$ coincide. Confusingly, literature on high energy physics often uses the terms "free energy", "thermodynamic potential" and "grand potential" interchangeably, even omitting the qualifier "density" altogether, yet always referring to the quantity defined here as the grand potential density Ω. For the purposes of this thesis the distinction between the various terms is not important, and we shall adopt this rather lax terminology in subsequent chapters.

The thermal average of an observable quantity A in the grand canonical ensemble is given by the expression

$$\langle A \rangle = \frac{1}{Z} \mathrm{tr}\,(\hat{A} e^{-\beta(\hat{H} - \mu_i \hat{Q}_i)}). \tag{3.22}$$

Thus, the average density of some charge Q_i is

$$\langle \rho_i \rangle = \frac{\langle Q_i \rangle}{V} = \frac{1}{VZ} \mathrm{tr}\,(\hat{Q}_i e^{-\beta(\hat{H} - \mu_i \hat{Q}_i)}), \tag{3.23}$$

which we can write as

$$\langle \rho_i \rangle = \frac{1}{\beta V Z} \frac{\partial Z}{\partial \mu_i} = \frac{1}{\beta V} \frac{\partial}{\partial \mu_i} \log Z = -\frac{\partial \Omega}{\partial \mu_i}. \tag{3.24}$$

In other words, once we know the grand potential, finding the average density of a specific charge is as simple as taking the derivative with respect to the corresponding chemical potential.

Eq. (3.22) can generally be extended to thermal field theory as the path integral expression

$$\langle A \rangle = \frac{1}{Z} \int \mathscr{D}\phi \; A \, e^{-S}. \tag{3.25}$$

3.4. The thermal scalar field

We will now obtain an expression for the free energy density of a real scalar field with Lagrangian

$$\mathscr{L} = \frac{1}{2} (\partial_\mu \phi)(\partial^\mu \phi) - \frac{1}{2} m^2 \phi^2, \tag{3.26}$$

where m is the mass. There are no conserved charges in this system, so we will not introduce any chemical potentials. In Euclidean space, the Lagrangian becomes

$$\mathscr{L}_E = \frac{1}{2} (\partial_\mu \phi)(\partial_\mu \phi) + \frac{1}{2} m^2 \phi^2, \tag{3.27}$$

giving the action

$$S = \int_0^\beta \mathrm{d}\tau \int \mathrm{d}^3 x \left[\frac{1}{2} (\partial_\mu \phi)(\partial_\mu \phi) + \frac{1}{2} m^2 \phi^2 \right] = \frac{1}{2} \int_0^\beta \mathrm{d}\tau \int \mathrm{d}^3 x \, \phi(-\partial^2 + m^2)\phi, \tag{3.28}$$

where we have integrated by parts and ignored the surface term, assuming the field falls off quickly as $x \to \infty$.

It is easier to work in frequency–momentum space, so we expand the field in a Fourier series,

$$\phi(\tau, \mathbf{x}) = \frac{1}{\sqrt{\beta V}} \sum_{n=-\infty}^{\infty} \sum_{\mathbf{p}} \phi_{n,\mathbf{p}} e^{i(\omega_n \tau + \mathbf{p}\cdot\mathbf{x})}, \tag{3.29}$$

where the coefficients are given by the inverse Fourier transform

$$\phi_{n,\mathbf{p}} = \frac{1}{\sqrt{\beta V}} \int_0^\beta \mathrm{d}\tau \int \mathrm{d}^3 x \, \phi(\tau, \mathbf{x}) e^{-i(\omega_n \tau + \mathbf{p}\cdot\mathbf{x})}. \tag{3.30}$$

The frequencies ω_n are called *Matsubara frequencies*[2] and follow from the τ-periodicity of ϕ. They are defined as

$$\omega_n = 2n\pi T, \qquad n = 0, \pm 1, \pm 2, \ldots \tag{3.31}$$

Additionally, we have applied periodic boundary conditions in a finite volume V, resulting in discrete momenta. This is just to simplify calculations a bit, and we will take the continuum limit in the end.

Next, we find the momentum representation of the action:

$$\begin{aligned} S &= \frac{1}{2} \int_0^\beta \mathrm{d}\tau \int \mathrm{d}^3 x \left[\frac{1}{\sqrt{\beta V}} \sum_{n,\mathbf{p}} \phi_{n,\mathbf{p}} e^{i(\omega_n \tau + \mathbf{p}\cdot\mathbf{x})} \right] (-\partial^2 + m^2) \\ &\qquad \times \left[\frac{1}{\sqrt{\beta V}} \sum_{m,\mathbf{q}} \phi_{m,\mathbf{q}} e^{i(\omega_m \tau + \mathbf{q}\cdot\mathbf{x})} \right] \\ &= \frac{1}{2} \sum_{n,\mathbf{p}} \phi_{n,\mathbf{p}} (\omega_n^2 + \mathbf{p}^2 + m^2) \phi_{-n,-\mathbf{p}}. \end{aligned} \tag{3.32}$$

Since $\phi(\tau, \mathbf{x})$ is real, we can use Eq. (3.30) to show that $\phi_{-n,-\mathbf{p}} = \phi^*_{n,\mathbf{p}}$. Furthermore, $\phi^*_{n,\mathbf{p}} \phi_{n,\mathbf{p}} = |\phi_{n,\mathbf{p}}|^2$. This means that we can write the action compactly as

$$S = \frac{1}{2} \varphi_\lambda M_{\lambda\kappa} \varphi_\kappa, \tag{3.33}$$

where we have employed the shorthand notation $\lambda = (n, \mathbf{p})$, and where we have defined $\varphi_\lambda \equiv |\phi_\lambda|$ and

$$M_{\lambda\kappa} \equiv M_{(n,\mathbf{p}),(m,\mathbf{q})} = (\omega_n^2 + \mathbf{p}^2 + m^2) \delta_{n,m} \delta_{\mathbf{p},\mathbf{q}}. \tag{3.34}$$

As in vacuum field theory, the matrix M is simply the inverse (bare) propagator. The *thermal propagator* of the nth Matsubara mode is therefore

$$G(\omega_n, \mathbf{p}) = \frac{1}{\omega_n^2 + \mathbf{p}^2 + m^2}. \tag{3.35}$$

[2] More precisely, these are the *bosonic* Matsubara frequencies. The fermionic Matsubara frequencies are slightly different due to the antiperiodicity requirement, and will be discussed in Sec. 3.5.

The partition function is now given by a Gaussian integral, easily evaluated using the standard formula:

$$Z = \int \mathscr{D}\varphi\, e^{-S} = \int \mathscr{D}\varphi\, e^{-\frac{1}{2}\varphi_\lambda M_{\lambda\kappa}\varphi_\kappa} = e^{-\frac{1}{2}\mathrm{tr}\log M}. \tag{3.36}$$

Thus, the free energy is given by

$$\mathscr{F} = \frac{1}{2\beta V}\mathrm{tr}\log M. \tag{3.37}$$

The trace is just the sum of the diagonal terms, and is easy to calculate since M is a diagonal matrix:

$$\mathrm{tr}\log M = \sum_\lambda \log M_{\lambda\lambda} = \sum_n \sum_{\mathbf{p}} \log(\omega_n^2 + \mathbf{p}^2 + m^2). \tag{3.38}$$

Taking the continuum limit $\sum_{\mathbf{p}} \to V\int \frac{\mathrm{d}^3p}{(2\pi)^3}$, we get the free energy

$$\mathscr{F} = \frac{1}{2}T\sum_n \int \frac{\mathrm{d}^3p}{(2\pi)^3}\, \log(\omega_n^2 + \mathbf{p}^2 + m^2) = \frac{1}{2}\sum\!\!\!\!\!\!\int_P \log(P^2 + m^2). \tag{3.39}$$

Here, we have introduced the notation

$$\sum\!\!\!\!\!\!\int_P \equiv T\sum_{n=-\infty}^{\infty}\int \frac{\mathrm{d}^3p}{(2\pi)^3}\,, \qquad P = (\omega_n, \mathbf{p}) \tag{3.40}$$

called a *sum-integral*. We will soon see how to evaluate the Matsubara sum in Eq. (3.39), but first we have a brief look at the necessary mathematical preliminaries.

3.4.1. Residue theory at a glance

Suppose that the function f has an isolated singularity at the point z_0 in the complex plane. Then, it has a Laurent series in an annulus around z_0:

$$f(z) = \cdots + \frac{a_{-2}}{(z-z_0)^2} + \frac{a_{-1}}{z-z_0} + a_0 + a_1(z-z_0) + a_2(z-z_0)^2 + \cdots. \tag{3.41}$$

The coefficient a_{-1} is called the *residue* of f at z_0, denoted $\mathrm{Res}(f, z_0)$.

If the function has a *simple pole* at z_0, i.e. $a_n = 0$ for $n \le -2$, the residue can be found using the simple formula

$$\mathrm{Res}(f, z_0) = \lim_{z\to z_0}(z-z_0)f(z). \tag{3.42}$$

Moreover, if we introduce another function g, which is analytic at z_0, then the residue of the product is

$$\mathrm{Res}[f(z)g(z), z_0] = g(z_0)\mathrm{Res}(f, z_0). \tag{3.43}$$

From this it follows that

$$\mathrm{Res}\left[\frac{g(z)}{z-z_0}, z_0\right] = g(z_0). \tag{3.44}$$

Finally, we state *Cauchy's residue theorem*: Let C be a simple closed positively oriented path in the complex plane. Suppose that f is analytic inside and on C, except at the isolated singularities $z_1, z_2, \ldots, z_n$ inside C. Then,

$$\oint_C \mathrm{d}z\, f(z) = 2\pi i \sum_{j=1}^{n} \mathrm{Res}(f, z_j). \tag{3.45}$$

3.4.2. Matsubara sums

We will now see how one can use complex contour integration to evaluate Matsubara sums like the one in Eq. (3.39).

First, we write

$$\mathscr{F} = \frac{1}{2}\int \frac{\mathrm{d}^3 p}{(2\pi)^3}\, A, \tag{3.46}$$

where we have defined

$$A \equiv T \sum_{n=-\infty}^{\infty} \log(\omega_n^2 + E_{\mathbf{p}}^2), \tag{3.47}$$

and $E_{\mathbf{p}}^2 \equiv \mathbf{p}^2 + m^2$.

Next, we rewrite the sum as

$$A = T\sum_n \log(-(i\omega_n)^2 + E_{\mathbf{p}}^2), \tag{3.48}$$

and differentiate with respect to $E_{\mathbf{p}}$:

$$\frac{\mathrm{d}A}{\mathrm{d}E_{\mathbf{p}}} = -2TE_{\mathbf{p}}\sum_n \frac{1}{(i\omega_n)^2 - E_{\mathbf{p}}^2}. \tag{3.49}$$

By using the residue theorem in reverse, we can express the sum over n as a contour integral over the complex variable ω,

$$\begin{aligned}\frac{\mathrm{d}A}{\mathrm{d}E_{\mathbf{p}}} &= -2TE_{\mathbf{p}}\sum_n \frac{\beta}{2}\mathrm{Res}\left\{\frac{1}{\omega^2 - E_{\mathbf{p}}^2}\coth\frac{\beta\omega}{2};\quad \omega = i\omega_n = i2\pi nT\right\} \\ &= -\frac{E_{\mathbf{p}}}{2\pi i}\oint_C \frac{\mathrm{d}\omega}{\omega^2 - E_{\mathbf{p}}^2}\coth\frac{\beta\omega}{2},\end{aligned} \tag{3.50}$$

because the hyperbolic cotangent has poles at $\frac{1}{2}\beta\omega = i\pi n$, that is, at $\omega = i\omega_n$, and the residues there are $\frac{2}{\beta}$. The contour C, shown in Fig. 3.1a, is closed at infinity and encircles all of these poles.

The hyperbolic cotangent is bounded everywhere except on the imaginary axis, and the factor $1/(\omega^2 - E_{\mathbf{p}}^2)$ decreases fast enough that we may instead close the contour around the poles at $\omega = \pm E_{\mathbf{p}}$, as shown in Fig. 3.1b. The contribution

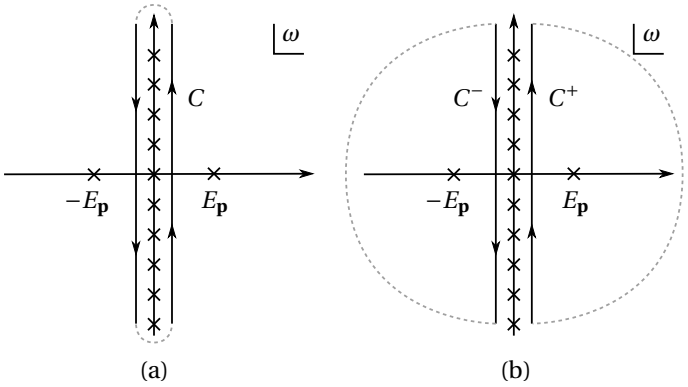

Figure 3.1.: (a) The original contour C, encircling the poles of the hyperbolic cotangent. (b) The contours C^+ and C^-, enclosing the poles at $\pm E_{\mathbf{p}}$.

from the semicircles vanishes when we take their radius to infinity. Then, using the residue theorem again, we find that

$$\begin{aligned}
\frac{\mathrm{d}A}{\mathrm{d}E_{\mathbf{p}}} &= -\frac{E_{\mathbf{p}}}{2\pi i}\oint_{(C^+\cup C^-)}\frac{\mathrm{d}\omega}{\omega^2-E_{\mathbf{p}}^2}\coth\frac{\beta\omega}{2} \\
&= E_{\mathbf{p}}\sum_{\omega=\pm E_{\mathbf{p}}}\mathrm{Res}\left\{\frac{1}{\omega^2-E_{\mathbf{p}}^2}\coth\frac{\beta\omega}{2}\right\} \\
&= E_{\mathbf{p}}\left(\frac{1}{2E_{\mathbf{p}}}\coth\frac{\beta E_{\mathbf{p}}}{2}-\frac{1}{2E_{\mathbf{p}}}\coth\frac{\beta(-E_{\mathbf{p}})}{2}\right) \\
&= \coth\frac{\beta E_{\mathbf{p}}}{2} \\
&= 1+\frac{2}{e^{\beta E_{\mathbf{p}}}-1}.
\end{aligned} \tag{3.51}$$

Note that the sign is switched in the second line because of the orientation of the contours. It is also worth noting that the second term in the final expression is the Bose–Einstein distribution function. Taking the antiderivative with respect to $E_{\mathbf{p}}$, we obtain

$$A = E_{\mathbf{p}} + 2T\log\left(1-e^{-\beta E_{\mathbf{p}}}\right). \tag{3.52}$$

3.4.3. Free energy

Plugging Eq. (3.52) back into Eq. (3.46), we arrive at the following result for the free energy:

$$\mathscr{F} = \frac{1}{2}\int\frac{\mathrm{d}^3p}{(2\pi)^3}\left\{E_{\mathbf{p}}+2T\log\left(1-e^{-\beta E_{\mathbf{p}}}\right)\right\}. \tag{3.53}$$

The first term in the integrand is temperature independent, while the second term depends on T and vanishes in the limit $T\to 0$. They are therefore the vac-

uum and thermal contributions to the free energy, respectively. The thermal contribution cannot be determined analytically when $m \neq 0$, but it is exponentially convergent and therefore easy to calculate numerically.

3.5. The thermal Dirac field

Next, we will obtain the grand potential of a Dirac field with Lagrangian

$$\mathscr{L} = \bar{\psi}(i\gamma^\mu \partial_\mu - m)\psi, \tag{3.54}$$

which corresponds to the Hamiltonian density

$$\mathscr{H} = \bar{\psi}(i\gamma^i \partial_i + m)\psi. \tag{3.55}$$

The number density of the fermions—that is, the density of particles minus the density of antiparticles—is given by the zeroth component of the Noether current density corresponding to U(1) invariance:

$$j^\mu = (n, \mathbf{j}) = \bar{\psi}\gamma^\mu \psi. \tag{3.56}$$

Redefining the Hamiltonian according to Eq. (3.8),

$$\mathscr{H} \to \bar{\psi}(i\gamma^i \partial_i + m)\psi - \mu n = \bar{\psi}(i\gamma^i \partial_i + m - \mu\gamma^0)\psi, \tag{3.57}$$

where μ is the chemical potential for particle number, we find that the Lagrangian must be

$$\mathscr{L} = \bar{\psi}(i\gamma^\mu \partial_\mu - m + \mu\gamma^0)\psi. \tag{3.58}$$

The Euclidean Lagrangian is then

$$\mathscr{L}_E = -\mathscr{L}(t = -i\tau) = \bar{\psi}\left(\tilde{\gamma}_0 \frac{\partial}{\partial\tau} + \tilde{\gamma}_i \partial_i + m - \mu\tilde{\gamma}_0\right)\psi, \tag{3.59}$$

where we have defined the *Euclidean gamma matrices* by

$$\tilde{\gamma}_0 = \gamma^0, \qquad \tilde{\gamma}_k = i\gamma^k \quad (k = 1, 2, 3). \tag{3.60}$$

Again, it is convenient to use a frequency–momentum representation of the fields,

$$\psi(\tau, \mathbf{x}) = \frac{1}{\sqrt{\beta V}} \sum_{n,\mathbf{p}} \psi_{n,\mathbf{p}} e^{i(\omega_n \tau + \mathbf{p}\cdot\mathbf{x})}, \tag{3.61}$$

with Fourier coefficients

$$\psi_{n,\mathbf{p}} = \frac{1}{\sqrt{\beta V}} \int_0^\beta \mathrm{d}\tau \int \mathrm{d}^3 x\, \psi(\tau, \mathbf{x}) e^{-i(\omega_n \tau + \mathbf{p}\cdot\mathbf{x})}. \tag{3.62}$$

Recall that ψ should be antiperiodic in imaginary time. This leads to a slightly different expression for the Matsubara frequencies than the one we found for bosons in Sec. 3.4:

$$\omega_n = (2n + 1)\pi T, \qquad n = 0, \pm 1, \pm 2, \ldots \tag{3.63}$$

We thus get the action

$$S = \sum_{n,\mathbf{p}} \bar{\psi}_{n,\mathbf{p}} \left[i\tilde{\gamma}_0 \omega_n + i\tilde{\gamma}_i p_i + m - \mu\tilde{\gamma}_0 \right] \psi_{n,\mathbf{p}} = \bar{\psi}_\lambda M_{\lambda\kappa} \psi_\kappa, \tag{3.64}$$

where

$$M_{\lambda\kappa} \equiv M_{(n,\mathbf{p}),(m,\mathbf{q})} = \left[i\tilde{\gamma}_0 \omega_n + i\tilde{\gamma} p_i + m - \mu\tilde{\gamma}_0 \right] \delta_{n,m} \delta_{\mathbf{p},\mathbf{q}}. \tag{3.65}$$

The partition function is then a Gaussian integral in Graßmann variables, easily evaluated using the standard formula:

$$Z = \int \mathscr{D}\bar{\psi}\mathscr{D}\psi \; e^{-\bar{\psi}_\lambda M_{\lambda\kappa} \psi_\kappa} = e^{\mathrm{tr}\log M}. \tag{3.66}$$

The matrix M is diagonal in frequency–momentum space, so that part of the trace is easy to evaluate:

$$\mathrm{tr}\log M = \sum_\lambda \mathrm{tr}\log M_{\lambda\lambda} = \sum_{n,\mathbf{p}} \mathrm{tr}\log\left[i\tilde{\gamma}_0 \omega_n + i\tilde{\gamma}_i p_i + m - \mu\tilde{\gamma}_0 \right]. \tag{3.67}$$

The remainder is an ordinary matrix trace, and by using the identity $\mathrm{tr}\,(\log M) = \log(\det M)$ we get

$$\begin{aligned} \mathrm{tr}\log M &= \sum_{n,\mathbf{p}} \log\det\left[i\tilde{\gamma}_0 \omega_n + i\tilde{\gamma}_i p_i + m - \mu\tilde{\gamma}_0 \right] \\ &= 2\sum_{n,\mathbf{p}} \left[\log(i\omega_n + \varepsilon_-) + \log(i\omega_n - \varepsilon_+) \right], \end{aligned} \tag{3.68}$$

where we have defined $\varepsilon_\pm \equiv E_\mathbf{p} \pm \mu = \sqrt{\mathbf{p}^2 + m^2} \pm \mu$.

Since we sum over both positive and negative values of n, the logarithmic terms can be symmetrised:

$$\begin{aligned} 2\sum_{n=-\infty}^{\infty} \log(i\omega_n + \varepsilon_-) &= \sum_{n=-\infty}^{\infty} \log(i\omega_n + \varepsilon_-) + \sum_{n=-\infty}^{\infty} \log(-i\omega_n + \varepsilon_-) \\ &= \sum_{n=-\infty}^{\infty} \log(\omega_n^2 + \varepsilon_-^2). \end{aligned} \tag{3.69}$$

Likewise, $2\sum_n \log(i\omega_n - \varepsilon_+) = \sum_n \log(\omega_n^2 + \varepsilon_+^2)$.

Taking the continuum limit, we find that the grand potential is

$$\Omega = -\frac{1}{\beta V}\log Z = -\sum\!\!\!\!\!\!\int_{\{P\}} \left[\log(\omega_n^2 + \varepsilon_-^2) + \log(\omega_n^2 + \varepsilon_+^2) \right], \tag{3.70}$$

where the curly brackets in the subscript to the sum-integral denote a summation over fermionic Matsubara frequencies. The sum-integral can be evaluated by the exact same method as in the bosonic case, using the residue theorem. We only have to replace the hyperbolic cotangent with the hyperbolic *tangent*, which has poles at $(n + \frac{1}{2})\pi$.

We then obtain

$$\Omega = -2\int \frac{\mathrm{d}^3 p}{(2\pi)^3} \left\{ E_\mathbf{p} + T\log\left[1 + e^{-\beta(E_\mathbf{p} - \mu)} \right] + T\log\left[1 + e^{-\beta(E_\mathbf{p} + \mu)} \right] \right\}. \tag{3.71}$$

Comparing this with the free energy of the scalar field, Eq. (3.53), we note four major differences:

- The thermal term has been split into two, differing only in the sign of the chemical potential. One is the contribution from the particles, the other is the contribution from the antiparticles.
- There is a plus sign inside the logarithms. This is because fermions are Fermi–Dirac distributed, as we will see below.
- There is an extra relative factor of 4, which is due to the four degrees of freedom inherent to spin-1/2 fermions.
- There is an overall minus sign, which means that the fermions give a *negative* contribution to the vacuum energy.

3.6. Conserved charges and chemical potentials

Since particles and antiparticles annihilate against each other we can express the number density of the fermions as a single quantity which is positive if there are more particles in the system and negative if there are more antiparticles. Using the formula (3.24) on Eq. (3.71), this *average number density* is

$$\langle n\rangle = -\frac{\partial\Omega}{\partial\mu} = 2\int\frac{\mathrm{d}^3p}{(2\pi)^3}\left\{\frac{1}{e^{\beta(E_{\mathbf{p}}-\mu)}+1} - \frac{1}{e^{\beta(E_{\mathbf{p}}+\mu)}+1}\right\}. \tag{3.72}$$

Not surprisingly, the Fermi–Dirac distribution appears in the integrand. If the particles are electrons, the electric charge density is $\langle\rho\rangle = -e\langle n\rangle$.

It is now clear how the density depends on the chemical potential: When $\mu > 0$ there are more particles than antiparticles in the system, and $\langle n\rangle > 0$. Likewise, when $\mu < 0$, then $\langle n\rangle < 0$. Finally, when $\mu = 0$, the numbers of particles and antiparticles are the same, and the average number density is zero. Thus, the chemical potential can be thought of as a "force" that induces a preference for a certain kind of particle, or charge, in the system.

Including multiple particle or charge types is simple. If we are dealing with a system that contains up and down quarks, for instance, ψ is written in flavour space as

$$\psi = \begin{pmatrix} u \\ d \end{pmatrix}, \tag{3.73}$$

and we still write the Lagrangian as in Eq. (3.58), only with separate chemical potentials for the different quark flavours:

$$\mu \to \begin{pmatrix} \mu_u & 0 \\ 0 & \mu_d \end{pmatrix}. \tag{3.74}$$

The number densities n_u and n_d are then simply given by

$$n_u = -\frac{\partial\Omega}{\partial\mu_u} \qquad \text{and} \qquad n_d = -\frac{\partial\Omega}{\partial\mu_d}. \tag{3.75}$$

The particle numbers n_u and n_d are examples of independently conserved charges. Another possibility is to use the total quark number density n_q and the isospin density n_I instead, which are related to n_u and n_d by

$$n_q = n_u + n_d \qquad \text{and} \qquad n_I = \frac{1}{2}(n_u - n_d). \tag{3.76}$$

Using Eq. (3.75) together with the corresponding relations for n_q and n_I, we find that the chemical potentials for quark number and isospin are, respectively

$$\mu_q = \frac{1}{2}(\mu_u + \mu_d), \tag{3.77}$$

$$\mu_I = \mu_u - \mu_d. \tag{3.78}$$

We can then write the Lagrangian compactly as

$$\mathscr{L} = \bar{\psi}(i\gamma^\mu \partial_\mu - m + \mu_q \gamma^0 + \mu_I I_3 \gamma^0)\psi, \tag{3.79}$$

where $I_3 = \frac{1}{2}\tau_3$ is the isospin operator. Again, the interpretation is clear: When μ_q is positive there are, on average, more particles in the system, and when it is negative there are more antiparticles. When μ_I is positive there are more up quarks than down quarks, and when it is negative there are more down quarks than up quarks.

4. High-temperature field theory

Due to asymptotic freedom the QCD coupling becomes small at high temperature. This indicates that we should be able to use perturbation theory to calculate physical quantities as series expansions in the coupling constant. However, a naïve attempt to do so will fail due to the appearance of infrared divergences in the theory.

These infrared divergences arise because of the masslessness of the gluons. According to special relativity the energy cost of creating a particle with mass m is $E = mc^2$. Creating a massless particle therefore requires zero energy, which means that one can in principle have infinitely many gluons at arbitrarily low energies. This is what causes the calculations to blow up. The same problem occurs in QED and in massless ϕ^4 theory.

At nonzero temperature, however, thermal fluctuations generate an effective mass for the massless particles in all of these theories, and the infrared divergences disappear. We say that the divergences are *screened* by the thermally generated mass. Somehow we need to take screening into account, and doing so requires a reorganisation of the perturbative series. Many methods have been developed for this purpose and in this chapter we will present several such techniques.

Due to the fact that massless ϕ^4 theory exhibits the same kind of infrared divergences as gauge theories, while at the same time being a much simpler model, it is very often used as a testbed for new computational techniques. In this chapter, and in Papers I and II, we use ϕ^4 theory exclusively, but we shall always keep in mind how the methods we present can be extended to more complicated theories.

In this chapter we therefore start by introducing ϕ^4 theory and its Feynman rules. Thereafter, in Sec. 4.2 we show how infrared divergences arise even in simple calculations, and how perturbation theory needs to be organised in order to take screening into account. In Secs. 4.3 and 4.4 we discuss *optimised perturbation theory* and *dimensional reduction*, respectively, which are different classes of methods for performing this reorganisation.

4.1. Feynman diagrams at finite temperature

In Secs. 3.4 and 3.5 we calculated the free energy of non-interacting scalar and Dirac field theories, respectively, at finite temperature. Closed-form solutions to path integrals such as Eqs. (3.36) and (3.66) are possible to obtain because the Lagrangians are only quadratic in the fields. If there are any higher-order

terms—interactions, that is—exact analytical solutions no longer exist. When the interactions are weak, the standard trick in quantum field theory is to use perturbation theory and expand observable quantities in orders of the coupling constants. Feynman diagrams have proved to be a very useful bookkeeping tool for perturbative calculations.

Thermal path integrals have more or less the same form as vacuum path integrals, with a few important differences. In vacuum field theory we usually work in a Minkowski spacetime, while in thermal field theory spacetime is Euclidean. Furthermore, at finite temperature we replace the integral over time with an integral over imaginary time that runs from 0 to β. We have seen that this is equivalent to replacing the integral over p_0 with a sum over Matsubara frequencies in the Fourier domain.

The Euclidean Lagrangian for ϕ^4 theory is given by

$$\mathscr{L} = \frac{1}{2}(\partial_\mu\phi)(\partial_\mu\phi) + \frac{1}{2}m^2\phi^2 + \frac{g^2}{24}\phi^4. \tag{4.1}$$

Using the rules above as a sort of "translation table" from vacuum to finite temperature field theory, we find that the Feynman rules for ϕ^4 theory are: To each internal line, assign a factor of

$$\text{——} = \frac{1}{P^2 + m^2}, \qquad P = (\omega_n, \mathbf{p}), \tag{4.2}$$

which is the thermal propagator for the nth Matsubara mode. P denotes a Euclidean momentum, so that $P^2 = \omega_n^2 + \mathbf{p}^2$. To each interaction vertex, assign a factor of

$$\times = -\frac{g^2}{24}. \tag{4.3}$$

Finally, for each internal momentum P, sum over Matsubara frequencies and integrate over spatial momenta:

$$\sum\!\!\!\!\!\!\int_P \cdots \tag{4.4}$$

As in vacuum field theory, one also needs to multiply each diagram by a symmetry factor that counts the possible permutations of the diagram.

Throughout this chapter we will use dimensional regularisation to calculate sum-integrals in $d+1$ dimensions and integrals over spatial momenta in d dimensions. For $d = 3-2\epsilon$ we then have that

$$\sum\!\!\!\!\!\!\int_P \equiv \left(\frac{e^\gamma\mu^2}{4\pi}\right)^\epsilon T\sum_n \int \frac{\mathrm{d}^{3-2\epsilon}p}{(2\pi)^{3-2\epsilon}}, \qquad P = (\omega_n, \mathbf{p}), \tag{4.5}$$

$$\int_{\mathbf{p}} \equiv \left(\frac{e^\gamma\mu^2}{4\pi}\right)^\epsilon \int \frac{\mathrm{d}^{3-2\epsilon}p}{(2\pi)^{3-2\epsilon}}, \tag{4.6}$$

where μ is an arbitrary renormalisation scale that ensures the correct dimensionality of the expression. The rest of the prefactor is chosen so that μ coincides with the renormalisation scale in the *minimal subtraction* ($\overline{\text{MS}}$) scheme. The constant γ is Euler's constant ($\gamma = 0.5772\ldots$).

4.2. The breakdown of naïve perturbation theory

In the Lagrangian (4.1) we now take the mass to be zero:

$$\mathscr{L} = \frac{1}{2}(\partial_\mu\phi)(\partial_\mu\phi) + \frac{g^2}{24}\phi^4. \tag{4.7}$$

The naïve approach to perturbation theory is to split the Lagrangian into a free part and an interaction part, i.e.

$$\mathscr{L}_{\text{free}} = \frac{1}{2}(\partial_\mu\phi)(\partial_\mu\phi), \tag{4.8}$$

$$\mathscr{L}_{\text{int.}} = \frac{g^2}{24}\phi^4, \tag{4.9}$$

and calculate radiative corrections in a loop expansion. At zero temperature the loop expansion is equivalent to a power series in g^2. This, however, turns out not to be the case at finite temperature.

To illustrate we will use this approach to calculate the self-energy $\Pi(P)$, where $P = (\omega_n, \mathbf{p})$ is the external momentum. The leading-order contribution comes from the one-loop diagram

$\Pi_1(P) =$ 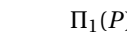 $= \frac{1}{2}g^2 \sum\!\!\!\!\!\!\int_Q \frac{1}{Q^2} = \frac{g^2T^2}{24}$ (4.10)

which is independent of P. In other words, the thermal fluctuations generate an effective mass of order gT.

We now move on to the two-loop diagrams and start with the double-bubble diagram which is also momentum independent:

$\Pi_{2a}(P) =$  $= -\frac{1}{4}g^4 \sum\!\!\!\!\!\!\int_{QR} \frac{1}{Q^2R^4}.$ (4.11)

The sum-integral is infrared divergent, indicating that naïve perturbation theory breaks down at finite temperature. The source of the divergence is the loop with two propagators, more specifically the $n = 0$ term in the Matsubara sum:

$$-\frac{1}{4}g^4 \sum\!\!\!\!\!\!\int_Q \frac{1}{Q^2} T\int_{\mathbf{r}} \frac{1}{\mathbf{r}^4}. \tag{4.12}$$

In practice, however, this infrared divergence is screened by the thermally generated mass. We can take this into account by using an effective propagator,

$$D(P) = \frac{1}{P^2 + m^2}, \tag{4.13}$$

where $m \sim gT$ since the leading order contribution to m^2 is given by Eq. (4.10). Using this propagator, the contribution from Eq. (4.12) would be

$$-\frac{1}{4}g^4 \sum\!\!\!\!\!\!\int_P \frac{1}{P^2} T\int_{\mathbf{q}} \frac{1}{(\mathbf{q}^2 + m^2)^2} = -\frac{1}{4}g^4\left(\frac{T^2}{12}\right)\left(\frac{T}{8\pi m}\right). \tag{4.14}$$

Thus, the double-bubble contributes at order g^3T^2 and not at order g^4T^3 as we would naïvely expect. At order g^3 we also get a contribution from the three-loop "Mickey Mouse" diagram,


$= \mathcal{O}(g^3).$ (4.15)

In fact, one can show that the order-g^3 correction to the thermal mass receives contributions from diagrams at *all* loop orders, and this is the fundamental reason why naïve perturbation theory breaks down. The diagram

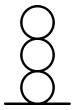
$= \mathcal{O}(g^4),$ (4.16)

however, along with an infinite number of other diagrams, contributes at subleading order. To get a consistent expansion in orders of the coupling one therefore has to resum a *subset* of diagrams from all loop orders. In order to see exactly which diagrams contribute at leading order, we can expand the one-loop self-energy obtained by using the effective propagator (4.13) as a series in m^2:

$$\sum\!\!\!\!\!\!\int_P \frac{1}{P^2+m^2} = \sum\!\!\!\!\!\!\int_P \frac{1}{P^2} + m^2 \sum\!\!\!\!\!\!\int_P \frac{1}{P^4} + m^4 \sum\!\!\!\!\!\!\int_P \frac{1}{P^6} + m^6 \sum\!\!\!\!\!\!\int_P \frac{1}{P^8} + \cdots \tag{4.17}$$

Since a factor of m^2 corresponds to a bubble and a factor of $1/P^2$ corresponds to a propagator, the above expansion yields the diagrams

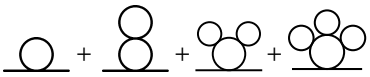
$+ \cdots,$ (4.18)

which are often referred to as *daisy diagrams*.

If we recalculate the one-loop contribution to the self-energy using the effective propagator, we obtain

$$\begin{aligned}
\Pi_1(P) &= \frac{1}{2}g^2 \sum\!\!\!\!\!\!\int_Q \frac{1}{Q^2+m^2} \\
&= \frac{1}{2}g^2 \left[T\int_{\mathbf{q}} \frac{1}{\mathbf{q}^2+m^2} + \sum\!\!\!\!\!\!\int_Q{}' \frac{1}{P^2} + \mathcal{O}(m^2) \right] \\
&= \frac{g^2T^2}{24}\left[1 - \frac{g\sqrt{6}}{4\pi} + \mathcal{O}(g^2) \right],
\end{aligned} \tag{4.19}$$

where the prime on the sum-integral denotes exclusion of the $n = 0$ mode. The term of order g^3 corresponds to the summation of daisy diagrams from all loop orders.

The one-loop diagram (4.10) is an example of a *hard thermal loop* (HTL); the only one in ϕ^4 theory. A hard thermal loop is a loop correction which is g^2T^2/P^2 times the corresponding tree-level amplitude, where P is an external momentum.

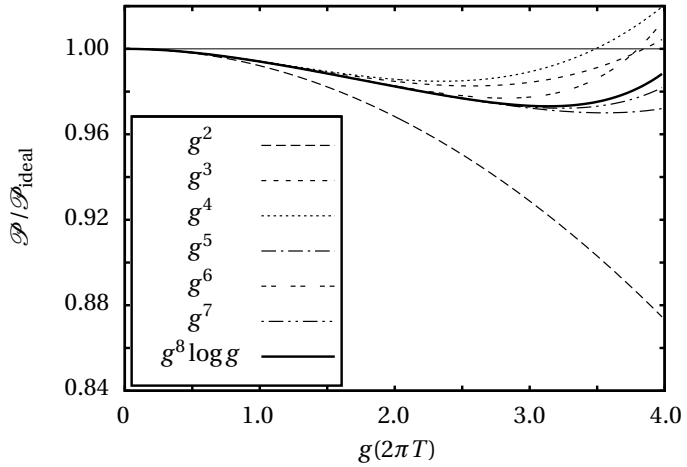

Figure 4.1.: Weak-coupling expansion of the pressure in massless ϕ^4 theory, normalised to the ideal gas pressure, $\pi^2 T^4/90$.

When P is soft the HTL is of order $g^0 = 1$ and is therefore as important as the tree-level contribution. When P is hard, on the other hand, the HTL is suppressed by g^2 and can be considered a perturbation.

In general, if we take the thermal mass to be equal to Eq. (4.10) and calculate physical quantities to some order in g using the effective propagator (4.13) we resum those diagrams, and *only* those diagrams, that contribute to this order. This is called the *weak-coupling expansion*. There are many methods to obtain the weak-coupling expansion, some of which will be presented in the following sections. Unfortunately, it turns out that this expansion converges rather poorly, in ϕ^4 theory as well as in gauge theories. As an example, in Fig. 4.1 we have plotted the pressure of ϕ^4 theory in the weak-coupling expansion for successive orders from g^2 through $g^8\log g$, as calculated in Paper II. Here we see that the successive corrections quickly become large as g increases, and furthermore that they oscillate back and forth as higher and higher orders are included. Similar behaviour is observed for the perturbative corrections in QCD [33]. It may therefore be desirable to resum other classes of diagrams as well, and the methods we present here are also used for this purpose.

4.3. Optimised perturbation theory

The simplest way of taking into account the screening of infrared divergences in the ϕ^4 Lagrangian is to decompose it into free and interacting parts as

$$\mathscr{L}_{\rm free} = \frac{1}{2}(\partial_\mu\phi)(\partial_\mu\phi) + \frac{1}{2}m^2\phi^2 \tag{4.20}$$

$$\mathscr{L}_{\rm int} = \frac{g^2}{24}\phi^4 - \frac{1}{2}m^2\phi^2. \tag{4.21}$$

In other words, we add a mass term to the free Lagrangian which acts as an infrared cutoff, while subtracting the same term from the interaction part of the Lagrangian. The latter is interpreted as a two-particle interaction and treated perturbatively on equal footing with the quartic term. One can then write physical quantities as a loop expansion in the massive theory. The self-energy, for instance, becomes

$\Pi(P)$ =

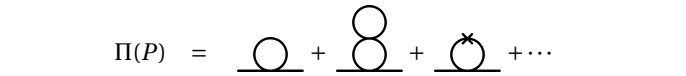

$$= \frac{1}{2}g^2 \sum\!\!\!\!\!\!\int_Q \frac{1}{Q^2+m^2} - \frac{1}{4}g^4 \sum\!\!\!\!\!\!\int_{QR} \frac{1}{Q^2+m^2}\frac{1}{(R^2+m^2)^2} + \frac{1}{2}g^2m^2 \sum\!\!\!\!\!\!\int_Q \frac{1}{(Q^2+m^2)^2} + \cdots \tag{4.22}$$

The cross in the third diagram is called a *mass insertion* and represents the two-particle interaction. Since $m^2 \sim g^2$ the mass insertion contributes at the same order as the ϕ^4 interaction, and it is therefore treated like a loop in the expansion.

If we set the mass parameter m^2 equal to $g^2T^2/24$, we can use this method to recover the weak-coupling expansion. There are, however, infinitely many other possible choices for m^2, and all correspond to different reorganisations of the perturbative series. In particular, it is common to determine m^2 from a variational principle like

$$\frac{\mathrm{d}\mathscr{F}}{\mathrm{d}m^2} = 0. \tag{4.23}$$

While it may seem inconsistent to organise the perturbative series differently from the strict weak-coupling expansion, we will show that the convergence properties of such expansions are often significantly better.

The reorganisation defined by Eqs. (4.20) and (4.21) is an example of *screened perturbation theory* (SPT), which will be discussed further in Sec. 4.3.2. SPT is part of a larger class of resummation schemes which we shall here refer to as *optimised perturbation theory* (OPT). Another commonly used term is *variational perturbation theory* (VPT), but we shall reserve this term for the case when the optimisation parameters (in this case only the mass m^2) are determined variationally.

To introduce and motivate the use of optimised perturbation theory and variational perturbation theory, we will now apply the methods to a simple integral. In particular, we will see that the convergence of the optimised expansion is significantly improved as compared to the naïve expansion.

4.3.1. A toy integral

Consider the simple integral

$$Z(\lambda) = \int_{-\infty}^{\infty} \mathrm{d}x\, e^{-\frac{1}{2}x^2 - \lambda x^4}. \tag{4.24}$$

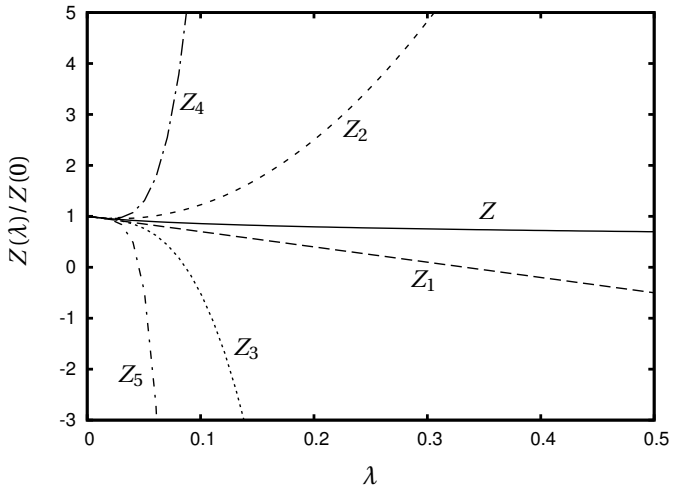

Figure 4.2.: The integral $Z(\lambda)$ evaluated numerically (solid line), together with successive perturbative approximations (dashed/dotted lines), all normalised to $Z(0) = \sqrt{2\pi}$.

As long as $\lambda > 0$, this integral is extremely well-behaved. It converges fast, and is therefore easy to calculate numerically. It can also be expressed analytically in terms of Bessel functions.

Now, suppose λ is a small parameter. It is then quite reasonable to believe that we can approximate this integral by a perturbative series—a series expansion in powers of λ:

$$Z(\lambda) = \int_{-\infty}^{\infty} \mathrm{d}x\, e^{-\frac{1}{2}x^2} \left(1 - \lambda x^4 + \frac{(\lambda x^4)^2}{2} + \cdots\right). \tag{4.25}$$

Let us use Z_N to denote the truncation of this series after N terms. That is,

$$Z_N(\lambda) = \sum_{n=0}^{N} \frac{(-\lambda)^n}{n!} \int_{-\infty}^{\infty} \mathrm{d}x\, x^{4n} e^{-\frac{1}{2}x^2} = \sum_{n=0}^{N} a_n \lambda^n, \tag{4.26}$$

where the expansion coefficients can be calculated analytically and are given by

$$a_n = \frac{(-1)^n}{n!} 2^{\frac{1}{2}+2n} \Gamma\left(\tfrac{1}{2} + 2n\right). \tag{4.27}$$

Naïvely, we expect that by including more and more terms in the expansion, the approximation to the original integral should become better and better. More precisely, we expect $Z_N(\lambda) \to Z(\lambda)$ as $N \to \infty$. As it turns out, this is not the case at all. In fact, the more terms we include, the *worse* the approximation becomes. This fact is clearly demonstrated in Fig. 4.2, in which the numerical evaluation of the original integral $Z(\lambda)$ is compared to the successive approximations $Z_0(\lambda), Z_1(\lambda), \ldots$

Closer inspection of Eq. (4.27) reveals the origin of this bad behaviour: The coefficients a_n grow factorially as n increases. This again means that the series $Z_\infty(\lambda)$ is an asymptotic series with zero radius of convergence.

Another thing worth noting is the fact that a_n is positive when n is even, but negative when n is odd. This, combined with the factorial growth of a_n, means that $Z_N(\lambda) > Z(\lambda)$ for even N, while $Z_N(\lambda) < Z(\lambda)$ for odd N, a feature which is also clearly evident in Fig. 4.2.

These two issues—the nonconvergence and oscillating nature of the successive perturbative approximations—are not specific to this particular problem. In fact, we saw in Fig. 4.1 that the same thing happens in the weak-coupling expansion of the pressure of ϕ^4 theory. To some extent this should not come as a surprise. After all, the partition function of ϕ^4 theory is just a generalisation of the integral (4.24).

In order to improve convergence, we will now perform a little trick. First, we add zero to the exponent. Specifically, we add an arbitrary term which is proportional to x^2, and then we subtract the same term again:

$$Z(\lambda) = \int_{-\infty}^{\infty} \mathrm{d}x\, e^{-\frac{1}{2}(1+\omega)x^2 + \frac{1}{2}\omega x^2 - \lambda x^4}. \tag{4.28}$$

Defining $r \equiv -\omega/2\lambda$, we can write this as

$$Z(\lambda) = \int_{-\infty}^{\infty} \mathrm{d}x\, e^{-\frac{1}{2}(1+\omega)x^2 - \lambda(r x^2 + x^4)}. \tag{4.29}$$

The trick is now that we expand this expression in λ, while pretending that r does *not* depend on λ. To avoid confusion with Eq. (4.26), we will label this expansion Z'_N. We then obtain

$$Z'_N(\lambda,\omega) = \sum_{n=0}^{N} \frac{(-\lambda)^n}{n!} \int_{-\infty}^{\infty} \mathrm{d}x\, (r x^2 + x^4)^n e^{-\frac{1}{2}(1+\omega)x^2}. \tag{4.30}$$

If we could include all orders of this expansion, we would recover the original integral, which is independent of the optimisation parameter ω. Since this is impossible, the result depends on the value of this parameter. Specifically, if we set $\omega = 0$ we recover Eq. (4.26), which corresponds to the "weak-coupling expansion" for this theory.

Of the infinitely many possible choices for ω, the *principle of minimal sensitivity* (PMS) provides us with a quite reasonable one: Since the value of the original integral is independent of ω, we should, at any given expansion order N, minimise the dependence of Z'_N on ω. That is, we should determine the value ω_N that satisfies the variational equation

$$\left.\frac{\mathrm{d}Z'_N}{\mathrm{d}\omega}\right|_{\omega=\omega_N} = 0. \tag{4.31}$$

The higher order terms in Eq. (4.30) quickly become very involved, so as an example of the procedure we will settle for calculating Z'_1:

$$Z'_1(\lambda,\omega) = \sqrt{2\pi}\left[\frac{1}{\sqrt{1+\omega}} + \frac{\omega}{2(1+\omega)^{3/2}} - \frac{3\lambda}{(1+\omega)^{5/2}}\right]. \tag{4.32}$$

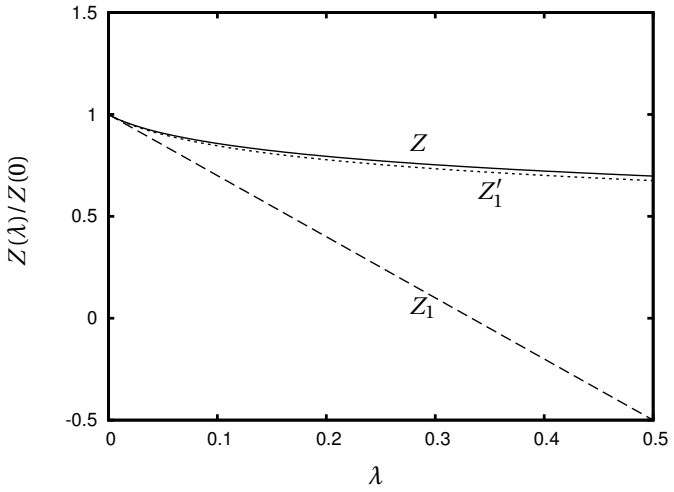

Figure 4.3.: The integral $Z(\lambda)$ evaluated numerically (solid line), the first-order perturbative approximation $Z_1(\lambda)$ (dashed line) and the first-order OPT approximation $Z_1'(\lambda)$ (dotted line), all normalised to $Z(0) = \sqrt{2\pi}$.

The PMS condition then becomes

$$0 = \left.\frac{\mathrm{d}Z_1'}{\mathrm{d}\omega}\right|_{\omega=\omega_1} = \frac{3\sqrt{2\pi}}{2}\left[-\frac{\omega_1}{2(1+\omega_1)^{5/2}} + \frac{5\lambda}{(1+\omega_1)^{7/2}}\right], \tag{4.33}$$

which, given that we must have $\omega > -1$ for the integral in Eq. (4.30) to converge, has the simple solution

$$\omega_1 = \omega_1(\lambda) = \frac{1}{2}(\sqrt{1+40\lambda} - 1). \tag{4.34}$$

In Fig. 4.3 we plot the first-order optimised expansion $Z_1'(\lambda) = Z_1'(\lambda, \omega = \omega_1(\lambda))$ and compare it to the nonperturbative numerical solution as well as the naïve first-order result $Z_1(\lambda)$, and it is evident that the optimised expansion is a much closer match. As an example, at $\lambda = 0.5$ the relative error in Z_1 is roughly 43%, while the error in Z_1' is only 3%. And it doesn't stop there. As is shown in Fig. 4.4, OPT also gives quite good results in the strong-coupling regime, where $\lambda > 0$ and ordinary perturbation theory is certain to fail. For $\lambda = 1000$, the relative error in Z_1' is still just 7%.

The example we have presented here is closely related to the problem of the anharmonic oscillator with potential

$$V(x) = \frac{\omega^2}{2}x^2 + \frac{g}{4}x^4. \tag{4.35}$$

The perturbative expansion of the ground state energy of this system diverges, because the successive corrections grow factorially in a manner similar to Eq.

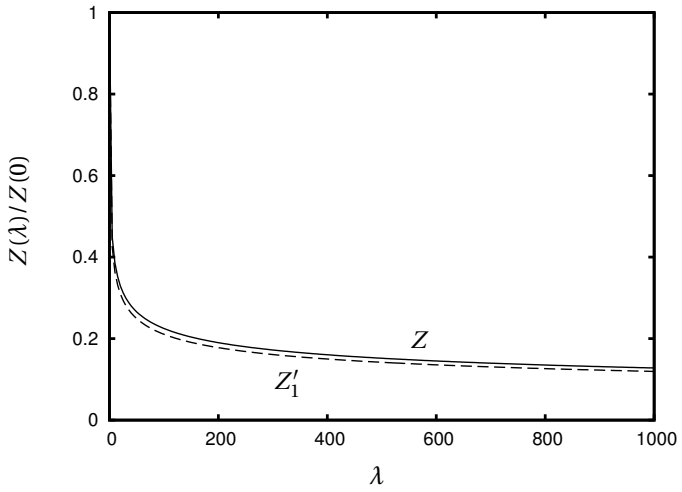

Figure 4.4.: The integral $Z(\lambda)$ evaluated numerically (solid line) and the first-order OPT approximation $Z_1'(\lambda)$ (dashed line), both normalised to $Z(0) = \sqrt{2\pi}$, for large values of λ

(4.27) [71, 72]. In Ref. [73] it was shown that variational perturbation theory can be applied to the problem, and that it yields a series of exponentially convergent approximations to the exact ground state energy.

4.3.2. Screened perturbation theory

Screened perturbation theory (SPT) is one example of optimised perturbation theory as applied to quantum field theories. It was introduced in the context of hot ϕ^4 theory in 1997 by Karsch, Patkós and Petreczky [74], who calculated the pressure at 2-loop level (and at 3 loops in the large-N limit). SPT was later used to calculate the pressure of ϕ^4 theory at the three-loop level [75, 76], and finally Paper I of this thesis pushed the calculation to four loops. A similar method has been used by Chiku and Hatsuda to study the O(N) linear sigma model with spontaneously broken symmetry [57].

We introduced the basics of SPT in the introduction to Sec. 4.3. We can generalise the method a bit by using different parameters m^2 and m_1^2 for the screening mass and the two-particle interaction, respectively:

$$\mathscr{L}_{\text{free}} = \frac{1}{2}(\partial_\mu\phi)(\partial_\mu\phi) + \frac{1}{2}m^2\phi^2, \tag{4.36}$$

$$\mathscr{L}_{\text{int}} = \frac{g^2}{24}\phi^4 - \frac{1}{2}m_1^2\phi^2. \tag{4.37}$$

This clearly separates the screening mass from the mass insertion and allows for better bookkeeping in intermediate calculations, and it also gives more flexibility

in the choice of a prescription for the mass. At the end of the day, m_1^2 is set equal to m^2 in all expressions.

Free energy

We can now write the expansion of the free energy to two loops as

$$\begin{aligned}\mathscr{F} &= \quad + \quad + \quad + \cdots \\ &= \frac{1}{2}\sum\!\!\!\!\!\!\int_P \log(P^2+m^2) + \frac{1}{8}g^2\left(\sum\!\!\!\!\!\!\int_P \frac{1}{P^2+m^2}\right)^2 \\ &\quad -\frac{1}{2}m_1^2\sum\!\!\!\!\!\!\int_P \frac{1}{P^2+m^2} + \cdots \end{aligned} \tag{4.38}$$

Massive sum-integrals such as these are unfortunately impossible to calculate analytically beyond three loops. To get an analytical expression we therefore have to make a second series expansion in orders of m/T, where m is taken to be of order gT [76]. For example, the one-loop sum-integral is expanded as

$$\begin{aligned}\sum\!\!\!\!\!\!\int_P \log(P^2+m^2) &= T\int_{\mathbf{p}} \log(\mathbf{p}^2+m^2) + \sum\!\!\!\!\!\!\int_P{}' \log(P^2+m^2) \\ &= T\int_{\mathbf{p}} \log(\mathbf{p}^2+m^2) + \sum\!\!\!\!\!\!\int_P{}' \log P^2 + m^2\sum\!\!\!\!\!\!\int_P{}' \frac{1}{P^2} \\ &\quad -\frac{1}{2}m^4\sum\!\!\!\!\!\!\int_P{}' \frac{1}{P^4} + \cdots \end{aligned} \tag{4.39}$$

In the $n=0$ term the momentum is not necessarily hard, so that term has to be singled out. The resulting integral, as well as the massless sum-integrals in the m/T expansion, can be evaluated analytically. In Paper I we show in detail the calculation of the free energy to four-loop order, where the m/T expansions are truncated at order g^7.

Mass prescriptions

The mass parameter m is in principle completely arbitrary, and if we were able to include all loop orders in calculations the result would be independent of m. In any given truncation, however, one has to select some prescription for the mass. Choosing $m^2 = g^2T^2/24$ we recover the weak-coupling expansion, and it is sensible to require that any mass prescription should reduce to this in the limit $g \to 0$.

One class of possibilities is to associate m with some physical mass in the system. The simplest choice is the Debye mass m_D defined by the location of the pole in the static propagator:

$$\mathbf{p}^2 + m^2 + \Pi(0,\mathbf{p}) = 0, \qquad \mathbf{p}^2 = -m_D^2. \tag{4.40}$$

The Debye mass is a well-defined quantity at any order of perturbation theory in scalar field theory and Abelian gauge theories. In non-Abelian gauge theories,

however, it is plagued by infrared divergences beyond leading order due to the magnetic mass problem [77]. Unfortunately, in scalar theories Eq. (4.40) has no solution for $g \gtrsim 2.6$ beyond one loop [75]. It would therefore be a poor choice for the purposes of Paper I.

Another class of prescriptions is based on the principle of minimal sensitivity: Since the results of SPT would be independent of m if we were able to calculate physical quantities to all orders, it is sensible to require that the result at any given finite order depends as little as possible on m. For the free energy this yields the variational equation

$$\frac{\mathrm{d}\mathscr{F}}{\mathrm{d}m^2} = 0. \tag{4.41}$$

The variational mass has the benefit of being well-defined at all orders in perturbation theory and can easily be generalised to gauge theories. In practice, however, it does not work very well beyond one loop because Eq. (4.41) only has solutions in the vicinity of $g = 0$ for a limited range of values for the renormalisation scale [75].

A prescription which works well for the scalar field theory is the *tadpole mass* prescription. The tadpole mass is calculated by taking the partial derivative of the free energy with respect to m^2 *before* setting $m_1 = m$:

$$m_t^2 = g^2 \left.\frac{\partial\mathscr{F}}{\partial m^2}\right|_{m_1=m}. \tag{4.42}$$

Thus,

$$\begin{aligned} m_t^2 &= -\frac{g^2}{\beta V Z}\frac{\partial}{\partial m^2}\int \mathscr{D}\phi\, e^{-\int_0^\beta \mathrm{d}\tau \int \mathrm{d}^3x\,[(\partial_\mu\phi)(\partial_\mu\phi)+m^2\phi^2+\mathscr{L}_\mathrm{int}]}\Big|_{m_1=m} \\ &= \frac{g^2}{\beta V}\int_0^\beta \mathrm{d}\tau \int \mathrm{d}^3x\,\frac{1}{Z}\int \mathscr{D}\phi\,\phi^2 e^{-S(m_1=m)} \\ &= g^2\langle\phi^2\rangle, \end{aligned} \tag{4.43}$$

where the expectation value $\langle\phi^2\rangle$ is the "tadpole". The tadpole mass is well-defined at all orders in scalar field theory, but the generalisation to gauge theories is problematic. The natural replacement of $\langle\phi^2\rangle$ would be $\langle A_\mu A_\mu\rangle$, which is a gauge variant quantity.

In Paper I we calculate the pressure to four loops using the three-loop tadpole mass prescription. The results clearly show that the convergence is improved as compared to the weak-coupling expansion.

Generalising to gauge theories

SPT cannot be generalised to gauge theories simply by adding and subtracting a local mass term in the Lagrangian, as this would violate gauge invariance. Instead one adds and subtracts a hard thermal loop improvement term [78, 79]. The free part of the Lagrangian includes the HTL self-energies while the remaining terms

are treated as perturbations. *HTL perturbation theory* (HTLPT) has been used to calculate the pressure of QED up to three loops [80], and recently calculations have been pushed to three loops in QCD as well [34, 81].

4.3.3. Other optimisation parameters

Here we have only discussed cases where the optimisation parameter is a single mass term. There are, however, many other possibilities. For instance, in the case of the linear sigma model with spontaneously broken O(N) symmetry, one could in principle introduce separate OPT terms for the sigma modes and the pions:

$$\mathscr{L} \to \mathscr{L} + \frac{1}{2}\chi_\sigma \sigma^2 + \frac{1}{2}\chi_\pi \pi_i \pi_i - \frac{1}{2}\chi_\sigma \sigma^2 - \frac{1}{2}\chi_\pi \pi_i \pi_i. \tag{4.44}$$

Furthermore, the optimisation terms do not necessarily have to be mass terms. In Ref. [58], OPT was generalised to optimise both the mass and the coupling of ϕ^4 theory at two loops.

Finally, we mention in passing the the *2PI formalism*, also referred to as the Φ-derivable approach. This does not fall under the category of optimised perturbation theory, but it is another example of a method where the parameters of the theory are determined based on a variational principle. Here, the exact propagator is treated as an infinite set of variational parameters [50]. The approach is based on the fact that the free energy can be written in terms of the two-particle irreducible (2PI) vacuum diagrams.

4.4. Dimensional reduction

Let ϕ be a massless bosonic field at finite temperature. In the Matsubara formalism it becomes periodic in imaginary time with a period equal to the inverse temperature, that is, $\phi(0,\mathbf{x}) = \phi(\beta,\mathbf{x})$. We can then write the field as a Fourier series in τ and a Fourier transform in $\mathbf{x}$:

$$\phi(\tau,\mathbf{x}) = \frac{1}{\sqrt{\beta}} \sum_n \int \frac{\mathrm{d}^d p}{(2\pi)^d}\, \varphi_n(\mathbf{p}) e^{i(\omega_n \tau + \mathbf{p}\cdot\mathbf{x})}. \tag{4.45}$$

Here, $\omega_n = 2n\pi T$ are the Matsubara frequencies and the free thermal propagator of the nth mode is

$$G_n(\mathbf{p}) = \frac{1}{\mathbf{p}^2 + \omega_n^2}. \tag{4.46}$$

Note that this has the same form as the vacuum propagator for a field with mass ω_n in d dimensions. In other words, one can view a thermal field theory in $d+1$ dimensions as a Euclidean vacuum field theory with infinitely many fields in d dimensions.

In this *dimensionally reduced* theory the nonzero Matsubara modes have masses on the scale of T, which we shall refer to as the *hard* scale. The φ_0 mode is massless, but we know that thermal fluctuations generate a screening mass on

the scale gT, called the *soft* scale. If the coupling g is small, the two scales are well separated; that is, $gT \ll T$. In this case one can construct an effective theory for the soft scale and treat it separately from the hard scale.

The coefficients of the effective theory are determined by calculating static correlators in the full theory and the effective theory and requiring that they be the same at long distance scales $R \gg 1/T$. This *matching* procedure is complicated by ultraviolet divergences. The ultraviolet divergences associated with the full 4-dimensional theory are removed by the standard renormalisation procedure. There are, however, new divergences in the effective theory, and these are taken care of by introducing an ultraviolet cutoff Λ which then marks the upper limit of validity for the effective theory. Λ is thus taken to be an intermediate momentum scale separating the soft scale from the hard, and is called the *factorisation* scale. Naturally, integrals in the effective theory will depend on the cutoff. The coefficients of the effective theory therefore also depend on Λ in such a way that it cancels out of all physical quantities.

We will now demonstrate the procedure for massless ϕ^4 theory, as defined by Eq. (4.1). To keep the discussion clear and simple, we shall only perform calculations to the fourth order in the coupling. The expansion has been carried out to order $g^8 \log g$ in Paper II. At the end, we will mention briefly how dimensional reduction can be applied to gauge theories such as QED and QCD. For an in-depth review of the method as applied to both scalar and gauge theories we refer to Ref. [82], on which the present discussion is based.

4.4.1. Effective theory

At the soft momentum scale, the nonzero Matsubara modes decouple. The three-dimensional effective theory obtained by dimensional reduction thus describes a single scalar field which, up to normalisation, can be associated with the zeroth Matsubara mode. Fourier expanding only in imaginary time,

$$\phi(\tau, \mathbf{x}) = \frac{1}{\sqrt{\beta}} \sum_n \varphi_n(\mathbf{x}) e^{i\omega_n \tau}, \tag{4.47}$$

we make the identification

$$\varphi(\mathbf{x}) \sim \varphi_0(\mathbf{x}) = \sqrt{T} \int_0^\beta \mathrm{d}\tau \, \phi(\tau, \mathbf{x}). \tag{4.48}$$

The original theory has a three-dimensional rotational symmetry in $\mathbf{x}$ as well as the symmetry $\phi \to -\phi$. The most general Lagrangian which exhibits these symmetries can be written

$$\mathscr{L}_{\mathrm{eff}} = \frac{1}{2}(\nabla\varphi)^2 + \frac{1}{2}m^2\varphi^2 + \frac{\lambda}{24}\varphi^4 + \cdots, \tag{4.49}$$

where the ellipsis denotes terms which are of higher order in φ^2 and $(\nabla\varphi)^2$. These will be ignored because they do not contribute at the order g^4. The φ^6 operator,

for instance, first contributes at order g^8. Note that this operator is not taken into account in Paper II either, because we only perform the formal expansion to order g^7. The additional contributions of order $g^8 \log g$ are calculated using renormalisation group equations.

One term which was omitted in Eq. (4.49), but which also respects the symmetries of the theory, is the unit operator. We include it now and denote its coefficient by f. The partition function is then

$$Z = \int \mathscr{D}\varphi \, e^{-\int \mathrm{d}^3x \, (f + \mathscr{L}_{\mathrm{eff}})} = e^{-Vf} Z_{\mathrm{eff}}, \tag{4.50}$$

where

$$Z_{\mathrm{eff}} \equiv \int \mathscr{D}\varphi \, e^{-\int \mathrm{d}^3x \, \mathscr{L}_{\mathrm{eff}}} \tag{4.51}$$

is the partition function of the effective theory. If we equate this with the partition function of the full theory,

$$Z = \int \mathscr{D}\phi \, e^{-\int_0^\beta \mathrm{d}\tau \int \mathrm{d}^3x \, \mathscr{L}}, \tag{4.52}$$

and take the logarithm on both sides, we find that

$$\log Z = -Vf + \log Z_{\mathrm{eff}}. \tag{4.53}$$

In other words, f is the contribution to the free energy from the hard scale.

4.4.2. Matching to the full theory

The factorisation scale Λ marks the upper limit of validity for the effective theory and thus acts as an ultraviolet cutoff. Physics at the hard scale gets encoded in f, as we have just seen, but also in m^2, λ and φ. The coefficients and the field therefore all depend on g, T and Λ, but in such a way that physical quantities do *not* depend on Λ, which is just an arbitrary intermediate scale. We will now discuss the matching procedure.

At the factorisation scale we can, assuming $\Lambda \gg gT$, treat the mass term in the effective theory as a perturbation. We thus decompose the Lagrangian according to

$$\mathscr{L}_{\mathrm{eff}}^{\mathrm{free}} = \frac{1}{2}(\nabla\varphi)^2, \tag{4.54}$$

$$\mathscr{L}_{\mathrm{eff}}^{\mathrm{int}} = \frac{1}{2}m^2\varphi^2 + \frac{\lambda}{24}\varphi^4 + \cdots \tag{4.55}$$

The matching procedure is carried out using *strict perturbation theory* which is identical to the naïve perturbation theory from Sec. 4.2. As we have seen, the expansion is plagued by infrared divergences which are screened by the generation of a soft thermal mass. Normally one has to take the screening into account by resumming an infinite set of higher-order diagrams. It is not necessary to do so

here, however, because the coefficients of the effective theory encode the physics at the hard scale which is insensitive to physics on the scale gT. If we make the same incorrect assumptions about screening in the effective theory, the infrared divergences will be the same in the two theories, and they will cancel in the matching procedure [83]. In the following we will use the symbol $\approxeq$ to denote an equality which only holds in strict perturbation theory.

Coefficient of the unit operator

We start by determining the coefficient of the unit operator, f. Eq. (4.53) can be written as

$$\mathscr{F} = \mathscr{F}_{\rm hard} + \mathscr{F}_{\rm soft}, \tag{4.56}$$

where $\mathscr{F}_{\rm hard} = Tf$ and $\mathscr{F}_{\rm soft} = -TV^{-1}\log Z_{\rm eff}$. In strict perturbation theory the free energy of the full theory is given by the expansion

$$\mathscr{F} \approxeq \mathscr{F}_0 + \mathscr{F}_1 + \mathscr{F}_{2a} + \mathscr{F}_{2b} + \frac{\Delta g^2}{g^2}\mathscr{F}_1 + \mathscr{O}(g^6), \tag{4.57}$$

where $\mathscr{F}_n$ denotes a term of order g^{2n}. Δg^2 is the coupling counterterm, calculated up to order g^{10} in Ref. [84]. The various terms are

$\mathscr{F}_0$ =  $= \frac{1}{2}\sum\!\!\!\!\!\!\int_P \log P^2,$ (4.58)

$\mathscr{F}_1$ =  $= \frac{1}{8}g^2\left(\sum\!\!\!\!\!\!\int_P \frac{1}{P^2}\right)^2,$ (4.59)

$\mathscr{F}_{2a}$ =  $= -\frac{1}{16}g^4\left(\sum\!\!\!\!\!\!\int_P \frac{1}{P^2}\right)^2 \sum\!\!\!\!\!\!\int_Q \frac{1}{Q^4},$ (4.60)

$\mathscr{F}_{2b}$ =  $= -\frac{1}{48}g^4 \sum\!\!\!\!\!\!\int_{PQR} \frac{1}{P^2Q^2R^2(P+Q+R)^2}.$ (4.61)

We evaluate the sum-integrals using dimensional regularisation in $3-2\epsilon$ dimensions, taking the momentum scale introduced by the regularisation to be the factorisation scale Λ. We then obtain

$$\begin{aligned}\mathscr{F} \approxeq -\frac{\pi^2 T^4}{90}\Bigg\{1 - \frac{5}{4}\alpha + \frac{15}{4}\alpha^2\Bigg[\log\frac{\Lambda}{4\pi T} + \frac{1}{3}\gamma + \frac{31}{45} \\ + \frac{4}{3}\frac{\zeta'(-1)}{\zeta(-1)} - \frac{2}{3}\frac{\zeta'(-3)}{\zeta(-3)}\Bigg]\Bigg\} + \mathscr{O}(\alpha^3),\end{aligned} \tag{4.62}$$

where

$$\alpha = \alpha(\Lambda) \equiv \frac{g^2(\Lambda)}{16\pi^2}. \tag{4.63}$$

The coupling satisfies the evolution equation [84]

$$\mu\frac{\mathrm{d}\alpha(\mu)}{\mathrm{d}\mu} = 3\alpha^2 + \mathscr{O}(\alpha^3), \tag{4.64}$$

which means that we can change the renormalisation scale from Λ to some arbitrary momentum scale μ by the substitution

$$\alpha(\Lambda) = \alpha(\mu)\left[1 - 3\alpha(\mu)\log\frac{\mu}{\Lambda}\right] + \mathcal{O}(\alpha^3). \tag{4.65}$$

Applying this to Eq. (4.62), we find that the term proportional to $\log\Lambda$ is exactly cancelled, meaning that $\mathscr{F}$ is independent of Λ to this order.

Since we are treating the mass parameter m^2 as a perturbation, a strict expansion of $\mathscr{F}_{\text{soft}}$ yields

$$\begin{aligned}\mathscr{F}_{\text{soft}} \quad \approxeq \quad & \frac{1}{2}\int_{\mathbf{p}} \log \mathbf{p}^2 + \frac{1}{8}\lambda\left(\int_{\mathbf{p}}\frac{1}{\mathbf{p}^2}\right)^2 - \frac{1}{16}\lambda^2\left(\int_{\mathbf{p}}\frac{1}{\mathbf{p}^2}\right)^2\int_{\mathbf{q}}\frac{1}{\mathbf{q}^4} \\ & -\frac{1}{48}\lambda^2\int_{\mathbf{pqr}}\frac{1}{\mathbf{p}^2\mathbf{q}^2\mathbf{r}^2(\mathbf{p}+\mathbf{q}+\mathbf{r})^2} + \mathcal{O}(\lambda^3).\end{aligned} \tag{4.66}$$

Note that there is no mass scale in either of these integrals, which means that they all vanish in dimensional regularisation. Thus $\mathscr{F}_{\text{soft}} \approxeq 0$, and we find that

$$\begin{aligned}f(\mu) \quad = \quad & -\frac{\pi^2 T^3}{90}\left\{1 - \frac{5}{4}\alpha(\mu) + \frac{15}{4}\alpha^2(\mu)\left[\log\frac{\mu}{4\pi T} + \frac{1}{3}\gamma + \frac{31}{45}\right.\right. \\ & \left.\left. + \frac{4}{3}\frac{\zeta'(-1)}{\zeta(-1)} - \frac{2}{3}\frac{\zeta'(-3)}{\zeta(-3)}\right]\right\}.\end{aligned} \tag{4.67}$$

At this order in α the coefficient f does not depend on the cutoff Λ of the effective theory, nor does it have any divergences. At order α^3, however, this is no longer the case. As shown in Paper II, f depends on Λ at this order and furthermore there is a pole in ϵ. The latter is cancelled by the inclusion of a vacuum counterterm δf in the effective theory[1].

Mass parameter

The easiest way to determine the mass parameter m^2 is to calculate the Debye mass in the full theory and in the effective theory and demand that they be the same. In the full theory the Debye mass is defined by the pole of the static propagator, that is, by

$$\mathbf{p}^2 + \Pi(0,\mathbf{p}) = 0, \qquad \mathbf{p}^2 = -m_D^2. \tag{4.68}$$

Here $\Pi(\omega_n,\mathbf{p})$ is the self-energy, naïvely expanded as

$$\Pi(P) \approxeq \Pi_1(P) + \Pi_{2a}(P) + \Pi_{2b}(P) + \frac{\Delta g^2}{g^2}\Pi_1(P) + \mathcal{O}(g^6), \tag{4.69}$$

[1] Here we have used δ to denote a counterterm in the three-dimensional theory, while Δ denotes a counterterm in the full theory.

where the various diagrams are

$$\Pi_1(P) \quad = \quad \text{  } \quad = \quad \frac{1}{2}g^2 \sum\!\!\!\!\!\!\int_Q \frac{1}{Q^2}, \tag{4.70}$$

$$\Pi_{2a}(P) \quad = \quad \text{  } \quad = \quad -\frac{1}{4}g^4 \sum\!\!\!\!\!\!\int_{QR} \frac{1}{Q^2R^4}, \tag{4.71}$$

$$\Pi_{2b}(P) \quad = \quad \text{  } \quad = \quad -\frac{1}{6}g^4 \sum\!\!\!\!\!\!\int_{QR} \frac{1}{Q^2R^2(P+Q+R)^2}. \tag{4.72}$$

Thus, the leading contribution to m_D is of order gT, and therefore $\mathbf{p}$ is a soft momentum. This allows us to greatly simplify the calculation of Π_{2b} by expanding the sum-integral around $\mathbf{p} = 0$,

$$\begin{aligned} \sum\!\!\!\!\!\!\int_{QR} \frac{1}{Q^2R^2(P+Q+R)^2} \quad &= \quad \sum\!\!\!\!\!\!\int_{QR} \frac{1}{Q^2R^2(Q+R)^2} \\ &\quad + \mathbf{p}^2 \sum\!\!\!\!\!\!\int_{QR} \frac{4\mathbf{q}^2/d - Q^2}{Q^6R^2(Q+R)^2} + \mathcal{O}(\mathbf{p}^4), \end{aligned} \tag{4.73}$$

thus making all the sum-integrals independent of the external momentum.

In the effective theory the Debye mass is similarly given by

$$\mathbf{p}^2 + \delta m^2 + \Pi_{\text{eff}}(\mathbf{p}) = 0, \qquad \mathbf{p}^2 = -m_D^2, \tag{4.74}$$

where we have included a mass counterterm to absorb poles which remain uncancelled in the full theory. Since the mass is treated as a perturbation, the self-energy can be expanded as

$$\begin{aligned} \Pi_{\text{eff}} \quad &\approx \quad m^2 + \frac{1}{2}\lambda \int_{\mathbf{q}} \frac{1}{\mathbf{q}^2} - \frac{1}{4}\lambda^2 \int_{\mathbf{qr}} \frac{1}{\mathbf{q}^2\mathbf{r}^4} - \frac{1}{6}\lambda^2 \int_{\mathbf{qr}} \frac{1}{\mathbf{q}^2\mathbf{r}^2(\mathbf{p}+\mathbf{q}+\mathbf{r})^2} \\ &\quad + \frac{1}{2}\lambda m^2 \int_{\mathbf{q}} \frac{1}{\mathbf{q}^2} + \mathcal{O}(\lambda^3). \end{aligned} \tag{4.75}$$

There is no mass scale in the first two integrals, nor in the last, and so these vanish in dimensional regularisation. The third integral contains the scale $\mathbf{p}$, but for the reasons stated above we can expand this integral around $\mathbf{p} = 0$ as well, causing it, too, to vanish in dimensional regularisation. Thus, we find that $\Pi_{\text{eff}}(\mathbf{p}) = m^2$ when $\mathbf{p}^2 = -m_D^2$. Combining Eqs. (4.68) and (4.74), we obtain

$$m^2 + \delta m^2 = \Pi(0, \mathbf{p}^2 = -m^2 - \delta m^2). \tag{4.76}$$

The details of the calculation can be found in Paper II, and the final result to order α^2 is:

$$\begin{aligned} m^2(\mu) \quad &= \quad \frac{2\pi^2T^2}{3}\alpha(\mu) \\ &\quad \times \left\{1 + \alpha^2(\mu)\left[4\log\frac{\Lambda}{4\pi T} - 3\log\frac{\mu}{4\pi T} + 2 - \gamma + 2\frac{\zeta'(-1)}{\zeta(-1)}\right]\right\}, \end{aligned} \tag{4.77}$$

$$\delta m^2(\mu) \quad = \quad \frac{2\pi^2T^2}{3\epsilon}\alpha^2(\mu). \tag{4.78}$$

Here we have also used the evolution equation (4.64) to isolate the contribution to m^2 from the cutoff Λ.

Coupling

In Paper II we use the effective theory to calculate the contribution from the soft scale to the pressure. If we perform this calculation to order g^4, we only need the coupling λ to order g^2, that is, the tree-level contribution. We obtain this by comparing the action of the full theory,

$$S = \int_0^\beta \mathrm{d}\tau \int \mathrm{d}^3x \, \mathscr{L}, \tag{4.79}$$

to the action of the effective theory,

$$S_{\mathrm{eff}} = \int \mathrm{d}^3x \, \mathscr{L}_{\mathrm{eff}}. \tag{4.80}$$

At the factorisation scale the hard modes decouple, and based on Eq. (4.47) we can therefore make the replacement $\phi(\tau,\mathbf{x}) \to \sqrt{T}\varphi(\mathbf{x})$ in Eq. (4.79). Comparing with Eq. (4.80) we find that

$$\lambda = g^2 T + \mathscr{O}(g^4). \tag{4.81}$$

In Paper II, however, where the pressure is calculated to $\mathscr{O}(g^7)$ in perturbation theory, we need the coupling to order g^4. Then it becomes necessary to include the following one-loop correction diagram:

Taking the external momenta to be soft, we then obtain

$$\lambda = T\left(g^2 - \frac{3}{2}g^4 \sum\!\!\!\!\!\!\int_P \frac{1}{P^4} + \Delta g^2\right) + \mathscr{O}(g^6). \tag{4.82}$$

When applying the evolution equation (4.64) we find that λ is independent of the factorisation scale Λ. Actually, since the coupling does not need renormalisation in three-dimensional ϕ^4 theory [85] this is true at all orders, and we can write

$$\Lambda \frac{\mathrm{d}\lambda}{\mathrm{d}\Lambda} = 0. \tag{4.83}$$

4.4.3. Calculations in the effective theory

Having determined the parameters of the effective theory, we can now use it to calculate contributions to physical quantities from the soft scale using perturbation theory. At this scale we need to take screening into account, that is, we can no longer treat m^2 as a perturbation. We thus decompose the Lagrangian as

$$\mathscr{L}_{\mathrm{eff}}^{\mathrm{free}} = \frac{1}{2}(\nabla\varphi)^2 + \frac{1}{2}m^2\varphi^2, \tag{4.84}$$

$$\mathscr{L}_{\mathrm{eff}}^{\mathrm{free}} = \frac{\lambda}{24}\varphi^4 + \cdots \tag{4.85}$$

The soft contribution to the pressure, for instance, can then be expanded to three loops as

$$
\begin{aligned}
\mathscr{F}_{\text{soft}} &= \quad + \quad + \quad + \quad + \cdots \\
&= \frac{1}{2}\int_{\mathbf{p}} \log(\mathbf{p}^2+m^2) - \frac{1}{2}\delta m^2 \int_{\mathbf{p}} \frac{1}{\mathbf{p}^2+m^2} + \frac{1}{8}\lambda\left(\int_{\mathbf{p}} \frac{1}{\mathbf{p}^2+m^2}\right)^2 \\
&\quad -\frac{1}{16}\lambda^2\left(\int_{\mathbf{p}} \frac{1}{\mathbf{p}^2+m^2}\right)^2 \int_{\mathbf{q}} \frac{1}{(\mathbf{q}^2+m^2)^2} \\
&\quad -\frac{1}{48}\lambda^2 \int_{\mathbf{pqr}} \frac{1}{\mathbf{p}^2+m^2}\frac{1}{\mathbf{q}^2+m^2}\frac{1}{\mathbf{r}^2+m^2}\frac{1}{(\mathbf{p}+\mathbf{q}+\mathbf{r})^2+m^2} \\
&\quad +\mathscr{O}(\lambda^3).
\end{aligned}
\tag{4.86}
$$

Here, the cross in the second diagram denotes the insertion of the counterterm δm^2. The total free energy, including both soft and hard contributions, is then given by

$$
\mathscr{F} = Tf + \mathscr{F}_{\text{soft}}. \tag{4.87}
$$

In Paper II we give a detailed account of how to calculate the pressure $\mathscr{P} = -\mathscr{F}$ to order g^7 using the effective theory. The advantage to using dimensional reduction as opposed to resummed perturbation theory, which is the topic of Sec. 4.3, is that the method is more economical and efficient. There is a clear separation between the two energy scales, and furthermore the three-dimensional integrals appearing in expansions such as Eq. (4.86) are easier to deal with than the corresponding 3+1-dimensional sum-integrals.

4.4.4. Gauge theories

Dimensional reduction is a very useful tool when applied to gauge theories as well. A detailed discussion can be found in Ref. [82], here we only mention a few important points.

QED and QCD contain both fermionic and bosonic degrees of freedom. The Matsubara frequencies of fermions are given by $\omega_n = (2n+1)\pi T$, which means that there are no soft fermionic modes. The degrees of freedom in the dimensionally reduced theory must therefore be associated with the zeroth Matsubara mode of the gauge fields.

In analogy with ϕ^4 theory there are two energy scales in QED at finite temperature: T and eT, where e is the coupling. These scales are associated with the typical momentum of a particle in the plasma, and the screening of static electric fields, respectively. The fields of the effective Lagrangian can be identified with the zero-frequency modes of the gauge field A_μ. In particular, the timelike component A_0 behaves like a real massive interacting field. The effective Lagrangian for the scale eT then has a three-dimensional rotational symmetry and a discrete symmetry $A_0 \to -A_0$, and it is invariant under gauge transformations of the spatial components A_i:

$$
\mathscr{L}_{\text{eff}} = \frac{1}{2}(\nabla A_0)^2 + \frac{1}{2}m_E^2 A_0^2 + \lambda_E A_0^4 + \frac{1}{4}F_{ij}F_{ij} + \cdots \tag{4.88}
$$

Using this approach, the free energy of QED has been calculated through order e^5 [86].

In QCD, and in non-Abelian gauge theories in general, there are actually *three* energy scales. These are the scale T which is the typical momentum of a particle in the plasma, the scale $g_s T$ which is associated with the screening of colour electric fields and the scale $g_s^2 T$ which is associated with the screening of colour magnetic fields. The hierarchy of momentum scales suggests that one constructs a sequence of *two* effective field theories that take care of the scales $g_s T$ and $g_s^2 T$. This strategy was first proposed by Braaten and Nieto [30, 31] who called the effective theories *electrostatic QCD* (EQCD) and *magnetostatic QCD* (MQCD), respectively. Dimensional reduction has been used to calculate the free energy of QCD up to order $g^6 \log g$ [33]. Interestingly, this is the highest order attainable in analytic calculations. Beyond this point perturbation theory breaks down due to nonperturbative contributions from the chromomagnetic scale.

5. The NJL model at finite temperature and density

NJL-type models are perhaps the most commonly used models for QCD at finite density. These are simplified models in which the strong interaction, mediated in QCD by the exchange of gluons, is approximated by a local four-point interaction between quarks. Gluons are completely absent from the theory. As such, NJL models have several shortcomings, most importantly the lack of confinement. At high temperatures confinement becomes less important, but any realistic description of quark–gluon plasma should take into account gluon degrees of freedom. At high *density*, on the other hand, it is expected that both confinement and gluon degrees of freedom play a minor role, and the use of NJL models seems justified [87]. Furthermore, the models share QCD's chiral symmetry breaking pattern, and are often used in studies of the chiral phase transition. The original NJL model only allows for two quark flavours and simple four-particle interactions. It has, however, been extended to more quark flavours and a plethora of interaction types, and a very rich phase diagram has emerged. A thorough NJL-model analysis of dense quark matter is provided in Ref. [87].

In Papers III and IV we use the two-flavour NJL model to study various aspects of the phase diagram of QCD. This chapter is meant to complement the discussion in these papers. First, we will review the specifics involved in the making of a phase diagram. In particular, we properly define terms like "phase" and "phase transition". Thereafter, in Sec. 5.2, we introduce the two-flavour NJL model that we will use in our calculations. Secs. 5.3 and 5.4 provide the theoretical background for the results of Papers III and IV, respectively.

5.1. Phases

Until now we have used the term "phase" rather offhand, without really defining it. A general, but not very precise, definition is "a state of matter which has a certain set of physical properties". This definition assumes that there is at least one other phase and that the physical properties of that phase are distinguishable from those of the first.

We need something a bit more precise. In particular, we need to define what we mean by "physical properties", and we need a way to distinguish between the various phases. To that end we introduce the notion of an *order parameter*.

5.1.1. Order parameters

An order parameter is normally a quantity which is zero in one phase and nonzero in the other. For the liquid–gas phase transition, for instance, the order parameter is the difference in density between the phases,

$$\Delta\rho = \rho - \rho_{\text{liquid}}. \tag{5.1}$$

Here, ρ is the density of the system and ρ_{liquid} is the density of the system in the liquid phase. Thus, when $\Delta\rho \simeq 0$ we know the system is in the liquid phase, and when $\Delta\rho > 0$ it is in the gas phase.

A better example is perhaps that of a ferromagnet. If we heat a ferromagnet, it will at some point lose its magnetisation because the electron spins are randomised due to thermal fluctuations. The temperature at which this happens is called the critical temperature[1], or T_c. The order parameter for this transition is the net magnetisation, $\mathbf{M}$. When $T < T_c$, the system is in the ferromagnetic phase, $\mathbf{M} \neq \mathbf{0}$, while for temperatures above T_c the net magnetisation is zero, $\mathbf{M} = \mathbf{0}$.

This example nicely illustrates a common connection between order parameters and symmetry. If there is no external magnetic field, the energy of a ferromagnet does not change when the magnet is rotated. In other words, the system has rotational symmetry. This symmetry is, however, spontaneously broken in the ferromagnetic phase, because the magnetisation necessarily points in a certain direction.

Inspired by this example, we shall define an order parameter as *a parameter which, when nonzero, spontaneously breaks one or more global symmetries*. This also allows us to define a phase more precisely as a set of states that have a certain symmetry.

Without explicitly stating as much, this is the definition we have been using in our discussions of the QCD phase diagram. For example, the order parameter for spontaneous chiral symmetry breaking is the chiral condensate, $\langle\bar{\psi}\psi\rangle$. It is nonzero in the hadronic phase, and vanishes in the quark–gluon plasma phase.

5.1.2. Phase transitions

The point at which an order parameter vanishes is called a phase transition. Generally, we distinguish between two types: *first-order* and *second-order* phase transitions.

In a first-order phase transition the order parameter is discontinuous, i.e. it makes a "jump" from some finite nonzero value to zero. This is shown schematically in Fig. 5.1a. Well-known examples of first-order phase transitions include the solid–liquid and liquid–gas transitions of water.

In a second-order phase transition, on the other hand, the order parameter goes continuously to zero but has a kink at the point where it vanishes. In other

[1] The critical temperature of the ferromagnetic phase transition is also called the *Curie* temperature.

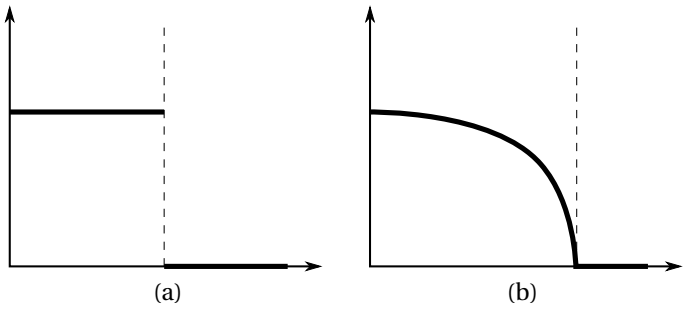

Figure 5.1.: The behaviour of the order parameter at (a) a first-order phase transition and (b) a second-order phase transition.

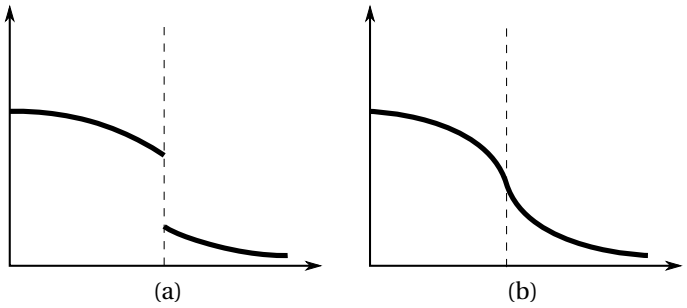

Figure 5.2.: The behaviour of the order parameter at (a) a first-order phase transition and (b) a crossover, when the symmetry is explicitly broken.

words, the first derivative of the order parameter is discontinuous. This is shown in Fig. 5.1b. The most famous example of a second-order phase transition is perhaps that of the ferromagnet.

If the symmetry is explicitly broken, the order parameter will never vanish entirely. Rather, it will approach zero asymptotically. If the symmetry is broken softly, the transition may still be discontinuous, and in this case it is still often referred to as a first-order phase transition. This is shown in Fig. 5.2a. If the transition is smooth, as in Fig. 5.2b, it is called a *crossover*. When we speak of the critical temperature in this case, we usually mean the point at which the transition happens most rapidly, i.e. the inflection point.

5.1.3. Equilibrium

When speaking of a phase, we are of course interested in the state of a system when it is in a stable equilibrium. A system is in a stable equilibrium state when it is not possible to gain energy by "pushing" the system into some other state, i.e. when the free energy is minimal. In other words, to determine the phase at a given point in the phase diagram, we need to find the values of the order

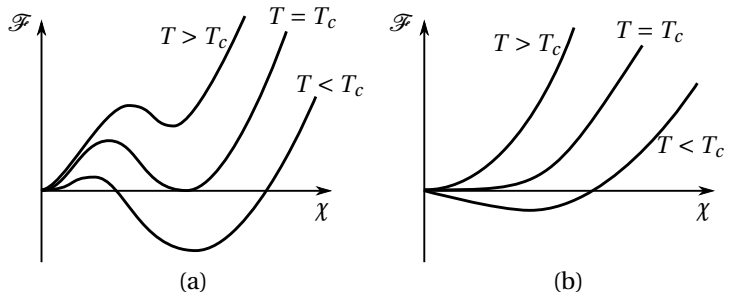

Figure 5.3.: The free energy as a function of a single order parameter at (a) a first-order phase transition and (b) a second-order phase transition.

parameters which correspond to the global minimum of the free energy.

Fig. 5.3 shows typical examples of how the free energy behaves as a function of a single order parameter χ near first- and second-order phase transitions. In the former case, the global minimum jumps discontinuously from some nonzero value to $\chi = 0$, whereas in the latter case the minimum moves continuously in towards zero. For $T > T_c$, the minimum is always at $\chi = 0$.

5.2. The NJL model

The Nambu–Jona-Lasinio (NJL) model was proposed by Nambu and Jona-Lasinio in two papers from 1961 [88, 89] as a model of interacting nucleons. This was before QCD, and even quarks, were known, so obviously, confinement was not an issue. On the other hand, there *were* already indications of (approximate) chiral symmetry. Since this would imply (almost) massless nucleons, the problem was to find a model that could explain the large nucleon mass without breaking chiral symmetry. They therefore introduced a Lagrangian for the nucleon field ψ with a chirally symmetric four-fermion point-like interaction,

$$\mathscr{L} = \bar{\psi}(i\gamma^\mu\partial_\mu - m_0)\psi + G\left[(\bar{\psi}\psi)^2 + (\bar{\psi}i\gamma^5\boldsymbol{\tau}\psi)^2\right], \tag{5.2}$$

where m_0 is a small bare nucleon mass, $\boldsymbol{\tau} = (\tau_1, \tau_2, \tau_3)$ is the vector of Pauli matrices acting in isospin space and G is a dimensionful coupling constant, the value of which is determined by experiment. It was shown that the self-energy induced by the interaction generates a large effective mass, which stays large even in the chiral limit $m_0 \to 0$.

In the 1970s, after it had become evident that the nucleons are *not* the most elementary particles, and after the ensuing development of QCD, the NJL model was reinterpreted as a model for quark–quark interactions where the local four-particle interaction represents the single gluon exchange.

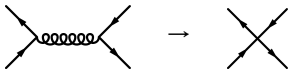

Still, it is common to use the Lagrangian shown in Eq. (5.2), with ψ being a quark field with two flavour and three colour degrees of freedom. This, however, is not the only possible choice. From a modern point of view, it is natural to write

$$\mathscr{L} = \mathscr{L}_{\text{free}} + \mathscr{L}_{\text{sym}} + \mathscr{L}_{\text{det}}, \tag{5.3}$$

where the various terms are

$$\begin{aligned}
\mathscr{L}_{\text{free}} &= \bar{\psi}(i\gamma^{\mu}\partial_{\mu} - m_0)\psi, && (5.4)\\
\mathscr{L}_{\text{sym}} &= G_1\left[(\bar{\psi}\psi)^2 + (\bar{\psi}i\gamma^5\boldsymbol{\tau}\psi)^2 + (\bar{\psi}i\gamma^5\psi)^2 + (\bar{\psi}\boldsymbol{\tau}\psi)^2\right], && (5.5)\\
\mathscr{L}_{\text{det}} &= G_2\left[(\bar{\psi}\psi)^2 + (\bar{\psi}i\gamma^5\boldsymbol{\tau}\psi)^2 - (\bar{\psi}i\gamma^5\psi)^2 - (\bar{\psi}\boldsymbol{\tau}\psi)^2\right], && (5.6)
\end{aligned}$$

and the original Lagrangian corresponds to setting $G_1 = G_2$. Here, $\mathscr{L}_{\text{free}}$ is just the free Dirac Lagrangian, while $\mathscr{L}_{\text{sym}}$ contains all possible chirally symmetric local 4-point interaction terms. In the chiral limit, both are symmetric under the groups

$$\text{SU}(N_c) \times \text{SU}(N_f)_L \times \text{SU}(N_f)_R \times \text{U}(1)_V \times \text{U}(1)_A. \tag{5.7}$$

Recall from Sec. 2.4 that the $\text{U}(1)_A$ symmetry of the QCD Lagrangian is broken in the quantum theory. To model this behaviour, we introduce the term $\mathscr{L}_{\text{det}}$, which was first suggested by 't Hooft [90, 91] to describe instanton induced interactions between quarks in QCD. It can be written in determinant form as

$$\mathscr{L}_{\text{det}} = 2G_2\left[\det\left\{\bar{\psi}(1+\gamma^5)\psi\right\} + \det\left\{\bar{\psi}(1-\gamma^5)\psi\right\}\right], \tag{5.8}$$

and breaks the $\text{U}(1)_A$ symmetry of $\mathscr{L}_{\text{free}}$ and $\mathscr{L}_{\text{sym}}$, while preserving the other symmetries. Note that the form (5.8) is the general form of the 't Hooft interaction. Specifically, Eq. (5.6) is only valid for two quark flavours. In the three-flavour case, Eq. (5.8) describes a six-body interaction.

5.3. The phase diagram of the NJL model

In Paper III we present a detailed study of the phase diagram of the two-flavour NJL model as a function of temperature, baryon chemical potential and isospin chemical potential, and it is discussed how the phase diagram is affected by imposing electric charge neutrality and weak equilibrium. The latter is interesting because of the possibility of there existing dense quark matter in the cores of compact neutron stars. Such stars must, on average, be electrically neutral, otherwise one would pay an enormous energy price. Furthermore, matter of this kind should be in β equilibrium, that is, weak-interaction processes like

$$u \leftrightarrow d + e^+ + \nu \tag{5.9}$$

should go with the same rate in both directions. In the following we demonstrate the calculation of the grand potential density in some detail, and we show how to enforce the constraints given above.

5.3.1. Chiral and pion condensates

In Eq. (5.3) we now set $G_1 = G_2 = G/2$ and include the chemical potentials μ_B and μ_I for baryon number and isospin, respectively. The Lagrangian can then be written

$$\mathscr{L} = \bar{\psi}(i\gamma^\mu\partial_\mu - m_0 + \mu_B\gamma^0 B + \mu_I\gamma^0 I_3)\psi + G\left[(\bar{\psi}\psi)^2 + (\bar{\psi}i\gamma^5\tau_i\psi)^2\right], \tag{5.10}$$

where $B = \mathrm{diag}(1/3, 1/3)$ and $I_3 = \tau_3/2$. We take the masses of the up and down quarks to be equal, $m_u = m_d = m_0$.

Assuming that the system is in thermodynamic equilibrium, we can rewrite the first interaction term in Eq. (5.10) as

$$(\bar{\psi}\psi)^2 = (\bar{\psi}\psi - \langle\bar{\psi}\psi\rangle)^2 + 2\bar{\psi}\psi\langle\bar{\psi}\psi\rangle - \langle\bar{\psi}\psi\rangle^2, \tag{5.11}$$

where $\langle\bar{\psi}\psi\rangle$ is the expectation value of the operator $\bar{\psi}\psi$. The fluctuations around this value are then given by the first term, $\bar{\psi}\psi - \langle\bar{\psi}\psi\rangle$. In the mean-field approximation we neglect the fluctuations, and obtain

$$(\bar{\psi}\psi)^2 \simeq 2\bar{\psi}\psi\langle\bar{\psi}\psi\rangle - \langle\bar{\psi}\psi\rangle^2. \tag{5.12}$$

The pseudoscalar interactions can be linearised in the same way, and we find that

$$(\bar{\psi}i\gamma^5\tau_i\psi)^2 \simeq 2\bar{\psi}i\gamma^5\tau_i\psi\langle\bar{\psi}i\gamma^5\tau_i\psi\rangle - \langle\bar{\psi}i\gamma^5\tau_i\psi\rangle^2. \tag{5.13}$$

Note that

$$\begin{aligned}
\langle\bar{\psi}i\gamma^5\tau_1\psi\rangle &= \langle\bar{u}i\gamma^5 d\rangle + \langle\bar{d}i\gamma^5 u\rangle, &(5.14)\\
\langle\bar{\psi}i\gamma^5\tau_2\psi\rangle &= -i\left(\langle\bar{u}i\gamma^5 d\rangle - \langle\bar{d}i\gamma^5 u\rangle\right), &(5.15)\\
\langle\bar{\psi}i\gamma^5\tau_1\psi\rangle &= \langle\bar{u}i\gamma^5 u\rangle - \langle\bar{d}i\gamma^5 d\rangle. &(5.16)
\end{aligned}$$

The expectation values $\langle\bar{\psi}i\gamma^5\tau_1\psi\rangle$ and $\langle\bar{\psi}i\gamma^5\tau_2\psi\rangle$ have the same quantum numbers as the charged pions, and when nonzero, they signal the formation of a Bose–Einstein condensate of charged pions. For a more compact notation and simpler equations we can use the $\mathrm{U}(1)_V$ symmetry to rotate away any nonzero value of $\langle\bar{\psi}i\gamma^5\tau_2\psi\rangle$, so we only have to consider one charged pion condensate. The expectation value $\langle\bar{\psi}i\gamma^5\tau_3\psi\rangle$, on the other hand, has the quantum numbers of the neutral pion, and we take this quantity to be zero as well.

We can then write the Lagrangian as

$$\begin{aligned}
\mathscr{L} &= \bar{\psi}\left[i\gamma^\mu\partial_\mu - m_0 + \mu_B\gamma^0 B + \mu_I\gamma^0 I_3 + 2G\langle\bar{\psi}\psi\rangle + 2Gi\gamma^5\tau_1\langle\bar{\psi}i\gamma^5\tau_1\psi\rangle\right]\psi\\
&\quad -G\left[\langle\bar{\psi}\psi\rangle^2 + \langle\bar{\psi}i\gamma^5\tau_1\psi\rangle^2\right]. &(5.17)
\end{aligned}$$

Here we see that we get an additional mass term proportional to the expectation value $\langle\bar{\psi}\psi\rangle$, which we identify as the chiral condensate. The pion condensate breaks parity and isospin symmetry as well as chiral symmetry.

For notational simplicity we now define the parameters

$$M \equiv m_0 - 2G\langle\bar{\psi}\psi\rangle, \qquad \rho \equiv -2G\langle\bar{\psi}i\gamma^5\tau_1\psi\rangle, \tag{5.18}$$

along with the chemical potentials

$$\mu \equiv \frac{\mu_B}{3}, \qquad \delta\mu \equiv \frac{\mu_I}{2}, \tag{5.19}$$

and thus obtain the Euclidean Lagrangian

$$\mathscr{L}_E = \bar{\psi}(\tilde{\gamma}_\mu\partial_\mu + M - \mu\tilde{\gamma}_0 - \delta\mu\tilde{\gamma}_0\tau_3 + i\tilde{\gamma}_5\tau_1\rho)\psi + \frac{(M-m_0)^2+\rho^2}{4G}. \tag{5.20}$$

M, which depends on both the bare quark mass and the chiral condensate, plays the role of an effective constituent quark mass[2]. μ is the quark number chemical potential.

5.3.2. Grand potential

The grand potential one obtains from the Lagrangian (5.20) can be written as

$$\Omega = \Omega_{\text{class}} + \Omega_{\text{corr}}. \tag{5.21}$$

Here, the classical potential is

$$\Omega_{\text{class}} = \frac{(M-m_0)^2+\rho^2}{4G}, \tag{5.22}$$

while the thermal quantum corrections are given by

$$\Omega_{\text{corr}} = \sum\!\!\!\!\!\!\int_{\{P\}} \text{tr}\log G^{-1}(P). \tag{5.23}$$

The sum-integral represents a trace over frequency–momentum space, and the remaining trace then has to be taken over Dirac space, flavour space and colour space. The inverse propagator is

$$G^{-1}(P) = i\tilde{\gamma}_\mu P_\mu + M - \mu\tilde{\gamma}_0 - \delta\mu\tilde{\gamma}_0\tau_3 + i\tilde{\gamma}_5\tau_1\rho. \tag{5.24}$$

Defining

$$E_\rho^\pm \equiv \sqrt{(E^\pm)^2+\rho^2}, \tag{5.25}$$

$$E^\pm \equiv E \pm \delta\mu, \tag{5.26}$$

$$E \equiv \sqrt{\mathbf{p}^2+M^2}, \tag{5.27}$$

[2] In Paper III, we refer to M as the chiral condensate. This is, strictly speaking, only a matter of definition, as m_0 is just an additive constant.

we can write the determinant of the inverse propagator as

$$\det G^{-1}(P) = \{[\,i\omega_n - E_u\,][\,i\omega_n - E_d\,][\,i\omega_n + E_{\bar{u}}\,][\,i\omega_n + E_{\bar{d}}\,]\}^{2N_c}, \tag{5.28}$$

where N_c is the number of colours and we have defined

$$\begin{aligned} E_u &= E_\rho^- - \mu, && (5.29)\\ E_d &= E_\rho^+ - \mu, && (5.30)\\ E_{\bar{u}} &= E_\rho^+ + \mu, && (5.31)\\ E_{\bar{d}} &= E_\rho^- + \mu, && (5.32) \end{aligned}$$

since the dispersion relations of the quasiparticles are given by the poles of the propagator upon analytic continuation back to Minkowski spacetime.

Using the identity $\mathrm{tr}\log G^{-1} = \log\det G^{-1}$ and inserting this into Eq. (5.23), we obtain

$$\begin{aligned} \Omega_{\mathrm{corr}} &= -2N_c \sum\!\!\!\!\!\!\int_{\{P\}} \big[\log(i\omega_n - E_u) + \log(i\omega_n - E_d) \\ &\qquad + \log(i\omega_n + E_{\bar{u}}) + \log(i\omega_n + E_{\bar{d}})\big]. \end{aligned} \tag{5.33}$$

Finally, we sum over Matsubara frequencies using the method described in Sec. 3.5 and add the classical potential, and thus obtain the mean-field grand potential of the two-flavour NJL model:

$$\begin{aligned} \Omega &= \frac{(M-m_0)^2+\rho^2}{4G} - 2N_c \int \frac{\mathrm{d}^3 p}{(2\pi)^3} \\ &\quad \times \Big\{ E_\rho^- + T\log[1+e^{-\beta(E_\rho^- - \mu)}] + T\log[1+e^{-\beta(E_\rho^- + \mu)}] \\ &\qquad + E_\rho^+ + T\log[1+e^{-\beta(E_\rho^+ - \mu)}] + T\log[1+e^{-\beta(E_\rho^+ + \mu)}] \Big\}. \end{aligned} \tag{5.34}$$

If we are to enforce charge neutrality and β equilibrium according to Eq. (5.9), we must also take electrons into account. We assume that the neutrinos are free to leave the system and that they can therefore be safely ignored. For simplicity, we describe the electrons as a noninteracting gas of massless particles. This is justified by the fact that the electromagnetic interaction is negligible compared to the strong interaction, and that the electrons are much lighter than the quark quasiparticles. The grand potential is then given by Eq. (3.71) in the limit when $m \to 0$, or

$$\Omega_e = -\frac{\mu_e^4}{12\pi} - \frac{\mu_e^2 T^2}{6} - \frac{7\pi T^4}{180}, \tag{5.35}$$

where μ_e is the electron number chemical potential. In this case the full potential is given by $\Omega = \Omega_{\mathrm{class}} + \Omega_{\mathrm{corr}} + \Omega_e$.

5.3.3. Phase diagram

When nonzero, the parameters M and ρ spontaneously break certain symmetries of the NJL Lagrangian, and they therefore fit our requirements for order parameters. The equilibrium values of these parameters are found by minimising the grand potential, that is, by solving the *gap equations*

$$\frac{\partial\Omega}{\partial M} = 0, \tag{5.36}$$

$$\frac{\partial\Omega}{\partial\rho} = 0. \tag{5.37}$$

In general, these equations cannot be solved analytically, and we therefore have to resort to numerical methods. Furthermore, the vacuum contributions are divergent and must therefore somehow be regulated. The most common regularisation method is to use an ultraviolet cutoff Λ, which is what we have done in Paper III. Another possibility is to include a form factor that falls off rapidly at large momenta, thus making the integrals convergent. This somewhat mimics asymptotic freedom, and was used e.g. in Ref. [92].

In vacuum—that is, when $T = \mu = \delta\mu = 0$—we know that chiral symmetry is spontaneously broken. M should therefore have a nonzero value in this case, and since it is effectively the constituent quark mass we require it to have a value on the order of ~ 300 MeV. However, in vacuum the potential Ω no longer depends on M and ρ separately. Rather, it depends on $M^2 + \rho^2$, thus taking on the "Mexican hat" shape with infinitely many equivalent vacua. The chiral condensate can be rotated into pseudoscalar condensates via the axial flavour transformations

$$\psi \to e^{i\gamma^5\alpha_i\tau_i}\psi. \tag{5.38}$$

In QCD, parity is conserved when $\mu_I = 0$, and to enforce this we always choose $\rho = 0$ when $\delta\mu = 0$. Given some Λ, we can then use Eq. (5.36) in vacuum to determine a value for the coupling G.

Various phase diagrams obtained from Eqs. (5.36) and (5.37) are discussed in detail in Paper III. In that paper we do, however, *not* show the phase diagram in the μ_B–T plane for vanishing isospin chemical potential, simply because it is "old news" [87]. It bears mentioning here, though, if nothing else for the sake of completeness.

The general structure of this phase diagram is shown in Fig. 5.4. (The exact quantitative details depend on the chosen values for M in vacuum, G and Λ.) There is a first-order phase transition starting at $(\mu_B, T) = (\mu_c, 0)$ and ending in a critical point. In the chiral limit, that is—when $m_0 = 0$—there is a second order phase transition extending from the critical point and meeting the T axis at $(\mu_B, T) = (0, T_c)$. Since we are working in a mean-field approximation, the critical exponent for the transition is $1/2$, that is, the chiral condensate for $T < T_c$ falls off as [93]

$$\langle\bar{\psi}\psi\rangle \propto (T_c - T)^{1/2}. \tag{5.39}$$

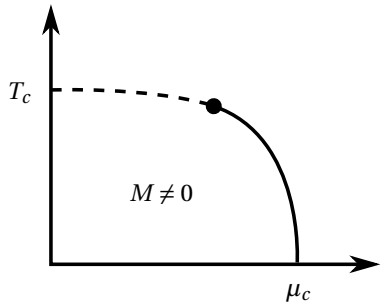

Figure 5.4.: The chiral phase transition in the μ–T plane. The solid line denotes a first-order phase transition, and the dashed line represents a second-order phase transition when $m_0 = 0$ or a crossover when $m_0 \neq 0$.

At the *physical point*, that is, when m_0 is chosen to reproduce the pion mass in vacuum, the transition to the left of the critical endpoint becomes a crossover. As reasoned above, no pion condensation takes place when $\mu_I = 0$.

5.3.4. Charge neutrality and weak equilibrium

The constraints of charge neutrality and β equilibrium can be stated as

$$\langle Q \rangle = 0 \tag{5.40}$$

and

$$\langle n_u \rangle = \langle n_d \rangle + \langle n_e \rangle, \tag{5.41}$$

respectively. The former translates into a new equation which must be solved simultaneously with Eqs. (5.36) and (5.37), namely

$$\frac{\partial \Omega}{\partial \mu_Q} = 0, \tag{5.42}$$

where μ_Q is the chemical potential for electric charge. Eq. (5.41), together with the fact that

$$\frac{Q}{e} = \frac{2}{3} n_u - \frac{1}{3} n_d - n_e, \tag{5.43}$$

means that we have the following relations between the chemical potentials:

$$\mu_u = \mu + \frac{2}{3}\mu_Q, \qquad \mu_d = \mu - \frac{1}{3}\mu_Q, \qquad \mu_e = -\mu_Q. \tag{5.44}$$

We refer to Paper III for an in-depth discussion of the phase diagram under these constraints.

5.4. The sign problem

In Paper IV we use the NJL model to study the sign problem of QCD. Specifically, we investigate the behaviour of the complex phase factor of the fermion determinant at finite density. In this section we will discuss in detail the meaning and importance of the phase factor, and mention some considerations that have to be made when studying it within the NJL model.

5.4.1. The phase factor

The fermionic part of the two-flavour QCD Lagrangian at finite baryon chemical potential and finite isospin chemical potential can be written as

$$\mathscr{L} = \bar{\psi}(D - m + \mu_B \gamma^0 B + \mu_I \gamma^0 I_3)\psi. \tag{5.45}$$

Here we have defined D to be the QCD fermion operator at vanishing chemical potentials,

$$D \equiv i\gamma^\mu \partial_\mu - g_s \gamma^\mu T^a A^a_\mu, \tag{5.46}$$

where T^a are the generators of SU(3) and A^a_μ are the gauge fields.

The Lagrangian is quadratic in the fermion fields and they can therefore be exactly integrated out of the path integral, yielding the *fermion determinant*:

$$\begin{aligned} Z_{\mathrm{QCD}} &= \int \mathscr{D}\bar{\psi}\mathscr{D}\psi\mathscr{D}A\, e^{-S} \\ &= \int \mathscr{D}A\, e^{-S_A} \det(D + m - \mu_B \tilde{\gamma}_0 B - \mu_I \tilde{\gamma}_0 I_3). \end{aligned} \tag{5.47}$$

Since $\tau_3 = \mathrm{diag}(1,-1)$, it is a trivial task to take the determinant over flavour space if we assume that the bare masses of the quarks are equal, that is, $m = \mathrm{diag}(m_0, m_0)$. Using the notation from Sec. 5.3.1 we find that

$$\begin{aligned} \det(D + m - \mu_B \tilde{\gamma}_0 B - \mu_I \tilde{\gamma}_0 I_3) &= \det(D + m_0 - \mu\tilde{\gamma}_0 - \delta\mu\tilde{\gamma}_0) \\ &\quad \times \det(D + m_0 - \mu\tilde{\gamma}_0 + \delta\mu\tilde{\gamma}_0). \end{aligned} \tag{5.48}$$

Thus, at vanishing isospin chemical potential, i.e. $\delta\mu = 0$, we can write the partition function as

$$Z_{\mathrm{QCD}} = \int \mathscr{D}A\, e^{-S_A} [\det(D + m_0 - \mu\tilde{\gamma}_0)]^2. \tag{5.49}$$

Here, and for the remainder of this section, the determinant is taken over spacetime, Dirac space and colour space, but not over flavour space as that was taken care of in Eq. (5.48).

At nonzero baryon number chemical potential, i.e. $\mu \neq 0$, the fermion determinant is generally complex, and the integral (5.49) can no longer be calculated on the lattice using Monte Carlo methods. This is the infamous *sign problem* in lattice QCD. We can then write the determinant as the product of its absolute value and a phase factor,

$$\det(D + m_0 - \mu\tilde{\gamma}_0) = e^{i\theta} |\det(D + m_0 - \mu\tilde{\gamma}_0)|, \tag{5.50}$$

where the phase factor determines the severity of the sign problem.

The *reweighting* technique [94] deals with the problem by including the phase factor in the observable rather than in the measure. While this method works in principle, it is limited by the strength of the fluctuations of the phase of the determinant. It is therefore of considerable interest to understand how the fluctuations of the phase factor depend on external parameters such as temperature and chemical potential [95].

To that end we wish to calculate the expectation value of the phase factor, and this is commonly done using *phase quenched QCD*—hereafter abbreviated |QCD|. In the phase quenched theory one replaces the fermion determinant by its absolute value:

$$Z_{|\mathrm{QCD}|} = \int \mathscr{D}A\, e^{-S_A} |\det(D + m_0 - \mu\tilde{\gamma}_0)|^2. \tag{5.51}$$

Thus |QCD| does not have a sign problem, and standard lattice techniques can be applied [96, 97, 98].

In the two-flavour case, the complex conjugate of the fermion determinant can be obtained simply by switching the sign of the chemical potential [99]:

$$\begin{aligned} [\det(D + m_0 - \mu\tilde{\gamma}_0)]^* &= \det[(D + m_0 - \mu\tilde{\gamma}_0)^\dagger] \\ &= \det[\tilde{\gamma}_5(D + m + \mu\tilde{\gamma}_0)\tilde{\gamma}_5] \\ &= \det(D + m + \mu\tilde{\gamma}_0). \end{aligned} \tag{5.52}$$

In the last line we used the cyclic property of the determinant. Thus, Eq. (5.51) can be written on the form

$$Z_{|\mathrm{QCD}|} = \int \mathscr{D}A\, e^{-S_A} \det(D + m_0 - \mu\tilde{\gamma}_0) \det(D + m_0 + \mu\tilde{\gamma}_0). \tag{5.53}$$

Comparing this to Eq. (5.48), we see that two-flavour phase quenched QCD with $\mu \neq 0$ and $\delta\mu = 0$ is equivalent to normal two-flavour QCD with $\mu = 0$ and $\delta\mu \neq 0$ if we in the former associate $\delta\mu$ with the quark number chemical potential.

The average of the (square of the) phase factor in |QCD| can then be written as

$$\begin{aligned} \langle e^{2i\theta} \rangle &= \frac{1}{Z_{|\mathrm{QCD}|}} \int \mathscr{D}A\, e^{-S_A} e^{2i\theta} |\det(D + m_0 - \mu\tilde{\gamma}_0)|^2 \\ &= \frac{1}{Z_{|\mathrm{QCD}|}} \int \mathscr{D}A\, e^{-S_A} [\det(D + m_0 - \mu\tilde{\gamma}_0)]^2 \\ &= \frac{Z_{\mathrm{QCD}}}{Z_{|\mathrm{QCD}|}}, \end{aligned} \tag{5.54}$$

i.e. as the ratio of the partition functions of normal QCD and the phase quenched theory. This makes sense on a quite intuitive level, since the sign problem is what separates QCD from |QCD|.

If $\langle e^{2i\theta} \rangle \simeq 0$, it means that the phase factor fluctuates strongly, and reweighting techniques can be expected to fail. If, on the other hand, $\langle e^{2i\theta} \rangle \simeq 1$, then the determinant is for the most part real and the sign problem can be controlled.

Chiral perturbation theory has been used to predict the behaviour of the average phase factor [95, 100, 101], and these predictions have been confirmed by lattice measurements. Unfortunately, χPT being a low-energy effective theory for chiral symmetry breaking, it cannot be trusted near and above the chiral phase transition. We therefore turn again to the NJL model.

5.4.2. The NJL model revisited

We introduced the two-flavour NJL model at finite baryon chemical potential and finite isospin chemical potential in Sec. 5.3. Using it as a model for QCD and denoting its partition function at finite μ and $\delta\mu$ by $Z_{\mathrm{NJL}}(\mu,\delta\mu)$, we can write the ratio (5.54) as

$$\langle e^{2i\theta}\rangle = \frac{Z_{\mathrm{NJL}}(\mu=\mu_q,\delta\mu=0)}{Z_{\mathrm{NJL}}(\mu=0,\delta\mu=\mu_q)}, \tag{5.55}$$

where μ_q is the quark number chemical potential. As suggested above, we have realised the phase quenched theory by associating the quark number chemical potential with the chemical potential for isospin.

The procedure for calculating the partition function is similar to what we described in Sec. 5.3, but there are some differences. These are described in detail in Paper IV, and we will therefore just mention a few important points here.

Firstly, as high-energy collision experiments are probing the area of the phase diagram in the vicinity of the critical endpoint of the chiral phase transition, it would be very interesting to be able to apply lattice QCD to this region as well. In order to study the interplay between the sign problem and the critical endpoint, we cannot limit ourselves to the "leading-order" mean-field approximation from Sec. 5.3. At the endpoint the correlation length of the sigma mode becomes infinite [16]. Hence, we need to somehow include the fluctuations we neglected in Eqs. (5.12) and (5.13). In particular, we need to take into account the masses of the fluctuating modes, since the sigma mass is inversely proportional to the correlation length. To that end we calculate the partition function in the saddle point approximation,

$$Z_{\mathrm{NJL}} = \frac{1}{\sqrt{\det H}} e^{-\beta V\Omega}. \tag{5.56}$$

Here, Ω is the grand potential density evaluated at its minimum, while H is the Hessian matrix—the matrix of second derivatives of the potential with respect to the fluctuations—also evaluated at the minimum. H measures the curvature of Ω at the minimum, and hence the particle masses.

Secondly, it is interesting to study the effect of the axial anomaly on the average phase factor. The strength of the $\mathrm{U}(1)_A$ breaking has been shown to have an impact on both the order of the phase transition [14] and the location of the critical endpoint [102]. To allow for an "adjustable" axial anomaly strength, we use the generalised NJL Lagrangian shown in Eqs. (5.3)–(5.6), and set the couplings equal to

$$G_1 = (1-\alpha)G, \qquad G_2 = \alpha G. \tag{5.57}$$

To ensure the stability of the theory we require that $0 \leq \alpha \leq 1/2$. Thus, when $\alpha = 1/2$ the $\mathrm{U}(1)_A$ symmetry is maximally broken and we recover the original NJL Lagrangian. When $\alpha = 0$ the axial symmetry is restored. However, because of the generalised couplings we must account for interactions (and thereby fluctuations) not only in the scalar–isoscalar and pseudoscalar–isovector channels, but also the pseudoscalar–isoscalar and scalar–isovector channels; eight fluctuating collective modes in all.

Bibliography

[1] J. O. Andersen and L. Kyllingstad, *Four-loop Screened Perturbation Theory*, *Phys.Rev.* **D78** (2008) 076008, [arXiv:0805.4478].

[2] J. O. Andersen, L. T. Kyllingstad, and L. E. Leganger, *Pressure to order $g^8 \log g$ of massless ϕ^4 theory at weak coupling*, *JHEP* **0908** (2009) 066, [arXiv:0903.4596].

[3] J. O. Andersen and L. T. Kyllingstad, *Pion Condensation in a two-flavor NJL model: the role of charge neutrality*, *J.Phys.* **G37** (2009) 015003, [hep-ph/0701033].

[4] J. O. Andersen, L. T. Kyllingstad, and K. Splittorff, *The Sign problem across the QCD phase transition*, *JHEP* **1001** (2010) 055, [arXiv:0909.2771].

[5] D. Griffiths, *Introduction to elementary particles*. John Wiley & Sons, 1987.

[6] M. Gell-Mann and Y. Ne'eman, *The eightfold way*. Frontiers in physics. W.A. Benjamin, New York, 1964.

[7] **Particle Data Group** Collaboration, K. Nakamura *et. al.*, *Review of particle physics*, *J.Phys.* **G37** (2010) 075021.

[8] E. Noether, *Invariant Variation Problems*, *Gott.Nachr.* **1918** (1918) 235–257, [physics/0503066].

[9] M. Tavel, *Milestones in mathematical physics: Noether's theorem*, *Transp.Theory Statist.Phys.* **1** (1971) 183–185.

[10] J. Goldstone, *Field Theories with Superconductor Solutions*, *Nuovo Cim.* **19** (1961) 154–164.

[11] J. Goldstone, A. Salam, and S. Weinberg, *Broken Symmetries*, *Phys.Rev.* **127** (1962) 965–970.

[12] H. B. Nielsen and S. Chadha, *On How to Count Goldstone Bosons*, *Nucl.Phys.* **B105** (1976) 445.

[13] T. Schäfer and E. V. Shuryak, *Instantons in QCD*, *Rev.Mod.Phys.* **70** (1998) 323–426, [hep-ph/9610451].

[14] R. D. Pisarski and F. Wilczek, *Remarks on the Chiral Phase Transition in Chromodynamics*, *Phys.Rev.* **D29** (1984) 338–341.

[15] D. H. Rischke, *The Quark gluon plasma in equilibrium*, *Prog.Part.Nucl.Phys.* **52** (2004) 197–296, [nucl-th/0305030].

[16] J. B. Kogut and M. A. Stephanov, *The Phases of Quantum Chromodynamics.* Cambridge monographs on particle physics, nuclear physics and cosmology. Cambridge University Press, Cambridge, 2010.

[17] M. Stephanov, *QCD phase diagram: An Overview*, *PoS* **LAT2006** (2006) 024, [hep-lat/0701002].

[18] A. Casher, *Chiral Symmetry Breaking in Quark Confining Theories*, *Phys.Lett.* **B83** (1979) 395.

[19] S. Hands, *The Phase diagram of QCD*, *Contemp.Phys.* **42** (2001) 209–225, [physics/0105022].

[20] **BRAHMS Collaboration** Collaboration, I. Arsene *et. al.*, *Quark gluon plasma and color glass condensate at RHIC? The Perspective from the BRAHMS experiment*, *Nucl.Phys.* **A757** (2005) 1–27, [nucl-ex/0410020].

[21] **PHENIX Collaboration** Collaboration, K. Adcox *et. al.*, *Formation of dense partonic matter in relativistic nucleus-nucleus collisions at RHIC: Experimental evaluation by the PHENIX collaboration*, *Nucl.Phys.* **A757** (2005) 184–283, [nucl-ex/0410003].

[22] B. Back, M. Baker, M. Ballintijn, D. Barton, B. Becker, *et. al.*, *The PHOBOS perspective on discoveries at RHIC*, *Nucl.Phys.* **A757** (2005) 28–101, [nucl-ex/0410022]. PHOBOS White Paper on discoveries at RHIC.

[23] **STAR Collaboration** Collaboration, J. Adams *et. al.*, *Experimental and theoretical challenges in the search for the quark gluon plasma: The STAR Collaboration's critical assessment of the evidence from RHIC collisions*, *Nucl.Phys.* **A757** (2005) 102–183, [nucl-ex/0501009].

[24] M. G. Alford, A. Schmitt, K. Rajagopal, and T. Schäfer, *Color superconductivity in dense quark matter*, *Rev.Mod.Phys.* **80** (2008) 1455–1515, [arXiv:0709.4635].

[25] E. V. Shuryak, *Theory of Hadronic Plasma*, *Sov.Phys.JETP* **47** (1978) 212–219.

[26] J. I. Kapusta, *Quantum Chromodynamics at High Temperature*, *Nucl.Phys.* **B148** (1979) 461–498.

[27] T. Toimela, *Perturbative QED and QCD at finite temperatures and densities*, *Int.J.Theor.Phys.* **24** (1985) 901.

[28] P. B. Arnold and C. Zhai, *The Three loop free energy for pure gauge QCD*, *Phys.Rev.* **D50** (1994) 7603–7623, [hep-ph/9408276].

[29] P. B. Arnold and C. Zhai, *The Three loop free energy for high temperature QED and QCD with fermions*, *Phys.Rev.* **D51** (1995) 1906–1918, [hep-ph/9410360].

[30] E. Braaten and A. Nieto, *On the convergence of perturbative QCD at high temperature*, *Phys.Rev.Lett.* **76** (1996) 1417–1420, [hep-ph/9508406].

[31] E. Braaten and A. Nieto, *Free energy of QCD at high temperature*, *Phys.Rev.* **D53** (1996) 3421–3437, [hep-ph/9510408].

[32] C. Zhai and B. M. Kastening, *The Free energy of hot gauge theories with fermions through g^5*, *Phys.Rev.* **D52** (1995) 7232–7246, [hep-ph/9507380].

[33] K. Kajantie, M. Laine, K. Rummukainen, and Y. Schroder, *The Pressure of hot QCD up to $g^6 \ln(1/g)$*, *Phys.Rev.* **D67** (2003) 105008, [hep-ph/0211321].

[34] J. O. Andersen, L. E. Leganger, M. Strickland, and N. Su, *NNLO hard-thermal-loop thermodynamics for QCD*, *Phys.Lett.* **B696** (2011) 468–472, [arXiv:1009.4644].

[35] C. Gattringer and C. B. Lang, *Quantum Chromodynamics on the Lattice*, vol. 788 of *Lecture Notes in Physics*. Springer-Verlag, Berlin, Heidelberg, 2010.

[36] O. Philipsen, *Lattice QCD at non-zero temperature and baryon density*, arXiv:1009.4089.

[37] H. J. Warringa, *Thermodynamics of QCD-inspired theories*. PhD thesis, Vrije Universiteit Amsterdam, 2006.

[38] A. Chodos, R. Jaffe, K. Johnson, C. B. Thorn, and V. Weisskopf, *A New Extended Model of Hadrons*, *Phys.Rev.* **D9** (1974) 3471–3495.

[39] A. Chodos, R. Jaffe, K. Johnson, and C. B. Thorn, *Baryon Structure in the Bag Theory*, *Phys.Rev.* **D10** (1974) 2599.

[40] T. A. DeGrand, R. Jaffe, K. Johnson, and J. Kiskis, *Masses and Other Parameters of the Light Hadrons*, *Phys.Rev.* **D12** (1975) 2060.

[41] D. Parganlija, F. Giacosa, and D. H. Rischke, *Vacuum Properties of Mesons in a Linear Sigma Model with Vector Mesons and Global Chiral Invariance*, *Phys.Rev.* **D82** (2010) 054024, [arXiv:1003.4934].

[42] J. O. Andersen, *Pion and kaon condensation at finite temperature and density*, *Phys.Rev.* **D75** (2007) 065011, [hep-ph/0609020].

[43] J. O. Andersen and L. E. Leganger, *Kaon condensation in the color-flavor-locked phase of quark matter, the Goldstone theorem, and the 2PI Hartree approximation*, *Nucl.Phys.* **A828** (2009) 360–389, [arXiv:0810.5510].

[44] S. R. Coleman, R. Jackiw, and H. Politzer, *Spontaneous Symmetry Breaking in the O(N) Model for Large N*, *Phys.Rev.* **D10** (1974) 2491.

[45] R. G. Root, *Effective Potential for the O(N) Model to Order 1/N*, *Phys.Rev.* **D10** (1974) 3322.

[46] H. Meyers-Ortmanns, H. J. Pirner, and B.-J. Schaefer, *Chiral Thermodynamics in the 1/N expansion*, *Phys.Lett.* **B311** (1993) 213–218.

[47] V. Jain, *Finite temperature scalar potential from a 1/N expansion*, *Nucl.Phys.* **B394** (1993) 707–727, [hep-ph/9205232].

[48] A. Bochkarev and J. I. Kapusta, *Chiral symmetry at finite temperature: Linear versus nonlinear sigma models*, *Phys.Rev.* **D54** (1996) 4066–4079, [hep-ph/9602405].

[49] J. O. Andersen, D. Boer, and H. J. Warringa, *Thermodynamics of O(N) sigma models: 1/N corrections*, *Phys.Rev.* **D70** (2004) 116007, [hep-ph/0408033].

[50] J. M. Cornwall, R. Jackiw, and E. Tomboulis, *Effective Action for Composite Operators*, *Phys.Rev.* **D10** (1974) 2428–2445.

[51] G. Baym and G. Grinstein, *Phase Transition in the Sigma Model at Finite Temperature*, *Phys.Rev.* **D15** (1977) 2897–2912.

[52] G. Amelino-Camelia and S.-Y. Pi, *Selfconsistent improvement of the finite temperature effective potential*, *Phys.Rev.* **D47** (1993) 2356–2362, [hep-ph/9211211].

[53] G. Amelino-Camelia, *Thermal effective potential of the O(N) linear sigma model*, *Phys.Lett.* **B407** (1997) 268–274, [hep-ph/9702403].

[54] H.-S. Roh and T. Matsui, *Chiral phase transition at finite temperature in the linear sigma model*, *Eur.Phys.J.* **A1** (1998) 205–220, [nucl-th/9611050].

[55] N. Petropoulos, *Linear sigma model and chiral symmetry at finite temperature*, *J.Phys.* **G25** (1999) 2225–2241, [hep-ph/9807331].

[56] J. T. Lenaghan and D. H. Rischke, *The O(N) model at finite temperature: Renormalization of the gap equations in Hartree and large N approximation*, *J.Phys.* **G26** (2000) 431–450, [nucl-th/9901049].

[57] S. Chiku and T. Hatsuda, *Optimized perturbation theory at finite temperature*, *Phys.Rev.* **D58** (1998) 076001, [hep-ph/9803226].

[58] S. Chiku, *Optimized perturbation theory at finite temperature: Two loop analysis*, *Prog.Theor.Phys.* **104** (2000) 1129–1150, [hep-ph/0012322].

[59] O. Scavenius, A. Mocsy, I. Mishustin, and D. Rischke, *Chiral phase transition within effective models with constituent quarks*, *Phys.Rev.* **C64** (2001) 045202, [nucl-th/0007030].

[60] A. Jakovac, A. Patkos, Z. Szep, and P. Szepfalusy, *T–μ phase diagram of the chiral quark model from a large flavor number expansion*, *Phys.Lett.* **B582** (2004) 179–186, [hep-ph/0312088].

[61] A. Mocsy, I. Mishustin, and P. Ellis, *Role of fluctuations in the linear sigma model with quarks*, *Phys.Rev.* **C70** (2004) 015204, [nucl-th/0402070].

[62] B.-J. Schaefer and J. Wambach, *The Phase diagram of the quark meson model*, *Nucl.Phys.* **A757** (2005) 479–492, [nucl-th/0403039].

[63] B.-J. Schaefer and J. Wambach, *Susceptibilities near the QCD (tri)critical point*, *Phys.Rev.* **D75** (2007) 085015, [hep-ph/0603256].

[64] B.-J. Schaefer and M. Wagner, *The Three-flavor chiral phase structure in hot and dense QCD matter*, *Phys.Rev.* **D79** (2009) 014018, [arXiv:0808.1491].

[65] E. Bowman and J. I. Kapusta, *Critical Points in the Linear Sigma Model with Quarks*, *Phys.Rev.* **C79** (2009) 015202, [arXiv:0810.0042].

[66] V. Skokov, B. Friman, E. Nakano, K. Redlich, and B.-J. Schaefer, *Vacuum fluctuations and the thermodynamics of chiral models*, *Phys.Rev.* **D82** (2010) 034029, [arXiv:1005.3166].

[67] J. W. Negele and H. Orland, *Quantum many-particle systems*. Addison-Wesley, Redwood City, California, 1988.

[68] M. Le Bellac, *Thermal field theory*. Cambridge monographs on mathematical physics. Cambridge University Press, Cambridge, 1996.

[69] J. I. Kapusta and C. Gale, *Finite-temperature field theory: principles and applications*. Cambridge monographs on mathematical physics. Cambridge University Press, Cambridge, 2006.

[70] M. E. Peskin and D. V. Schroeder, *An introduction to quantum field theory*. Westview Press, Boulder, Colorado, 1995.

[71] C. M. Bender and T. T. Wu, *Anharmonic oscillator*, *Phys. Rev.* **184** (1969) 1231–1260.

[72] C. M. Bender and T. T. Wu, *Anharmonic oscillator. ii. a study of perturbation theory in large order*, *Phys. Rev.* **D7** (1973) 1620–1636.

[73] W. Janke and H. Kleinert, *Convergent Strong-Coupling Expansions from Divergent Weak-Coupling Perturbation Theory*, *Phys.Rev.Lett.* **75** (1995) 2787–2791.

[74] F. Karsch, A. Patkós, and P. Petreczky, *Screened perturbation theory*, *Phys.Lett.* **B401** (1997) 69–73, [hep-ph/9702376].

[75] J. O. Andersen, E. Braaten, and M. Strickland, *Screened perturbation theory to three loops*, *Phys.Rev.* **D63** (2001) 105008, [hep-ph/0007159].

[76] J. O. Andersen and M. Strickland, *Mass expansions of screened perturbation theory*, *Phys.Rev.* **D64** (2001) 105012, [hep-ph/0105214].

[77] A. Rebhan, *Non-Abelian Debye mass at next-to-leading order*, *Phys.Rev.* **D48** (1993) 3967–3970, [hep-ph/9308232].

[78] E. Braaten and R. D. Pisarski, *Resummation and Gauge Invariance of the Gluon Damping Rate in Hot QCD*, *Phys.Rev.Lett.* **64** (1990) 1338.

[79] E. Braaten and R. D. Pisarski, *Soft Amplitudes in Hot Gauge Theories: A General Analysis*, *Nucl.Phys.* **B337** (1990) 569.

[80] J. O. Andersen, M. Strickland, and N. Su, *Three-loop HTL Free Energy for QED*, *Phys.Rev.* **D80** (2009) 085015, [arXiv:0906.2936].

[81] J. O. Andersen, L. E. Leganger, M. Strickland, and N. Su, *Three-loop HTL QCD thermodynamics*, arXiv:1103.2528.

[82] J. O. Andersen and M. Strickland, *Resummation in hot field theories*, *Annals Phys.* **317** (2005) 281–353, [hep-ph/0404164].

[83] E. Braaten and A. Nieto, *Effective field theory approach to high temperature thermodynamics*, *Phys.Rev.* **D51** (1995) 6990–7006, [hep-ph/9501375].

[84] H. Kleinert, J. Neu, V. Schulte-Frohlinde, K. Chetyrkin, and S. Larin, *Five loop renormalization group functions of O(n) symmetric ϕ^4 theory and ϵ-expansions of critical exponents up to ϵ^5*, *Phys.Lett.* **B272** (1991) 39–44, [hep-th/9503230].

[85] K. Farakos, K. Kajantie, K. Rummukainen, and M. E. Shaposhnikov, *3-D physics and the electroweak phase transition: Perturbation theory*, *Nucl.Phys.* **B425** (1994) 67–109, [hep-ph/9404201].

[86] J. O. Andersen, *The free energy of high temperature QED to order e^5 from effective field theory*, *Phys.Rev.* **D53** (1996) 7286–7292, [hep-ph/9509409].

[87] M. Buballa, *NJL model analysis of quark matter at large density*, *Phys.Rept.* **407** (2005) 205–376, [hep-ph/0402234].

[88] Y. Nambu and G. Jona-Lasinio, *Dynamical Model of Elementary Particles Based on an Analogy with Superconductivity. I*, *Phys.Rev.* **122** (1961) 345–358.

[89] Y. Nambu and G. Jona-Lasinio, *Dynamical Model of Elementary Particles Based on an Analogy with Superconductivity. II*, *Phys.Rev.* **124** (1961) 246–254.

[90] G. 't Hooft, *Computation of the Quantum Effects Due to a Four-Dimensional Pseudoparticle*, *Phys.Rev.* **D14** (1976) 3432–3450.

[91] G. 't Hooft, *How Instantons Solve the U(1) Problem*, *Phys.Rept.* **142** (1986) 357–387.

[92] M. G. Alford, K. Rajagopal, and F. Wilczek, *QCD at finite baryon density: Nucleon droplets and color superconductivity*, *Phys.Lett.* **B422** (1998) 247–256, [hep-ph/9711395].

[93] P. M. Chaikin and T. C. Lubensky, *Principles of condensed matter physics*. Cambridge University Press, Cambridge, 1995.

[94] I. M. Barbour, S. E. Morrison, E. G. Klepfish, J. B. Kogut, and M.-P. Lombardo, *Results on finite density QCD*, *Nucl.Phys.Proc.Suppl.* **60A** (1998) 220–234, [hep-lat/9705042].

[95] K. Splittorff and J. Verbaarschot, *The QCD Sign Problem for Small Chemical Potential*, *Phys.Rev.* **D75** (2007) 116003, [hep-lat/0702011].

[96] J. Kogut and D. Sinclair, *The Finite temperature transition for 2-flavor lattice QCD at finite isospin density*, *Phys.Rev.* **D70** (2004) 094501, [hep-lat/0407027].

[97] J. Kogut and D. Sinclair, *Lattice QCD at finite temperature and density in the phase-quenched approximation*, *Phys.Rev.* **D77** (2008) 114503, [arXiv:0712.2625].

[98] P. de Forcrand, M. A. Stephanov, and U. Wenger, *On the phase diagram of QCD at finite isospin density*, *PoS* **LAT2007** (2007) 237, [arXiv:0711.0023].

[99] M. G. Alford, A. Kapustin, and F. Wilczek, *Imaginary chemical potential and finite fermion density on the lattice*, *Phys.Rev.* **D59** (1999) 054502, [hep-lat/9807039].

[100] K. Splittorff and J. Verbaarschot, *The Approach to the thermodynamic limit in lattice QCD at mu not equal 0*, *Phys.Rev.* **D77** (2008) 014514, [arXiv:0709.2218].

[101] J. C. Bloch and T. Wettig, *Random matrix analysis of the QCD sign problem for general topology*, *JHEP* **0903** (2009) 100, [arXiv:0812.0324].

[102] J.-W. Chen, K. Fukushima, H. Kohyama, K. Ohnishi, and U. Raha, *U(A)(1) Anomaly in Hot and Dense QCD and the Critical Surface*, *Phys.Rev.* **D80** (2009) 054012, [arXiv:0901.2407].

Part II.

Papers

Paper I

Jens O. Andersen and Lars Kyllingstad:
"Four-loop screened perturbation theory",
Phys. Rev. **D78** (2008), 076008.

PHYSICAL REVIEW D **78,** 076008 (2008)

Four-loop screened perturbation theory

Jens O. Andersen* and Lars Kyllingstad+

Department of Physics, Norwegian University of Science and Technology, N-7491 Trondheim, Norway
(Received 27 June 2008; published 22 October 2008)

We study the thermodynamics of massless ϕ^4-theory using screened perturbation theory. In this method, the perturbative expansion is reorganized by adding and subtracting a thermal mass term in the Lagrangian. We calculate the free energy through four loops expanding in a double power expansion in m/T and g^2, where m is the thermal mass and g is the coupling constant. The expansion is truncated at order g^7 and the loop expansion is shown to have better convergence properties than the weak-coupling expansion. The free energy at order g^6 involves the four-loop triangle sum-integral evaluated by Gynther, Laine, Schröder, Torrero, and Vuorinen using the methods developed by Arnold and Zhai. The evaluation of the free energy at order g^7 requires the evaluation of a nontrivial three-loop sum-integral, which we calculate by the same methods.

DOI: 10.1103/PhysRevD.78.076008 PACS numbers: 11.10.Wx, 11.25.Db, 11.80.Fv, 12.38.Cy

I. INTRODUCTION

In recent years there has been significant progress in the understanding of thermal field theories in equilibrium [1–4]. For example, the thermodynamic functions can be calculated as power series in the coupling constant g at weak coupling and advanced calculational techniques have been developed in order to go beyond the first few corrections. The pressure has been calculated through order g^5 for massless ϕ^4-theory [5,6], massless QED [7–9], and massless non-Abelian gauge theories [10–12]. Very recently, the calculation frontier has been pushed to order g^6 in massless ϕ^4-theory by Gynther, Laine, Schröder, Torrero, and Vuorinen [13]. The calculation in Ref. [13] involves the computation of complicated four-loop vacuum diagrams and was motivated by the corresponding problem in non-Abelian gauge theories: There are three momentum scales—hard momenta of order T, soft momenta of order gT, and supersoft momenta of order g^2T, which give contributions to the free energy. The contribution from the hard scale T to the free energy can be calculated as a power series in g^2 using naïve perturbation theory without resummed propagators. The order g^6 is the first order at which all three momentum scales in QCD contribute to the free energy and so it is important to calculate the full g^6 term. Such a calculation involves the evaluation of four-loop vacuum diagrams in four dimensions.

However, it is well-known that the weak-coupling expansion is very sensitive to the renormalization scale, and it is furthermore convergent only if the coupling constant is tiny. The physical origin of this instability does not seem to be related to the magnetic mass problem in QCD, as it appears in ϕ^4-theory and QED as well. Rather, it seems to be associated with screening effects and quasiparticles.

In recent years there have been large efforts to reorganize the perturbative series such that it has improved convergence properties. Several of these methods are variational in nature, in which the thermodynamic potential Ω depends on one or more variational parameters m_i. The pressure and other thermodynamic quantities are then found by evaluating Ω and its derivatives at the variational point where $\delta\Omega/\delta m_i = 0$.

One of these methods is screened perturbation theory (SPT) which in the context of hot ϕ^4-theory was introduced by Karsch, Patkós, and Petreczky [14] (see also Refs. [15–17]). In this approach, one introduces a single variational parameter m^2 which is added to and subtracted from the original Lagrangian. The added piece is kept as a part of the free Lagrangian and the subtracted piece is treated as an interaction. The parameter m^2 has a simple interpretation of a thermal mass and satisfies a variational equation. SPT has been applied to calculate the pressure to three-loop order [18] and the convergence properties of the successive approximations are dramatically improved as compared to the weak-coupling expansion. The mass parameter is of order g and so it might be reasonable to carry out an additional expansion of the Feynman diagrams in powers of m/T, and truncate at the appropriate order. This was done in Ref. [19] and it was demonstrated that the double expansion in m/T and g converges quickly to the numerically exact result even for large values of the coupling.

The generalization of SPT to gauge theories cannot simply be made by adding and subtracting a local mass term as this would violate gauge invariance. Instead one adds and subtracts to the Lagrangian a hard thermal loop (HTL) improvement term [20]. The free piece of the Lagrangian includes the HTL self-energies, while the remaining terms are treated as perturbations. Hard thermal loop perturbation theory is a manifestly gauge invariant approach that can be used to calculate static as well as

*andersen@tf.phys.ntnu.no
+lars.kyllingstad@ntnu.no

dynamic quantities in a systematic expansion. HTL perturbation theory has been applied to calculate the pressure to two-loop order [21–25] in an m/T expansion and the convergence properties of the successive approximations are again improved as compared to the weak-coupling expansion.

Another variational method in which the propagator is a variational function was constructed by Luttinger and Ward [26] and by Baym [27] for nonrelativistic fermions in the early 1960s. Later, it was generalized to relativistic quantum field theories by Cornwall, Jackiw, and Tomboulis [28]. The approach is based on the fact that the thermodynamic potential Ω can be written in terms of the two-particle irreducible (2PI) vacuum diagrams. The propagator D satisfies the variational equation $\delta\Omega/\delta D = 0$. The 2PI effective action formalism is also referred to as Φ-derivable approximations.

Since the 2PI effective action formalism involves an effective propagator, a truncated calculation in the loop expansion or $1/N$-expansion involves a selective resummation of diagrams from all orders of perturbation theory. This fact makes renormalization of Φ-derivable approximations highly nontrivial. In recent years, there have been large efforts to prove renormalizability in the loop expansion, $1/N$-expansion, or the Hartree approximation, and, in particular, to prove that the counterterms are medium independent, i.e. independent of temperature and chemical potential [29–32].

The second issue is that of gauge-fixing dependence. While the exact 2PI effective action is gauge independent at the stationary point, this property is often lost in approximations. The problem has been examined by Arrizabalaga and Smit [33] as well as Carrington *et al.* [34]. In Ref. [33], it was shown that the n-loop Φ-derivable approximation, which is defined by the truncation of the action functional after n loops, has a gauge dependence that shows up at order g^{2n}. Furthermore, if the nth order solution to the gap equation is used to evaluate the complete effective action, the gauge dependence first shows up at order g^{4n}. Explicit examples of the gauge dependence of the three-loop Φ-derivable approximation can be found in Ref. [35].

The Φ-derivable approach has been used by Blaizot, Iancu, and Rebhan [36–38] and by Peshier [39] to calculate the thermodynamic quantities at the two-loop level in scalar field theory as well as in gauge theories. The calculations are based on the fact that the solution to the gap equation for the propagator for soft momenta is given by the HTL self-energies. Three-loop calculations have been performed in scalar field theory by Braaten and Petitgirard [40], and in QED in Ref. [35] using an m/T expansion similar to that employed in SPT in Ref. [19]. The convergence of the successive approximations to the pressure is improved significantly compared to the weak-coupling expansion and the sensitivity to the renormalization scale is also reduced. In Ref. [41], the authors carried out a numerically exact three-loop calculation of the pressure in ϕ^4-theory. Similarly, numerically exact two-loop calculations of the pressure in QED including an analysis of the gauge dependence of the results can be found in Ref. [42]. In these calculations no attempts to compare with the m/T expansions of Refs. [35,40] were made.

Finally, we mention other related resummation methods that have been applied in recent years, namely, the 2-particle point irreducible (2PPI) method [43,44] as well as the linear delta-expansion [45–48]. These methods are also variational in spirit. Moreover, it has been shown that they correctly predict a second-order phase transition when applied to ϕ^4-theory. In the case of the linear delta-expansion, the successive approximations of e.g. the pressure are remarkably stable as compared to the weak-coupling expansion.

The article is organized as follows. In Sec. II, we briefly discuss the systematics of screened perturbation theory. In Sec. III, we calculate the pressure to four-loop order in a double expansion in m/T and g^2. In Sec. IV, we discuss different gap equations that are used to determine the mass parameter in screened perturbation theory. We also present our numerical results and compare them with the weak-coupling expansion. In Sec. V, we summarize. In Appendix A and B, we list the sum-integrals and the integrals that we need. In Appendix C, we discuss the m/T expansion of typical sum-integrals that appear in the calculation. In Appendix D , we calculate explicitly a new three-loop sum-integral that contributes to order g^7 in the m/T expansion.

II. SCREENED PERTURBATION THEORY

The Lagrangian density for a massless scalar field with a ϕ^4 interaction is

$$\mathcal{L} = \frac{1}{2}\partial_\mu\phi\partial^\mu\phi - \frac{g^2}{24}\phi^4 + \Delta\mathcal{L}, \tag{1}$$

where g is the coupling constant and $\Delta\mathcal{L}$ includes counterterms. Renormalizability guarantees that $\Delta\mathcal{L}$ is of the form

$$\Delta\mathcal{L} = \frac{1}{2}\Delta Z\partial_\mu\phi\partial^\mu\phi - \frac{1}{24}\Delta g^2\phi^4. \tag{2}$$

Screened perturbation theory, which was introduced in thermal field theory by Karsch, Patkós, and Petreczky [14], is simply a reorganization of the perturbation series for thermal field theory. It can be made more systematic by using a framework called "optimized perturbation theory" that Chiku and Hatsuda [49] have applied to a spontaneously broken scalar field theory. The Lagrangian density is written as

$$\mathcal{L}_{\rm SPT} = -\mathcal{E}_0 + \frac{1}{2}\partial_\mu\phi\partial^\mu\phi - \frac{1}{2}(m^2 - m_1^2)\phi^2 - \frac{g^2}{24}\phi^4 + \Delta\mathcal{L} + \Delta\mathcal{L}_{\rm SPT}. \tag{3}$$

Here, $\mathcal{E}_0$ is the vacuum energy density term, and we have added and subtracted mass terms. If we set $\mathcal{E}_0 = 0$ and $m_1^2 = m^2$, we recover the original Lagrangian Eq. (1). Screened perturbation theory is defined by taking m^2 to be of order unity and m_1^2 to be of order g^2, expanding systematically in powers of g^2 and setting $m_1^2 = m^2$ at the end of the calculation. This defines a reorganization of the perturbative series in which the expansion is about the free field theory defined by

$$\mathcal{L}_{\text{free}} = -\mathcal{E}_0 + \frac{1}{2}\partial_\mu\phi\partial^\mu\phi - \frac{1}{2}m^2\phi^2. \tag{4}$$

The interacting term is

$$\mathcal{L}_{\text{int}} = \frac{1}{2}m_1^2\phi^2 - \frac{g^2}{24}\phi^4 + \Delta\mathcal{L} + \Delta\mathcal{L}_{\text{SPT}}. \tag{5}$$

Screened perturbation theory generates new ultraviolet divergences, but they can be canceled by the additional counterterm in $\Delta\mathcal{L}_{\text{SPT}}$. If we use dimensional regularization and minimal subtraction, the coefficients of these operators are polynomials in g^2 and $(m^2 - m_1^2)$. The counterterm $\Delta\mathcal{L}$ is

$$\Delta\mathcal{L} = -\frac{\Delta g^2}{24}\phi^4. \tag{6}$$

The additional counterterms required to remove the new divergences are

$$\Delta\mathcal{L}_{\text{SPT}} = -\Delta\mathcal{E}_0 - \frac{1}{2}(\Delta m^2 - \Delta m_1^2)\phi^2. \tag{7}$$

Several terms in the power series expansions of the counterterms are known from previous calculations at zero temperature. The counterterms Δg^2 and Δm^2 are known to order α^5, where $\alpha = g^2/(4\pi)^2$ [50]. We will need the coupling constant counterterm to next-to-leading order in α:

$$\Delta g^2 = \left[\frac{3}{2\epsilon}\alpha + \left(\frac{9}{4\epsilon^2} - \frac{17}{12\epsilon}\right)\alpha^2 + \cdots\right]g^2. \tag{8}$$

We need the mass counterterms Δm^2 and Δm_1^2 to next-to-leading order in α:

$$\Delta m^2 = \left[\frac{1}{2\epsilon}\alpha + \left(\frac{1}{2\epsilon^2} - \frac{5}{24\epsilon}\right)\alpha^2 + \cdots\right]m^2, \tag{9}$$

$$\Delta m_1^2 = \left[\frac{1}{2\epsilon}\alpha + \left(\frac{1}{2\epsilon^2} - \frac{5}{24\epsilon}\right)\alpha^2 + \cdots\right]m_1^2. \tag{10}$$

The counterterm for $\Delta\mathcal{E}_0$ has been calculated to order α^4 [51]. We will need its expansion only to first order in α and second order in m_1^2:

$$(4\pi)^2\Delta\mathcal{E}_0 = \left[\frac{1}{4\epsilon} + \frac{1}{8\epsilon^2}\alpha\right]m^4 - 2\left[\frac{1}{4\epsilon} + \frac{1}{8\epsilon^2}\alpha\right]m_1^2m^2 + \left[\frac{1}{4\epsilon} + \frac{1}{8\epsilon^2}\alpha\right]m_1^4. \tag{11}$$

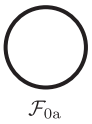

$\mathcal{F}_{0a}$

FIG. 1. One-loop vacuum diagram.

III. FREE ENERGY TO FOUR LOOPS

In this section, we calculate the m/T expansions of the pressure to four loops in screened perturbation theory. In performing the truncation, m is treated as a quantity that is $\mathcal{O}(g)$ and we include all terms which contribute to order g^7.

A. One-loop free energy

The free energy at leading order in g^2 is

$$\mathcal{F}_0 = \mathcal{E}_0 + \mathcal{F}_{0a} + \Delta_0\mathcal{E}_0, \tag{12}$$

where $\Delta_0\mathcal{E}_0$ is the term of order g^0 in the vacuum energy counterterm Eq. (11).

The expression for diagram $\mathcal{F}_{0a}$ in Fig. 1 is

$$\mathcal{F}_{0a} = \frac{1}{2}\sum\!\!\!\!\!\!\int_P \log[P^2 + m^2], \tag{13}$$

where the symbol $\sum\!\!\!\!\!\!\int_P$ is defined in Appendix A.

Treating m as $\mathcal{O}(gT)$ and including all terms which contribute through $\mathcal{O}(g^7)$, we obtain

$$\mathcal{F}_{0a} = \frac{1}{2}I_0' + \frac{1}{2}m^2I_1 + \frac{1}{2}TI_0' - \frac{1}{4}m^4I_2 + \frac{1}{6}m^6I_3, \tag{14}$$

where the sum-integrals I_0' and I_n are defined in Appendix A and the integral I_0' is defined in Appendix B. In Appendix C, we illustrate the m/T expansion of simple one-loop sum-integrals such as the one appearing in Eq. (13). We also note that most of the multiloop diagrams are products of simple one-loop sum-integrals.

The term I_2 is logarithmically divergent and the pole in ϵ is canceled by the zeroth-order term $\Delta_0\mathcal{E}_0$ in Eq. (11). The final result for the truncated one-loop free energy is

$$\mathcal{F}_0 = -\frac{\pi^2T^4}{90}\left[1 - 15\hat{m}^2 + 60\hat{m}^3 + 45(L + \gamma_E)\hat{m}^4 - \frac{15}{2}\zeta(3)\hat{m}^6\right], \tag{15}$$

where $\hat{m} = \frac{m}{2\pi T}$ and $L = \log\frac{\mu}{4\pi T}$.

B. Two-loop free energy

The contribution to the free energy at two loops is given by

$$\mathcal{F}_1 = \mathcal{F}_{1a} + \mathcal{F}_{1b} + \Delta_1\mathcal{E}_0 + \frac{\partial\mathcal{F}_{0a}}{\partial m^2}\Delta_1m^2, \tag{16}$$

where $\Delta_1\mathcal{E}_0$ and Δ_1m^2 are the vacuum and mass counter-

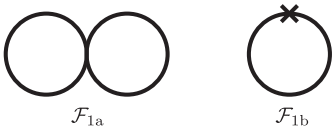

FIG. 2. Two-loop vacuum diagrams. The cross denotes a mass insertion.

terms of order g^2, respectively. The expressions for the diagrams $\mathcal{F}_{1a}$ and $\mathcal{F}_{1b}$ in Fig. 2 are

$$\mathcal{F}_{1a} = \frac{1}{8}g^2\Big(\sum\!\!\!\!\!\!\int_P \frac{1}{P^2+m^2}\Big)^2, \tag{17}$$

$$\mathcal{F}_{1b} = -\frac{1}{2}m_1^2\sum\!\!\!\!\!\!\int_P \frac{1}{P^2+m^2}. \tag{18}$$

Expanding the sum-integrals in Eqs. (17) and (18) to order $\mathcal{O}(g^7)$ yields

$$\mathcal{F}_{1a} = \frac{1}{8}g^2[I_1^2 + 2TI_1I_1 - 2m^2I_1I_2 + T^2I_1^2 - 2m^2I_1TI_2 + 2m^4I_1I_3 + m^4I_2^2 + 2m^4TI_1I_3], \tag{19}$$

$$\mathcal{F}_{1b} = -\frac{1}{2}m_1^2[I_1 + TI_1 - m^2I_2 + m^4I_3], \tag{20}$$

where the integral I_n is defined in Appendix B.

The poles in ϵ in Eqs. (19) and (20) are canceled by the counterterms in Eq. (16). The final result for the two-loop contribution to the free energy is

$$\mathcal{F}_1 = \frac{\pi^2T^4}{90}\alpha\Big[\frac{5}{4} - 15\hat{m} - 15(L+\gamma_E-3)\hat{m}^2 + 90(L+\gamma_E)\hat{m}^3 + 45\Big((L+\gamma_E)^2 + \frac{1}{12}\zeta(3)\Big)\hat{m}^4 - \frac{45}{2}\zeta(3)\hat{m}^5\Big] - \frac{\pi^2T^4}{90}15\hat{m}_1^2\Big[1 - 6\hat{m} - 6(L+\gamma_E)\hat{m}^2 + \frac{3}{2}\zeta(3)\hat{m}^4\Big]. \tag{21}$$

Note that we here and in the following have pulled out a factor of $\mathcal{F}_{\text{ideal}} = -\pi^2T^4/90$.

C. Three-loop free energy

The contribution to the free energy at three loops is

$$\mathcal{F}_2 = \mathcal{F}_{2a} + \mathcal{F}_{2b} + \mathcal{F}_{2c} + \mathcal{F}_{2d} + \Delta_2\mathcal{E}_0 + \frac{\partial\mathcal{F}_{0a}}{\partial m^2}\Delta_2m^2 + \frac{1}{2}\frac{\partial^2\mathcal{F}_{0a}}{(\partial m^2)^2}(\Delta_1m^2)^2 + \Big(\frac{\partial\mathcal{F}_{1a}}{\partial m^2} + \frac{\partial\mathcal{F}_{1b}}{\partial m^2}\Big)\Delta_1m^2 + \frac{\mathcal{F}_{1a}}{g^2}\Delta_1g^2 + \frac{\mathcal{F}_{1b}}{m_1^2}\Delta_1m_1^2, \tag{22}$$

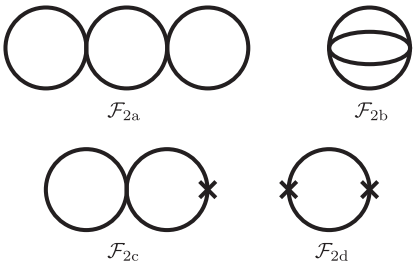

FIG. 3. Three-loop vacuum diagrams.

where we have included all necessary counterterms. The expressions for the diagrams $\mathcal{F}_{2a}$, $\mathcal{F}_{2b}$, $\mathcal{F}_{2c}$, and $\mathcal{F}_{2d}$ in Fig. 3 are

$$\mathcal{F}_{2a} = -\frac{1}{16}g^4\Big(\sum\!\!\!\!\!\!\int_P \frac{1}{P^2+m^2}\Big)^2\sum\!\!\!\!\!\!\int_Q \frac{1}{(Q^2+m^2)^2}, \tag{23}$$

$$\mathcal{F}_{2b} = -\frac{1}{48}g^4\sum\!\!\!\!\!\!\int_{PQR} \frac{1}{P^2+m^2}\frac{1}{Q^2+m^2}\frac{1}{R^2+m^2} \times \frac{1}{(P+Q+R)^2+m^2}, \tag{24}$$

$$\mathcal{F}_{2c} = \frac{1}{4}g^2m_1^2\sum\!\!\!\!\!\!\int_P \frac{1}{P^2+m^2}\sum\!\!\!\!\!\!\int_Q \frac{1}{(Q^2+m^2)^2}, \tag{25}$$

$$\mathcal{F}_{2d} = -\frac{1}{4}m_1^4\sum\!\!\!\!\!\!\int_P \frac{1}{(P^2+m^2)^2}. \tag{26}$$

Expanding in powers of m^2 to the appropriate order gives[1]

$$\mathcal{F}_{2a} = -\frac{1}{16}g^4[TI_1^2I_2 + I_1^2I_2 + 2T^2I_1I_1I_2 + T^3I_1^2I_2 + 2TI_1I_1I_2 - 2m^2TI_1I_2I_2 + T^2I_2I_1^2 - 2m^2I_1^2I_3 - 2m^2T^2I_2I_1I_2 - 2m^2I_1I_2^2 - 4m^2TI_1I_1I_3 - 2m^2TI_1I_2^2 + m^4TI_2I_2^2 + 2m^4TI_2I_1I_3], \tag{27}$$

$$\mathcal{F}_{2b} = -\frac{1}{48}g^4\Big[I_{\text{ball}} + T^3I_{\text{ball}} + 4TI_1I_{\text{sun}} + 6T^2I_2I_1^2 - 4m^2I'_{\text{ball}} - 8m^2TI_1\sum\!\!\!\!\!\!\int_{QR}\frac{Q^2+(2/d)\mathbf{q}^2}{Q^6R^2(Q+R)^2}\Big], \tag{28}$$

[1]Notice that the term TI_1I_{sun} in $\mathcal{F}_{2b}$ in Eq. (28) vanishes. However, we include this term because it gives rise to a finite term at four loops when renormalizing the coupling constant g.

$$\mathcal{F}_{2c} = \frac{1}{4} g^2 m_1^2 [T I_1 I_2 + I_1 I_2 + T^2 I_1 I_2 + T I_2 I_1 - m^2 T I_2 I_2 - m^2 I_2^2 - 2m^2 I_1 I_3 - 2m^2 T I_1 I_3 + m^4 T I_2 I_3], \quad (29)$$

$$\mathcal{F}_{2d} = -\frac{1}{4} m_1^4 [T I_2 + I_2 - 2m^2 I_3], \quad (30)$$

where $I_{\rm sun}$, $I_{\rm ball}$, and $I'_{\rm ball}$ are defined in Appendix A, and $I_{\rm ball}$ is defined in Appendix B.

The poles in ϵ in Eqs. (27)–(30) are canceled by the counterterms in Eq. (22).

The final result for the three-loop contribution to the free energy is

$$\begin{aligned}\mathcal{F}_2 = &-\frac{\pi^2 T^4}{90}\frac{5}{8}\frac{1}{\hat{m}}\alpha^2\Big[1 - 2\Big(\frac{59}{15} - \gamma_E - 3L - 4\frac{\zeta'(-1)}{\zeta(-1)} + 2\frac{\zeta'(-3)}{\zeta(-3)}\Big)\hat{m} \\ &- 12\hat{m}^2\Big(5 + 7L + 3\gamma_E - 8\log\hat{m} - 8\log 2 - 4\frac{\zeta'(-1)}{\zeta(-1)}\Big) \\ &+ \Big(268(L+\gamma_E) - 48(L+\gamma_E)^2 + \frac{\zeta'(-1)}{\zeta(-1)}(34 + 12\gamma_E) + 12\frac{\zeta''(-1)}{\zeta(-1)} + \gamma_E(17 - 21\gamma_E) + 34 + \frac{9\pi^2}{2} - 48\gamma_1 \\ &- \zeta(3) - 6C'_{\rm ball}\Big)\hat{m}^3 + (89 + 120(L+\gamma_E) + [18(L+\gamma_E)]^2 + 15\zeta(3))\hat{m}^4\Big] \\ &+ \frac{\pi^2 T^4}{90}\frac{15}{2}\frac{\hat{m}_1^2}{\hat{m}}\alpha\Big[1 + 2(L + \gamma_E - 3)\hat{m} - 18(L+\gamma_E)\hat{m}^2 - (12(L+\gamma_E)^2 + \zeta(3))\hat{m}^3 + \frac{15}{2}\zeta(3)\hat{m}^4\Big] \\ &- \frac{\pi^2 T^4}{90}\frac{45}{2}\frac{\hat{m}_1^4}{\hat{m}}[1 + 2(L+\gamma_E)\hat{m} - \zeta(3)\hat{m}^3]. \end{aligned} \quad (31)$$

Here $C'_{\rm ball} = 48.7976$ is the numerical constant in $I'_{\rm ball}$ [13].

D. Four-loop free energy

The contributions to the free energy at four loops are

$$\begin{aligned}\mathcal{F}_3 = &\mathcal{F}_{3a} + \mathcal{F}_{3b} + \mathcal{F}_{3c} + \mathcal{F}_{3d} + \mathcal{F}_{3e} + \mathcal{F}_{3f} + \mathcal{F}_{3g} + \mathcal{F}_{3h} + \mathcal{F}_{3i} + \mathcal{F}_{3j} + \Delta_3\mathcal{E}_0 + \frac{\partial\mathcal{F}_{0a}}{\partial m^2}\Delta_3 m^2 + \frac{1}{6}\frac{\partial^3\mathcal{F}_{0a}}{(\partial m^2)^3}(\Delta_1 m^2)^3 \\ &+ \frac{\partial^2\mathcal{F}_{0a}}{(\partial m^2)^2}(\Delta_1 m^2)(\Delta_2 m^2) + \Big(\frac{\partial\mathcal{F}_{1a}}{\partial m^2} + \frac{\partial\mathcal{F}_{1b}}{\partial m^2}\Big)\Delta_2 m^2 + \frac{\mathcal{F}_{1a}}{g^2}\Delta_2 g^2 + \Big(2\frac{\mathcal{F}_{2a}}{g^2} + 2\frac{\mathcal{F}_{2b}}{g^2} + \frac{\mathcal{F}_{2c}}{g^2}\Big)\Delta_1 g^2 \\ &+ \frac{1}{2}\Big(\frac{\partial\mathcal{F}_{1a}^2}{(\partial m^2)^2} + \frac{\partial\mathcal{F}_{1b}^2}{(\partial m^2)^2}\Big)(\Delta_1 m^2)^2 + \frac{\mathcal{F}_{1b}}{m_1^2}\Delta_2 m_1^2 + \frac{\partial\mathcal{F}_{1b}}{m_1^2\partial m^2}(\Delta_1 m^2)(\Delta_1 m_1^2) + \frac{1}{g^2}\frac{\partial\mathcal{F}_{1a}}{\partial m^2}(\Delta_1 g^2)(\Delta_1 m^2) \\ &+ \Big(\frac{\mathcal{F}_{2c}}{m_1^2} + 2\frac{\mathcal{F}_{2d}}{m_1^2}\Big)\Delta_1 m_1^2 + \Big(\frac{\partial\mathcal{F}_{2a}}{\partial m^2} + \frac{\partial\mathcal{F}_{2b}}{\partial m^2} + \frac{\partial\mathcal{F}_{2c}}{\partial m^2} + \frac{\partial\mathcal{F}_{2d}}{\partial m^2}\Big)\Delta_1 m^2. \end{aligned} \quad (32)$$

Note that some of the terms first contribute at order g^8 or higher. For example, the vacuum counterterm $\Delta_3\mathcal{E}_0$ first contributes at order $m^4\alpha^2 \sim g^8$.

The expressions for the diagrams $\mathcal{F}_{3a}$–$\mathcal{F}_{3j}$, in Fig. 4 are

$$\mathcal{F}_{3a} = \frac{1}{32} g^6 \Big(\oint_P \frac{1}{P^2 + m^2}\Big)^2 \Big(\oint_Q \frac{1}{(Q^2 + m^2)^2}\Big)^2, \quad (33)$$

$$\mathcal{F}_{3b} = \frac{1}{48} g^6 \Big(\oint_P \frac{1}{P^2 + m^2}\Big)^3 \oint_Q \frac{1}{(Q^2 + m^2)^3}, \quad (34)$$

$$\mathcal{F}_{3c} = \frac{1}{24} g^6 \oint_{PQR} \frac{1}{(P^2 + m^2)^2}\frac{1}{Q^2 + m^2}\frac{1}{R^2 + m^2} \times \frac{1}{(P + Q + R)^2 + m^2}\oint_S \frac{1}{S^2 + m^2} \quad (35)$$

$$\mathcal{F}_{3d} = \frac{1}{48} g^6 \oint_{PQRS} \frac{1}{Q^2 + m^2}\frac{1}{(P + Q)^2 + m^2}\frac{1}{R^2 + m^2} \times \frac{1}{(P + R)^2 + m^2}\frac{1}{S^2 + m^2}\frac{1}{(P + S)^2 + m^2}, \quad (36)$$

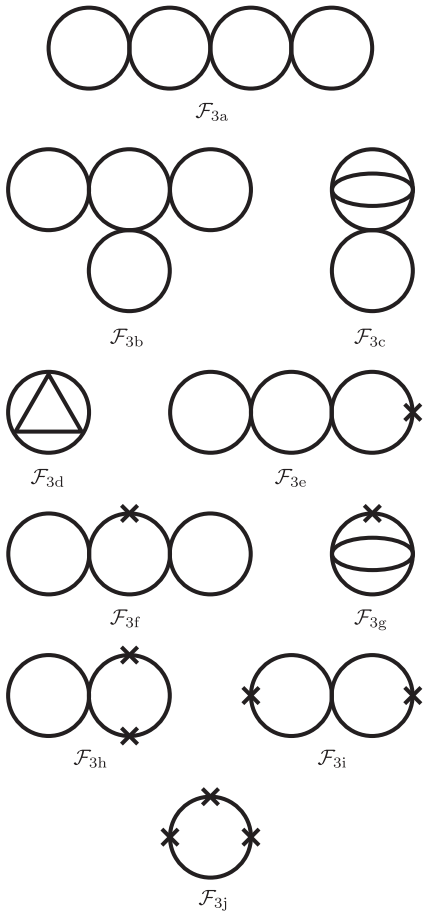

FIG. 4. Four-loop vacuum diagrams.

$$\mathcal{F}_{3e} = -\frac{1}{8}g^4m_1^2\oint_P \frac{1}{P^2+m^2}\left(\oint_Q \frac{1}{(Q^2+m^2)^2}\right)^2, \tag{37}$$

$$\mathcal{F}_{3f} = -\frac{1}{8}g^4m_1^2\left(\oint_P \frac{1}{P^2+m^2}\right)^2\oint_Q \frac{1}{(Q^2+m^2)^3}, \tag{38}$$

$$\mathcal{F}_{3g} = -\frac{1}{12}g^4m_1^2\oint_{PQR} \frac{1}{(P^2+m^2)^2}\,\frac{1}{Q^2+m^2}\,\frac{1}{R^2+m^2} \times \frac{1}{(P+Q+R)^2+m^2} \tag{39}$$

$$\mathcal{F}_{3h} = \frac{1}{4}g^2m_1^4\oint_P \frac{1}{P^2+m^2}\oint_Q \frac{1}{(Q^2+m^2)^3}, \tag{40}$$

$$\mathcal{F}_{3i} = \frac{1}{8}g^2m_1^4\left(\oint_P \frac{1}{(P^2+m^2)^2}\right)^2, \tag{41}$$

$$\mathcal{F}_{3j} = -\frac{1}{6}m_1^6\oint_P \frac{1}{(P^2+m^2)^3}. \tag{42}$$

Expanding the sum-integrals in powers of m^2 to the appropriate order gives

$$\begin{aligned}\mathcal{F}_{3a} = \frac{1}{32}g^6[&T^2I_2^2\mathcal{I}_1^2 + 2T^3I_1I_2^2\mathcal{I}_1 + 2TI_2\mathcal{I}_1^2\mathcal{I}_2 + \mathcal{I}_1^2\mathcal{I}_2^2 \\ &+ T^4I_1^2I_2^2 + 2TI_1\mathcal{I}_1\mathcal{I}_2^2 - 2m^2T^2I_2^2\mathcal{I}_1\mathcal{I}_2 \\ &- 2m^2T^3I_1I_2^2\mathcal{I}_2 + 4T^2I_1I_2\mathcal{I}_1\mathcal{I}_2 - 4m^2TI_2\mathcal{I}_1\mathcal{I}_2^2 \\ &+ 2T^3I_1^2I_2\mathcal{I}_2 - 4m^2TI_2\mathcal{I}_1^2\mathcal{I}_3],\end{aligned} \tag{43}$$

$$\begin{aligned}\mathcal{F}_{3b} = \frac{1}{48}g^6[&TI_3\mathcal{I}_1^3 + 3T^2I_1I_3\mathcal{I}_1^2 + 3T^3I_3I_1^2\mathcal{I}_1 \\ &- 3m^2TI_3\mathcal{I}_1^2\mathcal{I}_2 + \mathcal{I}_3\mathcal{I}_1^3 + T^4I_1^3I_3 \\ &- 6m^2T^2I_1I_3\mathcal{I}_1\mathcal{I}_2 + 3TI_1\mathcal{I}_1^2\mathcal{I}_3 - 3m^2T^3I_1^2I_3\mathcal{I}_2 \\ &+ 3m^4TI_3\mathcal{I}_1^2\mathcal{I}_3 + 3m^4TI_3\mathcal{I}_1\mathcal{I}_2^2],\end{aligned} \tag{44}$$

$$\begin{aligned}\mathcal{F}_{3c} = \frac{1}{24}g^6\Big[&(\mathcal{I}_1 + TI_1 - m^2\mathcal{I}_2)T^3I'_{\text{ball}} + (\mathcal{I}_1 + TI_1)\mathcal{I}'_{\text{ball}} \\ &+ 3T^2I_1I_2\mathcal{I}_1\mathcal{I}_2 - m^2TI_2\mathcal{I}_2\mathcal{I}_{\text{sun}} + 3T^3I_1^2I_2\mathcal{I}_2 \\ &+ 2\mathcal{I}_1(TI_1 - m^2TI_2)\oint_{QR}\frac{Q^2+(2/d)\mathbf{q}^2}{Q^6R^2(Q+R)^2}\Big],\end{aligned} \tag{45}$$

$$\begin{aligned}\mathcal{F}_{3d} = \frac{1}{48}g^6\Big[&\oint_P[\Pi(P)]^3 + T^4I_{\text{triangle}} \\ &+ 6TI_1\oint_P\frac{1}{P^2}[\Pi(P)]^2 + 3T^3\mathcal{I}_2I_{\text{ball}}\Big],\end{aligned} \tag{46}$$

$$\begin{aligned}\mathcal{F}_{3e} = -\frac{1}{8}g^4m_1^2[&T^2I_2^2\mathcal{I}_1 + T^3I_1I_2^2 + 2TI_2\mathcal{I}_1\mathcal{I}_2 \\ &- 2m^2TI_2\mathcal{I}_2^2 + \mathcal{I}_1\mathcal{I}_2^2 + 2T^2I_1I_2\mathcal{I}_2 - m^2T^2I_2^2\mathcal{I}_2 \\ &+ TI_1\mathcal{I}_2^2 - 4m^2TI_2\mathcal{I}_1\mathcal{I}_3],\end{aligned} \tag{47}$$

$$\begin{aligned}\mathcal{F}_{3f} = -\frac{1}{8}g^4m_1^2[&TI_3\mathcal{I}_1^2 + 2T^2I_3I_1\mathcal{I}_1 + T^3I_3I_1^2 \\ &- 2m^2TI_3\mathcal{I}_1\mathcal{I}_2 + \mathcal{I}_3\mathcal{I}_1^2 - 2T^2m^2I_3I_1\mathcal{I}_2 \\ &+ 2TI_1\mathcal{I}_1\mathcal{I}_3 + 2m^4TI_3\mathcal{I}_1\mathcal{I}_3 + m^4TI_3\mathcal{I}_2^2],\end{aligned} \tag{48}$$

$$\begin{aligned}\mathcal{F}_{3g} = -\frac{1}{12}g^4m_1^2\Big[&T^3I'_{\text{ball}} + \mathcal{I}'_{\text{ball}} + +3T^2I_1I_2\mathcal{I}_2 \\ &+ 2(TI_1 - m^2TI_2)\oint_{QR}\frac{Q^2+(2/d)\mathbf{q}^2}{Q^6R^2(Q+R)^2}\Big],\end{aligned} \tag{49}$$

$$\mathcal{F}_{3h} = \frac{1}{4} g^2 m_1^4 [T I_3 I_1 + T^2 I_1 I_3 + T I_1 I_3 - m^2 T I_2 I_3 + I_1 I_3 + m^4 T I_3 I_3], \quad (50)$$

$$\mathcal{F}_{3i} = \frac{1}{8} g^2 m_1^4 [T^2 I_2^2 + 2T I_2 I_2 + I_2^2 - 4m^2 T I_2 I_3], \quad (51)$$

$$\mathcal{F}_{3j} = -\frac{1}{6} m_1^6 [T I_3 + I_3], \quad (52)$$

where the self-energy $\Pi(P)$ is defined in Eq. (D2) and the integrals $I'_{\rm ball}$ and $I_{\rm triangle}$ are defined in Appendix B. The poles in Eqs. (43)–(52) are canceled by the counterterms in Eq. (32). The final result for the four-loop contribution to the free energy is

$$\begin{aligned}
\mathcal{F}_3 = {} & \frac{\pi^2 T^4}{90} \frac{5}{288} \frac{\alpha^3}{\hat{m}^3} \Bigg[1 + 18 \Bigg(11L + 3\gamma_E - 6 - 16\log 2 - 16\log\hat{m} - 8\frac{\zeta'(-1)}{\zeta(-1)} \Bigg) \hat{m}^2 \\
& + \Bigg(1236 + 108 C^a_{\rm triangle} + 36 C'_{\rm ball} + 288\gamma_1 - \frac{9198}{5}\gamma_E + 450\gamma_E^2 - \frac{6456}{5} L + 432\gamma_E L + 648 L^2 + 135\pi^2 \\
& - 54\pi^2 C^b_{\rm triangle} - 216\pi^2\gamma_E + (2100 - 72\gamma_E + 1728 L)\frac{\zeta'(-1)}{\zeta(-1)} + 432\Bigg(\frac{\zeta'(-1)}{\zeta(-1)}\Bigg)^2 - 432(\gamma_E + 2L)\frac{\zeta'(-3)}{\zeta(-3)} \\
& + 360\frac{\zeta''(-1)}{\zeta(-1)} + 1728\log 2 + 216\pi^2\log 2 + 432(4 - \pi^2)\log\hat{m} - 4534\zeta(3) \Bigg) \hat{m}^3 \\
& + \frac{9}{2} \Bigg(3742 - 288 C_I - 48 C'_{\rm ball} - 8064\gamma_1 - 6072\gamma_E - 2544\gamma_E^2 - 3904 L - 1872\gamma_E L - 2184 L^2 + 900\pi^2 \\
& + (1808 + 1824\gamma_E + 2496 L)\frac{\zeta'(-1)}{\zeta(-1)} - 288\frac{\zeta''(-1)}{\zeta(-1)} + 2688\gamma_E\log 2 + 4992 L\log 2 + 4992(\gamma_E + L)\log\hat{m} \\
& - 2304\gamma_E\log\pi + 2304\log^2(2\pi) - 15\zeta(3) \Bigg) \hat{m}^4 \Bigg] \\
& - \frac{\pi^2 T^4}{90} \frac{5}{16} \frac{\alpha^2 \hat{m}_1^2}{\hat{m}^3} \Bigg[1 + \Bigg(84 L + 36\gamma_E - 96\log\hat{m} - 36 - 96\log 2 - 48\frac{\zeta'(-1)}{\zeta(-1)} \Bigg) \hat{m}^2 \\
& + 2\Bigg(48(L + \gamma_E)^2 - 268(L + \gamma_E) - \gamma_E(17 - 21\gamma_E) + 48\gamma_1 - 34 - \frac{9\pi^2}{2} - \frac{\zeta'(-1)}{\zeta(-1)}(34 + 12\gamma_E) \\
& - 12\frac{\zeta''(-1)}{\zeta(-1)} + \zeta(3) + 6 C'_{\rm ball} \Bigg) \hat{m}^3 - 3(89 + 120(L + \gamma_E) + [18(L + \gamma_E)]^2 + 15\zeta(3))\hat{m}^4 \Bigg] \\
& + \frac{\pi^2 T^4}{90} \frac{15}{8} \frac{\alpha \hat{m}_1^4}{\hat{m}^3} \Bigg[1 + 18(L + \gamma_E)\hat{m}^2 + [24(L + \gamma_E)^2 + 2\zeta(3)]\hat{m}^3 - \frac{45}{2}\zeta(3)\hat{m}^4 \Bigg] - \frac{\pi^2 T^4}{90} \frac{15}{4} \frac{\hat{m}_1^6}{\hat{m}^3} [1 + 2\zeta(3)\hat{m}^3],
\end{aligned} \quad (53)$$

where the constants are

$$C'_{\rm ball} = 48.7976, \quad (54)$$

$$C^a_{\rm triangle} = -25.7055, \quad (55)$$

$$C^b_{\rm triangle} = 28.9250, \quad (56)$$

$$C_I = -38.5309. \quad (57)$$

There are a couple of calculational details that are worthwhile pointing out. The g^6 contribution arising from diagram $\mathcal{F}_{3d}$ when all momenta are hard (h) reads

$$\mathcal{F}^{\rm (hhhh)}_{3d} = \oint\!\!\!\!\!\!\sum_P [\Pi(P)]^3. \quad (58)$$

This term can be combined with the g^6 term arising from the counterterm $\mathcal{F}_{2b}\Delta_1 g^2 = -g^4 I_{\rm ball}\Delta_1 g^2/48$ and gives

$$\oint\!\!\!\!\!\!\sum_P \Bigg\{ [\Pi(P)]^3 - \frac{3}{(4\pi)^2\epsilon} [\Pi(P)]^2 \Bigg\}. \quad (59)$$

This particular combination was first calculated by Gynther *et al.* [13] using the methods of Arnold and Zhai. Similarly, we combine the g^7 term from $\mathcal{F}_{3d}$ with the term $T I_1 I_{\rm sun}$ from $\mathcal{F}_{2b}\Delta_1 g^2$, which gives

$$\oint\!\!\!\!\!\!\sum_P \frac{1}{P^2} \Bigg\{ [\Pi(P)]^2 - \frac{2}{(4\pi)^2\epsilon} [\Pi(P)] \Bigg\}. \quad (60)$$

We calculate this sum-integral in Appendix D. Finally, the term from $\mathcal{F}_{2b}\Delta_1 m^2$ which involves $I_{\rm sun}$ can be combined with the term $-m^2 I_2 I_2 I_{\rm sun}$ arising from $\mathcal{F}_{3c}$ to give

$$\frac{1}{24} g^6 m^2 I_2 \Bigg(\frac{1}{(4\pi)^2} \frac{1}{\epsilon} - I_2 \Bigg) I_{\rm sun}. \quad (61)$$

Since $I_{\rm sun}$ vanishes at order ϵ^0 and the term inside the parenthesis is finite, the particular combination (61) vanishes in the limit $\epsilon \to 0$.

E. Pressure to four loops

The pressure $\mathcal{P}$ is given by $-\mathcal{F}$. The contributions to the pressure of zeroth, first, second order, and third order in g^2 are given by Eqs. (15), (21), (31), and (53), respectively. Adding these contributions and setting $\mathcal{E}_0 = 0$ and $m_1^2 = m^2$, we obtain approximations to the pressure in screened perturbation theory which are accurate to $\mathcal{O}(g^7)$.

The one-loop approximation to the pressure is

$$\mathcal{P}_0 = \mathcal{P}_{\rm ideal}\Big[1 - 15\hat{m}^2 + 60\hat{m}^3 + 45\hat{m}^4(L+\gamma_E) - \frac{15}{2}\zeta(3)\hat{m}^6\Big], \tag{62}$$

where $\mathcal{P}_{\rm ideal} = \pi^2 T^4/90$ is the pressure of an ideal gas of massless particles.

The two-loop approximation to the pressure is obtained by adding Eq. (21) with $m_1^2 = m^2$:

$$\begin{aligned}\mathcal{P}_{0+1} = \mathcal{P}_{\rm ideal}\Big\{&1 - \frac{5}{4}\alpha + 15\hat{m}\alpha + 15\hat{m}^2(L+\gamma_E-3)\alpha \\ &- 30\hat{m}^3[1+3(L+\gamma_E)\alpha] \\ &- 45\hat{m}^4\Big[(L+\gamma_E) + \Big((L+\gamma_E)^2 + \frac{1}{12}\zeta(3)\Big)\alpha\Big] \\ &+ \frac{45}{2}\zeta(3)\hat{m}^5\alpha + 15\zeta(3)\hat{m}^6\Big\}.\end{aligned} \tag{63}$$

The three-loop approximation to the pressure is obtained by adding Eq. (31) with $m_1^2 = m^2$:

$$\begin{aligned}\mathcal{P}_{0+1+2} = \mathcal{P}_{\rm ideal}\Big\{&1 + \frac{5}{8\hat{m}}\alpha^2 - \frac{5}{4}\alpha + \Big(-\frac{59}{12} + \frac{15}{4}L + \frac{5}{4}\gamma_E + 5\frac{\zeta'(-1)}{\zeta(-1)} - \frac{5}{2}\frac{\zeta'(-3)}{\zeta(-3)}\Big)\alpha^2 \\ &+ \frac{15}{2}\hat{m}\Big[1 - \Big(5 + 3\gamma_E + 7L - 8\log\hat{m} - 8\log 2 - 4\frac{\zeta'(-1)}{\zeta(-1)}\Big)\alpha\Big]\alpha \\ &+ \frac{5}{8}\hat{m}^2\Big(268(L+\gamma_E) - 48(L+\gamma_E)^2 + \frac{\zeta'(-1)}{\zeta(-1)}(34+12\gamma_E) + 12\frac{\zeta''(-1)}{\zeta(-1)} + \gamma_E(17-21\gamma_E) + 34 \\ &+ \frac{9\pi^2}{2} - 48\gamma_1 - \zeta(3) - 6C'_{\rm ball}\Big)\alpha^2 - \frac{15}{2}\hat{m}^3\Big[1 - 6(L+\gamma_E)\alpha - \frac{1}{12}\Big(89 + 120(L+\gamma_E) + [18(L+\gamma_E)]^2 \\ &+ 15\zeta(3)\Big)\alpha^2\Big] + 45\hat{m}^4\Big((L+\gamma_E)^2 + \frac{1}{12}\zeta(3)\Big)\alpha - \frac{135}{4}\hat{m}^5\alpha\zeta(3) - \frac{15}{2}\hat{m}^6\zeta(3)\Big\}.\end{aligned} \tag{64}$$

The four-loop approximation to the pressure is obtained by adding Eq. (53) to Eq. (64), with $m_1^2 = m^2$:

$$\begin{aligned}\frac{\mathcal{P}_{0+1+2+3}}{\mathcal{P}_{\rm ideal}} = 1 &- \frac{5}{288}\frac{\alpha^3}{\hat{m}^3} + \frac{15}{16}\frac{1}{\hat{m}}\Big[\alpha^2 + \frac{1}{3}\Big(16\log\hat{m} + 6 - 3\gamma_E - 11L + 8\frac{\zeta'(-1)}{\zeta(-1)} + 16\log 2\Big)\alpha^3\Big] \\ &- \frac{5}{4}\Big[\alpha - \Big(3L - \frac{59}{15}\gamma_E + 4\frac{\zeta'(-1)}{\zeta(-1)} - 2\frac{\zeta'(-3)}{\zeta(-3)}\Big)\alpha^2 + \frac{1}{72}\Big(1236 + 36C'_{\rm ball} + 108C^a_{\rm triangle} + 288\gamma_1 \\ &- \frac{9198}{5}\gamma_E + 450\gamma_E^2 - \frac{6456}{5}L + 432\gamma_E L + 648L^2 + 135\pi^2 - 54\pi^2 C^b_{\rm triangle} - 216\pi^2\gamma_E \\ &+ (2100 - 72\gamma_E + 1728L)\frac{\zeta'(-1)}{\zeta(-1)} + 432\Big(\frac{\zeta'(-1)}{\zeta(-1)}\Big)^2 - 432(\gamma_E + 2L)\frac{\zeta'(-3)}{\zeta(-3)} + 360\frac{\zeta''(-1)}{\zeta(-1)} \\ &+ 1728\log 2 + 216\pi^2\log 2 + 432(4-\pi^2)\log\hat{m} - 4534\zeta(3)\Big)\alpha^3\Big] \\ &+ \frac{45}{8}\hat{m}\Big[\alpha - \frac{2}{3}\Big(13 + 3\gamma_E + 7L - 4\frac{\zeta'(-1)}{\zeta(-1)} - 8\log 2 - 8\log\hat{m}\Big)\alpha^2 \\ &- \frac{1}{72}\Big(3742 - 288C_I - 48C'_{\rm ball} - 8064\gamma_1 - 6072\gamma_E - 2544\gamma_E^2 - 3904L - 1872\gamma_E L - 2184L^2 + 900\pi^2 \\ &+ (1808 + 1824\gamma_E + 2496L)\frac{\zeta'(-1)}{\zeta(-1)} - 288\frac{\zeta''(-1)}{\zeta(-1)} + 2688\gamma_E\log 2 + 4992L\log 2 + 4992(\gamma_E + L)\log\hat{m} \\ &- 2304\gamma_E\log\pi + 2304\log^2(2\pi) - 15\zeta(3)\Big)\alpha^3\Big] - \frac{15}{4}\hat{m}^3\Big[1 - 3(L+\gamma_E)\alpha + \frac{1}{12}(89 + 120(L+\gamma_E) \\ &+ [18(L+\gamma_E)]^2 + 15\zeta(3))\alpha^2\Big] + \frac{135}{16}\zeta(3)\hat{m}^5\alpha.\end{aligned} \tag{65}$$

The final result for the pressure is given by Eq. (65). If we use the weak-coupling expansion for the mass parameter, $\hat{m}^2 = \alpha/6$, our result reduces to the weak-coupling expansion result through order α^3.[2] Inserting $\hat{m}^2$ into Eq. (65), we obtain

$$\mathcal{P} = \mathcal{P}_{\rm ideal}\Bigg\{1 - \frac{5}{4}\alpha + \frac{5\sqrt{6}}{3}\alpha^{3/2} + \frac{15}{4}\Bigg[\log\frac{\mu}{4\pi T} + C_4\Bigg]\alpha^2 - \frac{15\sqrt{6}}{2}\Bigg[\log\frac{\mu}{4\pi T} - \frac{2}{3}\log\alpha + C_5\Bigg]\alpha^{5/2} - \frac{45}{4}\Bigg[\log^2\frac{\mu}{4\pi T} - \frac{1}{3}\Bigg(\frac{269}{45} - 2\gamma_E - 8\frac{\zeta'(-1)}{\zeta(-1)} + 4\frac{\zeta'(-3)}{\zeta(-3)}\Bigg)\log\frac{\mu}{4\pi T} + \frac{1}{3}(4 - \pi^2)\log\alpha + C_6\Bigg]\alpha^3\Bigg\}, \tag{66}$$

where the constants C_4–C_6 are

$$C_4 \equiv -\frac{59}{45} + \frac{1}{3}\gamma_E + \frac{4}{3}\frac{\zeta'(-1)}{\zeta(-1)} - \frac{2}{3}\frac{\zeta'(-3)}{\zeta(-3)}, \tag{67}$$

$$C_5 \equiv \frac{5}{6} + \frac{1}{3}\gamma_E - \frac{2}{3}\log\frac{2}{3} - \frac{2}{3}\frac{\zeta'(-1)}{\zeta(-1)}, \tag{68}$$

$$C_6 \equiv \frac{1}{3}(4 - \pi^2)\log\frac{2}{3} + \frac{103}{54} + \frac{1}{18}C'_{\rm ball} - \frac{1}{6}C^a_{\rm triangle} - \frac{\pi^2}{12}C^b_{\rm triangle} + \frac{4}{9}\gamma_1 - \frac{511}{180}\gamma_E + \frac{25}{36}\gamma_E^2 + \frac{5\pi^2}{24} - \frac{\pi^2}{3}\gamma_E + \pi^2\log 2 + \Bigg(\frac{175}{54} - \frac{1}{9}\gamma_E\Bigg)\frac{\zeta'(-1)}{\zeta(-1)} + \frac{2}{3}\Bigg(\frac{\zeta'(-1)}{\zeta(-1)}\Bigg)^2 + \frac{5}{9}\frac{\zeta''(-1)}{\zeta(-1)} - \frac{2}{3}\gamma_E\frac{\zeta'(-3)}{\zeta(-3)} - \frac{2267}{324}\zeta(3). \tag{69}$$

The numerical values of C_4–C_6 are

$$C_4 = 1.097\,75, \tag{70}$$

$$C_5 = -0.027\,320\,5, \tag{71}$$

$$C_6 = -6.593\,63. \tag{72}$$

Gynther *et al.* [13] have calculated the pressure for an $O(N)$-symmetric theory at weak coupling through order g^6 using effective field theory methods. Our result agrees with theirs for $N = 1$.

Using the renormalization group equation for the running coupling constant to next-to-leading order,

$$\mu\frac{d\alpha}{d\mu} = 3\alpha^2 - \frac{17}{3}\alpha^3, \tag{73}$$

it is straightforward to verify that the result (66) is independent of the renormalization scale μ through order $g^6\log g$.

IV. GAP EQUATIONS AND NUMERICAL RESULTS

The mass parameter m in screened perturbation theory is completely arbitrary. In order to complete a calculation using SPT, we need a prescription for the mass parameter m as a function of g and T. One of the complications which arises from the ultraviolet divergences is that the parameters $\mathcal{E}_0$, m^2, m_1^2, and g^2 are all running parameters that depend on the renormalization scale μ.

The prescription of Karsch, Patkós, and Petreczky for $m_*(T)$ is the solution to the one-loop gap equation

$$m_*^2 = \frac{1}{2}\alpha(\mu_*)\Bigg[J_1(\beta m_*)T^2 - \Bigg(2\log\frac{\mu_*}{m_*} + 1\Bigg)m_*^2\Bigg], \tag{74}$$

where μ^* is the renormalization scale and $J_1(\beta m)$ is the function

$$J_1(\beta m) = 8\beta^2\int_0^\infty \frac{dpp^2}{(p^2+m^2)^{1/2}}\frac{1}{e^{\beta(p^2+m^2)^{1/2}} - 1}. \tag{75}$$

Their choice for the scale was $\mu_* = T$. In the weak-coupling limit, the solution to (74) is $m_* = g(\mu_*)T/\sqrt{24}$. The gap equation (74) is the renormalized version of the following equation:

$$m^2 = \frac{1}{2}g^2\sum\!\!\!\!\!\!\int_P \frac{1}{P^2 + m^2}. \tag{76}$$

There are many possibilities for generalizing (74) to higher orders in g. We will consider three different possibilities in the following.

A. Debye mass

One class of possibilities is to identify m_* with some physical mass in the system. The simplest choice is the Debye mass m_D defined by the location of the pole in the static propagator:

$$p^2 + m^2 + \Sigma(0, p) = 0, \qquad p^2 = -m_D^2. \tag{77}$$

The Debye mass is a well-defined quantity in scalar field theory and Abelian gauge theories at any order in perturbation theory. However, in non-Abelian gauge theories, it is plagued by infrared divergences beyond leading order [52].

B. Tadpole mass

The *tadpole mass* is another generalization of Eq. (74) to higher loops. It can be calculated by taking the partial derivative of the free energy $\mathcal{F}$ with respect to m^2 *before* setting $m_1 = m$:

[2]It is important to point out that we have only calculated part of the g^7 term in the weak-coupling expansion. See the discussion in Sec. V.

$$m_t^2 = g^2 \frac{\partial \mathcal{F}}{\partial m^2}\bigg|_{m_1=m}. \tag{78}$$

From this equation, we see that m_t^2 is proportional to the expectation value $\langle\phi^2\rangle$. The tadpole mass is well-defined at all orders in scalar field theory, but the generalization to gauge theories is problematic. The natural replacement of $\langle\phi^2\rangle$ would be $\langle A_\mu A_\mu\rangle$, which is a gauge-variant quantity.

C. Variational mass

There is another class of prescriptions that is variational in spirit. The results of SPT would be independent of m if they were calculated to all orders. This suggests choosing m to minimize the dependence of some physical quantity on m. The *variational mass* is defined by minimizing the free energy:

$$\frac{\partial \mathcal{F}}{\partial m^2} = 0. \tag{79}$$

The variational mass has the benefit that it is well-defined at all orders in perturbation theory and can easily be generalized to gauge theories.

D. Comparison

At one loop, the three different prescriptions give the same gap equation, Eq. (74). Moreover, it turns out that the two-loop tadpole mass coincides with the one-loop tadpole mass [18]. However, at two loops the screening and variational masses are ill-behaved [18]. The screening mass solution ceases to exist beyond $g \sim 2.6$ and the variational gap equation only has solutions in the vicinity of $g = 0$ for some values of L. In the following, we therefore restrict ourselves to the tadpole gap equation.

E. Tadpole gap equation through three loops

At one loop, the renormalized gap equation follows from Eq. (15) upon differentiation with respect to m^2 and can be written as

$$0 = \hat{m}^2 - \frac{1}{6}\alpha\bigg[1 - 6\hat{m} - 6\hat{m}^2(L + \gamma_E) + \frac{3}{2}\zeta(3)\hat{m}^4\bigg]. \tag{80}$$

At two loops, the renormalized gap equation follows from differentiating the sum of Eqs. (15) and (21) with respect to m, and setting $m_1 = m$. It can be written in the form

$$\begin{aligned} 0 = {} & \hat{m}^2 + \frac{\alpha^2}{12\hat{m}} - \frac{\alpha}{6}[1 + \alpha(3 - \gamma_E - L)] \\ & + \frac{1}{2}\hat{m}\alpha[1 - 3\alpha(\gamma_E + L)] \\ & - \hat{m}^2\alpha^2\bigg[(\gamma_E + L)^2 + \frac{\zeta(3)}{12}\bigg] + \frac{5}{8}\hat{m}^3\alpha^2\zeta(3) \\ & + \frac{1}{4}m^4\alpha\zeta(3). \end{aligned} \tag{81}$$

At three loops, the renormalized gap equation follows from differentiating the sum of Eqs. (15), (21), and (31) and setting $m_1 = m$. This yields

$$\begin{aligned} 0 = {} & \hat{m}^2 + \frac{1}{8}\frac{\alpha^2}{\hat{m}}\bigg\{1 + \alpha\bigg[1 - \gamma_E - \frac{7}{3}L + \frac{4}{3}\frac{\zeta'(-1)}{\zeta(-1)} + \frac{8}{3}\log 2 + \frac{8}{3}\log\hat{m}\bigg]\bigg\} - \frac{\alpha}{6}\bigg\{1 - \alpha(L + \gamma_E - 3) \\ & + \alpha^2\bigg[2(L + \gamma_E)^2 - \frac{17}{12} + 2\gamma_1 - \frac{67}{6}(L + \gamma_E) - \frac{1}{24}\gamma_E(17 - 21\gamma_E) - \frac{3\pi^2}{16} - \frac{17}{12}\frac{\zeta'(-1)}{\zeta(-1)} - \frac{1}{2}\gamma_E\frac{\zeta'(-1)}{\zeta(-1)} \\ & - \frac{1}{2}\frac{\zeta''(-1)}{\zeta(-1)} + \frac{1}{24}\zeta(3) + \frac{1}{4}C'_{\rm ball}\bigg]\bigg\} + \frac{3}{8}\hat{m}\alpha\bigg\{1 - 2\alpha(L + \gamma_E) + \alpha^2\bigg[9(L + \gamma_E)^2 + \frac{10}{3}(L + \gamma_E) + \frac{89}{36} + \frac{5}{12}\zeta(3)\bigg]\bigg\} \\ & - \frac{5}{16}\hat{m}^3\alpha^2\zeta(3). \end{aligned} \tag{82}$$

F. Numerical results

The two-loop SPT-improved approximation to the pressure is obtained by inserting the solution to the one-loop gap equation (80) into the two-loop pressure (63). In Fig. 5 (a) we show the various truncations to the two-loop SPT-improved approximation to the $\mathcal{P}/\mathcal{P}_{\rm ideal}$ as a function of $g(2\pi T)$. We notice that the various truncations converge quickly. The order-g^4 to order-g^7 results are almost indistinguishable and essentially equal to the exact numerical two-loop result in Ref. [18]. In the three-loop case, we insert the solution to the two-loop gap equation (81) into the three-loop pressure (64). In Fig. 5(b), we show the various truncations to the three-loop SPT-improved approximation to $\mathcal{P}/\mathcal{P}_{\rm ideal}$ as a function of $g(2\pi T)$. The three-loop result also converges to the exact numerical three-loop result, albeit not as fast as in the two-loop case. At four loops, we insert the solution to the three-loop gap equation (82) into the four-loop pressure (65). In Fig. 5(c), we show the various truncations to the four-loop SPT-improved approximation to $\mathcal{P}/\mathcal{P}_{\rm ideal}$ as a function of $g(2\pi T)$. Although we cannot compare our successive approximations with a numerically exact four-loop result for the pressure, we expect them to converge reasonably fast. Based on the experience with the two- and three-loop approximations, we expect that the g^7 truncation provides a good approximation to the numerically exact result.

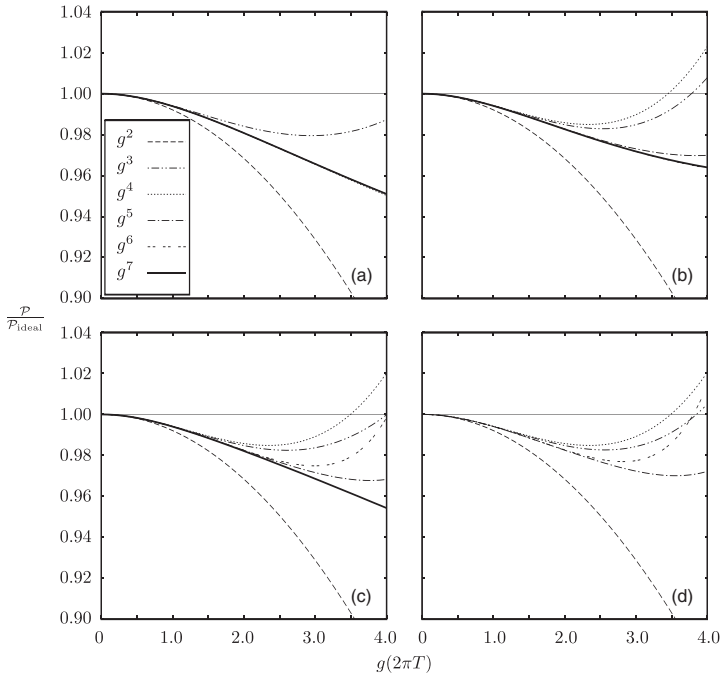

FIG. 5. (a) Two-loop pressure, (b) three-loop pressure, (c) four-loop pressure, (d) weak-coupling expansion of the pressure, all normalized to $\mathcal{P}_{\rm ideal}$.

Clearly, however, only a calculation through g^8 can settle this issue firmly. In Fig. 5(d), we show the weak-coupling expansion of $\mathcal{P}/\mathcal{P}_{\rm ideal}$ to orders g^2, g^3, g^4, g^5, and g^6 as a function of $g(2\pi T)$ for comparison. Note that the results to order g^2 are identical in SPT and in the weak-coupling expansion since there is no m-dependence at this order.

In Fig. 6(a), we show the two-, three-, and four-loop pressure through order g^7 normalized to $\mathcal{P}/\mathcal{P}_{\rm ideal}$ as a function of $g(2\pi T)$. In Fig. 6(b), we show the weak-coupling expansion of $\mathcal{P}/\mathcal{P}_{\rm ideal}$ to orders g^2, g^3, g^4, g^5, and g^6 as a function of $g(2\pi T)$ for comparison. The successive approximations using screened perturbation theory have better convergence properties than the weak-coupling results. The improved stability is partly due to the fact that we are using a thermal mass determined by a gap equation and not by the perturbative value for the Debye mass.

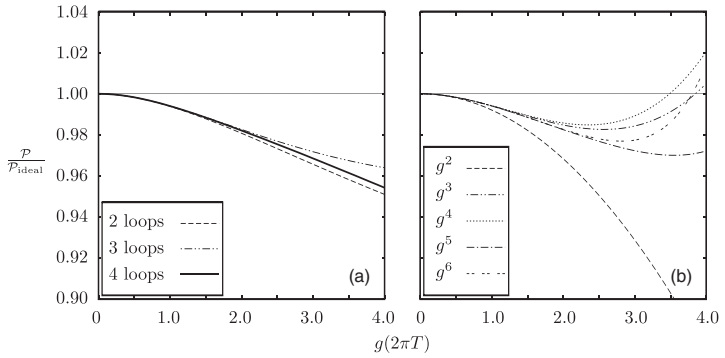

FIG. 6. (a) Pressure normalized to $\mathcal{P}_{\rm ideal}$ through g^7 for various loop orders, (b) weak-coupling pressure at various orders of g.

V. SUMMARY AND OUTLOOK

In this paper, we have calculated the pressure of massless scalar field theory to four loops using screened perturbation theory expanding in a double expansion in powers of g^2 and m/T. Treating m as $\mathcal{O}(gT)$, we truncated our expansion at order g^7. The expansion required the evaluation of a new nontrivial three-loop diagram, where we evaluated the sum-integral using the techniques developed in Ref. [10]. We have seen that the successive approximations are more stable than the weak-coupling expansion. In particular, it is interesting to note that the four-loop curve lies between the two-loop curve and the three-loop curve. The apparent improved convergence seemed to be linked to the fact that SPT basically is an expansion about an ideal gas of massive particles instead of an expansion about an ideal gas of massless particles which is the case for the weak-coupling expansion.

Using the weak-coupling value for the mass parameter m, our result reduces to the weak-coupling result for the pressure through g^6. In particular, we have reproduced the pressure at weak coupling for $N = 1$ obtained by Gynther *et al.* [13]. Using effective-field theory methods, the authors in Ref. [13] have calculated the hard and soft contributions to the pressure through order g^6 separately. It appears that the convergence properties in the hard sector are better than in the soft sector even for moderate values of the coupling.

We have mentioned that our result only includes part of the full g^7 term in the weak-coupling expansion. This is straightforward to see, if one uses the effective-field theory approach developed in [6]. The contributions to the free energy comes from the two momentum scales T and gT. The contribution from the hard scale T can be calculated by evaluating the sum-integrals with bare propagators and so is therefore a series in g^2 starting at order g^0. The contribution to the free energy from the soft scale gT can be calculated using an effective Euclidean three-dimensional field theory whose coefficients depend on g and T. This contribution to the free energy is a series in g starting at g^3. The contributions to the free energy that are odd in powers in g are therefore entirely coming from three-dimensional vacuum diagrams and power-counting tells you immediately that part of the g^7 term is arising from the five-loop vacuum diagrams. Our four-loop calculation therefore agrees with the weak-coupling expansion through order g^6.

In order to evaluate the free energy to order g^7, we must determine all the coefficients in the effective theory to sufficiently high order in g. The only nontrivial calculation that is required is to determine the mass parameter in the effective theory to order g^6. This involves the expression for the diagram calculated in Appendix D i.e. the sum-integral

$$I \equiv \sum\!\!\!\!\!\!\int_P \frac{1}{P^2}\left\{[\Pi(P)]^2 - \frac{2}{(4\pi)^2\epsilon}\Pi(P)\right\}. \tag{83}$$

The evaluation of the free energy to order g^7 is in progress [53].

ACKNOWLEDGMENTS

J. O. A. would like to thank E. Braaten, M. Laine, and M. Strickland for valuable discussions, and thank E. Braaten and M. Strickland for collaboration on related work on SPT.

APPENDIX A: SUM-INTEGRALS

In the imaginary-time formalism for thermal field theory, the four-momentum $P = (P_0, \mathbf{p})$ is Euclidean with $P^2 = P_0^2 + \mathbf{p}^2$. The Euclidean energy p_0 has discrete values: $P_0 = 2n\pi T$ for bosons, where n is an integer. Loop diagrams involve sums over P_0 and integrals over $\mathbf{p}$. With dimensional regularization, the integral is generalized to $d = 3 - 2\epsilon$ spatial dimensions. We define the dimensionally regularized sum-integral by

$$\sum\!\!\!\!\!\!\int_P \equiv \left(\frac{e^\gamma\mu^2}{4\pi}\right)^\epsilon T \sum_{P_0=2n\pi T} \int \frac{d^{3-2\epsilon}p}{(2\pi)^{3-2\epsilon}}, \tag{A1}$$

where $3 - 2\epsilon$ is the dimension of space and μ is an arbitrary momentum scale. The factor $(e^\gamma/4\pi)^\epsilon$ is introduced so that, after minimal subtraction of the poles in ϵ due to ultraviolet divergences, μ coincides with the renormalization scale of the $\overline{\text{MS}}$ renormalization scheme.

1. One-loop sum-integrals

The massless one-loop sum-integral is given by

$$\begin{aligned} I_n &\equiv \sum\!\!\!\!\!\!\int_P \frac{1}{P^{2n}} \\ &= (e^{\gamma_E}\mu^2)^\epsilon \frac{\zeta(2n-3+2\epsilon)}{8\pi^2} \frac{\Gamma(n-\frac{3}{2}+\epsilon)}{\Gamma(\frac{1}{2})\Gamma(n)} \\ &\quad \times (2\pi T)^{4-2n-2\epsilon}, \end{aligned} \tag{A2}$$

where $\zeta(x)$ is Riemann's zeta function. Specifically, we need the sum-integrals:

$$I'_0 \equiv \sum\!\!\!\!\!\!\int_P \log P^2 = -\frac{\pi^2 T^4}{45}[1 + \mathcal{O}(\epsilon)], \tag{A3}$$

$$\begin{aligned} I_1 = \frac{T^2}{12}\left(\frac{\mu}{4\pi T}\right)^{2\epsilon}\Bigg[1 + \left(2 + 2\frac{\zeta'(-1)}{\zeta(-1)}\right)\epsilon \\ + \left(4 + \frac{\pi^2}{4} + 4\frac{\zeta'(-1)}{\zeta(-1)} + 2\frac{\zeta''(-1)}{\zeta(-1)}\right)\epsilon^2 + \mathcal{O}(\epsilon^3)\Bigg], \end{aligned} \tag{A4}$$

$$I_2 = \frac{1}{(4\pi)^2}\left(\frac{\mu}{4\pi T}\right)^{2\epsilon}\left[\frac{1}{\epsilon} + 2\gamma_E + \left(\frac{\pi^2}{4} - 4\gamma_1\right)\epsilon + \mathcal{O}(\epsilon^2)\right], \tag{A5}$$

$$I_3 = \frac{1}{(4\pi)^4 T^2}[2\zeta(3) + \mathcal{O}(\epsilon)]. \tag{A6}$$

2. Two-loop sum-integrals

We need two two-loop sum-integrals that are listed below:

$$I_{\rm sun} = \sum\!\!\!\!\!\!\int_{PQ} \frac{1}{P^2Q^2(P+Q)^2} = \mathcal{O}(\epsilon), \tag{A7}$$

$$\sum\!\!\!\!\!\!\int_{PQ} \frac{P^2 + (2/d)p^2}{P^6Q^2(P+Q)^2} = \frac{3}{4(4\pi)^4}\left(\frac{\mu}{4\pi T}\right)^{4\epsilon} \times\left[\frac{1}{\epsilon^2} + \left(\frac{5}{6} + 4\gamma_E\right)\frac{1}{\epsilon} + \frac{89}{36} + \frac{\pi}{2} + \frac{10}{3}\gamma_E + 4\gamma_E^2 - 8\gamma_1 + \mathcal{O}(\epsilon)\right]. \tag{A8}$$

The setting-sun sum-integral was first calculated by Arnold and Zhai in Ref. [10], while Eq. (A8) was calculated in Ref. [40].

3. Three-loop sum-integrals

We need the following three-loop sum-integrals:

$$I_{\rm ball} = \sum\!\!\!\!\!\!\int_{PQR} \frac{1}{P^2Q^2R^2(P+Q+R)^2} = \frac{T^4}{24(4\pi)^2}\left(\frac{\mu}{4\pi T}\right)^{6\epsilon}\left[\frac{1}{\epsilon} + \frac{91}{15} + 8\frac{\zeta'(-1)}{\zeta(-1)} - 2\frac{\zeta'(-3)}{\zeta(-3)} + \mathcal{O}(\epsilon)\right], \tag{A9}$$

$$I'_{\rm ball} = \sum\!\!\!\!\!\!\int_{PQR} \frac{1}{P^4Q^2R^2(P+Q+R)^2} = \frac{T^2}{8(4\pi)^4}\left(\frac{\mu}{4\pi T}\right)^{6\epsilon}\left[\frac{1}{\epsilon^2} + \left(\frac{17}{6} + 4\gamma_E + 2\frac{\zeta'(-1)}{\zeta(-1)}\right)\frac{1}{\epsilon} + \frac{1}{2}\gamma_E\left(17 + 15\gamma_E + 12\frac{\zeta'(-1)}{\zeta(-1)}\right) + C'_{\rm ball} + \mathcal{O}(\epsilon)\right], \tag{A10}$$

$$\sum\!\!\!\!\!\!\int_P \frac{1}{P^2}\left\{[\Pi(P)]^2 - \frac{2}{(4\pi)^2\epsilon}\Pi(P)\right\} = -\frac{T^2}{4(4\pi)^4}\left(\frac{\mu}{4\pi T}\right)^{6\epsilon}\left\{\frac{1}{\epsilon^2} + \frac{1}{\epsilon}\left[\frac{4}{3} + 2\frac{\zeta'(-1)}{\zeta(-1)} + 4\gamma_E\right] + \frac{1}{3}\left[46 - 8\gamma_E - 16\gamma_E^2 - 104\gamma_1 - 24\gamma_E\log(2\pi) + 24\log^2(2\pi) + \frac{45\pi^2}{4} + 24\frac{\zeta'(-1)}{\zeta(-1)} + 2\frac{\zeta''(-1)}{\zeta(-1)} + 16\gamma_E\frac{\zeta'(-1)}{\zeta(-1)}\right] + C_I + \mathcal{O}(\epsilon)\right\}, \tag{A11}$$

where $C'_{\rm ball} = 48.7976$ and $C_I = -38.5309$. The massless basketball sum-integral was first calculated in Ref. [10] and $I'_{\rm ball}$in Ref. [13]. The expression for the sum-integral Eq. (A11) appears here for the first time and is calculated in Appendix D.

4. Four-loop sum-integrals

We also need a single four-loop sum-integral which was calculated in Ref. [13]:

$$\sum\!\!\!\!\!\!\int_P \left\{[\Pi(P)]^3 - \frac{3}{(4\pi)^2\epsilon}[\Pi(P)]^2\right\} = -\frac{T^4}{16(4\pi)^4}\left[\frac{1}{\epsilon^2} + \left(\frac{10}{3} + 4\frac{\zeta'(-1)}{\zeta(-1)} + 4L\right)\frac{1}{\epsilon} + (2L+\gamma_E)^2 + \left(\frac{6}{5} - 2\gamma_E + 4\frac{\zeta'(-3)}{\zeta(-3)}\right)(2L+\gamma_E) + C^a_{\rm triangle}\right] - \frac{T^4}{512(4\pi)^2}\left[\frac{1}{\epsilon} + 8L + 4\gamma_E + C^b_{\rm triangle}\right] + \mathcal{O}(\epsilon), \tag{A12}$$

where $C^a_{\rm triangle} = -25.7055$ and $C^b_{\rm triangle} = 28.9250$.

APPENDIX B: THREE-DIMENSIONAL INTEGRALS

Dimensional regularization can be used to regularize both the ultraviolet divergences and infrared divergences in three-dimensional integrals over momenta. The spatial dimension is generalized to $d = 3 - 2\epsilon$ dimensions. Integrals are evaluated at a value of d for which they converge and then analytically continued to $d = 3$. We use the integration measure

$$\int_p \equiv \left(\frac{e^\gamma\mu^2}{4\pi}\right)^\epsilon \int \frac{d^{3-2\epsilon}p}{(2\pi)^{3-2\epsilon}}. \tag{B1}$$

1. One-loop integrals

The one-loop integral is given by

$$I_n \equiv \int_p \frac{1}{(p^2+m^2)^n} = \frac{1}{8\pi}(e^{\gamma_E}\mu^2)^\epsilon \frac{\Gamma(n - \frac{3}{2} + \epsilon)}{\Gamma(\frac{1}{2})\Gamma(n)} m^{3-2n-2\epsilon}. \tag{B2}$$

Specifically, we need:

$$I'_0 \equiv \int_p \log(p^2+m^2) = -\frac{m^3}{6\pi}\left(\frac{\mu}{2m}\right)^{2\epsilon}\left[1 + \frac{8}{3}\epsilon + \left(\frac{52}{9} + \frac{\pi^2}{4}\right)\epsilon^2 + \mathcal{O}(\epsilon^3)\right], \tag{B3}$$

$$I_1 = -\frac{m}{4\pi}\left(\frac{\mu}{2m}\right)^{2\epsilon}\left[1 + 2\epsilon + \left(4 + \frac{\pi^2}{4}\right)\epsilon^2 + \mathcal{O}(\epsilon^3)\right], \tag{B4}$$

$$I_2 = \frac{1}{8\pi m}\left(\frac{\mu}{2m}\right)^{2\epsilon}\left[1 + \frac{\pi^2}{4}\epsilon^2 + \mathcal{O}(\epsilon^3)\right], \tag{B5}$$

$$I_3 = \frac{1}{32\pi m^3}\left(\frac{\mu}{2m}\right)^{2\epsilon}\left[1 + 2\epsilon + \frac{\pi^2}{4}\epsilon^2 + \mathcal{O}(\epsilon^3)\right]. \tag{B6}$$

2. Three-loop integrals

We need two three-loop integrals:

$$\begin{aligned} I_{\text{ball}} &= \int_{pqr} \frac{1}{p^2+m^2}\frac{1}{q^2+m^2}\frac{1}{r^2+m^2}\frac{1}{(\mathbf{p}+\mathbf{q}+\mathbf{r})^2+m^2} \\ &= -\frac{m}{(4\pi)^3}\left(\frac{\mu}{2m}\right)^{6\epsilon}\left[\frac{1}{\epsilon} + 8 - 4\log 2\right. \\ &\quad \left. + 4\left(13 + \frac{17}{48}\pi^2 - 8\log 2 + \log^2 2\right)\epsilon + \mathcal{O}(\epsilon^2)\right], \end{aligned} \tag{B7}$$

$$\begin{aligned} I'_{\text{ball}} &= \int_{pqr} \frac{1}{(p^2+m^2)^2}\frac{1}{q^2+m^2}\frac{1}{r^2+m^2} \\ &\quad \times \frac{1}{(\mathbf{p}+\mathbf{q}+\mathbf{r})^2+m^2} \\ &= \frac{1}{8m(4\pi)^3}\left(\frac{\mu}{2m}\right)^{6\epsilon}\left[\frac{1}{\epsilon} + 2 - 4\log 2\right. \\ &\quad \left. + 4\left(1 + \frac{17}{48}\pi^2 - 2\log 2 + \log^2 2\right)\epsilon + \mathcal{O}(\epsilon^2)\right]. \end{aligned} \tag{B8}$$

The massive basketball was calculated in Ref. [6] to order ϵ^0, and to order ϵ in Ref. [54]. The other three-loop integral is obtained by differentiating the massive basketball with respect to the mass m.

3. Four-loop integrals

We need a single four-loop integral, namely, the triangle integral. This integral was calculated in Ref. [54] and reads

$$\begin{aligned} I_{\text{triangle}} &= \int_{pqrs} \frac{1}{q^2+m^2}\frac{1}{(\mathbf{p}+\mathbf{q})^2+m^2}\frac{1}{r^2+m^2} \\ &\quad \times \frac{1}{(\mathbf{p}+\mathbf{r})^2+m^2}\frac{1}{s^2+m^2}\frac{1}{(\mathbf{p}+\mathbf{s})^2+m^2} \\ &= \frac{\pi^2}{32(4\pi)^4}\left(\frac{\mu}{2m}\right)^{8\epsilon}\left[\frac{1}{\epsilon} + 2 + 4\log 2 - \frac{84}{\pi^2}\zeta(3)\right. \\ &\quad \left. + \mathcal{O}(\epsilon)\right]. \end{aligned} \tag{B9}$$

APPENDIX C: m/T EXPANSIONS

In this appendix, we list the m/T expansions of the sum-integrals we need. The sum-integrals include sums over the Matsubara frequencies $P_0 = 2\pi nT$ and integrals over the three-momentum $\mathbf{p}$. In the sum-integrals, two important mass scales appear. These are the *hard* scale $2\pi T$ and the *soft* scale m. The soft scale m is of order gT and at weak coupling this scale is well-separated from the hard scale, $m \ll 2\pi T$. We can therefore expand the sum-integrals as a Taylor series in powers of m/T.

First consider the simple one-loop sum-integral appearing in the expression for the one-loop free energy in Eq. (13):

$$\begin{aligned} \mathcal{F}_{0a} &= \frac{1}{2}\sum\!\!\!\!\!\!\int_P \log[P^2 + m^2] \\ &= \frac{1}{2}\sum\!\!\!\!\!\!\int_P^{(\text{h})} \log[P^2 + m^2] + \frac{1}{2}\sum\!\!\!\!\!\!\int_P^{(\text{s})} \log[P^2 + m^2], \end{aligned} \tag{C1}$$

where the superscripts (h) and (s) denote the hard and soft contributions, respectively. In the hard region, the momentum P is of order T and so we can expand in powers of m^2/P^2. This yields

$$\begin{aligned} \sum\!\!\!\!\!\!\int_P^{(\text{h})} \log[P^2 + m^2] &= \sum\!\!\!\!\!\!\int_P \log P^2 + m^2\sum\!\!\!\!\!\!\int_P \frac{1}{P^2} \\ &\quad - \frac{1}{2}m^4\sum\!\!\!\!\!\!\int_P \frac{1}{P^4} + \cdots. \end{aligned} \tag{C2}$$

The contribution from soft momenta is given by the $p_0 = 0$ mode alone and reads

$$\sum\!\!\!\!\!\!\int_P^{(\text{s})} \log[P^2 + m^2] = T\int_p \log(p^2 + m^2). \tag{C3}$$

The other simple one-loop sum-integrals are expanded in a similar manner.

We next consider the massive basketball diagram in Eq. (24):

$$\mathcal{I}_{\text{ball}}(m^2) = \sum\!\!\!\!\!\!\int_{PQR} \frac{1}{(P^2+m^2)(Q^2+m^2)(R^2+m^2)[(P+Q+R)^2+m^2]}. \tag{C4}$$

Equation (C4) involves three sum-integrals and so receives contributions from four momentum regions: (hhh), (hhs), (hss), and (sss). In the first case, where all the loop momenta are hard, we can expand the sum-integral in powers of m^2. This

yields

$$\mathcal{I}^{(\mathrm{hhh})}_{\mathrm{ball}}(m^2) = \oint\!\!\!\!\!\!\sum_{PQR} \frac{1}{P^2Q^2R^2(P+Q+R)^2} - 4m^2 \oint\!\!\!\!\!\!\sum_{PQR} \frac{1}{P^4Q^2R^2(P+Q+R)^2} + \cdots. \tag{C5}$$

When two momenta are hard and one is soft, the contribution reads

$$\begin{aligned}\mathcal{I}^{(\mathrm{hhs})}_{\mathrm{ball}}(m^2) &= 4T \int_p \frac{1}{p^2+m^2} \oint\!\!\!\!\!\!\sum_{QR} \frac{1}{Q^2+m^2} \frac{1}{R^2+m^2} \frac{1}{(\mathbf{p}+Q+R)^2+m^2} \\ &= 4T \int_p \frac{1}{p^2+m^2} \oint\!\!\!\!\!\!\sum_{QR} \frac{1}{Q^2R^2(Q+R)^2} - 8m^2T \int_p \frac{1}{p^2+m^2} \Big[\oint\!\!\!\!\!\!\sum_{QR} \frac{Q^2+(2/d)\mathbf{q}^2}{Q^6R^2(Q+R)^2} \Big] + \cdots. \end{aligned} \tag{C6}$$

When one momentum is hard and two are soft, the contribution is given by

$$\mathcal{I}^{(\mathrm{hss})}_{\mathrm{ball}}(m^2) = 6T^2 \int_{pq} \frac{1}{p^2+m^2} \frac{1}{q^2+m^2} \oint\!\!\!\!\!\!\sum_{R} \frac{1}{R^2+m^2} \frac{1}{(\mathbf{p}+\mathbf{q}+R)^2+m^2} = 6T^2 \int_{pq} \frac{1}{p^2+m^2} \frac{1}{q^2+m^2} \oint\!\!\!\!\!\!\sum_{R} \frac{1}{R^4} + \cdots. \tag{C7}$$

Finally, when all momenta are soft, the contribution is given by the massive basketball diagram I_{ball} in three dimensions:

$$\mathcal{I}^{(\mathrm{sss})}_{\mathrm{ball}}(m^2) = T^3 \int_{pqr} \frac{1}{p^2+m^2} \frac{1}{q^2+m^2} \frac{1}{r^2+m^2} \frac{1}{(\mathbf{p}+\mathbf{q}+\mathbf{r})^2+m^2}. \tag{C8}$$

The basketball diagram with a single mass insertion $\mathcal{I}'_{\mathrm{ball}}(m^2)$ can be calculated by differentiating the massive basketball diagram with respect to m^2. This yields

$$\begin{aligned}\mathcal{I}'_{\mathrm{ball}}(m^2) &= \oint\!\!\!\!\!\!\sum_{PQR} \frac{1}{(P^2+m^2)^2} \frac{1}{Q^2+m^2} \frac{1}{R^2+m^2} \frac{1}{(P+Q+R)^2+m^2} \\ &= \oint\!\!\!\!\!\!\sum_{PQR} \frac{1}{P^4Q^2R^2(P+Q+R)^2} + T \int_p \frac{1}{(p^2+m^2)^2} \oint\!\!\!\!\!\!\sum_{QR} \frac{1}{Q^2R^2(Q+R)^2} \\ &\quad + 2T \int_p \frac{p^2}{(p^2+m^2)^2} \Big[\oint\!\!\!\!\!\!\sum_{QR} \frac{Q^2+(2/d)\mathbf{q}^2}{Q^6R^2(Q+R)^2} \Big] + 3T^2 \int_{pq} \frac{1}{p^2+m^2} \frac{1}{(q^2+m^2)^2} \oint\!\!\!\!\!\!\sum_{R} \frac{1}{R^4} \\ &\quad + T^3 \int_{pqr} \frac{1}{(p^2+m^2)^2} \frac{1}{q^2+m^2} \frac{1}{r^2+m^2} \frac{1}{(\mathbf{p}+\mathbf{q}+\mathbf{r})^2+m^2} + \cdots. \end{aligned} \tag{C9}$$

Note that the second term is formally of order g^5, but it vanishes at order ϵ^0 due to the fact that $\mathcal{I}_{\mathrm{sun}} = \mathcal{O}(\epsilon)$.

The massive four-loop triangle sum-integral reads

$$\mathcal{I}_{\mathrm{triangle}}(m^2) = \oint\!\!\!\!\!\!\sum_{PQRS} \frac{1}{Q^2+m^2} \frac{1}{(P+Q)^2+m^2} \frac{1}{R^2+m^2} \frac{1}{(P+R)^2+m^2} \frac{1}{S^2+m^2} \frac{1}{(P+S)^2+m^2}. \tag{C10}$$

When all four momenta are hard, the leading contribution is given by setting $m = 0$, i.e.

$$\mathcal{I}^{(\mathrm{hhhh})}_{\mathrm{triangle}}(m^2) = \oint\!\!\!\!\!\!\sum_{PQRS} \frac{1}{Q^2(P+Q)^2R^2(P+R)^2S^2(P+S)^2}. \tag{C11}$$

When one of the momenta is hard and three are soft, we find

$$\mathcal{I}^{(\mathrm{hsss})}_{\mathrm{triangle}}(m^2) = 3T^3 \int_{pqr} \frac{1}{p^2+m^2} \frac{1}{q^2+m^2} \frac{1}{r^2+m^2} \frac{1}{(\mathbf{p}+\mathbf{q}+\mathbf{r})^2+m^2} \oint\!\!\!\!\!\!\sum_{S} \frac{1}{S^4} + \cdots.$$

This contribution is of order g^7. When one momentum is soft and three momenta are hard, the contribution is

$$\begin{aligned}\mathcal{I}^{(\mathrm{shhh})}_{\mathrm{triangle}}(m^2) &= 6T \int_s \frac{1}{s^2+m^2} \oint\!\!\!\!\!\!\sum_{PQR} \frac{1}{P^2+m^2} \frac{1}{Q^2+m^2} \frac{1}{(P+Q)^2+m^2} \frac{1}{R^2+m^2} \frac{1}{(P+R)^2+m^2} \\ &= 6T \int_s \frac{1}{s^2+m^2} \oint\!\!\!\!\!\!\sum_{PQR} \frac{1}{P^2Q^2R^2(P+Q)(P+R)^2} + \cdots. \end{aligned} \tag{C12}$$

This contribution is of order g^7. When all four loop momenta are soft, the contribution is given by the massive three-dimensional triangle diagram I_{triangle}:

$$\mathcal{I}^{(\mathrm{ssss})}_{\mathrm{triangle}}(m^2) = T^4 \int_{pqrs} \frac{1}{q^2+m^2}\frac{1}{(\mathbf{p}+\mathbf{q})^2+m^2}\frac{1}{r^2+m^2}\frac{1}{(\mathbf{p}+\mathbf{r})^2+m^2}\frac{1}{s^2+m^2}\frac{1}{(\mathbf{p}+\mathbf{s})^2+m^2}. \tag{C13}$$

This contribution is of order g^6. Finally, we notice that the contribution when two momenta are soft and two momenta are hard, is of higher order in the coupling g.

APPENDIX D: EXPLICIT CALCULATIONS

In this appendix, we illustrate the use of the calculational techniques developed by Arnold and Zhai in Ref. [10] to evaluate complicated multiloop diagrams. The strategy is to rewrite the original sum-integral into two sets of terms. The first type is ultraviolet divergent, but is sufficiently simple to be evaluated analytically using dimensional regularization. The second type is finite both in the ultraviolet and the infrared, but is normally so complicated that it must be evaluated numerically. In order to isolate the divergences in terms that are tractable, typically one or more subtractions are required.

We need to calculate the following three-loop diagram:

$$I \equiv \sum\!\!\!\!\!\!\int_P \frac{1}{P^2}\left\{[\Pi(P)]^2 - \frac{2}{(4\pi)^2\epsilon}\Pi(P)\right\}, \tag{D1}$$

where the self-energy $\Pi(P)$ is defined by

$$\Pi(P) = \sum\!\!\!\!\!\!\int_Q \frac{1}{Q^2(P+Q)^2}. \tag{D2}$$

The first term in Eq. (D1) arises from the m/T-expansion of the triangle sum-integral in four dimensions, while the second term arises from the term $TI_1\mathcal{I}_{\mathrm{sun}}$ which is a part of the counterterm $\mathcal{F}_{2\mathrm{b}}\Delta_1 g^2/g^2$.

At zero temperature, the self-energy is denoted by $\Pi^0(P)$ and reads

$$\Pi^0(P) = \frac{1}{(4\pi)^2}\left(\frac{e^{\gamma_E}\mu^2}{P^2}\right)^{\epsilon}\frac{\Gamma(\epsilon)\Gamma^2(1-\epsilon)}{\Gamma(2-2\epsilon)}. \tag{D3}$$

In order to isolate the UV divergences and simplify the calculations, we write the self-energy as

$$\Pi(P) = \frac{1}{(4\pi)^2\epsilon} + \Pi^0_s(P) + \Pi^T(P), \tag{D4}$$

where $\Pi^0_s(P)$ is the finite part of $\Pi^0(P)$, i.e. we have subtracted the divergent piece in Eq. (D3) from $\Pi^0(P)$:

$$\Pi^0_s(P) = \frac{1}{(4\pi)^2}\left\{\left(\frac{e^{\gamma_E}\mu^2}{P^2}\right)^{\epsilon}\frac{\Gamma(\epsilon)\Gamma^2(1-\epsilon)}{\Gamma(2-2\epsilon)} - \frac{1}{\epsilon}\right\}, \tag{D5}$$

and $\Pi^T(P)$ is the finite-temperature piece of $\Pi(P)$. In three dimensions, $\Pi^T(P)$ reads [10]

$$\Pi^T(P) = \frac{T}{(4\pi)^2}\int\frac{d^3r}{r^2}e^{i\mathbf{p}\cdot\mathbf{r}}\left(\coth\bar{r} - \frac{1}{\bar{r}}\right)e^{-|p_0|r}, \tag{D6}$$

where $\bar{r} = 2\pi T r$. In the following we need the UV limit of $\Pi^T(P)$. This happens to be given by the UV limit of the full self-energy (D2) and is given by [10]

$$\Pi^T_{\mathrm{UV}}(P) = \frac{2}{P^2}\sum\!\!\!\!\!\!\int_Q \frac{1}{Q^2}. \tag{D7}$$

Using the decomposition (D4), the integral in Eq. (D1) can be written as

$$I = -\frac{1}{(4\pi)^4\epsilon^2}\sum\!\!\!\!\!\!\int_P \frac{1}{P^2} + \sum\!\!\!\!\!\!\int_P \frac{1}{P^2}[\Pi^0_s(P)]^2 + 2\sum\!\!\!\!\!\!\int_P \frac{1}{P^2}\Pi^0_s(P)\Pi^T(P) + \sum\!\!\!\!\!\!\int_P \frac{1}{P^2}[\Pi^T(P)]^2. \tag{D8}$$

We now consider the different contributions to I. The first term in Eq. (D8) is a simple one-loop sum-integral and reads

$$I_1 = -\frac{1}{(4\pi)^4\epsilon^2}\sum\!\!\!\!\!\!\int_P \frac{1}{P^2} = -\left(\frac{\mu}{4\pi T}\right)^{2\epsilon}\frac{T^2}{12(4\pi)^4}\left[\frac{1}{\epsilon^2} + 2\left(1+\frac{\zeta'(-1)}{\zeta(-1)}\right)\frac{1}{\epsilon} + \frac{\pi^2}{4} + 4 + 4\frac{\zeta'(-1)}{\zeta(-1)} + 2\frac{\zeta''(-1)}{\zeta(-1)} + \mathcal{O}(\epsilon)\right]. \tag{D9}$$

The second term in Eq. (D8) contains no logarithmic UV divergences and so it is finite in dimensional regularization:

$$I_2 = \sum\!\!\!\!\!\!\int_P \frac{1}{P^2}[\Pi^0_s(P)]^2 = \frac{T^2}{12(4\pi)^4}\left[4 + \frac{\pi^2}{3} + 8\frac{\zeta'(-1)}{\zeta(-1)}\left(2+\log\frac{\mu}{4\pi T}\right) + 4\frac{\zeta''(-1)}{\zeta(-1)} + 4\left(2+\log\frac{\mu}{4\pi T}\right)^2\right] + \mathcal{O}(\epsilon). \tag{D10}$$

The third term requires a little more thought. Since the UV behavior of $\Pi^T(P)$ is $1/P^2$, the integrand $\Pi^0_s(P)\Pi^T(P)/P^2$ is logarithmically divergent in the ultraviolet. In order to isolate this divergence, we add and subtract $\Pi^T_{\mathrm{UV}}(P)$ from $\Pi^0_s(P)\Pi^T(P)/P^2$. Thus the third sum-integral in Eq. (D8) becomes

$$I_3 = 2\sum\!\!\!\!\!\!\int_P \frac{1}{P^2}\Pi^0_s(P)\Pi^T(P) = 2\sum\!\!\!\!\!\!\int{}'_P \frac{1}{P^2}\Pi^0_s(P)[\Pi^T(P) - \Pi^T_{\mathrm{UV}}(P)] + 2\sum\!\!\!\!\!\!\int{}'_P \frac{1}{P^2}\Pi^0_s(P)\Pi^T_{\mathrm{UV}}(P) + 2T\int_p \frac{1}{p^2}\Pi^0_s(p_0=0,p)\Pi^T(p_0=0,p), \tag{D11}$$

where we have isolated the contribution from the $p_0 = 0$ term since the contribution to I_3 from this term is infrared

divergent. In order to calculate the first term in Eq. (D11), we need $\Pi^T_{\rm UV}(P)$ in coordinate space. It is given by the small-r behavior of $\Pi^T(P)$ and reads

$$\Pi^T_{\rm UV}(P) = \frac{T}{(4\pi)^2}\int \frac{d^3r}{r^2} e^{i\mathbf{p}\cdot\mathbf{r}} \frac{\bar{r}}{3} e^{-|p_0|r}. \tag{D12}$$

This yields

$$\begin{aligned} I_3^{\rm a} &= 2{\sum\!\!\!\!\!\!\int}'_P \frac{1}{P^2}\Pi_s^0(P)[\Pi^T(P) - \Pi^T_{\rm UV}(P)] \\ &= \frac{2T^2}{(4\pi)^4}\int d^3r \frac{1}{r^2}\left(\coth\bar{r} - \frac{1}{\bar{r}} - \frac{\bar{r}}{3}\right)\sum_{p_0\neq 0} e^{-|p_0|r} \\ &\quad\times \int \frac{d^3p}{(2\pi)^3}\frac{e^{i\mathbf{p}\cdot\mathbf{r}}}{p_0^2+p^2}\left(2 + \log\frac{\mu^2}{p_0^2+p^2}\right). \end{aligned} \tag{D13}$$

The integral over three-momentum can be done analytically. We write it as

$$\int \frac{d^3p}{(2\pi)^3}\frac{e^{i\mathbf{p}\cdot\mathbf{r}}}{p_0^2+p^2}\left(2 + 2\log\frac{\mu}{4\pi T} + \log\frac{(4\pi T)^2}{p_0^2+p^2}\right), \tag{D14}$$

where the first two terms in the parentheses are independent of p, making this part of the integral a simple Fourier transform:

$$\begin{aligned} &\int \frac{d^3p}{(2\pi)^3}\frac{e^{i\mathbf{p}\cdot\mathbf{r}}}{p_0^2+p^2}\left(2 + 2\log\frac{\mu}{4\pi T}\right) \\ &\quad = \frac{e^{-|p_0|r}}{4\pi r}\left(2 + 2\log\frac{\mu}{4\pi T}\right). \end{aligned} \tag{D15}$$

Averaging over angles, the last term can be rewritten as

$$\begin{aligned} &\int \frac{d^3p}{(2\pi)^3}\frac{e^{i\mathbf{p}\cdot\mathbf{r}}}{p_0^2+p^2}\log\frac{(4\pi T)^2}{p_0^2+p^2} \\ &\quad = \frac{1}{4\pi^2 ir}\int_{-\infty}^{\infty} dp\, p \frac{e^{ipr}}{p_0^2+p^2}\log\frac{(4\pi T)^2}{p_0^2+p^2}. \end{aligned} \tag{D16}$$

The integrand has a branch cut starting at $p = i|p_0|$ running to $p = i\infty$, and a pole in $p = i|p_0|$. The contour can be deformed to wrap around the pole and the branch cut, and taking care to include contributions from both, one arrives at the result

$$\begin{aligned} &\int \frac{d^3p}{(2\pi)^3}\frac{e^{i\mathbf{p}\cdot\mathbf{r}}}{p_0^2+p^2}\log\frac{(4\pi T)^2}{p_0^2+p^2} \\ &\quad = \frac{e^{-|p_0|r}}{4\pi r}\left(\log\frac{2\bar{r}}{|\bar{p}_0|} + \gamma_E + e^{2|p_0|r}\mathrm{Ei}(-2|p_0|r)\right), \end{aligned} \tag{D17}$$

where $\bar{p}_0 = p_0/2\pi T = n$ and the exponential-integral function $\mathrm{Ei}(z)$ is defined as

$$\mathrm{Ei}\,(z) = -\int_{-z}^{\infty}\frac{dte^{-t}}{t}. \tag{D18}$$

Thus Eq. (D13) can be rewritten as

$$\begin{aligned} I_3^a &= \frac{2T^2}{(4\pi)^4}\int d^3r\frac{1}{r^2}\left(\coth\bar{r} - \frac{1}{\bar{r}} - \frac{\bar{r}}{3}\right)\sum_{p_0\neq 0}\frac{e^{-2|p_0|r}}{4\pi r} \\ &\quad\times\left(2 + \gamma_E + 2\log\frac{\mu}{4\pi T} + \log\frac{2\bar{r}}{|\bar{p}_0|}\right. \\ &\quad\left. + e^{2|p_0|r}\mathrm{Ei}(-2|p_0|r)\right). \end{aligned} \tag{D19}$$

The first three terms in the last parentheses are independent of r and p_0 and, for these terms, the integral over r and the sum over Matsubara modes can be evaluated analytically. In particular, we are able to find the coefficient of $\log\mu$. This is fortunate, because it allows us to check the consistency of our final result for the free energy. Let

$$\xi \equiv \frac{2T^2}{(4\pi)^4}\int d^3r\frac{1}{r^2}\left(\coth\bar{r} - \frac{1}{\bar{r}} - \frac{\bar{r}}{3}\right)\sum_{p_0\neq 0}\frac{e^{-2|p_0|r}}{4\pi r}. \tag{D20}$$

Integrating over angles and summing over Matsubara frequencies yields

$$\begin{aligned} \xi &= \frac{2T^2}{(4\pi)^4}\int_0^\infty \frac{d\bar{r}}{\bar{r}}\left(\coth\bar{r} - \frac{1}{\bar{r}} - \frac{\bar{r}}{3}\right)\frac{2}{e^{2\bar{r}}-1} \\ &= \frac{4T^2}{(4\pi)^4}\int_0^\infty \frac{d\bar{r}}{\bar{r}}\left(\frac{2}{e^{2\bar{r}}-1} + 1 - \frac{1}{\bar{r}} - \frac{\bar{r}}{3}\right)\frac{1}{e^{2\bar{r}}-1}. \end{aligned} \tag{D21}$$

The integral above is finite, but the individual terms are divergent for small $\bar{r}$. We therefore regulate them by multiplying by an extra factor $(2\bar{r})^\alpha$ and taking the limit $\alpha \to 0$ in the end. The basic integrals we need are

$$\int_0^\infty \frac{dtt^x}{e^t-1} = \Gamma(x+1)\zeta(x+1), \tag{D22}$$

$$\int_0^\infty \frac{dtt^x}{(e^t-1)^2} = \Gamma(x+1)[\zeta(x) - \zeta(x+1)]. \tag{D23}$$

This yields

$$\begin{aligned} \xi = \frac{4T^2}{(4\pi)^4}\Big[&2\Gamma(\alpha)[\zeta(\alpha-1) - \zeta(\alpha)] + \Gamma(\alpha)\zeta(\alpha) \\ &- 2\Gamma(\alpha-1)\zeta(\alpha-1) - \frac{1}{6}\Gamma(\alpha+1)\zeta(\alpha+1)\Big]. \end{aligned} \tag{D24}$$

The limit $\alpha \to 0$ is regular, and we obtain

$$\xi = -\frac{2T^2}{3(4\pi)^4}\left(1 + \gamma_E - 3\log(2\pi) + 2\frac{\zeta'(-1)}{\zeta(-1)}\right). \tag{D25}$$

The remaining integral over the coordinate r as well as the Matsubara sum in Eq. (D19) must be done numerically. Equation (D19) can then be written as

$$\begin{aligned} I_3^{\rm a} = -\frac{2T^2}{3(4\pi)^4}\Big[&\left(2 + \gamma_E + 2\log\frac{\mu}{4\pi T}\right) \\ &\times\left(1 + \gamma_E - 3\log(2\pi) + 2\frac{\zeta'(-1)}{\zeta(-1)}\right) + C\Big], \end{aligned} \tag{D26}$$

where the numerical constant C is

$$C = -\frac{3}{4\pi}\int\frac{d^3r}{r^3}\Big(\coth\bar{r} - \frac{1}{\bar{r}} - \frac{\bar{r}}{3}\Big)\sum_{p_0\neq 0}\Big(e^{-2|p_0|r}\log\frac{2\bar{r}}{|\bar{p}_0|} + \mathrm{Ei}(-2|p_0|r)\Big) = 0.003\,481\,4. \tag{D27}$$

The subtraction term in Eq. (D11) can be calculated with dimensional regularization and reads

$$\begin{aligned} I_3^{\rm b} &= 2\sum\!\!\!\!\!\!\int_P \frac{1}{P^2}\,\Pi_s^0(P)\Pi_{\rm UV}^T(P) \\ &= \frac{4}{(4\pi)^2}\sum\!\!\!\!\!\!\int_Q \frac{1}{Q^2}\sum\!\!\!\!\!\!\int_P \frac{1}{P^4}\Big\{\Big(\frac{e^{\gamma_E}\mu^2}{P^2}\Big)^{\epsilon}\frac{\Gamma(\epsilon)\Gamma^2(1-\epsilon)}{\Gamma(2-2\epsilon)} - \frac{1}{\epsilon}\Big\} \\ &= -\frac{T^2}{6(4\pi)^4}\Big[\frac{1}{\epsilon^2} + \Big(2\log\frac{\mu}{4\pi T} + 2\frac{\zeta'(-1)}{\zeta(-1)} + 1\Big)\frac{1}{\epsilon} \\ &\quad - 2\log^2\frac{\mu}{4\pi T} - 2\log\frac{\mu}{4\pi T}\Big(1 + 4\gamma_E - 2\frac{\zeta'(-1)}{\zeta(-1)}\Big) \\ &\quad + 2\frac{\zeta'(-1)}{\zeta(-1)} + 2\frac{\zeta''(-1)}{\zeta(-1)} - 1 - \frac{\pi^2}{12} - 4\gamma_E + 8\gamma_1\Big]. \end{aligned} \tag{D28}$$

The last term in Eq. (D11) is

$$\begin{aligned} I_3^{\rm c} &= 2T\int_p \frac{1}{p^2}\,\Pi_s^0(p_0=0,p)\Pi^T(p_0=0,p) \\ &= 2T\int_p \frac{1}{p^2}\,\Pi_s^0(p_0=0,p) \\ &\quad\times[\Pi(p_0=0,p) - \Pi^0(p_0=0,p)]. \end{aligned} \tag{D29}$$

The second term vanishes in dimensional regularization since there is no mass scale in the integral, i.e.

$$2T\int_p \frac{1}{p^2}\,\Pi_s^0(p_0=0,p)\Pi^0(p_0=0,p) = 0. \tag{D30}$$

In order to evaluate the first term in Eq. (D29), we must calculate $\Pi(p_0=0,p)$. Using Feynman parameters, we obtain

$$\begin{aligned} \Pi(p_0=0,p) &= \sum\!\!\!\!\!\!\int_Q \frac{1}{Q^2(\mathbf{p}+Q)^2} \\ &= T\Big(\frac{e^{\gamma_E}\mu^2}{4\pi}\Big)^{\epsilon}\frac{\Gamma(1/2+\epsilon)}{(4\pi)^{(3/2)-\epsilon}} \\ &\quad\times\sum_{q_0}\int_0^1\frac{dx}{[x(1-x)p^2+q_0^2]^{(1/2)+\epsilon}}. \end{aligned} \tag{D31}$$

Inserting the expression for $\Pi_s^0(p_0=0,p)$ and $\Pi(p_0=0,p)$, we obtain

$$\begin{aligned} I_3^{\rm c} &= \frac{2T^2}{(4\pi)^2}\Big(\frac{e^{\gamma_E}\mu^2}{4\pi}\Big)^{\epsilon}\frac{\Gamma(1/2+\epsilon)}{(4\pi)^{(3/2)-\epsilon}}\int_p\frac{1}{p^2} \\ &\quad\times\Big[\Big(\frac{e^{\gamma_E}\mu^2}{p^2}\Big)^{\epsilon}\frac{\Gamma(\epsilon)\Gamma^2(1-\epsilon)}{\Gamma(2-2\epsilon)} - \frac{1}{\epsilon}\Big] \\ &\quad\times\sum_{q_0}\int_0^1\frac{dx}{[x(1-x)p^2+q_0^2]^{(1/2)+\epsilon}}. \end{aligned} \tag{D32}$$

$$\begin{aligned} I_3^{\rm c} &= \frac{2T^2}{(4\pi)^4}\frac{(e^{\gamma}\mu^2)^{2\epsilon}}{2\pi}\frac{\Gamma(\frac{1}{2}+\epsilon)}{\Gamma(\frac{3}{2}-\epsilon)}\Big[(e^{\gamma}\mu^2)^{\epsilon}\frac{\Gamma(\epsilon)\Gamma^2(1-\epsilon)}{\Gamma(2-2\epsilon)}\int_0^{\infty}dp\,\frac{p^{-4\epsilon}}{(p^2+1)^{(1/2)+\epsilon}}\int_0^1 dx[x(1-x)]^{-(1/2)+2\epsilon}\sum_{q_0}{}'\frac{1}{|q_0|^{6\epsilon}} \\ &\quad - \frac{1}{\epsilon}\int_0^{\infty}dp\,\frac{p^{-2\epsilon}}{(p^2+1)^{(1/2)+\epsilon}}\int_0^1 dx[x(1-x)]^{-(1/2)+\epsilon}\sum_{q_0}{}'\frac{1}{|q_0|^{4\epsilon}}\Big] \\ &= \frac{2T^2}{(4\pi)^4}\Big(\frac{e^{\gamma}\mu^2}{4\pi^2T^2}\Big)^{2\epsilon}\frac{\Gamma(\frac{1}{2}+\epsilon)}{\Gamma(\frac{3}{2}-\epsilon)}\Big[\Big(\frac{e^{\gamma}\mu^2}{4\pi^2T^2}\Big)^{\epsilon}\frac{1}{2^{1+4\epsilon}\sqrt{\pi}}\frac{\Gamma(\epsilon)\Gamma^2(1-\epsilon)\Gamma(\frac{1}{2}-2\epsilon)\Gamma(3\epsilon)\Gamma(\frac{1}{2}+2\epsilon)}{\Gamma(2-2\epsilon)\Gamma(\frac{1}{2}+\epsilon)\Gamma(1+2\epsilon)}\zeta(6\epsilon) \\ &\quad - \frac{1}{4\pi\epsilon}\frac{\Gamma(\frac{1}{2}-\epsilon)\Gamma(\epsilon)\Gamma(\frac{1}{2}+\epsilon)}{\Gamma(1+\epsilon)}\zeta(4\epsilon)\Big], \end{aligned} \tag{D33}$$

where the prime indicates that we have omitted the $p_0=0$ mode from the sum. Expanding Eq. (D33) in powers of ϵ, we obtain

$$\begin{aligned} I_3^{\rm c} &= \frac{T^2}{6(4\pi)^4}\Big[\frac{1}{\epsilon^2} - \frac{2}{\epsilon} - 12 - \frac{11\pi^2}{3} - 24\log(2\pi) - 12\log^2(2\pi) - 24\log\frac{\mu}{4\pi T} - 12\log^2\frac{\mu}{4\pi T} \\ &\quad - 24\log(2\pi)\log\frac{\mu}{4\pi T} + 12\gamma_E^2 + 24\gamma_1\Big] + \mathcal{O}(\epsilon). \end{aligned} \tag{D34}$$

The last term in Eq. (D8) is

$$I_4 = \sum\!\!\!\!\!\!\int_P \frac{1}{P^2}[\Pi^T(P)]^2. \tag{D35}$$

Since the UV behavior of $\Pi^T(P)$ is $1/P^2$, the sum-integral in Eq. (D35) is UV finite. However, $\Pi_T(P)$ has a logarithmic infrared divergence for the $p_0 = 0$ mode. This implies that the sum-integral I_4 has linear and logarithmic IR divergences. The linear divergence is set to zero in dimensional regularization while the logarithmic is not. In order to isolate these divergences, we rewrite the sum-integral as

$$I_4 = \sum\!\!\!\!\!\!\int_P{}' \frac{1}{P^2}[\Pi^T(P)]^2 + T\int_p \frac{1}{p^2}[\Pi^T(p_0 = 0, p)]^2, \tag{D36}$$

where the prime indicates that we have omitted the $p_0 = 0$ mode from the sum. The primed sum-integral in Eq. (D36) is finite both in the ultraviolet and in the infrared. Using the three-dimensional representation of the $\Pi_T(P)$, Eq. (D6), the first term in Eq. (D36) can be written as

$$\begin{aligned} I_4^{\mathrm{a}} &= \sum\!\!\!\!\!\!\int_P{}' \frac{1}{P^2}[\Pi^T(P)]^2 \\ &= \frac{T^3}{(4\pi)^4}\sum_{p_0}{}' \int\frac{d^3p}{(2\pi)^3}\int\frac{d^3r}{r^2}\frac{d^3r'}{(r')^2}\frac{1}{p_0^2+p^2}\left(\coth\bar{r}-\frac{1}{\bar{r}}\right) \\ &\quad\times\left(\coth\bar{r}'-\frac{1}{\bar{r}'}\right)e^{i\mathbf{p}\cdot(\mathbf{r}+\mathbf{r}')}e^{-|p_0|(r+r')}. \end{aligned} \tag{D37}$$

The integral over three-momentum p corresponds to a Fourier transform of a massive propagator and so gives rise to a Yukawa potential. The sum over nonzero Matsubara frequencies can also be done analytically and we obtain

$$\begin{aligned} I_4^{\mathrm{a}} &= \frac{2T^3}{(4\pi)^5}\int\frac{d^3r}{r^2}\frac{d^3r'}{(r')^2}\frac{1}{|\mathbf{r}+\mathbf{r}'|}\left(\coth\bar{r}-\frac{1}{\bar{r}}\right)\left(\coth\bar{r}'-\frac{1}{\bar{r}'}\right) \\ &\quad\times\frac{1}{e^{\bar{r}+\bar{r}'+|\bar{\mathbf{r}}+\bar{\mathbf{r}}'|}-1}. \end{aligned} \tag{D38}$$

Averaging over angles, one finds

$$\begin{aligned} I_4^{\mathrm{a}} &= \frac{2T^2}{(4\pi)^4}\int_0^\infty\frac{d\bar{r}d\bar{r}'}{\bar{r}\bar{r}'}\left(\coth\bar{r}-\frac{1}{\bar{r}}\right)\left(\coth\bar{r}'-\frac{1}{\bar{r}'}\right) \\ &\quad\times[\log(e^{2(\bar{r}+\bar{r}')}-1)-\log(e^{\bar{r}+\bar{r}'+|\bar{r}-\bar{r}'|}-1) \\ &\quad+|\bar{r}-\bar{r}'|-\bar{r}-\bar{r}']. \end{aligned} \tag{D39}$$

The remaining integrals over $\bar{r}$ and $\bar{r}'$ must be done numerically and we obtain

$$I_4^{\mathrm{a}} = \frac{T^2}{(4\pi)^4}[0.058\,739\,2]. \tag{D40}$$

The second term in Eq. (D36) is rewritten as

$$\begin{aligned} I_4^{\mathrm{b}} &= T\int_p\frac{1}{p^2}[\Pi^T(p_0=0,p)]^2 \\ &= T\int_p\frac{1}{p^2}\{[\Pi^T(p_0=0,p)-\Pi_{\mathrm{IR}}^T(p)]^2 \\ &\quad+2\Pi^T(p_0=0,p)\Pi_{\mathrm{IR}}^T(p)-[\Pi_{\mathrm{IR}}^T(p)]^2\}, \end{aligned} \tag{D41}$$

where $\Pi_{\mathrm{IR}}(p)$ is given by the $q_0 = 0$ term in Eq. (D31):

$$\begin{aligned} \Pi_{\mathrm{IR}}^T(p) &= T\int_q\frac{1}{q^2(\mathbf{p}+\mathbf{q})^2} \\ &= T\left(\frac{e^{\gamma_E}\mu^2}{4\pi}\right)^\epsilon\frac{4^\epsilon\sqrt{\pi}}{(4\pi)^{(3/2)-\epsilon}} \\ &\quad\times\frac{\Gamma(1/2+\epsilon)\Gamma(1/2-\epsilon)}{\Gamma(1-\epsilon)}p^{-1-2\epsilon}. \end{aligned} \tag{D42}$$

The first integral in Eq. (D41) is now well-behaved in both the ultraviolet and the infrared. It can be evaluated numerically using the representation of $\Pi^T(p_0 = 0, p)$ in three dimensions. The subtracted terms are infrared divergent and are calculated with dimensional regularization. The first integral can be calculated directly in three dimensions. In this case, $\Pi_{\mathrm{IR}}^T(p)$ reduces to

$$\Pi_{\mathrm{IR}}^T(p) = \frac{T}{8p}. \tag{D43}$$

Using the three-dimensional representation (D6) for $\Pi^T(P)$ with $p_0 = 0$ and Eq. (D43), we get

$$\begin{aligned} I_4^{\mathrm{b1}} &= T\int_p\frac{1}{p^2}[\Pi^T(p_0=0,p)-\Pi_{\mathrm{IR}}^T(p)]^2 \\ &= T^3\int_p\frac{1}{p^2}\left[\frac{1}{(4\pi)^4}\int\frac{d^3r}{r^2}\frac{d^3r'}{(r')^2}e^{i\mathbf{p}\cdot(\mathbf{r}+\mathbf{r}')}\left(\coth r-\frac{1}{r}\right)\right. \\ &\quad\times\left(\coth\bar{r}'-\frac{1}{\bar{r}'}\right)-\frac{1}{4(4\pi)^2p}\int\frac{d^3r}{r^2}e^{i\mathbf{p}\cdot\mathbf{r}}\left(\coth\bar{r}-\frac{1}{\bar{r}}\right) \\ &\quad\left.+\frac{1}{64p^2}\right]. \end{aligned} \tag{D44}$$

The averages over the angles between $\mathbf{p}$ and $\mathbf{r}$, and between $\mathbf{p}$ and $\mathbf{r}'$ can be done analytically and we obtain

$$\begin{aligned} I_4^{\mathrm{b1}} &= T^3\int_p\frac{1}{p^2}\left[\frac{1}{(4\pi)^2}\int_0^\infty dr\int_0^\infty dr'\frac{\sin pr}{pr}\frac{\sin pr'}{pr'}\right. \\ &\quad\times\left(\coth r-\frac{1}{r}\right)\left(\coth\bar{r}'-\frac{1}{\bar{r}'}\right) \\ &\quad\left.-\frac{1}{4(4\pi)p}\int_0^\infty dr\frac{\sin pr}{pr}\left(\coth\bar{r}-\frac{1}{\bar{r}}\right)+\frac{1}{64p^2}\right]. \end{aligned} \tag{D45}$$

The integrals over r, r', and p must be done numerically. The result is

$$I_4^{\mathrm{b1}} = \frac{T^2}{(4\pi)^4}[9.5763]. \tag{D46}$$

The first subtraction term in Eq. (D41) is

$$I_4^{\rm b2} = 2T\int_p \frac{1}{p^2}\Pi_T(p_0=0,p)\Pi^T_{\rm IR}(p)$$
$$= 2T\int_p \frac{1}{p^2}[\Pi(p_0=0,p)-\Pi^0(p_0=0,p)]\Pi^T_{\rm IR}(p)$$
$$= 2T\int_p \frac{1}{p^2}\Pi(p_0=0,p)\Pi^T_{\rm IR}(p), \tag{D47}$$

where we have used the fact that the second term vanishes in dimensional regularization. This term is logarithmically divergent both in the infrared and in the ultraviolet. If we use the same scale for the regularization of ultraviolet and infrared divergences, the integral vanishes [6].

Inserting the expressions for $\Pi^0(p_0=0,p)$ and $\Pi^T_{\rm IR}(p)$ into Eq. (D47), we obtain

$$I_4^{\rm b2} = \frac{T^3}{(4\pi)^{4-3\epsilon}}\left(\frac{e^{\gamma_E}\mu^2}{4\pi}\right)^{3\epsilon}2^{1+2\epsilon}\frac{\Gamma^2(\frac{1}{2}+\epsilon)\Gamma(\frac{1}{2}-\epsilon)}{\Gamma(\frac{3}{2}-\epsilon)\Gamma(1-\epsilon)}\int_0^\infty dp\int_0^1 dx\sum_{q_0}\frac{p^{-1-4\epsilon}}{[x(1-x)p^2+q_0^2]^{(1/2)+\epsilon}}$$
$$= \frac{T^3}{(4\pi)^{4-3\epsilon}}\left(\frac{e^{\gamma_E}\mu^2}{4\pi}\right)^{3\epsilon}2^{1+2\epsilon}\frac{\Gamma^2(\frac{1}{2}+\epsilon)\Gamma(\frac{1}{2}-\epsilon)}{\Gamma(\frac{3}{2}-\epsilon)\Gamma(1-\epsilon)}\int_0^\infty dp\frac{p^{-1-4\epsilon}}{(p^2+1)^{(1/2)+\epsilon}}\int_0^1 dx[x(1-x)]^{2\epsilon}{\sum_{q_0}}'\frac{1}{|q_0|^{1+6\epsilon}}$$
$$= \frac{T^2}{(4\pi)^4}\left(\frac{e^{\gamma_E}\mu^2}{4\pi^2T^2}\right)^{3\epsilon}\frac{4^\epsilon}{\pi}\frac{\Gamma(\frac{1}{2}+\epsilon)\Gamma(\frac{1}{2}-\epsilon)\Gamma(-2\epsilon)\Gamma(\frac{1}{2}+3\epsilon)\Gamma^2(1+2\epsilon)}{\Gamma(\frac{3}{2}-\epsilon)\Gamma(1-\epsilon)\Gamma(2+4\epsilon)}\zeta(1+6\epsilon). \tag{D48}$$

The prime on the sum in the second line indicates that we have excluded the zero mode $q_0=0$ from the sum. This mode gives rise to an integral that is linearly divergent in the infrared. Since there is no mass scale in this integral, it vanishes. Note also that the integral over p is logarithmically divergent in the infrared and this divergence is *not* set to zero in dimensional regularization [13]. Expanding Eq. (D48) in powers of ϵ, we obtain

$$I_4^{\rm b2} = -\frac{T^2}{6(4\pi)^4}\left[\frac{1}{\epsilon^2}+\left(6\log\frac{\mu}{4\pi T}+6\gamma_E-2\right)\frac{1}{\epsilon}+12+\frac{25}{12}\pi^2-12\log\frac{\mu}{4\pi T}+18\log^2\frac{\mu}{4\pi T}+36\gamma_E\log\frac{\mu}{4\pi T}\right.$$
$$\left.-12\gamma_E-36\gamma_1\right]+\mathcal{O}(\epsilon). \tag{D49}$$

Finally, we consider the last subtraction term in Eq. (D41). Since $\Pi^T_{\rm IR}(p_0=0,p)$ goes like $1/p$ for small p, the integrand has a linear infrared divergence. This divergence is set to zero in dimensional regularization. In fact, since there is no mass scale in the integral, it vanishes:

$$T\int_p\frac{1}{p^2}[\Pi^T_{\rm IR}(p)]^2=0. \tag{D50}$$

Adding Eqs. (D9), (D10), (D26), (D28), (D34), (D40), (D46), and (D49), we can write I in the following form:

$$I = -\frac{T^2}{4(4\pi)^4}\left(\frac{\mu}{4\pi T}\right)^{6\epsilon}\left\{\frac{1}{\epsilon^2}+\frac{1}{\epsilon}\left[\frac{4}{3}+2\frac{\zeta'(-1)}{\zeta(-1)}+4\gamma_E\right]\right.$$
$$+\frac{1}{3}\left[46-8\gamma_E-16\gamma_E^2-104\gamma_1-24\gamma_E\log(2\pi)+24\log^2(2\pi)+\frac{45\pi^2}{4}+24\frac{\zeta'(-1)}{\zeta(-1)}+2\frac{\zeta''(-1)}{\zeta(-1)}+16\gamma_E\frac{\zeta'(-1)}{\zeta(-1)}\right]$$
$$\left.-38.5309+\mathcal{O}(\epsilon)\right\}. \tag{D51}$$

[1] J.-P. Blaizot, E. Iancu, and A. K. Rebhan, in *Quark Gluon Plasma 3*, edited by R. C. Hwa and X. N. Wang (World Scientific, Singapore, 2004), p. 60.
[2] D. H. Rischke, Prog. Part. Nucl. Phys. **52**, 197 (2004).
[3] U. Kraemmer and A. K. Rebhan, Rep. Prog. Phys. **67**, 351 (2004).
[4] J. O. Andersen and M. Strickland, Ann. Phys. (N.Y.) **317**, 281 (2005).
[5] R. R. Parwani and H. Singh, Phys. Rev. D **51**, 4518 (1995).
[6] E. Braaten and A. Nieto, Phys. Rev. D **51**, 6990 (1995).
[7] C. Coriano and R. R. Parwani, Phys. Rev. Lett. **73**, 2398 (1994).

[8] R. R. Parwani, Phys. Lett. B **334**, 420 (1994); **342**, 454(E) (1994); R. R. Parwani and C. Coriano, Nucl. Phys. **B434**, 56 (1995).
[9] J. O. Andersen, Phys. Rev. D **53**, 7286 (1996).
[10] P. Arnold and C. Zhai, Phys. Rev. D **50**, 7603 (1994); **51**, 1906 (1995).
[11] C. Zhai and B. Kastening, Phys. Rev. D **52**, 7232 (1995).
[12] E. Braaten and A. Nieto, Phys. Rev. D **53**, 3421 (1996).
[13] A. Gynther, M. Laine, Y. Schröder, C. Torrero, and A. Vuorinen, J. High Energy Phys. 04 (2007) 094.
[14] F. Karsch, A. Patkós, and P. Petreczky, Phys. Lett. B **401**, 69 (1997).
[15] V. I. Yukalov, Moscow University Physics Bulletin **31**, 10 (1976).
[16] P. M. Stevenson, Phys. Rev. D **23**, 2916 (1981).
[17] W. Janke and H. Kleinert, Phys. Rev. Lett. **75**, 2787 (1995).
[18] J. O. Andersen, E. Braaten, and M. Strickland, Phys. Rev. D **63**, 105008 (2001).
[19] J. O. Andersen and M. Strickland, Phys. Rev. D **64**, 105012 (2001).
[20] E. Braaten and R. D. Pisarski, Phys. Rev. Lett. **64**, 1338 (1990); Nucl. Phys. **B337**, 569 (1990); V. V. Klimov, Sov. Phys. JETP **55**, 199 (1982).
[21] J. O. Andersen, E. Braaten, and M. Strickland, Phys. Rev. Lett. **83**, 2139 (1999).
[22] J. O. Andersen, E. Braaten, and M. Strickland, Phys. Rev. D **61**, 014017 (1999).
[23] J. O. Andersen, E. Braaten, E. Petitgirard, and M. Strickland, Phys. Rev. D **66**, 085016 (2002).
[24] J. O. Andersen, E. Braaten, and M. Strickland, Phys. Rev. D **61**, 074016 (2000).
[25] J. O. Andersen, E. Petitgirard, and M. Strickland, Phys. Rev. D **70**, 045001 (2004).
[26] J. M. Luttinger and J. C. Ward, Phys. Rev. **118**, 1417 (1960).
[27] G. Baym, Phys. Rev. **127**, 1391 (1962).
[28] J. M. Cornwall, R. Jackiw, and E. Tomboulis, Phys. Rev. D **10**, 2428 (1974).
[29] H. van Hees and J. Knoll, Phys. Rev. D **65**, 025010 (2001); **65**, 105005 (2002).
[30] J.-P. Blaizot, E. Iancu, and U. Reinosa, Phys. Lett. B **568**, 160 (2003); Nucl. Phys. **A736**, 149 (2004).
[31] J. Berges, S. Borsanyi, U. Reinosa, and J. Serreau, Ann. Phys. (N.Y.) **320**, 344 (2005).
[32] G. Fejos, A. Patkos, and Zs. Szep, Nucl. Phys. **A803**, 115 (2008).
[33] A. Arrizabalaga and J. Smit, Phys. Rev. D **66**, 065014 (2002).
[34] M. E. Carrington, G. Kunstatter, and H. Zaraket, Eur. Phys. J. C **42**, 253 (2005).
[35] J. O. Andersen and M. Strickland, Phys. Rev. D **71**, 025011 (2005).
[36] J.-P. Blaizot, E. Iancu, and A. Rebhan, Phys. Lett. B **470**, 181 (1999).
[37] J.-P. Blaizot, E. Iancu, and A. Rebhan, Phys. Rev. Lett. **83**, 2906 (1999).
[38] J.-P. Blaizot, E. Iancu, and A. Rebhan, Phys. Rev. D **63**, 065003 (2001).
[39] A. Peshier, Phys. Rev. D **63**, 105004 (2001).
[40] E. Braaten and E. Petitgirard, Phys. Rev. D **65**, 041701(R) (2002); **65**, 085039 (2002).
[41] J. Berges, Sz. Borsanyi, U. Reinosa, and J. Serreau, Phys. Rev. D **71**, 105004 (2005).
[42] S. Borsanyi and U. Reinosa, Phys. Lett. B **661**, 88 (2008).
[43] H. Verschelde and J. De Pessemier, Eur. Phys. J. C **22**, 771 (2002).
[44] G. Smet, T. Vanzielighem, K. Van Acoleyen, and H. Verschelde, Phys. Rev. D **65**, 045015 (2002).
[45] M. B. Pinto and R. O. Ramos, Phys. Rev. D **60**, 105005 (1999).
[46] M. B. Pinto and R. O. Ramos, Phys. Rev. D **61**, 125016 (2000).
[47] R. L. S. Farias, G. Krein, and R. O. Ramos, arXiv:0809.1449.
[48] T. S. Evans, H. F. Jones, and D. Winder, Nucl. Phys. **B598**, 578 (2001).
[49] S. Chiku and T. Hatsuda, Phys. Rev. D **58**, 076001 (1998).
[50] H. Kleinert *et al.*, Phys. Lett. B **272**, 39 (1991); **319**, 545 (E) (1993).
[51] B. Kastening, Phys. Rev. D **54**, 3965 (1996).
[52] A. K. Rebhan, Phys. Rev. D **48**, R3967 (1993).
[53] J. O. Andersen and L. Kyllingstad (unpublished).
[54] K. Kajantie, M. Laine, K. Rummukainen, and Y. Schröder, J. High Energy Phys. 04 (2003) 036.

Paper II

Jens O. Andersen, Lars T. Kyllingstad and Lars E. Leganger:
"Pressure to order $g^8 \log g$ of massless ϕ^4 theory at weak coupling",
JHEP **0908** (2009), 066.

Published by IOP Publishing for SISSA

Received: *May 26, 2009*
Accepted: *July 30, 2009*
Published: *August 18, 2009*

Pressure to order $g^8 \log g$ of massless ϕ^4 theory at weak coupling

Jens O. Andersen,[a,1] **Lars T. Kyllingstad**[b] **and Lars E. Leganger**[b]

[a] *Niels Bohr International Academy, Niels Bohr Institute, Blegdamsvej 17, DK-2100 Copenhagen, Denmark*
[b] *Department of Physics, Norwegian University of Science and Technology, Høgskoleringen 5, N-7491 Trondheim, Norway*
E-mail: andersen@tf.phys.ntnu.no, lars.kyllingstad@ntnu.no, lars.leganger@ntnu.no

Abstract: We calculate the pressure of massless ϕ^4-theory to order $g^8 \log(g)$ at weak coupling. The contributions to the pressure arise from the hard momentum scale of order T and the soft momentum scale of order gT. Effective field theory methods and dimensional reduction are used to separate the contributions from the two momentum scales: The hard contribution can be calculated as a power series in g^2 using naive perturbation theory with bare propagators. The soft contribution can be calculated using an effective theory in three dimensions, whose coefficients are power series in g^2. This contribution is a power series in g starting at order g^3. The calculation of the hard part to order g^6 involves a complicated four-loop sum-integral that was recently calculated by Gynther, Laine, Schröder, Torrero, and Vuorinen. The calculation of the soft part requires calculating the mass parameter in the effective theory to order g^6 and the evaluation of five-loop vacuum diagrams in three dimensions. This gives the free energy correct up to order g^7. The coefficients of the effective theory satisfy a set of renormalization group equations that can be used to sum up leading and subleading logarithms of T/gT. We use the solutions to these equations to obtain a result for the free energy which is correct to order $g^8 \log(g)$. Finally, we investigate the convergence of the perturbative series.

Keywords: NLO Computations, Thermal Field Theory, Renormalization Group

ArXiv ePrint: 0903.4596

[1] On leave from: Department of Physics, Norwegian University of Science and Technology, N-7491 Trondheim, Norway

doi:10.1088/1126-6708/2009/08/066

Contents

1 Introduction

In recent years there has been significant progress in our understanding of thermal field theories in equilibrium [1–4]. Part of the progress is based on the developement of the calculational technology necessary to perform loop calculations beyond the first correction. The motivation to carry out such difficult higher-order calculations of e.g. the pressure in thermal QCD is its relevance to heavy-ion collisions and the early universe. The pressure in nonabelian gauge theories has been calculated perturbatively through order g^4 in ref. [5, 6], to order g^5 in refs. [7, 8], and to order $g^6 \log(g)$ in ref. [9]. There are three momentum scales that contribute to the pressure in thermal QCD - hard momenta of order T, soft momenta

of order gT, and supersoft momenta of order g^2T. The next order — order g^6 — is the first order at which all three momentum scales contribute to the pressure and it is also the order at which perturbation theory breaks down due to infrared divergences [10, 11]. The pressure contains a nonperturbative contribution from the supersoft scale that can be estimated numerically [12–14]. It also contains a presently unknown contribution from the hard scale. This contribution can be calculated by evaluating highly nontrivial four-loop vacuum diagrams with unresummed propagators. As a step in this direction, Gynther, Laine, Schröder, Torrero, and Vuorinen considered the simpler problem of ϕ^4-theory at finite temperature and calculated the free energy to order g^6 [15]. A difficult part of the calculation was to evaluate the four-loop triangle sum-integral, using the techniques developed by Arnold and Zhai in refs. [5, 6].

In hot field theories at weak coupling, the momentum scales in the plasma are well separated and it is advantageous to use effective field theory methods to organize the calculations of the pressure into separate contributions from the hard, soft and supersoft scales. The basic idea is that the mass of the nonzero Matsubara modes are of order T and heavy. Since these modes are heavy, they decouple from the light modes, i.e. the static Matsubara modes. In particular, all fermionic modes decouple since their masses are always of order T. The contributions from the nonzero Matsubara modes to thermodynamic quantities can be calculated using bare propagators and are encoded in the parameters of the effective theory. Integrating out the hard scale T, i.e. integrating out the nonzero Matsubara frequencies, leaves us with an effective dimensionally reduced theory for the scales gT and g^2T [8]. In the case of QCD, the effective theory is an SU(N) gauge theory coupled to an adjoint Higgs. The process is known as dimensional reduction [16–20]. The next step is to construct a second effective theory for the scale g^2T by integrating out the scale gT from the problem [8]. It amounts to integrating out the adjoint Higgs and this step can also be made in perturbation theory. This effective theory is a nonabelian gauge theory in three dimensions, which is confining with a nonperturbative mass gap of order g^2T [11]. This theory must be treated nonperturbatively and gives the nonperturbative contribution to the pressure mentioned above.

In the present paper we consider the thermodynamics of massless ϕ^4-theory and calculate the pressure through order $g^8\log(g)$ in a weak-coupling expansion using effective field theory. Calculations in scalar field theory are simplified by the fact that the supersoft scale g^2T does not appear and so we only need to construct a single effective theory for the soft scale gT. This theory is infrared safe to all orders in perturbation theory due to the generation of a thermal mass of order gT. Compared to the g^6-calculations of ref. [15], the next order requires the matching of the mass parameter to three loops and the evaluation of some five-loop vacuum diagrams in the effective theory. The matching involves a nontrivial three-loop sum-integral that was calculated recently in ref. [21].

The paper is organized as follows. In section II, we briefly discuss effective field theory and determine the coefficients of the dimensionally reduced theory. In section III, we use the effective theory and calculate the soft contributions to the pressure. In section IV, we present and discuss our final results for the pressure. In section V, we summarize. In appendix A and B, we list the necessary sum-integrals and integrals. In appendix C, we

calculate explicitly some of the new three-dimensional integrals that we need.

2 Effective field theory

In this section, we briefly discuss the three-dimensional effective field theory and the matching procedure used to determine its coefficients. For a detailed discussion, see e.g. refs. [19, 20].

The Euclidean Lagrangian density for a massless scalar field with a Φ^4-interaction is

$$\mathcal{L} = \frac{1}{2}(\partial_\mu \Phi)^2 + \frac{g^2}{24}\Phi^4 + \Delta\mathcal{L} \,, \tag{2.1}$$

where g is the coupling constant and $\Delta\mathcal{L}$ includes counterterms. This term reads

$$\Delta\mathcal{L} = \frac{1}{2}\Delta Z_\Phi (\partial_\mu \Phi)^2 + \frac{1}{24}\Delta g^2 \Phi^4 \,. \tag{2.2}$$

In the present case we need the counterterm Δg^2 to next-to-leading order i g^2. It is given by

$$\Delta g^2 = \left[\frac{3}{2\epsilon}\alpha + \left(\frac{9}{4\epsilon^2} - \frac{17}{12\epsilon}\right)\alpha^2\right] g^2 \,, \tag{2.3}$$

where $\alpha = g^2/(4\pi)^2$. We denote by $\phi(x)$ the field in the effective theory. It can be approximately, i.e. up to field redefinitions, be identified with zero-frequency mode of the field Φ in the original theory. The Lagrangian of the effective theory can be then be written as

$$\mathcal{L}_{\text{eff}} = \frac{1}{2}(\nabla\phi)^2 + \frac{1}{2}m^2\phi^2 + \frac{g_3^2}{24}\phi^4 + \cdots \,, \tag{2.4}$$

where m is the mass of the theory and g_3^2 is the quartic coupling. The dots indicate an infinite series of higher-order operators consistent with the symmetries, such as rotational invariance and the discrete symmetry $\phi \to -\phi$. In eq. (2.4), we have omitted a coefficient f of the unit operator. Its interpretation is that it gives the contribution to the free energy from the hard scale T.

For the calculation of the pressure to order $g^8\log(g)$, we need to know f and the mass parameter m^2 to order g^6 and the coupling constant g_3^2 to order g^4, i.e. we consider ϕ^4-theory in three spatial dimensions.[1] This theory is superrenormalizable and only the mass needs renormalization [22]. The parameters in the effective Lagrangian (2.4) are determined by calculating static correlation functions in the two theories at long distances R, i.e. $R \gg 1/T$, and demanding that they be the same [19]. In the matching calculations, we are employing *strict perturbation theory* [19]. This amounts to doing perturbative calculations in power series in g^2 in which we treat the mass parameter as a perturbation in the effective theory. The Lagrangian is therefore split into a free and an interacting part according to

$$\mathcal{L}_{\text{eff}}^{\text{free}} = \frac{1}{2}(\nabla\phi)^2 \,, \tag{2.5}$$

$$\mathcal{L}_{\text{eff}}^{\text{int}} = \frac{1}{2}m^2\phi^2 + \frac{g_3^2}{24}\phi^4 + \cdots \,. \tag{2.6}$$

[1] Power counting tells one that the operator $(\phi\nabla\phi)^2$ contributes to the free energy first at order g^8.

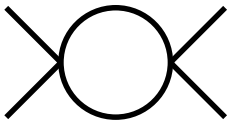

Figure 1. One-loop Feynman graph that contributes to the coupling g_3^2 in the effective theory.

Strict perturbation theory gives rise to infrared divergences in the calculation that physically are cut off by the generation of a thermal mass m. The same infrared divergences appear in the loops in the full theory and so they cancel in the matching calculations. The incorrect treatment of the infrared divergences and the physics on the scale gT is not problematic since this will be taken care of by calculations in the effective theory. The matching calculations treat the physics on the hard scale correctly and the physics on that scale is encoded in the parameters of the three-dimensional effective Lagrangian.

However, the matching calculations of the parameters in $\mathcal{L}_{\text{eff}}$ are complicated by ultraviolet divergences. Those divergences that are associated with the full four-dimensional theory are removed by renormalization of the coupling constant g. The remaining divergences are cancelled by the extra counterterms that are determined by the ultraviolet divergences in the effective theory. These divergences are regulated by introducing a cutoff Λ. The cutoff Λ can be thought of as an arbitrary factorization scale that separates the scale T from the scale gT (or smaller) which can be treated in the effective theory [19]. The parameters in the effective theory therefore depend on the cutoff Λ in order to cancel the Λ-dependence of the loop integrals in the effective theory.

2.1 Coupling constant

To leading order in the coupling g^2, we can simply read off the coupling g_3^2 from the Lagrangian of the full theory. Making the replacement $\Phi \to \sqrt{T}\phi$ in the Lagrangian (2.1) and comparing $\int_0^\beta d\tau\, \mathcal{L}$ with $\mathcal{L}_{\text{eff}}$, we conclude that $g_3^2 = g^2 T$. The one-loop graph needed for the matching of the coupling g_3^2 to next-to-leading order in g^2 is shown in figure 1. Since the loop correction vanishes in the effective theory due to the fact that we are using massless propagators, the matching equation reduces to

$$g_3^2 = g^2 T - \frac{3}{2} g^4 T \sum\!\!\!\!\!\!\int_P \frac{1}{P^4} + \Delta_1 g^2 T \,, \tag{2.7}$$

where $\Delta_1 g^2$ is the order-g^4 coupling constant counterterm in eq. (2.3). After renormalization, we find

$$\begin{aligned} g_3^2(\Lambda) = g^2(\mu) T \Bigg[1 - \frac{3g^2}{(4\pi)^2} \left(\log \frac{\mu}{4\pi T} + \gamma_E \right) - \\ - \frac{3g^2}{(4\pi)^2} \left(\log^2 \frac{\mu}{4\pi T} + 2\gamma_E \log \frac{\mu}{4\pi T} + \frac{\pi^2}{8} - 2\gamma_1 \right) \epsilon \Bigg] \,, \end{aligned} \tag{2.8}$$

where $g^2 = g^2(\mu)$ is the coupling constant at the scale μ in the $\overline{\text{MS}}$ scheme and we have kept the order-ϵ terms in g_3^2 for later use. We have used the renormalization group equation

Figure 2. One-loop vacuum diagram.

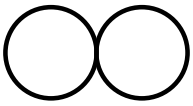

Figure 3. Two-loop vacuum diagram.

for the running coupling constant g^2,

$$\mu\frac{\partial}{\partial\mu}\alpha = 3\alpha^2 - \frac{17}{3}\alpha^3 \,, \tag{2.9}$$

to change the scale from Λ to μ. The right-hand side of eq. (2.8) is independent of Λ. In fact, since the coupling g_3^2 does not require renormalization in three dimensions, it satisfies the renormalization group equation

$$\Lambda\frac{\partial}{\partial\Lambda}g_3 = 0 \,. \tag{2.10}$$

2.2 Coefficient of unit operator

The partition function in the full theory is given by the path integral

$$Z = \int \mathcal{D}\Phi\, e^{-\int_0^\beta d\tau \int d^3x \mathcal{L}} \,, \tag{2.11}$$

and the pressure is then given by $\mathcal{P} = T\log\mathcal{Z}/V$, where V is the volume of the system. In terms of the effective theory, the partition function can be written as

$$\mathcal{Z} = e^{-fV}\int \mathcal{D}\phi\, e^{-\int d^3x \mathcal{L}_{\rm eff}} \,. \tag{2.12}$$

The matching then yields

$$\log\mathcal{Z} = -fV + \log\mathcal{Z}_{\rm eff} \,, \tag{2.13}$$

where $\mathcal{Z}_{\rm eff}$ is the partitition function of the three-dimensional theory. Equivalently, we can write $\mathcal{F} = \mathcal{F}_{\rm hard} + \mathcal{F}_{\rm soft}$, where $\mathcal{F}_{\rm hard} = fT$ and $\mathcal{F}_{\rm soft} = -T\log\mathcal{Z}_{\rm eff}/V$. Now since calculations in strict perturbation theory in the effective theory is carried out using bare propagators, there is no scale in the vacuum graphs. This implies that they vanish in dimensional regularization and that $\log\mathcal{Z}_{\rm eff} = 0$. Eq. (2.13) then tells us that f is given by a strict loop expansion in four dimensions.

The vacuum diagrams through four loops are shown in figures 2–5.

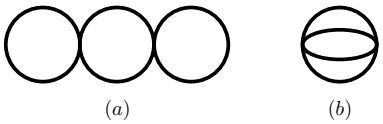

Figure 4. Three-loop vacuum diagrams.

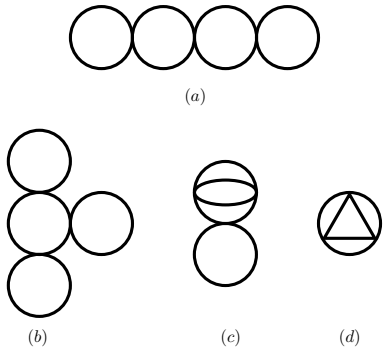

Figure 5. Four-loop vacuum diagrams.

We can then write

$$\mathcal{F}_{\rm hard} = \mathcal{F}_0^{(h)} + \mathcal{F}_1^{(h)} + \mathcal{F}_{\rm 2a}^{(h)} + \mathcal{F}_{\rm 2b}^{(h)} + \mathcal{F}_{\rm 3a}^{(h)} + \mathcal{F}_{\rm 3b}^{(h)} + \mathcal{F}_{\rm 3c}^{(h)} + \mathcal{F}_{\rm 3d}^{(h)} + \\ + \frac{\mathcal{F}_1^{(h)}}{g^2}(\Delta_1 g^2 + \Delta_2 g^2) + 2\left(\frac{\mathcal{F}_{\rm 2a}^{(h)}}{g^2} + \frac{\mathcal{F}_{\rm 2b}^{(h)}}{g^2}\right)\Delta_1 g^2 \,, \tag{2.14}$$

where $\Delta_1 g^2$ and $\Delta_2 g^2$ are the order-g^4 and order-g^6 coupling constant counterterms, respectively, given in eq. (2.3). The superscript h indicates that the expression gives the hard contribution to the free energy. The expressions for the diagrams are

$$\mathcal{F}_0^{(h)} = \frac{1}{2}\sum\!\!\!\!\!\!\int_P \log P^2 \,, \tag{2.15}$$

$$\mathcal{F}_1^{(h)} = \frac{1}{8}g^2\left(\sum\!\!\!\!\!\!\int_P \frac{1}{P^2}\right)^2 \,, \tag{2.16}$$

$$\mathcal{F}_{\rm 2a}^{(h)} = -\frac{1}{16}g^4\left(\sum\!\!\!\!\!\!\int_P \frac{1}{P^2}\right)^2 \sum\!\!\!\!\!\!\int_Q \frac{1}{Q^4} \,, \tag{2.17}$$

$$\mathcal{F}_{\rm 2b}^{(h)} = -\frac{1}{48}g^4 \sum\!\!\!\!\!\!\int_{PQR} \frac{1}{P^2Q^2R^2(P+Q+R)^2} \,, \tag{2.18}$$

$$\mathcal{F}_{\rm 3a}^{(h)} = \frac{1}{32}g^6\left(\sum\!\!\!\!\!\!\int_P \frac{1}{P^2}\right)^2\left(\sum\!\!\!\!\!\!\int_Q \frac{1}{Q^4}\right)^2 \,, \tag{2.19}$$

$$\mathcal{F}_{\rm 3b}^{(h)} = \frac{1}{48}g^6 \sum\!\!\!\!\!\!\int_P \frac{1}{Q^6}\left(\sum\!\!\!\!\!\!\int_P \frac{1}{P^2}\right)^3 \,, \tag{2.20}$$

$$\mathcal{F}_{3c}^{(c)} = \frac{1}{24} g^6 \sum\!\!\!\!\!\!\int_P \frac{1}{P^2} \sum\!\!\!\!\!\!\int_{KQR} \frac{1}{K^4 Q^2 R^2 (K+Q+R)^2} \,, \tag{2.21}$$

$$\mathcal{F}_{3d}^{(h)} = \frac{1}{48} g^6 \sum\!\!\!\!\!\!\int_P [\Pi(P)]^3 \,, \tag{2.22}$$

where the symbol $\sum\!\!\!\!\!\!\int$ is defined in eq. (A.1) and the self-energy $\Pi(P)$ is defined in eq. (A.13). The expressions for the sum-integrals are listed in appendix A. After renormalization, the final expression is [15]

$$\begin{aligned}
\mathcal{F}_{\rm hard}(\Lambda) = &-\frac{\pi^2 T^4}{90} \times \\
&\times \Bigg\{ 1 - \frac{5}{4}\alpha + \frac{15}{4}\alpha^2 \left[\log\frac{\mu}{4\pi T} + \frac{1}{3}\gamma_E + \frac{31}{45} + \frac{4}{3}\frac{\zeta'(-1)}{\zeta(-1)} - \frac{2}{3}\frac{\zeta'(-3)}{\zeta(-3)} \right] + \\
&\quad + \frac{15}{16}\alpha^3 \times \\
&\quad \times \Bigg[\frac{\pi^2}{\epsilon} - 12\log^2\frac{\mu}{4\pi T} - \left(\frac{1084}{45} + 8\gamma_E + 32\frac{\zeta'(-1)}{\zeta(-1)} - 16\frac{\zeta'(-3)}{\zeta(-3)} \right) \times \\
&\qquad \times \log\frac{\mu}{4\pi T} + 8\pi^2 \log\frac{\Lambda}{4\pi T} - \frac{134}{9} - \frac{25}{3}\gamma_E^2 - \frac{1}{27}\zeta(3) + \frac{31}{15}\gamma_E - \\
&\qquad - \frac{\pi^2}{2} + 4\gamma_E\pi^2 - \frac{206}{9}\frac{\zeta'(-1)}{\zeta(-1)} - \frac{16}{3}\gamma_1 + 8\gamma_E\frac{\zeta'(-3)}{\zeta(-3)} + \\
&\qquad + \frac{4}{3}\gamma_E\frac{\zeta'(-1)}{\zeta(-1)} - 8\left(\frac{\zeta'(-1)}{\zeta(-1)}\right)^2 - \frac{20}{3}\frac{\zeta''(-1)}{\zeta(-1)} - \\
&\qquad - \frac{2}{3}C'_{\rm ball} + 2C^a_{\rm triangle} + \pi^2 C^b_{\rm triangle} \Bigg] + \mathcal{O}(\epsilon) \Bigg\} \,,
\end{aligned} \tag{2.23}$$

where $\alpha = \alpha(\mu)$, $C'_{\rm ball} = 48.7976$, $C^a_{\rm triangle} = -25.7055$, and $C^b_{\rm triangle} = 28.9250$. We have used the renormalization group equation for g^2 to change the renormalization scale from Λ to μ. Note that the final results contains a pole in ϵ. We cancel it by adding a counterterm $T\delta f$ [8]. The term δf can be determined by calulating the ultraviolet divergences in the effective theory. The triangle diagram in three dimensions has a logarithmic ultraviolet divergence and the counterterm needed to cancel this divergence is given by

$$\delta f = \frac{g_3^6 \pi^2}{1536(4\pi)^4 \epsilon} \,. \tag{2.24}$$

If we express the counterterm in terms of the coupling g of the full theory, we must take into account that g_3^6 multiplies a pole in ϵ and it therefore picks up finite terms. These terms will be of order g^8 and can be neglected in the present calculation.[2] The coefficient f satisfies the evolution equation

$$\Lambda\frac{\partial}{\partial\Lambda} f = -\frac{\pi^2}{192(4\pi)^4} g_3^6 \,. \tag{2.25}$$

This follows from the scale dependence of the triangle diagram in three dimensions and the fact that the Λ-dependence of f must cancel the scale dependence in the effective theory.

[2] Note that minimal subtraction in the full theory and in the effective theory are not equivalent. The difference is the finite terms mentioned above [8].

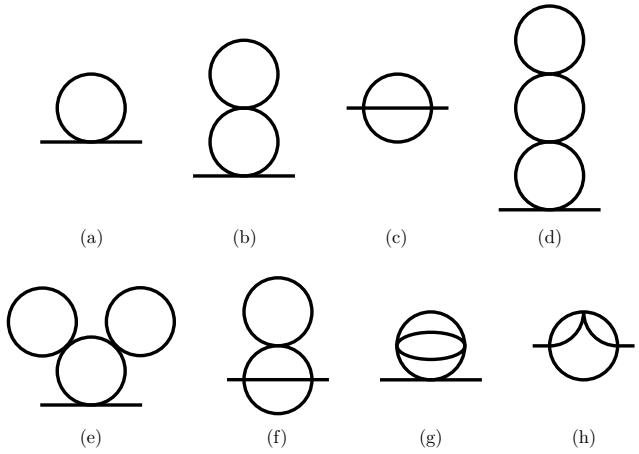

Figure 6. Feynman graphs that contribute to the self-energy through three loops.

2.3 Mass parameter

The simplest way of determining the mass parameter m^2 is by matching the Debye or screening mass m_D in the full theory and in the effective theory [19]. The Debye mass m_D is given by the pole of static propagator, i.e. by

$$p^2 + \tilde{\Pi}(p_0 = 0, p) = 0 \,, \qquad p^2 = -m_D^2 \,, \tag{2.26}$$

where $\tilde{\Pi}(p_0, p)$ denotes the self-energy function. In the effective theory, the equation is

$$p^2 + m^2 + \Pi_{\text{eff}}(p) = 0 \,, \qquad p^2 = -m_D^2 \,, \tag{2.27}$$

where $\Pi_{\text{eff}}(p)$ is the self-energy in the effective theory. Since the self-energy in the full theory is expanded around $p = 0$, we should do to the same in the effective theory (see discussion below). The loop integrals are therefore evaluated at zero external momentum and since the matching is carried out using massless propagators there is no scale in the loop integrals. They therefore vanish in in dimensional regularization, i.e. $\Pi_{\text{eff}}(0) = \Pi'_{\text{eff}}(0) = \cdots = 0$. Using this fact and equating (2.26) and (2.27), we obtain $m^2 \approx m_D^2$ [3]

$$m_D^2 = \tilde{\Pi}(p_0 = 0, p = i m_D) \,. \tag{2.28}$$

The diagrams that contribute to the self-energy $\tilde{\Pi}(P)$ through three loops are shown in figure 6. The self-energy $\tilde{\Pi}(P)$ is given by

$$\begin{aligned} \tilde{\Pi}(P) = {} & \tilde{\Pi}_1^{(h)}(P) + \tilde{\Pi}_2^{(h)}(P) + \tilde{\Pi}_3^{(h)}(P) + \\ & + \frac{\tilde{\Pi}_1^{(h)}(P)}{g^2} \left(\Delta_1 g^2 + \Delta_2 g^2 \right) + 2 \frac{\tilde{\Pi}_2^{(h)}(P)}{g^2} \Delta_1 g^2 \,. \end{aligned} \tag{2.29}$$

[3] Note that we use the symbol "$\approx$" to emphasize that the the mass parameter m^2 is equal to the Debye mass m_D^2 only in strict perturbation theory. The interpretation is that m gives the contribution to the Debye mass from the hard scale T.

The expression for the various terms in the self-energy are given by

$$\tilde{\Pi}_1^{(h)}(P) = \frac{1}{2}g^2 \sum\!\!\!\!\!\!\int_Q \frac{1}{Q^2} \,, \tag{2.30}$$

$$\tilde{\Pi}_{2a}^{(h)}(P) = -\frac{1}{4}g^4 \sum\!\!\!\!\!\!\int_{QR} \frac{1}{Q^4R^2} \,, \tag{2.31}$$

$$\tilde{\Pi}_{2b}^{(h)}(P) = -\frac{1}{6}g^4 \sum\!\!\!\!\!\!\int_{QR} \frac{1}{Q^2R^2(P+Q+R)^2} \,, \tag{2.32}$$

$$\tilde{\Pi}_{3a}^{(h)}(P) = \frac{1}{8}g^6 \sum\!\!\!\!\!\!\int_Q \frac{1}{Q^2}\left(\sum\!\!\!\!\!\!\int_R \frac{1}{R^4}\right)^2 \,, \tag{2.33}$$

$$\tilde{\Pi}_{3b}^{(h)}(P) = \frac{1}{8}g^6 \sum\!\!\!\!\!\!\int_Q \frac{1}{Q^6}\left(\sum\!\!\!\!\!\!\int_R \frac{1}{R^2}\right)^2 \tag{2.34}$$

$$\tilde{\Pi}_{3c}^{(h)}(P) = \frac{1}{4}g^6 \sum\!\!\!\!\!\!\int_K \frac{1}{K^2} \sum\!\!\!\!\!\!\int_{QR} \frac{1}{Q^4R^2(P+Q+R)^2} \,, \tag{2.35}$$

$$\tilde{\Pi}_{3d}^{(h)}(P) = \frac{1}{12}g^6 \sum\!\!\!\!\!\!\int_{KQR} \frac{1}{K^4Q^2R^2(K+Q+R)^2} \,, \tag{2.36}$$

$$\tilde{\Pi}_{3e}^{(h)}(P) = \frac{1}{4}g^6 \sum\!\!\!\!\!\!\int_Q \frac{1}{(P+Q)^2}[\Pi(Q)]^2 \,. \tag{2.37}$$

Since the leading-order solution to eq. (2.28) gives a value of p that is of the order gT, it is justified to expand the loop diagrams in a Taylor series around $p = 0$. We can then write eq. (2.28) as

$$m_D^2 = \tilde{\Pi}_1^{(h)}(0) + \tilde{\Pi}_2^{(h)}(0) + \tilde{\Pi}_2^{(h)\prime}(0)p^2 + \tilde{\Pi}_3(0) + \cdots \,, \;\; p^2 = -m_D^2 \,, \tag{2.38}$$

or $m_D^2 = \tilde{\Pi}_1^{(h)}(0) + \tilde{\Pi}_2^{(h)}(0) + \tilde{\Pi}_3^{(h)}(0) - \tilde{\Pi}_1(0)\tilde{\Pi}_2'(0)$. We then need the two-loop self-energy diagram $\tilde{\Pi}_{2\mathrm{b}}(P)$ to order p^2, while the three-loop self-energy diagrams $\tilde{\Pi}_{3\mathrm{c}}^{(h)}(P)$ and $\tilde{\Pi}_{3\mathrm{e}}^{(h)}(P)$ can be evaluated at $p = 0$. This yields

$$\tilde{\Pi}_{2\mathrm{b}}^{(h)}(P) = -\frac{1}{6}g^4 \sum\!\!\!\!\!\!\int_{QR} \frac{1}{Q^2R^2(Q+R)^2} - \frac{1}{6}g^4p^2 \sum\!\!\!\!\!\!\int_{QR} \frac{(4/d)q^2 - Q^2}{Q^6R^2(Q+R)^2} + \mathcal{O}(p^4) \,, \tag{2.39}$$

$$\tilde{\Pi}_{3\mathrm{c}}^{(h)}(0) = \frac{1}{4}g^6 \sum\!\!\!\!\!\!\int_K \frac{1}{K^2} \sum\!\!\!\!\!\!\int_{QR} \frac{1}{Q^4R^2(Q+R)^2} \,, \tag{2.40}$$

$$\tilde{\Pi}_{3\mathrm{e}}^{(h)}(0) = \frac{1}{4}g^6 \sum\!\!\!\!\!\!\int_Q \frac{1}{Q^2}[\Pi(Q)]^2 \,. \tag{2.41}$$

The sum-integrals needed are listed in appendix A. After renormalization, we obtain

$$\begin{aligned} m^2(\Lambda) = {} & \frac{1}{24}g^2(\Lambda)T^2 \times \\ & \times\left\{1 + \frac{g^2}{(4\pi)^2}\left[\frac{1}{\epsilon} + \log\frac{\Lambda}{4\pi T} + 2 - \gamma_E + 2\frac{\zeta'(-1)}{\zeta(-1)}\right] - \frac{6g^4}{(4\pi)^4} \times \right. \\ & \times\left[\frac{1}{\epsilon}\left(\log\frac{\Lambda}{4\pi T} + \gamma_E\right) + \frac{7}{2}\log^2\frac{\Lambda}{4\pi T} + \left(\frac{19}{18} + 5\gamma_E + 2\frac{\zeta'(-1)}{\zeta(-1)}\right)\log\frac{\Lambda}{4\pi T} + \right. \\ & \left. \left. + \frac{2851}{864} - \frac{95}{48}\gamma_E^2 - \frac{119}{144}\gamma_E - \frac{1}{144}\zeta(3) - 9\gamma_1 + \frac{\zeta'(-1)}{\zeta(-1)}\left(\frac{113}{72} + \frac{17}{12}\gamma_E\right) - \right. \right. \end{aligned}$$

$$-\frac{1}{4}\frac{\zeta''(-1)}{\zeta(-1)}+\frac{29}{32}\pi^2-2\gamma_E\log(2\pi)+2\log^2(2\pi)-\frac{1}{24}C'_{\rm ball}+\frac{1}{4}C_I\Bigg]+$$
$$+\mathcal{O}(\epsilon)\Bigg\}\,, \tag{2.42}$$

where $g=g(\Lambda)$ and $C_I=-38.4672$. The mass parameter through order g^4 is known to order ϵ [9], but we only need it to order ϵ^0. We notice that the mass parameter contains uncancelled poles in ϵ. It is advantageous to write the mass term as a sum of a finite piece $\tilde{m}^2$ and a counterterm Δm^2, where

$$\begin{aligned}
\tilde{m}^2(\Lambda) &= \frac{1}{24}g^2(\mu)T^2\times\\
&\times\Bigg\{1+\frac{g^2}{(4\pi)^2}\left[4\log\frac{\Lambda}{4\pi T}-3\log\frac{\mu}{4\pi T}+2-\gamma_E+2\frac{\zeta'(-1)}{\zeta(-1)}\right]-\\
&\quad-\frac{6g^4}{(4\pi)^4}\left[4\log^2\frac{\Lambda}{4\pi T}-\frac{3}{2}\log^2\frac{\mu}{4\pi T}+\left(\frac{19}{18}-\gamma_E+2\frac{\zeta'(-1)}{\zeta(-1)}\right)\log\frac{\mu}{4\pi T}+\right.\\
&\qquad+4\gamma_E\log\frac{\Lambda}{4\pi T}+\frac{2851}{864}-\frac{95}{48}\gamma_E^2-\frac{119}{144}\gamma_E-\frac{1}{144}\zeta(3)-7\gamma_1+\\
&\qquad+\frac{\zeta'(-1)}{\zeta(-1)}\left(\frac{113}{72}+\frac{17}{12}\gamma_E\right)-\frac{1}{4}\frac{\zeta''(-1)}{\zeta(-1)}+\frac{25}{32}\pi^2-2\gamma_E\log(2\pi)+\\
&\qquad\left.+2\log^2(2\pi)-\frac{1}{24}C'_{\rm ball}+\frac{1}{4}C_I\right]+\mathcal{O}(\epsilon)\Bigg\}\,,
\end{aligned} \tag{2.43}$$

$$\begin{aligned}
\Delta m^2(\Lambda) &= \frac{g^4T^2}{24(4\pi)^2\epsilon}\left[1-\frac{6g^2}{(4\pi)^2}\left(\log\frac{\mu}{4\pi T}+\gamma_E\right)-\right.\\
&\qquad\left.-\frac{6g^2}{(4\pi)^2}\left(\log^2\frac{\mu}{4\pi T}+2\gamma_E\log\frac{\mu}{4\pi T}+\frac{\pi^2}{8}-2\gamma_1\right)\epsilon\right]\,,\\
&= \frac{g_3^4(\Lambda)}{24(4\pi)^2\epsilon}\,,
\end{aligned} \tag{2.44}$$

where $g=g(\mu)$ and we have used eq. (2.9) to change the renormalization scale from Λ to μ. The term Δm^2 acts as a counterterm in the effective theory. In fact, the sunset diagram in three dimensions that contribute to the self-energy is logarithmically divergent, whose divergence exactly is given by the right-hand side of eq. (2.44) [22]. The mass parameter $\tilde{m}$ in three dimensions therefore satisfies the evolution equation

$$\Lambda\frac{\partial}{\partial\Lambda}\tilde{m}^2=\frac{1}{6}\frac{g_3^4}{(4\pi)^2}\,. \tag{2.45}$$

In the remainder of the paper, we will use m instead of $\tilde{m}$ for covenience.

3 Soft contributions

In this section, we calculate the soft contributions $\mathcal{P}_{\rm soft}$ to the pressure. This requires the calculations of vacuum diagrams in the effective theory (2.4) through five loops. In order to take into account the soft scale gT, we now include the mass term m^2 in the free part of the Lagrangian and only the quartic term in eq. (2.4) is treated as an interaction. The

inclusion of the mass term in the propagators cuts off the infrared divergences that plagues naive perturbation theory in the full theory.

The one-loop vacuum diagram is shown in figure 2. Its contribution to the free energy is given by

$$\mathcal{F}_0^{(s)} = \frac{1}{2} T \int_p \log\left(p^2 + m^2\right) \,, \tag{3.1}$$

where the superscript (s) indicates that the expression gives the soft contribution to the free energy. Using the expression in the appendix B, we obtain

$$\mathcal{F}_0^{(s)} = -\frac{m^3 T}{12\pi} \,. \tag{3.2}$$

The two-loop vacuum diagram is shown in figure 3. Its contribution to the free energy is given by

$$\mathcal{F}_1^{(s)} = \frac{1}{8} g_3^2 T \left(\int_p \frac{1}{p^2 + m^2}\right)^2 \,. \tag{3.3}$$

Using the expression in the appendix B, we obtain

$$\mathcal{F}_1^{(s)} = \frac{g_3^2 m^2 T}{8(4\pi)^2} \,. \tag{3.4}$$

The three-loop vacuum diagrams are shown in figure 4. The contribution to the free energy is given by

$$\mathcal{F}_2^{(s)} = \mathcal{F}_{2\mathrm{a}}^{(s)} + \mathcal{F}_{2\mathrm{b}}^{(s)} + \frac{\partial \mathcal{F}_0^{(s)}}{\partial m^2} \Delta m^2 \,, \tag{3.5}$$

where Δm^2 is the mass counterterm (2.44) in the effective theory and

$$\mathcal{F}_{2\mathrm{a}}^{(s)} = -\frac{1}{16} g_3^4 T \left(\int_p \frac{1}{p^2 + m^2}\right)^2 \int_q \frac{1}{(q^2 + m^2)^2} \,, \tag{3.6}$$

$$\mathcal{F}_{2\mathrm{b}}^{(s)} = -\frac{1}{48} g_3^4 T \int_{pqr} \frac{1}{p^2 + m^2} \frac{1}{q^2 + m^2} \frac{1}{r^2 + m^2} \frac{1}{(\mathbf{p} + \mathbf{q} + \mathbf{r})^2 + m^2} \,. \tag{3.7}$$

Using the expression in the appendix B, we obtain

$$\mathcal{F}_2^{(s)} = \frac{g_3^4 m T}{96(4\pi)^3} \left[8 \log \frac{\Lambda}{2m} + 9 - 8 \log 2\right] \,. \tag{3.8}$$

We note that all poles in ϵ cancel as they must since there are no divergences from the hard part proportional to $g_3^4 m$.

The four-loop vacuum diagrams are shown in figure 5. The contribution to the free energy is given by

$$\mathcal{F}_3^{(s)} = \mathcal{F}_{3\mathrm{a}}^{(s)} + \mathcal{F}_{3\mathrm{b}}^{(s)} + \mathcal{F}_{3\mathrm{c}}^{(s)} + \mathcal{F}_{3\mathrm{d}}^{(s)} + \frac{\partial \mathcal{F}_1^{(s)}}{\partial m^2} \Delta m^2 \,, \tag{3.9}$$

where the expressions for the diagrams are

$$\mathcal{F}_{3a}^{(s)} = \frac{1}{32} g_3^6 T \left(\int_p \frac{1}{p^2+m^2} \right)^2 \left(\int_q \frac{1}{(q^2+m^2)^2} \right)^2 , \tag{3.10}$$

$$\mathcal{F}_{3b}^{(s)} = \frac{1}{48} g_3^6 T \left(\int_p \frac{1}{p^2+m^2} \right)^3 \int_q \frac{1}{(q^2+m^2)^3} , \tag{3.11}$$

$$\mathcal{F}_{3c}^{(s)} = \frac{1}{24} g_3^6 T \int_{pqr} \frac{1}{(p^2+m^2)^2} \frac{1}{q^2+m^2} \frac{1}{r^2+m^2} \frac{1}{(\mathbf{p}+\mathbf{q}+\mathbf{r})^2+m^2} \times \\ \times \int_s \frac{1}{s^2+m^2} , \tag{3.12}$$

$$\mathcal{F}_{3d}^{(s)} = \frac{1}{48} g_3^6 T \int_{pqrs} \frac{1}{q^2+m^2} \frac{1}{(\mathbf{p}+\mathbf{q})^2+m^2} \frac{1}{r^2+m^2} \frac{1}{(\mathbf{p}+\mathbf{r})^2+m^2} \times \\ \times \frac{1}{s^2+m^2} \frac{1}{(\mathbf{p}+\mathbf{s})^2+m^2} . \tag{3.13}$$

Using the expressions in the appendix B, we obtain

$$\mathcal{F}_3^{(s)} = \frac{g_3^6 T}{768(4\pi)^4} \left[-4\left(4-\pi^2\right) \log \frac{\Lambda}{2m} - 4 + 16\log 2 - 42\zeta(3) + \pi^2(1+2\log 2) \right] + \\ + \frac{g_3^6 T \pi^2}{1536(4\pi)^4 \epsilon} . \tag{3.14}$$

The pole in ϵ in eq. (3.14) arises from the triangle diagram in eq. (3.13). This pole is cancelled by the counterterm in eq. (2.24).

The five-loop vacuum diagrams are shown in figure 7. The contributions to the free energy are given by

$$\mathcal{F}_4^{(s)} = \mathcal{F}_{4a}^{(s)} + \mathcal{F}_{4b}^{(s)} + \mathcal{F}_{4c}^{(s)} + \mathcal{F}_{4d}^{(s)} + \mathcal{F}_{4e}^{(s)} + \mathcal{F}_{4f}^{(s)} + \mathcal{F}_{4g}^{(s)} + \mathcal{F}_{4h}^{(s)} + \mathcal{F}_{4i}^{(s)} + \mathcal{F}_{4j}^{(s)} + \\ + \frac{\partial \mathcal{F}_2^{(s)}}{\partial m^2} \Delta m^2 + \frac{1}{2} \frac{\partial^2 \mathcal{F}_0^{(s)}}{(\partial m^2)^2} (\Delta m^2)^2 . \tag{3.15}$$

where the expressions for the diagrams are

$$\mathcal{F}_{4a}^{(s)} = -\frac{1}{64} g_3^8 T \left(\int_p \frac{1}{p^2+m^2} \right)^2 \left(\int_q \frac{1}{(q^2+m^2)^2} \right)^3 , \tag{3.16}$$

$$\mathcal{F}_{4b}^{(s)} = -\frac{1}{32} g_3^8 T \left(\int_p \frac{1}{p^2+m^2} \right)^3 \int_q \frac{1}{(q^2+m^2)^2} \int_r \frac{1}{(r^2+m^2)^3} , \tag{3.17}$$

$$\mathcal{F}_{4c}^{(s)} = -\frac{1}{128} g_3^8 T \left(\int_p \frac{1}{p^2+m^2} \right)^4 \int_q \frac{1}{(q^2+m^2)^4} , \tag{3.18}$$

$$\mathcal{F}_{4d}^{(s)} = -\frac{1}{16} g_3^8 T \int_{pqrs} \frac{1}{(q^2+m^2)^2} \frac{1}{(\mathbf{p}+\mathbf{q})^2+m^2} \frac{1}{r^2+m^2} \frac{1}{(\mathbf{p}+\mathbf{r})^2+m^2} \times \\ \times \frac{1}{s^2+m^2} \frac{1}{(\mathbf{p}+\mathbf{s})^2+m^2} \int_t \frac{1}{t^2+m^2} , \tag{3.19}$$

$$\mathcal{F}_{4e}^{(s)} = -\frac{1}{48} g_3^8 T \int_{pqr} \frac{1}{(p^2+m^2)^3} \frac{1}{q^2+m^2} \frac{1}{r^2+m^2} \frac{1}{(\mathbf{p}+\mathbf{q}+\mathbf{r})^2+m^2} \times \\ \times \left(\int_s \frac{1}{s^2+m^2} \right)^2 , \tag{3.20}$$

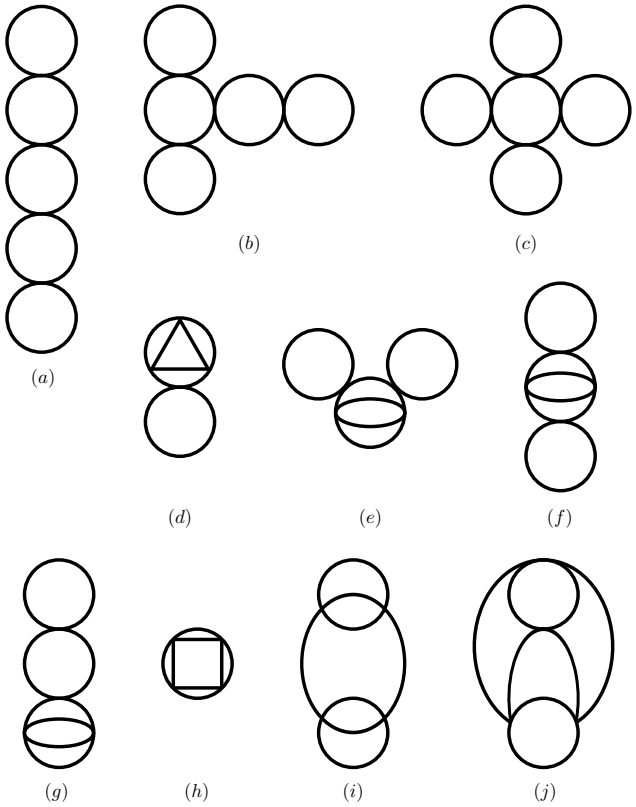

Figure 7. Five-loop vacuum diagrams that contribute to the soft part of the free energy.

$$\mathcal{F}_{4\mathrm{f}}^{(s)} = -\frac{1}{32} g_3^8 T \int_{pqr} \frac{1}{(p^2+m^2)^2} \frac{1}{(q^2+m^2)^2} \frac{1}{r^2+m^2} \frac{1}{(\mathbf{p}+\mathbf{q}+\mathbf{r})^2+m^2} \times \\ \times \left(\int_s \frac{1}{s^2+m^2} \right)^2 , \tag{3.21}$$

$$\mathcal{F}_{4\mathrm{g}}^{(s)} = -\frac{1}{48} g_3^8 T \int_{pqr} \frac{1}{(p^2+m^2)^2} \frac{1}{q^2+m^2} \frac{1}{r^2+m^2} \frac{1}{(\mathbf{p}+\mathbf{q}+\mathbf{r})^2+m^2} \times \\ \times \int_s \frac{1}{s^2+m^2} \int_t \frac{1}{(t^2+m^2)^2} , \tag{3.22}$$

$$\mathcal{F}_{4\mathrm{h}}^{(s)} = -\frac{1}{128} g_3^8 T \int_{pqrst} \frac{1}{q^2+m^2} \frac{1}{(\mathbf{p}+\mathbf{q})^2+m^2} \frac{1}{r^2+m^2} \frac{1}{(\mathbf{p}+\mathbf{r})^2+m^2} \times \\ \times \frac{1}{s^2+m^2} \frac{1}{(\mathbf{p}+\mathbf{s})^2+m^2} \frac{1}{t^2+m^2} \frac{1}{(\mathbf{p}+\mathbf{t})^2+m^2} , \tag{3.23}$$

$$\mathcal{F}_{4\mathrm{i}}^{(s)} = -\frac{1}{144} g_3^8 T \int_p \frac{1}{(p^2+m^2)^2} \int_{qr} \frac{1}{q^2+m^2} \frac{1}{r^2+m^2} \frac{1}{(\mathbf{p}+\mathbf{q}+\mathbf{r})^2+m^2} \times$$

$$\times \int_{st} \frac{1}{s^2+m^2}\frac{1}{t^2+m^2}\frac{1}{(\mathbf{p}+\mathbf{s}+\mathbf{t})^2+m^2}\,, \tag{3.24}$$

$$\mathcal{F}_{4\mathrm{j}}^{(s)} = -\frac{1}{32}g_3^8 T\int_{pqrst}\frac{1}{q^2+m^2}\frac{1}{(\mathbf{p}+\mathbf{q})^2+m^2}\frac{1}{(\mathbf{p}+\mathbf{r})^2+m^2}\frac{1}{(\mathbf{t}+\mathbf{r})^2+m^2}\frac{1}{r^2+m^2}\times$$
$$\times\frac{1}{(\mathbf{p}+\mathbf{s})^2+m^2}\frac{1}{(\mathbf{s}+\mathbf{t})^2+m^2}\frac{1}{s^2+m^2}\,. \tag{3.25}$$

Using the expressions in the appendix B, we obtain

$$\mathcal{F}_4^{(s)} = -\frac{g_3^8 T}{288m(4\pi)^5}\times$$
$$\times\left[\log^2\frac{\Lambda}{2m}+\frac{1}{4}(1-8\log 2)\log\frac{\Lambda}{2m}-\frac{15}{64}-\frac{3}{8}\pi^2+\frac{9}{8}\pi^2\log 2+\right.$$
$$\left.+\frac{23}{4}\log 2+6\log^2 2-6\log 3-\frac{81}{16}\zeta(3)+5\mathrm{Li}_2(\tfrac{1}{4})+9\mathrm{C}_{4\mathrm{j}}\right]\,, \tag{3.26}$$

where $C_{4j} = 0.443166$. We note that all poles in ϵ cancel as they must since there are no divergences from the hard part proportional to g_3^8/m. Adding eqs. (3.2), (3.3), (3.8), (3.14), and (3.26) as well as the counterterm eq. (2.24), we obtain the soft contribution to the free energy through five loops

$$\mathcal{F}_{0+1+2+3+4}^{(s)} = -\frac{m^3T}{12\pi}+\frac{g_3^2m^2T}{8(4\pi)^2}+\frac{g_3^4mT}{96(4\pi)^3}\left[8\log\frac{\Lambda}{2m}+9-8\log 2\right]+$$
$$+\frac{g_3^6T}{768(4\pi)^4}\times$$
$$\times\left[-4(4-\pi^2)\log\frac{\Lambda}{2m}-4+16\log 2-42\zeta(3)+\pi^2(1+2\log 2)\right]-$$
$$-\frac{g_3^8T}{288m(4\pi)^5}\times$$
$$\times\left[\log^2\frac{\Lambda}{2m}+\frac{1}{4}(1-8\log 2)\log\frac{\Lambda}{2m}-\frac{15}{64}-\frac{3}{8}\pi^2+\frac{9}{8}\pi^2\log 2+\right.$$
$$\left.+\frac{23}{4}\log 2+6\log^2 2-6\log 3-\frac{81}{16}\zeta(3)+5\mathrm{Li}_2(\tfrac{1}{4})+9\mathrm{C}_{4\mathrm{j}}\right]\,. \tag{3.27}$$

Using the evolution equations for g_3^2 and m^2, it easy to check that the free energy, eq. (2.23) plus eq. (3.27) is independent of the factorization scale Λ.

By expanding the coupling g_3^2 (2.8) and the mass parameter m^2 (2.43) to the appropriate orders in the various terms in (3.27), we obtain the soft contribution through order g^7. This yields

$$\mathcal{F}_{\mathrm{soft}} = -\frac{\pi^2T^4}{90}\times$$
$$\times\left\{\frac{5\sqrt{6}}{3}\alpha^{3/2}-\frac{15}{2}\alpha^2-\frac{15\sqrt{6}}{2}\alpha^{5/2}\left[\log\frac{\mu}{4\pi T}-\frac{2}{3}\log\alpha+C_5\right]-\right.$$
$$\left.-\frac{15}{16}\alpha^3\times\right.$$

$$
\begin{aligned}
&\times \left[-48 \log \frac{\mu}{4\pi T} + 16 \frac{\zeta'(-1)}{\zeta(-1)} - 32\gamma_E - 84\zeta(3) + 8 + 16 \log \frac{2}{3} + \right. \\
&\qquad \left. + 16 \log \alpha + \pi^2 \left(2 + 12 \log 2 - 4 \log \frac{2}{3} - 4 \log \alpha + 8 \log \frac{\Lambda}{4\pi T} \right) \right] + \\
&+ \frac{225\sqrt{6}}{8} \alpha^{7/2} \times \\
&\times \left[\log^2 \frac{\mu}{4\pi T} + \left(\frac{221}{135} + \frac{2}{3}\gamma_E - \frac{4}{3} \log \frac{2}{3} - \frac{4}{3} \frac{\zeta'(-1)}{\zeta(-1)} - \frac{4}{3} \log \alpha \right) \log \frac{\mu}{4\pi T} + \right. \\
&\qquad + \left(\frac{2}{15} + \frac{8}{45} \frac{\zeta'(-1)}{\zeta(-1)} - \frac{52}{45}\gamma_E + \frac{8}{45} \log \frac{2}{3} \right) \log \alpha + \frac{4}{45} \log^2 \alpha + \\
&\qquad \left. + C_7 \right] \Bigg\} \,, \qquad (3.28)
\end{aligned}
$$

where the constants C_5 and C_7 are defined below.

4 Results and discussion

The full pressure is given by minus the sum of eq. (2.23) and eq. (3.27). The strict weak-coupling result for the pressure through order g^7 is minus the sum of eq. (2.23) and eq. (3.28). This yields

$$
\begin{aligned}
\mathcal{P} = \mathcal{P}_{\rm ideal} &\times \\
&\times \Bigg\{ 1 - \frac{5}{4}\alpha + \frac{5\sqrt{6}}{3}\alpha^{3/2} + \frac{15}{4}\alpha^2 \left[\log \frac{\mu}{4\pi T} + C_4 \right] - \\
&- \frac{15\sqrt{6}}{2}\alpha^{5/2} \left[\log \frac{\mu}{4\pi T} - \frac{2}{3} \log \alpha + C_5 \right] - \\
&- \frac{45}{4}\alpha^3 \left[\log^2 \frac{\mu}{4\pi T} - \frac{1}{3} \left(\frac{269}{45} - 2\gamma_E - 8 \frac{\zeta'(-1)}{\zeta(-1)} + 4 \frac{\zeta'(-3)}{\zeta(-3)} \right) \log \frac{\mu}{4\pi T} + \right. \\
&\qquad \left. + \frac{1}{3}(4 - \pi^2) \log \alpha + C_6 \right] + \\
&+ \frac{225\sqrt{6}}{8}\alpha^{7/2} \times \\
&\times \left[\log^2 \frac{\mu}{4\pi T} + \left(\frac{221}{135} + \frac{2}{3}\gamma_E - \frac{4}{3} \log \frac{2}{3} - \frac{4}{3} \frac{\zeta'(-1)}{\zeta(-1)} - \frac{4}{3} \log \alpha \right) \log \frac{\mu}{4\pi T} + \right. \\
&\qquad \left. + \left(\frac{2}{15} + \frac{8}{45} \frac{\zeta'(-1)}{\zeta(-1)} - \frac{52}{45}\gamma_E - \frac{8}{45} \log \frac{2}{3} \right) \log \alpha + \frac{4}{45} \log^2 \alpha + C_7 \right] \Bigg\}, \qquad (4.1)
\end{aligned}
$$

where $\mathcal{P}_{\rm ideal} = \pi^2 T^4/90$ and where the constants $C_4 - C_7$ are

$$
C_4 \equiv -\frac{59}{45} + \frac{1}{3}\gamma_E + \frac{4}{3}\frac{\zeta'(-1)}{\zeta(-1)} - \frac{2}{3}\frac{\zeta'(-3)}{\zeta(-3)} \,, \qquad (4.2)
$$

$$
C_5 \equiv \frac{5}{6} + \frac{1}{3}\gamma_E - \frac{2}{3}\log\frac{2}{3} - \frac{2}{3}\frac{\zeta'(-1)}{\zeta(-1)} \,, \qquad (4.3)
$$

$$
C_6 \equiv \frac{1}{3}(4 - \pi^2)\log\frac{2}{3} + \frac{103}{54} + \frac{1}{18}C'_{\rm ball} - \frac{1}{6}C^a_{\rm triangle} - \frac{\pi^2}{12}C^b_{\rm triangle} + \frac{4}{9}\gamma_1 - \frac{511}{180}\gamma_E +
$$

$$+\frac{25}{36}\gamma_E^2+\frac{5\pi^2}{24}-\frac{\pi^2}{3}\gamma_E+\pi^2\log 2+\left(\frac{175}{54}-\frac{1}{9}\gamma_E\right)\frac{\zeta'(-1)}{\zeta(-1)}+\frac{2}{3}\left(\frac{\zeta'(-1)}{\zeta(-1)}\right)^2+$$
$$+\frac{5}{9}\frac{\zeta''(-1)}{\zeta(-1)}-\frac{2}{3}\gamma_E\frac{\zeta'(-3)}{\zeta(-3)}-\frac{2267}{324}\zeta(3)\,, \tag{4.4}$$

$$C_7=-\frac{1457}{810}+\frac{1}{45}C'_{\rm ball}-\frac{2}{15}C_I+\frac{749}{270}\gamma_E+\frac{56}{15}\gamma_1-\frac{11}{20}\pi^2+\frac{2}{15}\frac{\zeta''(-1)}{\zeta(-1)}+$$
$$+\frac{16}{15}\gamma_E\log(2\pi)-\frac{16}{15}\log^2(2\pi)-\frac{52}{45}\gamma_E\log\frac{2}{3}-\frac{19}{27}\frac{\zeta'(-1)}{\zeta(-1)}-\frac{38}{45}\gamma_E\frac{\zeta'(-1)}{\zeta(-1)}+$$
$$+\frac{4}{45}\left(\frac{\zeta'(-1)}{\zeta(-1)}\right)^2+\frac{34}{15}\log\frac{2}{3}+\frac{2}{5}\pi^2\log 2+\frac{4}{45}\log^2 3+\frac{28}{15}\log^2 2-$$
$$-\frac{8}{45}\log 2\log 3+\frac{8}{45}\frac{\zeta'(-1)}{\zeta(-1)}\log\frac{2}{3}-\frac{97}{54}\zeta(3)+\frac{16}{9}{\rm Li}_2(\tfrac{1}{4})+\frac{97}{90}\gamma_E^2+\frac{16}{5}C_{4\rm j}\,, \tag{4.5}$$

where $C^a_{\rm triangle}=-25.7055$ and $C^b_{\rm triangle}=28.9250$. The numerical values of C_4-C_7 are

$$C_4 = 1.09775\,, \tag{4.6}$$
$$C_5 = -0.0273205\,, \tag{4.7}$$
$$C_6 = -6.5936\,, \tag{4.8}$$
$$C_7 = -0.862\,. \tag{4.9}$$

Note that the Λ-dependence cancels in the result (4.1). Using eq. (2.9) for the running of α, it is straightforward to check that the final result eq. (4.1) is RG invariant up to higher-order corrections. The order-g^4 result was obtained by Frenkel, Saa, and Taylor [23], the order-g^5 result by Parwani and Singh [24], the order-$g^6\log(g)$ result by Braaten and Nieto [19], and the order-g^6 result by Gynther et al. [15]. The latter was later reproduced in ref. [21] using screened perturbation theory [25–27] by taking the weak-coupling limit for the mass parameter, $m=gT/\sqrt{24}$.

An expansion of the pressure in powers of g is given in eq. (4.1). It is accurate up to corrections of order $g^8\log(g)$. A more accurate expression can be obtained by using the fact that our short-distance coefficients satisfy a set of evolution equations. The solutions to the evolution equations are

$$g_3^2(\Lambda) = g_3^2(2\pi T)\,, \tag{4.10}$$
$$f(\Lambda) = f(2\pi T)-\frac{\pi^2 g_3^6(2\pi T)}{192(4\pi)^4}\log\frac{\Lambda}{2\pi T}\,, \tag{4.11}$$
$$m^2(\Lambda) = m^2(2\pi T)+\frac{g_3^4(2\pi T)}{6(4\pi)^2}\log\frac{\Lambda}{2\pi T}\,. \tag{4.12}$$

If we substitute the short-distance coefficients (4.10) and (4.12) into eq. (3.27) and add the short-distance contribution (4.11), setting $\Lambda=gT/\sqrt{24}$ everwhere, and expand the resulting expression in powers of g, we obtain the complete result for the pressure, which is correct up to order $g^8\log(g)$. The contributions to the free energy $\mathcal{F}$ of order $g^8\log(g)$ come from (4.11) and from using (4.12) to expand the $g_3^2m^2T$ term in (3.27). This yields

$$\mathcal{F}_{\rm g^8\,log(g)} = \frac{3g^8T^4}{64(4\pi)^6}\,(\log 2-\gamma_E)\,(4-\pi^2)\log(g)\,. \tag{4.13}$$

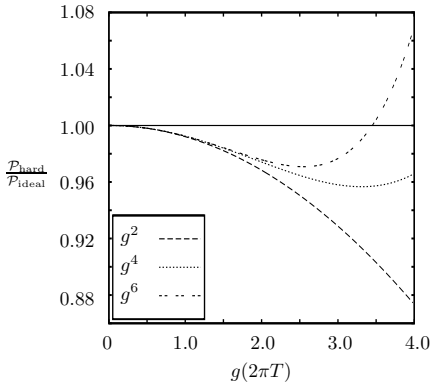

Figure 8. Hard contributions $\mathcal{P}_{\rm hard}$ to the pressure $\mathcal{P}$ normalized to $\mathcal{P}_{\rm ideal}$ to order g^2, g^4, and g^6.

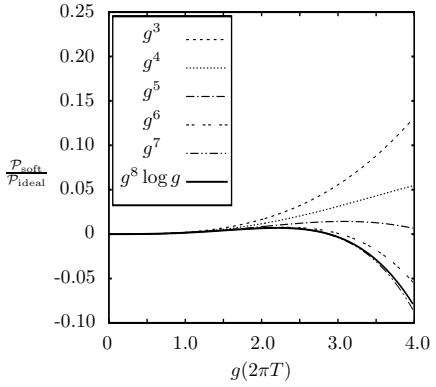

Figure 9. Soft contributions $\mathcal{P}_{\rm soft}$ to the pressure $\mathcal{P}$ normalized to $\mathcal{P}_{\rm ideal}$ to order g^3, g^4, g^5, g^6, g^7, and $g^8 \log(g)$.

Moreover, using the solutions to the flow equations, we are summing up leading logarithms of the form $g^{2n+3}\log^n(g)$ and e.g. subleading logarithms of the form $g^{2n+5}\log^n(g)$, where $n = 2, 3, \ldots$. These terms are obtained by expanding out the m^3T and $g_3^4 mT$ terms in (3.27), respectively.

In figure 8, we show the various loop orders of $\mathcal{P}_{\rm hard}$ normalized to $\mathcal{P}_{\rm ideal}$ to orders g^2, g^4, and g^6, where $\mathcal{P}_{\rm hard}$ is given by minus eq. (2.23).[4] We have chosen $\mu = 2\pi T$ and $\Lambda = 2\pi T$. We notice that the successive approximations are larger than the previous one. In figure 9, we show the weak-coupling expansion of $\mathcal{P}_{\rm soft}$ normalized to $\mathcal{P}_{\rm ideal}$ to orders g^3, g^4, g^5 g^6, g^7, and $g^8\log(g)$, where $\mathcal{P}_{\rm soft}$ is given by minus the sum of eqs. (3.28) and (4.13).

In figure 10, we show the weak-coupling expansion of the pressure $\mathcal{P}$ given by (4.1) minus (4.13) normalized to $\mathcal{P}_{\rm ideal}$ to orders g^2, g^3 g^4, g^5 g^6, g^7, and $g^8\log(g)$. The convergence properties of the successive approximations of the sum $\mathcal{P} = \mathcal{P}_{\rm hard} + \mathcal{P}_{\rm soft}$

[4]Note that we omit the pole in ϵ in eq. (2.23) in the plots of the hard part.

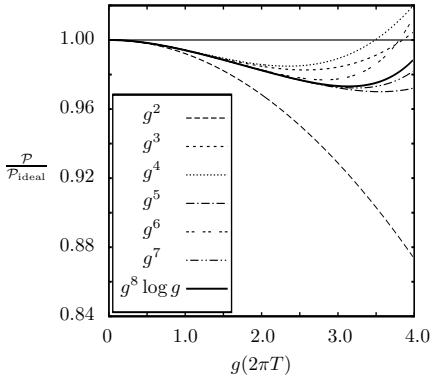

Figure 10. Weak-coupling expansion of the pressure $\mathcal{P}$ normalized to $\mathcal{P}_{\rm ideal}$ to order g^2, g^3, g^4, g^5, g^6, g^7, and $g^8 \log(g)$.

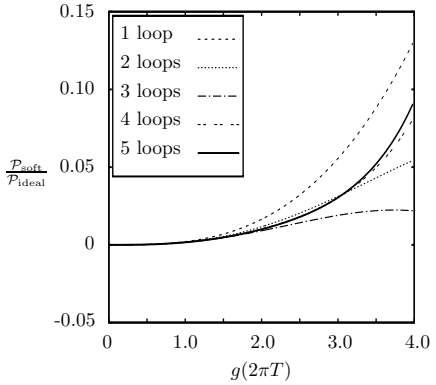

Figure 11. Soft contributions $\mathcal{P}_{\rm soft}$ to the pressure $\mathcal{P}$ normalized to $\mathcal{P}_{\rm ideal}$ at one through five loops.

clearly is better than the convergence properties of the successive approximations to $\mathcal{P}_{\rm hard}$ and $\mathcal{P}_{\rm soft}$ separately.

In figure 11, we plot the successive loop orders of minus eq. (3.27) normalized to $\mathcal{P}_{\rm ideal}$. In the one- and two-loop approximations, we use the leading-order results for g_3^2 and for m^2. At three and four loops, we use the leading-order result for g_3^2 and next-to-leading order result for m^2. Finally, at five loops, we use the solutions to the evolution equations for g_3^2, f, and m^2. The renormalization scale is $\mu = 2\pi T$ and the factorization scale is $\Lambda = gT/\sqrt{24}$. These approximations represent a selective resummation of higher-order terms. Clearly, the convergence is better than the strict perturbative expansion. In particular, the three-, four-, and five-loop approximations are very close.

In figure 12, we plot the successive loop orders of the the pressure which is given by the sum of minus eq. (2.23) minus eq. (3.27), and minus (4.13), normalized to $\mathcal{P}_{\rm ideal}$, starting

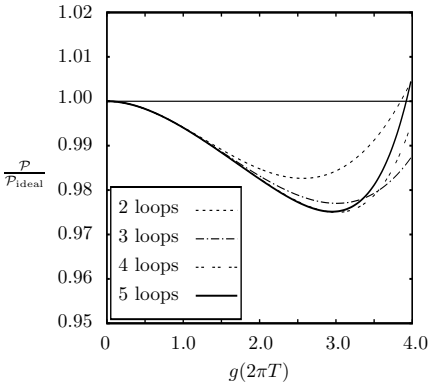

Figure 12. Successive approximations to the pressure $\mathcal{P}$ normalized to $\mathcal{P}_{\rm ideal}$ at two through five loops.,

at two loops. We are using the same approximations for g_3^2 and m^2 as in the previous plot. Again we notice that the convergence of P is better than $P_{\rm hard}$ and $P_{\rm soft}$ separately. In fact the convergence is very good as the 3-loop through 5-loop approximations are very close. It is not surprising that a selective resummation improves the convergence of the series. This was also notice in screened perturbation theory [21, 25–27].

5 Summary

In the present paper, we have calculated the pressure to order $g^8\log(g)$ in massless ϕ^4-theory at weak coupling. The first step is the determination of the coefficients in the dimensionally reduced effective field theory. This calculation encodes the physics of the hard scale T. The mass parameter was needed to order g^6 and involves a nontrivial three-loop sum-integral that was recently calculated in ref. [21]. The second step consists of using the effective theory to calculate the vacuum diagrams through five loops. All loop diagrams in the effective theory but one could be calculated analytically with dimensional regularization. This way of organizing the calculations is more economical and efficient than resummed perturbation theory.

The parameters of the effective theory, g_3^2, f, and m^2, satisfy a set of evolution equations. The solutions of these equations show that the parameters depend explicitly on the renormalization scale. This dependence is necessary to cancel the dependence on the scale in the effective theory [19]. The fact the our final result for the pressure is independent of the renormalization scale is a nontrivial check of the calculations. Furthermore, by choosing $\Lambda = gT/\sqrt{24}$ and using the solutions to the evolution equations, we were able to sum up leading logarithms of the form $g^{2n+3}\log^n(g)$ and e.g. subleading logarithms of the form $g^{2n+5}\log^n(g)$, where $n = 2, 3, \ldots$. as well as obtaining the coefficient of the $g^8\log(g)$ term.

As pointed out in ref. [15], it would be advantageous to develop the machinery of calculating complicated multiloop sum-integrals in an automated fashion as has been done for

Feynman diagrams at zero temperature. Perhaps such techniques could provide analytical expressions for the constants that today are known only numerically. This is necessary if one wants to tackle the formidable problem of calculating the hard part of the g^6-contribution to the free energy of QCD.

Acknowledgments

The authors would like to thank T. Brauner, B. Kastening, and M. Laine for useful discussions. The authors would like to thank the Niels Bohr International Academy for kind hospitality.

A Sum-integrals

In the imaginary-time formalism for thermal field theory, the 4-momentum $P = (P_0, \mathbf{p})$ is Euclidean with $P^2 = P_0^2 + \mathbf{p}^2$. The Euclidean energy p_0 has discrete values: $P_0 = 2n\pi T$ for bosons, where n is an integer. Loop diagrams involve sums over P_0 and integrals over $\mathbf{p}$. With dimensional regularization, the integral is generalized to $d = 3-2\epsilon$ spatial dimensions. We define the dimensionally regularized sum-integral by

$$\sum\!\!\!\!\!\!\int_P \equiv \left(\frac{e^\gamma \mu^2}{4\pi}\right)^\epsilon T \sum_{P_0 = 2n\pi T} \int \frac{d^{3-2\epsilon}p}{(2\pi)^{3-2\epsilon}} , \tag{A.1}$$

where $3-2\epsilon$ is the dimension of space and μ is an arbitrary momentum scale. The factor $(e^\gamma/4\pi)^\epsilon$ is introduced so that, after minimal subtraction of the poles in ϵ due to ultraviolet divergences, μ coincides with the renormalization scale of the $\overline{\rm MS}$ renormalization scheme.

A.1 One-loop sum-integrals

The massless one-loop sum-integral is given by

$$\begin{aligned}
\mathcal{I}_n &\equiv \sum\!\!\!\!\!\!\int_P \frac{1}{P^{2n}} \\
&= (e^{\gamma_E}\mu^2)^\epsilon \frac{\zeta(2n-3+2\epsilon)}{8\pi^2} \frac{\Gamma(n-\frac{3}{2}+\epsilon)}{\Gamma(\frac{1}{2})\Gamma(n)} (2\pi T)^{4-2n-2\epsilon} ,
\end{aligned} \tag{A.2}$$

where $\zeta(x)$ is Riemann's zeta function. Specifically, we need the sum-integrals

$$\begin{aligned}
\mathcal{I}'_0 &\equiv \sum\!\!\!\!\!\!\int_P \log P^2 \\
&= -\frac{\pi^2 T^4}{45} \left[1 + \mathcal{O}(\epsilon)\right] , \qquad (A.3) \\
\mathcal{I}_1 &= \frac{T^2}{12} \left(\frac{\mu}{4\pi T}\right)^{2\epsilon} \left[1 + \left(2 + 2\frac{\zeta'(-1)}{\zeta(-1)}\right)\epsilon + \right. \\
&\qquad \left. + \left(4 + \frac{\pi^2}{4} + 4\frac{\zeta'(-1)}{\zeta(-1)} + 2\frac{\zeta''(-1)}{\zeta(-1)}\right)\epsilon^2 + \mathcal{O}(\epsilon^3)\right] , \qquad (A.4) \\
\mathcal{I}_2 &= \frac{1}{(4\pi)^2} \left(\frac{\mu}{4\pi T}\right)^{2\epsilon} \left[\frac{1}{\epsilon} + 2\gamma_E + \left(\frac{\pi^2}{4} - 4\gamma_1\right)\epsilon + \mathcal{O}(\epsilon^2)\right] , \qquad (A.5)
\end{aligned}$$

$$\mathcal{I}_3 = \frac{1}{(4\pi)^4 T^2}\left[2\zeta(3) + \mathcal{O}(\epsilon)\right] . \tag{A.6}$$

A.2 Two-loop sum-integrals

We need three two-loop sum-integral that are listed below:

$$\begin{aligned}
\mathcal{I}_{\rm sun} &= \sum\!\!\!\!\!\!\int_{PQ} \frac{1}{P^2Q^2(P+Q)^2} \\
&= \mathcal{O}(\epsilon) , \qquad\qquad (A.7)\\
\sum\!\!\!\!\!\!\int_{PQ} \frac{P^2+(2/d)p^2}{P^6Q^2(P+Q)^2} &= \frac{3}{4(4\pi)^4}\left(\frac{\mu}{4\pi T}\right)^{4\epsilon}\left[\frac{1}{\epsilon^2}+\left(\frac{5}{6}+4\gamma_E\right)\frac{1}{\epsilon}+\frac{89}{36}+\frac{\pi}{2}+\right.\\
&\qquad \left.+\frac{10}{3}\gamma_E+4\gamma_E^2-8\gamma_1+\mathcal{O}(\epsilon)\right] , \qquad (A.8)\\
\sum\!\!\!\!\!\!\int_{PQ} \frac{P^2-(4/d)p^2}{P^6Q^2(P+Q)^2} &= \frac{1}{4(4\pi)^4}\left(\frac{\mu}{4\pi T}\right)^{4\epsilon}\left[\frac{1}{\epsilon}+\frac{19}{6}+4\gamma_E+\mathcal{O}(\epsilon)\right] . \qquad (A.9)
\end{aligned}$$

The setting-sun sum-integral was first calculated by Arnold and Zhai in refs. [5, 6]. The remaining two-loop sum-integrals were calculated by Braaten and Petitgirard [28, 29] using the techniques developed in [5, 6].

A.3 Three-loop sum-integrals

We need the following three-loop sum-integrals:

$$\begin{aligned}
\mathcal{I}_{\rm ball} &= \sum\!\!\!\!\!\!\int_{PQR} \frac{1}{P^2Q^2R^2(P+Q+R)^2} \\
&= \frac{T^4}{24(4\pi)^2}\left(\frac{\mu}{4\pi T}\right)^{6\epsilon}\left[\frac{1}{\epsilon}+\frac{91}{15}+8\frac{\zeta'(-1)}{\zeta(-1)}-2\frac{\zeta'(-3)}{\zeta(-3)}+\mathcal{O}(\epsilon)\right] , \qquad (A.10)\\
\mathcal{I}'_{\rm ball} &= \sum\!\!\!\!\!\!\int_{PQR} \frac{1}{P^4Q^2R^2(P+Q+R)^2} \\
&= \frac{T^2}{8(4\pi)^4}\left(\frac{\mu}{4\pi T}\right)^{6\epsilon}\left[\frac{1}{\epsilon^2}+\left(\frac{17}{6}+4\gamma_E+2\frac{\zeta'(-1)}{\zeta(-1)}\right)\frac{1}{\epsilon}+\right.\\
&\quad \left.+\frac{1}{2}\gamma_E\left(17+15\gamma_E+12\frac{\zeta'(-1)}{\zeta(-1)}\right)+C'_{\rm ball}+\mathcal{O}(\epsilon)\right] , \qquad (A.11)
\end{aligned}$$

and

$$\begin{aligned}
&\sum\!\!\!\!\!\!\int_P \frac{1}{P^2}\left\{[\Pi(P)]^2-\frac{2}{(4\pi)^2\epsilon}\Pi(P)\right\} = \\
&\quad = -\frac{T^2}{4(4\pi)^4}\left(\frac{\mu}{4\pi T}\right)^{6\epsilon}\times \\
&\qquad \times\left\{\frac{1}{\epsilon^2}+\frac{1}{\epsilon}\left[\frac{4}{3}+2\frac{\zeta'(-1)}{\zeta(-1)}+4\gamma_E\right]+\right. \\
&\qquad\quad +\frac{1}{3}\left[46-8\gamma_E-16\gamma_E^2-104\gamma_1-24\gamma_E\log(2\pi)+24\log^2(2\pi)+\frac{45\pi^2}{4}+\right. \\
&\qquad\qquad \left.\left.+24\frac{\zeta'(-1)}{\zeta(-1)}+2\frac{\zeta''(-1)}{\zeta(-1)}+16\gamma_E\frac{\zeta'(-1)}{\zeta(-1)}\right]+C_I+\mathcal{O}(\epsilon)\right\} , \qquad (A.12)
\end{aligned}$$

where the self-energy $\Pi(P)$ is defined as

$$\Pi(P) = \sum\!\!\!\!\!\!\int_Q \frac{1}{Q^2(P+Q)^2} \,, \tag{A.13}$$

and $C'_{\rm ball} = 48.7976$ and $C_I = -38.4672$. The massless basketball sum-integral was first calculated by Arnold and Zhai in refs. [5, 6]. The sum-integral eq. (A.11) was calculated by Gynther *et al.* in ref. [15]. The expression for the sum-integral eq. (A.12) was calculated in ref. [21].

A.4 Four-loop sum-integrals

We also need a single four-loop sum-integral which was calculated in ref. [15]:

$$\begin{aligned}
&\sum\!\!\!\!\!\!\int_P \left\{ [\Pi(P)]^3 - \frac{3}{(4\pi)^2\epsilon}[\Pi(P)]^2 \right\} = \\
&\quad = -\frac{T^4}{16(4\pi)^4} \times \\
&\qquad \times \left[\frac{1}{\epsilon^2} + \left(4\log\frac{\mu}{4\pi T} + \frac{10}{3} + 4\frac{\zeta'(-1)}{\zeta(-1)} \right) \frac{1}{\epsilon} + (2\log\frac{\mu}{4\pi T} + \gamma_E)^2 + \right. \\
&\qquad\quad \left. + \left(\frac{6}{5} - 2\gamma_E + 4\frac{\zeta'(-3)}{\zeta(-3)} \right) (2\log\frac{\mu}{4\pi T} + \gamma_E) + C^a_{\rm triangle} \right] - \\
&\qquad - \frac{T^4}{512(4\pi)^2} \left[\frac{1}{\epsilon} + 8\log\frac{\mu}{4\pi T} + 4\gamma_E + C^b_{\rm triangle} \right] + \mathcal{O}(\epsilon) \,,
\end{aligned} \tag{A.14}$$

where $C^a_{\rm triangle} = -25.7055$ and $C^b_{\rm triangle} = 28.9250$.

B Three-dimensional integrals

Dimensional regularization can be used to regularize both the ultraviolet divergences and infrared divergences in 3-dimensional integrals over momenta. The spatial dimension is generalized to $d = 3 - 2\epsilon$ dimensions. Integrals are evaluated at a value of d for which they converge and then analytically continued to $d = 3$. We use the integration measure

$$\int_p \equiv \left(\frac{e^\gamma \mu^2}{4\pi} \right)^\epsilon \int \frac{d^{3-2\epsilon}p}{(2\pi)^{3-2\epsilon}} \,. \tag{B.1}$$

B.1 One-loop integrals

The one-loop integral is given by

$$\begin{aligned}
I_n &\equiv \int_p \frac{1}{(p^2+m^2)^n} \\
&= \frac{1}{8\pi} (e^{\gamma_E}\mu^2)^\epsilon \frac{\Gamma(n - \frac{3}{2} + \epsilon)}{\Gamma(\frac{1}{2})\Gamma(n)} m^{3-2n-2\epsilon} \,.
\end{aligned} \tag{B.2}$$

Specifically, we need

$$\begin{aligned}
I'_0 &\equiv \int_p \log(p^2+m^2) \\
&= -\frac{m^3}{6\pi} \left(\frac{\mu}{2m} \right)^{2\epsilon} \left[1 + \frac{8}{3}\epsilon + \left(\frac{52}{9} + \frac{\pi^2}{4} \right) \epsilon^2 + \mathcal{O}\left(\epsilon^3\right) \right] \,,
\end{aligned} \tag{B.3}$$

$$I_1 = -\frac{m}{4\pi}\left(\frac{\mu}{2m}\right)^{2\epsilon}\left[1+2\epsilon+\left(4+\frac{\pi^2}{4}\right)\epsilon^2+\mathcal{O}\left(\epsilon^3\right)\right], \tag{B.4}$$

$$I_2 = \frac{1}{8\pi m}\left(\frac{\mu}{2m}\right)^{2\epsilon}\left[1+\frac{\pi^2}{4}\epsilon^2+\mathcal{O}\left(\epsilon^3\right)\right], \tag{B.5}$$

$$I_3 = \frac{1}{32\pi m^3}\left(\frac{\mu}{2m}\right)^{2\epsilon}\left[1+2\epsilon+\frac{\pi^2}{4}\epsilon^2+\mathcal{O}\left(\epsilon^3\right)\right], \tag{B.6}$$

$$I_4 = \frac{1}{64\pi m^5}\left(\frac{\mu}{2m}\right)^{2\epsilon}\left[1+\frac{8}{3}\epsilon+\left(\frac{4}{3}+\frac{\pi^2}{4}\right)\epsilon^2+\mathcal{O}\left(\epsilon^3\right)\right]. \tag{B.7}$$

B.2 Two-loop integrals

We need the following two-loop integral

$$\begin{aligned} I_{\rm sun}(p=im) &= \int_{qr}\frac{1}{q^2+m^2}\frac{1}{r^2+m^2}\frac{1}{(\mathbf{p}+\mathbf{q}+\mathbf{r})^2+m^2}\bigg|_{p=im} \\ &= \frac{1}{4(4\pi)^2}\left(\frac{\mu}{2m}\right)^{4\epsilon}\times \\ &\quad\times\left[\frac{1}{\epsilon}+6-8\log 2+\left(36-\frac{\pi^2}{6}-48\log 2+8\log^2 2\right)\epsilon+\mathcal{O}(\epsilon^2)\right]. \end{aligned} \tag{B.8}$$

This integral was calculated to order ϵ^0 in ref. [19] and to order ϵ in refs. [28, 29].

B.3 Three-loop integrals

We need the following three-loop integrals:

$$\begin{aligned} I_{\rm ball} &= \int_{pqr}\frac{1}{p^2+m^2}\frac{1}{q^2+m^2}\frac{1}{r^2+m^2}\frac{1}{(\mathbf{p}+\mathbf{q}+\mathbf{r})^2+m^2} \\ &= -\frac{m}{(4\pi)^3}\left(\frac{\mu}{2m}\right)^{6\epsilon}\times \\ &\quad\times\left[\frac{1}{\epsilon}+8-4\log 2+4\left(13+\frac{17}{48}\pi^2-8\log 2+\log^2 2\right)\epsilon+\mathcal{O}\left(\epsilon^2\right)\right], \end{aligned} \tag{B.9}$$

$$\begin{aligned} I'_{\rm ball} &= \int_{pqr}\frac{1}{(p^2+m^2)^2}\frac{1}{q^2+m^2}\frac{1}{r^2+m^2}\frac{1}{(\mathbf{p}+\mathbf{q}+\mathbf{r})^2+m^2} \\ &= \frac{1}{8m(4\pi)^3}\left(\frac{\mu}{2m}\right)^{6\epsilon}\times \\ &\quad\times\left[\frac{1}{\epsilon}+2-4\log 2+4\left(1+\frac{17}{48}\pi^2-2\log 2+\log^2 2\right)\epsilon+\mathcal{O}\left(\epsilon^2\right)\right], \end{aligned} \tag{B.10}$$

$$\begin{aligned} J &= \int_{pqr}\frac{1}{(q^2+m^2)^2}\frac{1}{(\mathbf{p}+\mathbf{q})^2+m^2}\frac{1}{(r^2+m^2)^2}\frac{1}{(\mathbf{p}+\mathbf{r})^2+m^2} \\ &= \frac{1}{16m^3(4\pi)^3}\left(\frac{\mu}{2m}\right)^{6\epsilon}\left[1+\mathcal{O}\left(\epsilon\right)\right], \end{aligned} \tag{B.11}$$

$$\begin{aligned} K &= \int_{pqr}\frac{1}{(q^2+m^2)^3}\frac{1}{(\mathbf{p}+\mathbf{q})^2+m^2}\frac{1}{r^2+m^2}\frac{1}{(\mathbf{p}+\mathbf{r})^2+m^2} \\ &= \frac{1}{32m^3(4\pi)^3}\left(\frac{\mu}{2m}\right)^{6\epsilon}\left[\frac{1}{\epsilon}+5-4\log 2+\mathcal{O}\left(\epsilon\right)\right]. \end{aligned} \tag{B.12}$$

The massive basketball was calculated in ref. [19] to order ϵ^0, and to order ϵ in ref. [9]. $I'_{\rm ball}$ can be obtained by differentiation of $I_{\rm ball}$ with respect to m. The 3-loop integrals J and K are calculated in appendix C.

B.4 Four-loop integrals

We need the following two four-loop integrals

$$\begin{aligned} I_{\rm triangle} &= \int_{pqrs} \frac{1}{q^2+m^2}\frac{1}{(\mathbf{p}+\mathbf{q})^2+m^2}\frac{1}{r^2+m^2}\frac{1}{(\mathbf{p}+\mathbf{r})^2+m^2}\frac{1}{s^2+m^2}\frac{1}{(\mathbf{p}+\mathbf{s})^2+m^2} \\ &= \frac{\pi^2}{32(4\pi)^4}\left(\frac{\mu}{2m}\right)^{8\epsilon}\left[\frac{1}{\epsilon}+2+4\log 2-\frac{84}{\pi^2}\zeta(3)+\mathcal{O}(\epsilon)\right], \qquad \text{(B.13)} \\ I'_{\rm triangle} &= \int_{pqrs} \frac{1}{(q^2+m^2)^2}\frac{1}{(\mathbf{p}+\mathbf{q})^2+m^2}\frac{1}{r^2+m^2}\frac{1}{(\mathbf{p}+\mathbf{r})^2+m^2}\frac{1}{s^2+m^2}\frac{1}{(\mathbf{p}+\mathbf{s})^2+m^2} \\ &= \frac{\pi^2}{48m^2(4\pi)^4}\left(\frac{\mu}{2m}\right)^{8\epsilon}\left[1+\mathcal{O}(\epsilon)\right]. \qquad \text{(B.14)} \end{aligned}$$

The triangle diagram was calculated in ref. [30]. The diagram $I'_{\rm triangle}$ follows from the triangle diagram upon differentiation with respect to m^2.

B.5 Five-loop integrals

$$\begin{aligned} I_{\rm rung} &= \int_{pqrst} \frac{1}{q^2+m^2}\frac{1}{(\mathbf{p}+\mathbf{q})^2+m^2}\frac{1}{r^2+m^2}\frac{1}{(\mathbf{p}+\mathbf{r})^2+m^2}\frac{1}{s^2+m^2}\frac{1}{(\mathbf{p}+\mathbf{s})^2+m^2}\times \\ &\qquad \times\frac{1}{t^2+m^2}\frac{1}{(\mathbf{p}+\mathbf{t})^2+m^2} \\ &= \frac{1}{2m(4\pi)^5}\left(\frac{\mu}{2m}\right)^{10\epsilon}\left[\pi^2\log 2-\frac{9}{2}\zeta(3)+\mathcal{O}(\epsilon)\right], \qquad \text{(B.15)} \\ I_{\rm doublesun} &= \int_{pqrst} \frac{1}{(p^2+m^2)^2}\frac{1}{q^2+m^2}\frac{1}{r^2+m^2}\frac{1}{(\mathbf{p}+\mathbf{q}+\mathbf{r})^2+m^2}\times \\ &\qquad \times\frac{1}{s^2+m^2}\frac{1}{t^2+m^2}\frac{1}{(\mathbf{p}+\mathbf{s}+\mathbf{t})^2+m^2} \\ &= \frac{1}{32m(4\pi)^5}\left(\frac{\mu}{2m}\right)^{10\epsilon}\times \\ &\qquad \times\left[\frac{1}{\epsilon^2}+(4-8\log 2)\frac{1}{\epsilon}-4+\frac{31}{12}\pi^2-96\log 3+64\log 2+104\log^2 2\right. \\ &\qquad\quad \left.+80\mathrm{Li}_2(\tfrac{1}{4})+\mathcal{O}(\epsilon)\right], \qquad \text{(B.16)} \\ I_{\rm 4j} &= \int_{pqrst} \frac{1}{q^2+m^2}\frac{1}{(\mathbf{p}+\mathbf{q})^2+m^2}\frac{1}{(\mathbf{p}+\mathbf{r})^2+m^2}\frac{1}{(\mathbf{t}+\mathbf{r})^2+m^2}\frac{1}{r^2+m^2}\times \\ &\qquad \times\frac{1}{(\mathbf{p}+\mathbf{s})^2+m^2}\frac{1}{(\mathbf{t}+\mathbf{s})^2+m^2}\frac{1}{s^2+m^2} \\ &= \frac{1}{m(4\pi)^5}\left(\frac{\mu}{2m}\right)^{10\epsilon}\left[C_{\rm 4j}+\mathcal{O}(\epsilon)\right], \qquad \text{(B.17)} \end{aligned}$$

where $C_{\rm 4j}=0.443166$. The integrals are calculated in appendix C.

C Explicit calculations

In this appendix, we calculate explicitly some of the multi-loop vacuum diagrams in three dimensions.

The three-loop integral J in eq. (B.11) can be written as

$$J = \int_p \left[I'_{\rm bubble}(p)\right]^2 , \tag{C.1}$$

where

$$I'_{\rm bubble}(p) = \int_q \frac{1}{(q^2+m^2)^2}\frac{1}{(\mathbf{p}+\mathbf{q})^2+m^2} . \tag{C.2}$$

By power counting it is easy to see that both J and $I'_{\rm bubble}$ are finite in three spatial dimension. The latter then reduces to

$$I'_{\rm bubble}(p) = \frac{1}{8\pi m}\frac{1}{p^2+4m^2} . \tag{C.3}$$

Inserting eq. (C.3) into eq. (C.1) and using eq. (B.5) with $\epsilon = 0$ and a mass of $2m$. we obtain eq. (B.11).

The integral K can be calculated by noting the relation

$$I''_{\rm ball} = -2K - 3J . \tag{C.4}$$

The integral $I_{\rm rung}$ in (B.15) can be written as

$$I_{\rm rung} = \int_p I^4_{\rm bubble}(p) , \tag{C.5}$$

where

$$I_{\rm bubble}(p) = \int_q \frac{1}{q^2+m^2}\frac{1}{(\mathbf{p}+\mathbf{q})^2+m^2} . \tag{C.6}$$

The integrals $I_{\rm rung}$ and $I_{\rm bubble}(p)$ are convergent in three dimensions. The latter then reduces to

$$I_{\rm bubble}(p) = \frac{1}{4\pi p}\arctan\frac{p}{2m} . \tag{C.7}$$

$I_{\rm rung}$ can now be easily found and the result is given by eq. (B.15).

The diagram appearing in $\mathcal{F}_{5i}$ can be written as

$$I_{\rm doublesun} = \int_p \frac{1}{(p^2+m^2)^2} I^2_{\rm sun}(p) , \tag{C.8}$$

where $I_{\rm sun}(p)$ is

$$I_{\rm sun}(p) = \int_{qr} \frac{1}{q^2+m^2}\frac{1}{r^2+m^2}\frac{1}{(\mathbf{p}+\mathbf{q}+\mathbf{r})^2+m^2} . \tag{C.9}$$

In order to isolate the divergences in (C.8), we add and subtract $I_{\rm sun}(p=im)$, and rewrite it as

$$\begin{aligned} I_{\rm doublesun} = & \int_p \frac{1}{(p^2+m^2)^2} \times \\ & \times \Big\{ [I_{\rm sun}(p) - I_{\rm sun}(p=im)]^2 + 2 I_{\rm sun}(p) I_{\rm sun}(p=im) - \\ & - I^2_{\rm sun}(p=im) \Big\} \ . \end{aligned} \tag{C.10}$$

We denote the three terms above by $I_{\rm ds1}$, $I_{\rm ds2}$, and $I_{\rm ds3}$. We first consider $I_{\rm ds1}$. The difference $I_{\rm sun}(p) - I_{\rm sun}(p=im)$ is finite and can be calculated directly in three dimensions. We obtain

$$\begin{aligned} & I_{\rm sun}(p) - I_{\rm sun}(p=im) = \\ & \quad = -\frac{1}{(4\pi)^2} \left(\frac{\mu}{2m}\right)^{4\epsilon} \left[\frac{3m}{p} \arctan \frac{p}{3m} + \frac{1}{2} \ln \frac{p^2+9m^2}{64 m^2} + \mathcal{O}(\epsilon) \right] \ . \end{aligned} \tag{C.11}$$

The first term $I_{\rm ds1}$ is finite in three dimensions. Using eq. (C.11), we obtain

$$I_{\rm ds1} = \frac{1}{2m(4\pi)^5} \left(\frac{\mu}{2m}\right)^{10\epsilon} \left[6 \log^2 2 - 6 \log 3 + 4 \log 2 + 5 {\rm Li}_2(\tfrac{1}{4}) + \mathcal{O}(\epsilon) \right] \ . \tag{C.12}$$

The second term $I_{\rm ds2}$ can be written as

$$I_{\rm ds2} = 2 I_{\rm sun}(p=im) \int_{pqr} \frac{1}{(p^2+m^2)^2} \frac{1}{q^2+m^2} \frac{1}{r^2+m^2} \frac{1}{(\mathbf{p}+\mathbf{q}+\mathbf{r})^2+m^2} \ . \tag{C.13}$$

Using eqs. (B.8) and (B.10), we obtain

$$\begin{aligned} I_{\rm ds2} = & \frac{1}{16m(4\pi)^5} \left(\frac{\mu}{2m}\right)^{10\epsilon} \times \\ & \times \left[\frac{1}{\epsilon^2} + (8 - 12 \log 2) \frac{1}{\epsilon} + 52 + \frac{5}{4} \pi^2 - 96 \log 2 + 44 \log^2 2 + \mathcal{O}(\epsilon) \right] \ . \end{aligned} \tag{C.14}$$

Similarly, $I_{\rm ds3}$ can be written as

$$\begin{aligned} I_{\rm ds3} = & -I^2_{\rm sun}(p=im) I_2 \\ = & -\frac{1}{32m(4\pi)^5} \left(\frac{\mu}{2m}\right)^{10\epsilon} \times \\ & \times \left[\frac{1}{\epsilon^2} + (12 - 16 \log 2) \frac{1}{\epsilon} + 108 - \frac{\pi^2}{12} - 192 \log 2 + 80 \log^2 2 + \mathcal{O}(\epsilon) \right] . \end{aligned} \tag{C.15}$$

Adding eqs. (C.12), (C.14), and (C.15), we obtain

$$\begin{aligned} I_{\rm doublesun} = & \frac{1}{32m(4\pi)^5} \left(\frac{\mu}{2m}\right)^{10\epsilon} \times \\ & \times \left[\frac{1}{\epsilon^2} + (4 - 8 \log 2) \frac{1}{\epsilon} - 4 + \frac{31}{12} \pi^2 - 96 \log 3 + 64 \log 2 + 104 \log^2 2 + \right. \\ & \left. + 80 {\rm Li}_2(\tfrac{1}{4}) + \mathcal{O}(\epsilon) \right] . \end{aligned} \tag{C.16}$$

Let us finally discuss the five-loop integral appearing in eq. (B.17). It can be written as

$$I_{4\mathrm{j}} = \int_{pq} I_{\mathrm{bubble}}(p) \left[\Pi_{\mathrm{tri}}(p,q)\right]^2 \ , \tag{C.17}$$

where

$$\Pi_{\mathrm{tri}}(p,q) = \int_r \frac{1}{r^2+m^2} \frac{1}{(\mathbf{p}+\mathbf{r})^2+m^2} \frac{1}{(\mathbf{q}+\mathbf{r})^2+m^2} \ . \tag{C.18}$$

The diagram (C.18) is finite in three dimensions and can be written as [31, 32]

$$\Pi_{\mathrm{tri}}(p,q) = \frac{\arctan(\sqrt{D}/C)}{8\pi\sqrt{D}} \ , \tag{C.19}$$

where

$$C = \frac{p^2+q^2+\mathbf{p}\cdot\mathbf{q}+4m^2}{m^2} \ , \tag{C.20}$$

$$D = \frac{p^2q^2(\mathbf{p}-\mathbf{q})^2+4m^2[p^2q^2-(\mathbf{p}\cdot\mathbf{q})^2]}{4m^6} \ . \tag{C.21}$$

The integral (C.17) can now be evaluated numerically by first averaging over angles and then integrating over p and q. This yields

$$I_{4\mathrm{j}} = \frac{1}{m(4\pi)^5} \left(\frac{\mu}{2m}\right)^{10\epsilon} [0.443166] \ . \tag{C.22}$$

References

[1] J.-P. Blaizot, E. Iancu and A. Rebhan, *Thermodynamics of the high-temperature quark gluon plasma*, hep-ph/0303185 [SPIRES].

[2] D.H. Rischke, *The quark-gluon plasma in equilibrium*, *Prog. Part. Nucl. Phys.* **52** (2004) 197 [nucl-th/0305030] [SPIRES].

[3] U. Kraemmer and A. Rebhan, *Advances in perturbative thermal field theory*, *Rept. Prog. Phys.* **67** (2004) 351 [hep-ph/0310337] [SPIRES].

[4] J.O. Andersen and M. Strickland, *Resummation in hot field theories*, *Ann. Phys.* **317** (2005) 281 [hep-ph/0404164] [SPIRES].

[5] P. Arnold and C.-X. Zhai, *The three loop free energy for pure gauge QCD*, *Phys. Rev.* **D 50** (1994) 7603 [hep-ph/9408276] [SPIRES].

[6] P. Arnold and C.-X. Zhai, *The three loop free energy for high temperature QED and QCD with fermions*, *Phys. Rev.* **D 51** (1995) 1906 [hep-ph/9410360] [SPIRES].

[7] C.-X. Zhai and B.M. Kastening, *The Free energy of hot gauge theories with fermions through* g^5, *Phys. Rev.* **D 52** (1995) 7232 [hep-ph/9507380] [SPIRES].

[8] E. Braaten and A. Nieto, *Renormalization effects in a dilute Bose gas*, *Phys. Rev.* **B 55** (1997) 8090 [hep-th/9609047] [SPIRES].

[9] K. Kajantie, M. Laine, K. Rummukainen and Y. Schroder, *Four-loop vacuum energy density of the* SU(N_c) *+ adjoint Higgs theory*, *JHEP* **04** (2003) 036 [hep-ph/0304048] [SPIRES].

[10] A.D. Linde, *Infrared problem in thermodynamics of the Yang-Mills gas*, *Phys. Lett.* **B 96** (1980) 289 [SPIRES].

[11] D.J. Gross, R.D. Pisarski and L.G. Yaffe, *QCD and instantons at finite temperature*, *Rev. Mod. Phys.* **53** (1981) 43 [SPIRES].

[12] A. Hietanen, K. Kajantie, M. Laine, K. Rummukainen and Y. Schroder, *Plaquette expectation value and gluon condensate in three dimensions*, *JHEP* **01** (2005) 013 [hep-lat/0412008] [SPIRES].

[13] A. Hietanen and A. Kurkela, *Plaquette expectation value and lattice free energy of three-dimensional* SU(N) *gauge theory*, *JHEP* **11** (2006) 060 [hep-lat/0609015] [SPIRES].

[14] F. Di Renzo, M. Laine, V. Miccio, Y. Schroder and C. Torrero, *The leading non-perturbative coefficient in the weak-coupling expansion of hot QCD pressure*, *JHEP* **07** (2006) 026 [hep-ph/0605042] [SPIRES].

[15] A. Gynther, M. Laine, Y. Schroder, C. Torrero and A. Vuorinen, *Four-loop pressure of massless O(N) scalar field theory*, *JHEP* **04** (2007) 094 [hep-ph/0703307] [SPIRES].

[16] P.H. Ginsparg, *First order and second order phase transitions in gauge theories at finite temperature*, *Nucl. Phys.* **B 170** (1980) 388 [SPIRES].

[17] T. Appelquist and R.D. Pisarski, *High-temperature Yang-Mills theories and three-dimensional quantum chromodynamics*, *Phys. Rev.* **D 23** (1981) 2305 [SPIRES].

[18] N.P. Landsman, *Limitations to dimensional reduction at high temperature*, *Nucl. Phys.* **B 322** (1989) 498 [SPIRES].

[19] E. Braaten and A. Nieto, *Effective field theory approach to high temperature thermodynamics*, *Phys. Rev.* **D 51** (1995) 6990 [hep-ph/9501375] [SPIRES].

[20] K. Kajantie, M. Laine, K. Rummukainen and M.E. Shaposhnikov, *Generic rules for high temperature dimensional reduction and their application to the standard model*, *Nucl. Phys.* **B 458** (1996) 90 [hep-ph/9508379] [SPIRES].

[21] J.O. Andersen and L. Kyllingstad, *Four-loop screened perturbation theory*, *Phys. Rev.* **D 78** (2008) 076008 [arXiv:0805.4478] [SPIRES].

[22] K. Farakos, K. Kajantie, K. Rummukainen and M.E. Shaposhnikov, 3D *physics and the electroweak phase transition: perturbation theory*, *Nucl. Phys.* **B 425** (1994) 67 [hep-ph/9404201] [SPIRES].

[23] J. Frenkel, A.V. Saa and J.C. Taylor, *The pressure in thermal scalar field theory to three loop order*, *Phys. Rev.* **D 46** (1992) 3670 [SPIRES].

[24] R. Parwani and H. Singh, *The pressure of hot* $(g^2\phi^4)$ *theory at order* g^5, *Phys. Rev.* **D 51** (1995) 4518 [hep-th/9411065] [SPIRES].

[25] F. Karsch, A. Patkos and P. Petreczky, *Screened perturbation theory*, *Phys. Lett.* **B 401** (1997) 69 [hep-ph/9702376] [SPIRES].

[26] J.O. Andersen, E. Braaten and M. Strickland, *Screened perturbation theory to three loops*, *Phys. Rev.* **D 63** (2001) 105008 [hep-ph/0007159] [SPIRES].

[27] J.O. Andersen and M. Strickland, *Mass expansions of screened perturbation theory*, *Phys. Rev.* **D 64** (2001) 105012 [hep-ph/0105214] [SPIRES].

[28] E. Braaten and E. Petitgirard, *Solution to the 3-loop ϕ-derivable approximation for scalar thermodynamics*, *Phys. Rev.* **D 65** (2002) 041701 [hep-ph/0106045] [SPIRES].

[29] E. Braaten and E. Petitgirard, *Solution to the 3-loop ϕ-derivable approximation for massless scalar thermodynamics*, *Phys. Rev.* **D 65** (2002) 085039 [hep-ph/0107118] [SPIRES].

[30] A. Vuorinen, *The pressure of QCD at finite temperature and quark number density*, hep-ph/0402242 [SPIRES].

[31] B.G. Nickel, *Evaluation of simple Feynman graphs*, *J. Math. Phys.* **19** (1978) 542 [SPIRES].

[32] B. Kastening, private communication.

Paper III

Jens O. Andersen and Lars T. Kyllingstad:
"Pion condensation in a two-flavour NJL model: the role of charge neutrality",
J. Phys. G **37** (2009), 015003.

IOP PUBLISHING JOURNAL OF PHYSICS G: NUCLEAR AND PARTICLE PHYSICS

J. Phys. G: Nucl. Part. Phys. **37** (2010) 015003 (19pp) doi:10.1088/0954-3899/37/1/015003

Pion condensation in a two-flavour NJL model: the role of charge neutrality

J O Andersen and L T Kyllingstad

Department of Physics, Norwegian University of Science and Technology, N-7491 Trondheim, Norway

E-mail: andersen@tf.phys.ntnu.no and lars.kyllingstad@ntnu.no

Received 12 August 2009
Published 23 November 2009
Online at stacks.iop.org/JPhysG/37/015003

Abstract

We study pion condensation and the phase structure in a two-flavour Nambu–Jona-Lasinio model in the presence of baryon chemical potential μ and isospin chemical potential $\mu_{\rm I}$ at zero and finite temperature. There is a competition between the chiral condensate and a Bose–Einstein condensate of charged pions. In the chiral limit, the chiral condensate vanishes for any finite value of the isospin chemical potential, while there is a charged pion condensate that depends on the chemical potentials and the temperature. At the physical point, the chiral condensate is always nonzero, while the charged pion condensate depends on $\mu_{\rm I}$ and T. For $T = \mu = 0$, the critical isospin chemical potential $\mu_{\rm I}^c$ for the onset of Bose–Einstein condensation is always equal to the pion mass. For $\mu = 0$, we compare our results with chiral perturbation theory, sigma-model calculations and lattice simulations. Finally, we examine the effects of imposing electric charge neutrality and weak equilibrium on the phase structure of the model. In the chiral limit, there is a window of baryon chemical potential and temperature where the charged pions condense. At the physical point, the charged pions do not condense.

1. Introduction

There has been a tremendous effort in recent years to map out the phase diagram of QCD as a function of temperature and baryon chemical potential [1–7]. It is generally accepted that one can calculate the properties of strongly interacting matter at asymptotically high temperature or at asymptotically high densities using perturbative QCD.

At sufficiently high density and low temperature, we know that QCD is in the colour-flavour locked (CFL) phase. This state is a colour superconducting state because the quarks form Cooper pairs in analogy to electrons in an ordinary superconductor. In this case, the original symmetry group of QCD, $SU(3)_{\rm c} \times SU(3)_L \times SU(3)_R \times U(1)_{\rm B}$, is broken down to

$SU(3)_{c+L+R}$ which is a linear combination of the generators of the original group. This linear combination locks rotation in colour space to rotations in flavour space and this has given the name to the phase. In the CFL phase there is an octet of Goldstone modes which arises from the breaking of chiral symmetry and a singlet arising from the breaking of the baryon-number conserving group $U(1)_{\rm B}$. The CFL phase is a superfluid due to the breaking of the global $U(1)_{\rm B}$ symmetry. This is analogous to the superfluidity encountered in condensed-matter systems such as ^{4}He. At very high densities, all nine modes are effectively massless since one can ignore the quark masses. This implies that the low-energy properties of the CFL phase can be described in terms of an effective field theory for the massless mesons [8–11]. At moderate densities, one cannot neglect the quark masses and chiral symmetry is broken explicitly. Thus only the superfluid mode is exactly massless, while the other mesons acquire masses. The lightest massive modes are expected to be the charged and neutral kaons and if the chemical potentials are large enough, there is a transition to a Bose condensed phase. Bose condensation of kaons in the CFL phase has been studied in detail in [12–22].

QCD at finite baryon chemical potential $\mu_{\rm B}$ is not accessible by Monte Carlo simulations due to the complex fermion determinant. This is in contrast to QCD at finite isospin chemical potential $\mu_{\rm I}$ (still at zero $\mu_{\rm B}$) where lattice simulations are possible since the functional determinant is real. Thus, this is a system whose phase diagram one can study on the lattice as a function of a conserved charge.

Lattice simulations [23–25] suggest that there is a deconfinement transition of pions at high temperature and low density, and Bose–Einstein condensation of charged pions at high isospin density and low temperature. In fact, the deconfinement transition and the transition to a charged pion condensate seem to coincide. The deconfinement transition is found by measuring the Polyakov loop and the measurements show a sharp increase (indicating deconfinement) at approximately the same temperature as the onset of pion condensation.

Pion condensation and the phase diagram of two-flavour QCD have been investigated using chiral perturbation theory [26–28], ladder QCD [29], the chiral quark model [30], the linear sigma models [31–36], NJL models [33, 37–43] and Polyakov-loop NJL models [44, 45]. The PNJL models suggest that deconfinement and the onset of Bose–Einstein condensation are two different transitions. Very recently, Abuki *et al* [46] have considered the possibility of probing the phase diagram of electrically neutral QCD at finite isospin chemical potential using an equilibrated gas of neutrinos. They found that a condensate of charged pions arises at large enough neutrino densities and small baryon densities, and that at even larger neutrino densities there is condensation of charged kaons as well.

We note in passing the similarity between three-colour QCD at finite $\mu_{\rm I}$ and two-colour QCD at finite $\mu_{\rm B}$ [23]. The correspondence is given by identifying $\mu_{\rm I}/2$ with $\mu_{\rm B}$, the charged pion condensate with the diquark condensate[1], and the isospin density with the quark density.

Bose-condensed states or colour-superconducting states may be found in the interior of compact stars if the density is high enough. In contrast to hadronic matter in heavy-ion collisions, bulk matter in compact stars must (on average) be electrically neutral and so a neutrality constraint must be imposed [47, 48]. Similarly, bulk matter must be colour neutral and if the system is in a colour superconducting phase, one sometimes has to impose this constraint explicitly. It is automatically satisfied if one uses the QCD Lagrangian, but this is not so if one describes the system using NJL-type models. This is due to the fact that there are no gauge fields in this model and the $SU(N_{\rm c})$ colour symmetry is global [18, 49–51].

[1] The diquark condensate in two-colour QCD does not break any local symmetries, only global ones. The system is therefore a superfluid but not a colour superconductor.

The advantage of models with quarks as microscopic degrees of freedom, such as the NJL model, is that one can investigate simultaneously the effects of finite baryon chemical potential and isospin chemical potential. In the present paper, we consider the two-flavour NJL model at finite baryon chemical potential and isospin chemical potential. We compute the phase diagram at zero and finite temperature as a function of these variables. We restrict ourselves to sufficiently low values of the baryon chemical potential such that there are no superconducting phases [48, 52]. We also investigate the effects on the phase diagram by imposing electric charge neutrality and β-equilibrium. Our work is a generalization of the papers by Ebert and Klimenko [38, 39] to finite temperature and finite pion mass.

The paper is organized as follows. In section 2, we discuss the Lagrangian and the gap equations of the NJL model. In section 3, we discuss the phase diagram at zero as well as finite temperature. In section 4, we discuss the issues of charge neutrality and β-equilibrium. In section 5, we investigate the phase diagram at zero and finite temperatures imposing charge neutrality and β-equilibrium. In section 6, we summarize and conclude.

2. Lagrangian and gap equations

In this section, we discuss the properties of the Lagrangian of the two-flavour NJL model. The Lagrangian can be written as [53]

$$\mathcal{L} = \mathcal{L}_0 + \mathcal{L}_1 + \mathcal{L}_2, \tag{1}$$

where the various terms are

$$\mathcal{L}_0 = \bar{\psi}(\mathrm{i}\gamma^\mu \partial_\mu - m_0)\psi, \tag{2}$$

$$\mathcal{L}_1 = G_1[(\bar{\psi}\psi)^2 + (\bar{\psi}\boldsymbol{\tau}\psi)^2 + (\bar{\psi}\mathrm{i}\gamma_5\psi)^2 + (\bar{\psi}\mathrm{i}\gamma_5\boldsymbol{\tau}\psi)^2], \tag{3}$$

$$\mathcal{L}_2 = G_2[(\bar{\psi}\psi)^2 - (\bar{\psi}\boldsymbol{\tau}\psi)^2 - (\bar{\psi}\mathrm{i}\gamma_5\psi)^2 + (\bar{\psi}\mathrm{i}\gamma_5\boldsymbol{\tau}\psi)^2]. \tag{4}$$

Here, m_0 is the quark-mass matrix, which is diagonal in flavour space and contains the bare quark masses m_u and m_d. Moreover, $\boldsymbol{\tau} = (\tau_1, \tau_2, \tau_3)$ where τ_i $(i = 1, 2, 3)$ are the Pauli matrices. G_1 and G_2 are coupling constants. The quark field ψ is an isospin doublet

$$\psi = \begin{pmatrix} \mathrm{u} \\ \mathrm{d} \end{pmatrix}. \tag{5}$$

In the following, we take $m_\mathrm{u} = m_\mathrm{d}$. The Lagrangian (1) has a global $SU(N_\mathrm{c})$ symmetry as well as a $U(1)_\mathrm{B}$ baryon symmetry. The latter reflects baryon number conservation. In the chiral limit, the Lagrangian (1) has an $SU(2)_L \times SU(2)_R$ symmetry. Away from the chiral limit, this symmetry is reduced to $SU(2)_{L+R}$ isospin symmetry. $\mathcal{L}_1$ has an additional $U(1)_A$ axial symmetry. $\mathcal{L}_2$ is 't Hooft's instanton-induced interaction term and breaks explicitly the $U(1)_A$ axial symmetry of $\mathcal{L}_1$ [54, 55]. In the following, we shall limit ourselves to study the standard NJL Lagrangian by choosing $G_1 = G_2 \equiv G/2$ [53] and so equation (1) reduces to

$$\mathcal{L} = \bar{\psi}(\mathrm{i}\gamma^\mu \partial_\mu - m_0)\psi + G[(\bar{\psi}\psi)^2 + (\bar{\psi}\mathrm{i}\gamma_5\boldsymbol{\tau}\psi)^2]. \tag{6}$$

We can characterize the system described by the Lagrangian (6) by the expectation values of the different conserved charges associated with the continuous symmetries. For each conserved charge Q_i, we introduce a chemical potential μ_i. Note, however, that it is possible to specify the expectation values of different charges simultaneously only if they commute. In the present case, we introduce a chemical potential μ_B associated with the $U(1)_\mathrm{B}$ baryon symmetry, as well as a chemical potential μ_I associated with the third component of the $SU(2)_{L+R}$ isospin

group. This is done by adding to the Lagrangian (6), the terms

$$\mathcal{L}_{\mathrm{B}} = \mu_{\mathrm{B}} \bar{\psi} \gamma^0 B \psi, \tag{7}$$

$$\mathcal{L}_{\mathrm{I}} = \mu_{\mathrm{I}} \bar{\psi} \gamma^0 I_3 \psi, \tag{8}$$

where $B = \mathrm{diag}(1/3, 1/3)$ and $I_3 = \tau_3/2$. We can then write the Lagrangian as

$$\mathcal{L} = \bar{\psi}[\mathrm{i}\gamma^\mu \partial_\mu - m_0 + \mu\gamma^0 + \delta\mu\gamma^0\tau_3]\psi + G[(\bar{\psi}\psi)^2 + (\bar{\psi}\mathrm{i}\gamma^5\tau_i\psi)^2], \tag{9}$$

where we have defined the quark chemical potential μ as well as $\delta\mu$ by

$$\mu \equiv \frac{\mu_{\mathrm{B}}}{3}, \tag{10}$$

$$\delta\mu \equiv \frac{\mu_{\mathrm{I}}}{2}. \tag{11}$$

In the remainder of the paper, we assume $\mu \geqslant 0$ and $\delta\mu \geqslant 0$ for simplicity. In terms of the chemical potentials for the u and the d-quarks, μ_{u} and μ_{d}, the chemical potentials μ and $\delta\mu$ can be written as

$$\mu = \tfrac{1}{2}(\mu_{\mathrm{u}} + \mu_{\mathrm{d}}), \tag{12}$$

$$\delta\mu = \tfrac{1}{2}(\mu_{\mathrm{u}} - \mu_{\mathrm{d}}). \tag{13}$$

In the chiral limit, the inclusion of the isospin chemical potential breaks the $SU(2)_L \times SU(2)_R$-symmetry of the Lagrangian to $U(1)_L \times U(1)_R$. At the physical point, it breaks the $SU(2)_{L+R}$-symmetry down to $U(1)_{L+R}$.

From the path-integral representation of the free energy density Ω

$$\mathrm{e}^{-\beta V\Omega} = \int \mathcal{D}\psi^*\mathcal{D}\psi\, \mathrm{e}^{-\int_0^\beta \mathrm{d}\tau \int \mathrm{d}^3x \mathcal{L}}, \tag{14}$$

the expression for the charge density Q_i associated with the chemical potential μ_i can be written as

$$Q_i = -\frac{\partial\Omega}{\partial\mu_i}. \tag{15}$$

We next introduce the auxiliary fields σ and π_i by

$$\sigma = -2G\bar{\psi}\psi, \tag{16}$$

$$\pi_i = -2G\bar{\psi}\mathrm{i}\gamma_5\tau_i\psi. \tag{17}$$

The Lagrangian (9) can now compactly be written as

$$\mathcal{L} = \bar{\psi}[\mathrm{i}\gamma^\mu\partial_\mu - m_0 + \mu\gamma^0 + \delta\mu\gamma^0\tau_3 - \sigma - \mathrm{i}\gamma^5\pi_a\tau_a]\psi - \frac{1}{4G}(\sigma^2 + \pi_a\pi_a). \tag{18}$$

The original Lagrangian (9) can be recovered by using the equations of motion for the auxiliary fields σ and π_i to eliminate them from equation (18). The Lagrangian is now bilinear in the quark fields and so we can integrate them out exactly. We then obtain the following effective action for the composite fields σ and π:

$$S_{\mathrm{eff}} = -\frac{1}{2}N_{\mathrm{c}}\mathrm{Tr}\log[\mathrm{i}\gamma^\mu\partial_\mu - m_0 + \mu\gamma^0 + \delta\mu\gamma^0\tau_3 - \sigma - \mathrm{i}\gamma^5\pi_a\tau_a] - \int \mathrm{d}^3x \int_0^\beta \mathrm{d}\tau \frac{1}{4G}(\sigma^2 + \pi_a\pi_a), \tag{19}$$

where Tr denotes the trace and is over Dirac indices as well as spacetime.

We next introduce a nonzero expectation value for the fields σ and π_1 to allow for a chiral condensate and a charged pion condensate. The fields are then written as

$$\sigma = -2G\langle\bar{\psi}\psi\rangle + \tilde{\sigma}, \tag{20}$$

$$\pi_1 = -2G\langle\bar{\psi}\mathrm{i}\gamma^5\tau_1\psi\rangle + \tilde{\pi}_1, \tag{21}$$

where $\tilde{\sigma}$ and $\tilde{\pi}_1$ are quantum fluctuating fields. In the mean-field approximation, we neglect the fluctuations of the quantum fields $\tilde{\sigma}$ and $\tilde{\pi}_1$ in the functional determinant. This approximation coincides with the leading order of the $1/N_\mathrm{c}$-expansion, where N_c is the number of colours[2].

For notational simplicity, we introduce the quantities M and ρ given by

$$M \equiv m_0 - 2G\langle\bar{\psi}\psi\rangle, \tag{22}$$

$$\rho \equiv -2G\langle\bar{\psi}\mathrm{i}\gamma^5\tau_1\psi\rangle, \tag{23}$$

where M is the constituent quark mass. Note that in the chiral limit, the chiral condensate breaks the $SU(2)_L \times SU(2)_R$ symmetry spontaneously down to $SU(2)_{L+R}$ in the usual manner. Moreover, we can always use the remaining $U(1)$-symmetry to rotate away any nonzero value of $\langle\bar{\psi}\mathrm{i}\gamma^5\tau_2\psi\rangle$.

Note that we have introduced a single chiral condensate and not separate chiral condensates $\langle\bar{\mathrm{u}}\mathrm{u}\rangle$ and $\langle\bar{\mathrm{d}}\mathrm{d}\rangle$ for the u and the d quarks. We have chosen $G_1 = G_2$ and in this case the effective action (19) only depends on the sum of these condensates. In fact, it is easy to show that the two chiral condensates must be equal. This is in contrast to the calculations of Barducci *et al* [37], where the authors choose $G_1 = G/2$ and $G_2 = 0$. In that case the effective action is not symmetric under permutation of the two chiral condensates and they are different. Our choice is motivated by the fact that $U(1)_A$ symmetry is broken in QCD due to instanton effects [56]. In fact, setting $G_1 = G_2 \neq 0$ in the present model means that axial symmetry is maximally violated. When $G_2 = 0$, on the other hand, the Lagrangian (1) is $U(1)_A$-symmetric.

Also note that we take the condensates M and ρ to be spacetime independent. Though it has been demonstrated that the phase diagram may contain phases where the condensates are non-uniform [57], also within the framework of the two-flavour NJL model [58–62], taking this possibility into account is beyond the scope of this study. Still, it would be interesting to see how these non-uniform phases are affected by imposing neutrality constraints.

Using standard techniques to evaluate the trace and using $\Omega = -S_\mathrm{eff}/\beta V$, where Ω is the thermodynamic potential and V is the volume of the system, we obtain

$$\begin{aligned}\Omega = \frac{(M-m_0)^2+\rho^2}{4G} - 2N_\mathrm{c}\int\frac{\mathrm{d}^3p}{(2\pi)^3}\Big\{E_\rho^- + T\ln\Big[1+\mathrm{e}^{-\beta(E_\rho^- - \mu)}\Big] \\ + T\ln\Big[1+\mathrm{e}^{-\beta(E_\rho^- + \mu)}\Big] + E_\rho^+ + T\ln\Big[1+\mathrm{e}^{-\beta(E_\rho^+ - \mu)}\Big] + T\ln\Big[1+\mathrm{e}^{-\beta(E_\rho^+ + \mu)}\Big]\Big\},\end{aligned} \tag{24}$$

where the energy $E_\rho^\pm$ is defined by

$$E_\rho^\pm = \sqrt{(E^\pm)^2 + \rho^2} \tag{25}$$

where

$$E^\pm = E \pm \delta\mu, \tag{26}$$

$$E = \sqrt{p^2 + M^2}. \tag{27}$$

[2] In fact, every power of the quantum fluctuating fields that arises from expanding the functional determinant gives an additional factor of $1/\sqrt{N_\mathrm{c}}$ and so equation (19) is a convenient way of organizing a $1/N_\mathrm{c}$-expansion.

In the limit $T \to 0$, the thermodynamic potential (24) reduces to

$$\Omega = \frac{(M-m_0)^2+\rho^2}{4G} - 2N_c \int \frac{d^3p}{(2\pi)^3}\{E_\rho^- + (\mu - E_\rho^-)\theta(\mu - E_\rho^-) + E_\rho^+ + (\mu - E_\rho^+)\theta(\mu - E_\rho^+)\}, \tag{28}$$

which is in agreement with the result of [38]. The values of M and ρ are found by minimizing the thermodynamic potential Ω, that is by solving the following gap equations:

$$\frac{\partial\Omega}{\partial M} = 0, \tag{29}$$

$$\frac{\partial\Omega}{\partial\rho} = 0. \tag{30}$$

Differentiating the effective potential (24) with respect to M and ρ, we obtain the gap equations

$$0 = \frac{M-m_0}{2G} - 2N_c M \int \frac{d^3p}{(2\pi)^3}\left\{\frac{E^+}{EE_\rho^+}\left[1-n(E_\rho^+-\mu)-n(E_\rho^++\mu)\right] + \frac{E^-}{EE_\rho^-}\left[1-n(E_\rho^--\mu)-n(E_\rho^-+\mu)\right]\right\}, \tag{31}$$

$$0 = \frac{\rho}{2G} - 2N_c\rho \int \frac{d^3p}{(2\pi)^3}\left\{\frac{1}{E_\rho^+}\left[1-n(E_\rho^+-\mu)-n(E_\rho^++\mu)\right] + \frac{1}{E_\rho^-}\left[1-n(E_\rho^--\mu)-n(E_\rho^-+\mu)\right]\right\}, \tag{32}$$

where n is the Fermi–Dirac distribution,

$$n(E) = \frac{1}{e^{\beta E}+1}. \tag{33}$$

Taking the limit $T \to 0$, these equations reduce to those obtained by Ebert and Klimenko [38]:

$$0 = \frac{M-m_0}{2G} - 2N_c M \int \frac{d^3p}{(2\pi)^3}\left\{\frac{\theta(E_\rho^+-\mu)E^+}{EE_\rho^+} + \frac{\theta(E_\rho^--\mu)E^-}{EE_\rho^-}\right\}, \tag{34}$$

$$0 = \frac{\rho}{2G} - 2N_c\rho \int \frac{d^3p}{(2\pi)^3}\left\{\frac{\theta(E_\rho^+-\mu)}{E_\rho^+} + \frac{\theta(E_\rho^--\mu)}{E_\rho^-}\right\}. \tag{35}$$

The dispersion relations for the quasiparticles are determined by the zeros of the functional determinant in equation (19). One finds [38]

$$E_u = E_\rho^- - \mu, \qquad E_d = E_\rho^+ - \mu, \tag{36}$$

$$E_{\bar{u}} = E_\rho^- + \mu, \qquad E_{\bar{d}} = E_\rho^+ + \mu. \tag{37}$$

It is easy to show that the dispersion relations for the $\bar{u}$ and $\bar{d}$ quarks are always gapped, while the dispersion relations for the u and d quarks can be gapped or ungapped depending on the values of μ. In the chiral limit, it follows directly from the gap equations (31) and (32) that there are no nonzero values for μ, $\delta\mu$ and T for which M and ρ are nonzero simultaneously.

In the pion-condensed phase the dispersion relations for u and d quarks then reduce to

$$E_{\mathrm{u}} = \sqrt{(p-\delta\mu)^2+\rho^2} - \mu \tag{38}$$

$$E_{\mathrm{d}} = \sqrt{(p+\delta\mu)^2+\rho^2} - \mu. \tag{39}$$

For the u quark, the dispersion relation is gapped or ungapped according to

$$\rho > \mu, \qquad \text{gapped spectrum,} \tag{40}$$

$$\rho = \mu, \qquad \text{ungapped quadratic spectrum,} \tag{41}$$

$$\rho < \mu, \qquad \text{ungapped linear spectrum.} \tag{42}$$

The possibility of an ungapped quadratic quark spectrum in the context of dense baryonic matter was first discussed in [63]. The gaplessness of the d quark is determined by the line that is defined implicitly by the equation $\mu = \sqrt{(\delta\mu)^2+\rho^2}$, which follows from equation (39). The window in the pion-condensed phase where the fermionic excitations are gapless is coined *gapless pion condensation* [38]. The situation here is analogous to what happens in colour superconductivity, except that in this case it is $\delta\mu$ that dictates the onset of gaplessness: $\delta\mu = \Delta$, where Δ is the superconducting gap [6, 64]. Moreover, in colour superconductivity $\delta\mu$ is called a stress parameter because it gives rise to a mismatch between the Fermi surfaces of the u and the d quarks, which imposes an extra energy cost (stress) on the formation of Cooper pairs. As long as the stress parameter is small enough compared to Δ, BCS pairing can occur [64]. In the context of pion condensation, μ plays the role as a stress parameter since the mismatch is between the Fermi surfaces of the u and $\bar{\mathrm{d}}$ quarks. Similarly, if the stress parameter μ is small enough relative to ρ, pion condensation can occur. We will return to this point below.

The integrals appearing in equations (24), (31) and (32) are ultraviolet divergent and one may impose a three-dimensional UV cutoff Λ to regulate them. Alternatively, one can introduce a form factor [65], which falls off for large momenta. This ensures that the integrals converge in the ultraviolet. Given an ultraviolet cutoff Λ, the coupling constant G and the quark mass m_0, we can use the Dyson equation for the quark propagator to determine the value for the chiral condensate in the vacuum. The Dyson equation reads [53]

$$M = m_0 + 4N_{\mathrm{f}}N_{\mathrm{c}}G\int \frac{\mathrm{d}^3p}{(2\pi)^3}\frac{M}{\sqrt{p^2+M^2}}, \tag{43}$$

where N_{f} is the number of flavours and N_{c} is the number of colours. In the remainder of the paper, we also set $N_{\mathrm{f}} = 2$ and $N_{\mathrm{c}} = 3$. This is simply the gap equation (31) in the vacuum, i.e. for $\mu = \delta\mu = 0$.

3. Phase diagram

In this section, we study the phase diagram at zero and finite temperature without taking charge neutrality into account. Since we are not considering colour superconductivity, we restrict ourselves to quark chemical potentials $\mu < 350$ MeV. Since we are using an ultraviolet cutoff of approximately 650 MeV (see below), one should not trust results for the chemical potentials μ and $\delta\mu$ above approximately 400 MeV. We therefore do not consider values above $\mu = 350$ MeV and $\delta\mu = 400$ MeV in the calculations. The equilibrium values of M and ρ are obtained by solving numerically the gap equations (31) and (32).

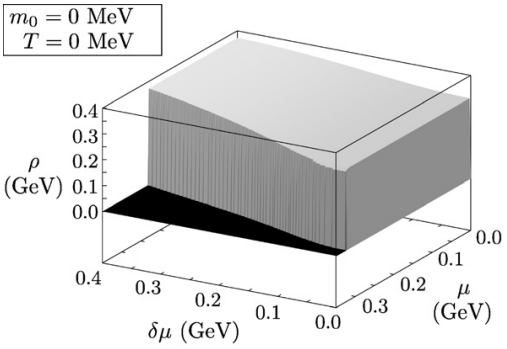

Figure 1. Pion condensate in the chiral limit as a function of quark chemical potential μ and $\delta\mu$ at zero temperature.

3.1. Chiral limit

In the chiral limit, the current quark mass vanishes, $m_0 = 0$. For the numerical calculations, we choose an ultraviolet cutoff $\Lambda = 650.9$ MeV and a coupling constant $G = 5.04$ (GeV)$^{-2}$. Solving the Dyson equation (43), this gives a constituent quark mass in the vacuum of $M = 309.9$ MeV.

We mentioned in the previous section that there are no values of μ, $\delta\mu$ and T such that M and ρ are simultaneously nonzero. In other words, the possible solutions to the gap equations are (a) $M = \rho = 0$, (b) $M \neq 0$, $\rho = 0$ and (c) $\rho \neq 0$, $M = 0$. In case (a), the full symmetry of the Lagrangian is intact, while in case (b) the $U(1)_L \times U(1)_R$ symmetry is broken spontaneously down to $U(1)_{L+R}$ by the chiral condensate. The breaking of the $U(1)$-symmetry gives rise to a conventional Goldstone mode[3]. In case (c) the pion condensate breaks parity as well as the $U(1)_L \times U(1)_R$ symmetry down to $U(1)_{AI_3}$. The latter transforms the left-handed and right-handed flavour doublet as $\psi_L \to \mathrm{e}^{\mathrm{i}\alpha\tau_3}\psi_L$, $\psi_R \to \mathrm{e}^{-\mathrm{i}\alpha\tau_3}\psi_R$. The breaking of the $U(1)$-symmetry gives rise to a conventional Goldstone boson with a linear dispersion relation for small values of the 3-momentum. The ground state is therefore a pion superfluid[4]. The dispersion relations for the composite fields σ and π in equations (16) and (17) are found by first expanding the effective action (19) to second order in the quantum fluctuating fields $\tilde{\sigma}$ and $\tilde{\pi}_i$. This gives rise to a 4×4 fluctuation matrix $\Gamma(\omega, p)$, where the solutions to $\det \Gamma(\omega, p) = 0$ determine the dispersion relations $\omega(p)$. Details can be found in [39]. At finite chemical potential there is a mixing between the fields $\tilde{\pi}_1$ and $\tilde{\pi}_2$ and one of the linear combinations is massless [38].

The pion condensate of the two-flavour NJL model at zero temperature is shown in figure 1. It is worth noting that along the μ-axis, i.e. for $\delta\mu = 0$, the effective potential no longer depends on M and ρ separately, but rather on the combination $M^2 + \rho^2$ [39]. The effective potential then has the usual Mexican-hat shape with infinitely many equivalent vacua, where we can choose any one we wish. The chiral condensate can be rotated into pseudoscalar condensates

[3] For $\mu = \delta\mu = 0$, i.e. in the vacuum, there is a broken $SU(2)$-symmetry which gives rise to the three massless pions in the usual manner.

[4] At finite density, Lorentz invariance is broken and the number of broken generators need not be the same as the number of Goldstone bosons [66–68]. Goldstone bosons with quadratic dispersion relations appear and the system is not a superfluid in this case.

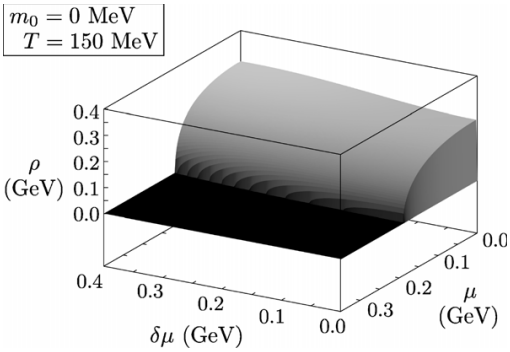

Figure 2. Pion condensate in the chiral limit as a function of μ and $\delta\mu$ for $T = 150$ MeV.

via the axial flavour transformations

$$\psi \to \mathrm{e}^{\mathrm{i}\theta_a \gamma_5 \tau_a}\psi, \qquad a = 1, 2, 3. \tag{44}$$

This is analogous to what happens in colour superconductivity, where diquark condensates are rotated into pseudoscalar diquark ones via rotations similar to those in equation (44) [12]. At finite quark mass or finite isospin chemical potential, the system becomes unstable against developing a nonzero pion condensate. At vanishing isospin chemical potential, parity is conserved in QCD and to enforce this we choose $\rho = 0$ along the line $\delta\mu = 0$. Consequently, the chiral condensate is nonvanishing and chiral symmetry is broken along the line $\delta\mu = 0$. Figure 1 shows that the charged pions condense for any nonzero value of the isospin chemical potential. This result is in accordance with that of Ebert and Klimenko [38] and calculations in the linear sigma model at finite isospin chemical potential [33, 34]. Finally, we note that the phase transition from the pion condensed phase to the chirally symmetric phase is first order. Note that the critical isospin chemical potential $\delta\mu$ is decreasing as a function of μ.

In figure 2, we show the pion condensate as a function of the quark chemical potential and isospin chemical potential at $T = 150$ MeV. The region of pion condensation is smaller than at $T = 0$ and the transition to a chirally symmetric phase is now second order everywhere.

In figure 3, we show the pion condensate in the chiral limit as a function of μ and T for fixed value of the isospin chemical potential, $\delta\mu = 200$ MeV. As the temperature and the quark chemical potential increase, the region of pion condensation decreases. For $T = 0$, the transition is first order. There is a line of first-order transitions starting at $T = 0$ which ends at a critical point given by $T = 0.11$ GeV and $\mu = 0.22$ GeV. The transition is of second order for larger values of T and smaller values of μ.

As mentioned above, the quark chemical potential induces a stress in the system and for sufficiently large values of μ it is no longer energetically favourable to form a Bose condensate of charged pions. This is clearly seen in figure 4, where we have plotted the thermodynamic potential $\Omega(\rho)$ minus $\Omega(\rho = 0)$ for three different values of μ with $\delta\mu = 200$ MeV and $T = 0$. From this figure it is evident that the transition is first order.

3.2. Physical point

At the physical point, we choose the parameters $m_0 = 5.5$ MeV, $\Lambda = 650.9$ MeV and $G = 5.04$ (GeV)$^{-2}$. Solving the Dyson equation (43), this gives a constituent quark vacuum mass $M = 325.2$ MeV, and the model reproduces the pion mass of $m_\pi = 140$ MeV.

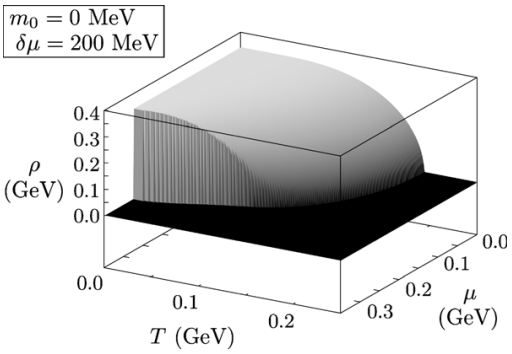

Figure 3. Pion condensate in the chiral limit as a function of quark chemical potential μ and temperature T for $\delta\mu = 200$ MeV.

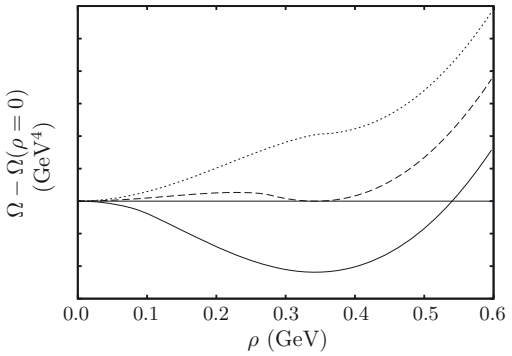

Figure 4. $\Omega(\rho) - \Omega(\rho = 0)$ in the chiral limit at $T = 0$ as a function of ρ for $\delta\mu = 200$ MeV and three different values of μ. Solid line: 100 MeV, dashed line: 275.87 MeV and dotted line: 350 MeV.

Due to the nonzero current quark mass, the chiral condensate M will always be nonzero and so chiral symmetry is never restored. For sufficiently high temperature or chemical potentials, the chiral condensate goes towards zero since the temperature-independent value of m_0 becomes irrelevant.

The two possible solutions of the gap equations are therefore (a) $\rho = 0$ and (b) $\rho \neq 0$. In case (a) the full symmetry of the Lagrangian is intact, while in case (b) parity and the $U(1)_{L+R}$ symmetry are spontaneously broken. In the latter case, there is a conventional Goldstone mode and the ground state is a pion superfluid.

In figure 5, we show the pion condensate as a function of T and $\delta\mu$ for $\mu = 0$. The transition is second order everywhere with mean-field critical exponents, which is in agreement with the analysis using chiral perturbation theory [26, 27]. However, lattice calculations [23] suggest that the transition is first order for μ_I large enough. The line of first-order transitions ends at a tricritical point and the line of second-order transitions extends down to $T = 0$. This discrepancy between mean-field calculations and lattice calculations is most likely due to shortcomings of mean-field theory itself. Lattice simulations also suggest that the transition

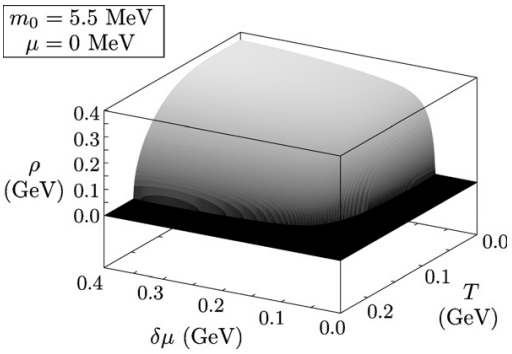

Figure 5. Pion condensate for $\mu = 0$ as a function of T and $\delta\mu$.

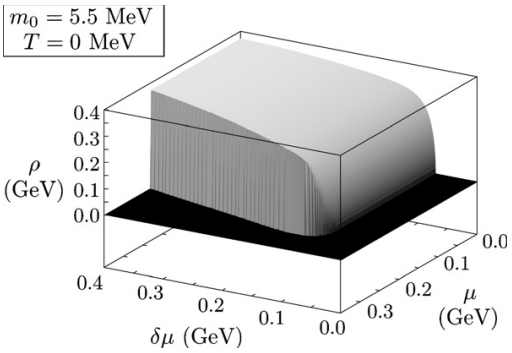

Figure 6. Pion condensate at the physical point as a function of quark chemical potential μ and $\delta\mu$ at zero temperature.

to a Bose–Einstein condensed state coincides with the deconfinement phase transition to a quark–gluon plasma.

In figure 6, we show the pion condensate as a function of μ and $\delta\mu$ at the physical point for $T = 0$. Along the axis $\mu = 0$, the transition to the pion condensed phase occurs at $\delta\mu_c = m_\pi/2 = 70$ MeV. The phase transition for $\mu = 0$ is second order. The transition remains second order for $\delta\mu^c$ smaller than approximately 80 MeV. For larger values of $\delta\mu$ it turns into a first-order transition. This is also shown in figure 7, where the solid curve shows a first-order transition ending at a critical point, while the dashed line indicates a second-order transition. This figure is very similar to figure 3 of [43].

The results for the pion condensate are in qualitative agreement with those obtained by Barducci *et al* [37]. Quantitative differences are due to different quark–antiquark interaction terms in the Lagrangian as well as different ways of regulating the loop integrals.

In figure 8, we show the chiral and pion condensates as functions of the isospin chemical potential for $\mu = T = 0$. The chiral condensate is constant from $\delta\mu = 0$ to $\delta\mu \approx m_\pi/2$, after which it drops rapidly towards zero at large $\delta\mu$. This behaviour is in agreement with the lattice simulations of Kogut and Sinclair [23] and the sigma-model calculations of He *et al* [33]. We

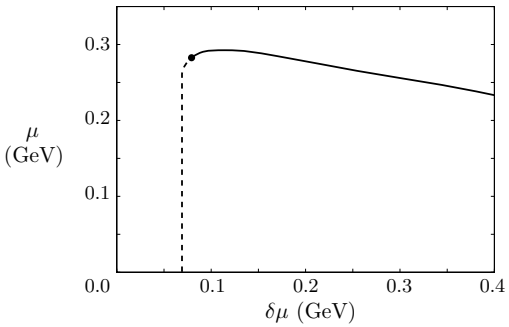

Figure 7. Phase diagram at the physical point at $T = 0$. The solid curve indicates a first-order transition which ends at a critical point. The dashed curve indicates a second-order transition.

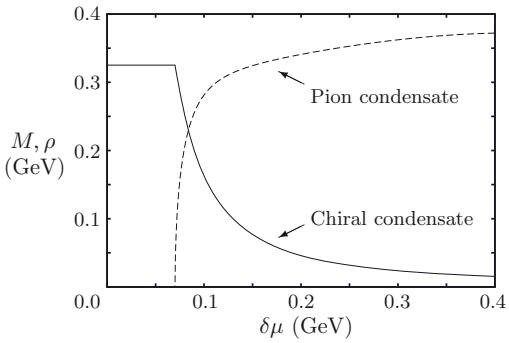

Figure 8. Pion condensate (dashed curve) and chiral condensate (solid curve) of the two-flavour NJL model at the physical point as a function of $\delta\mu$ at $\mu = T = 0$.

note the onset of pion condensation at $\delta\mu \approx m_\pi/2$ and that the condensate increases rapidly thereafter. This illustrates the competition between the two condensates.

In figure 9, we show the pion condensate as a function of μ and $\delta\mu$ at the physical point for $T = 150$ MeV. The region of Bose condensation becomes smaller as the temperature increases, as expected. The phase transition is now second order everywhere.

In figure 10, we show the phase diagram of the two-flavour NJL model as a function of T and $\delta\mu$ for $\mu = 0$. The solid line is the chiral limit and the dashed line is at the physical point. We note that the two curves are approaching each other for large values of $\delta\mu$, as expected.

In figure 11, we show the chiral condensate as a function of μ and $\delta\mu$ at the physical point and for $T = 0$. The chiral condensate goes to zero as the chemical potentials become large.

4. Electric charge neutrality and β-equilibrium

In the previous section, we have calculated the phase diagram by finding the solutions to the gap equations (29) and (30). Dense matter inside stars should be neutral with respect to electric as well as colour charge, otherwise one would pay an enormous energy price [47, 48].

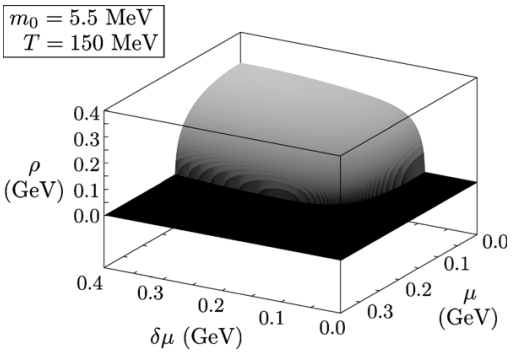

Figure 9. Pion condensate of the two-flavour NJL model at the physical point as a function of μ and $\delta\mu$ for $T = 150$ MeV.

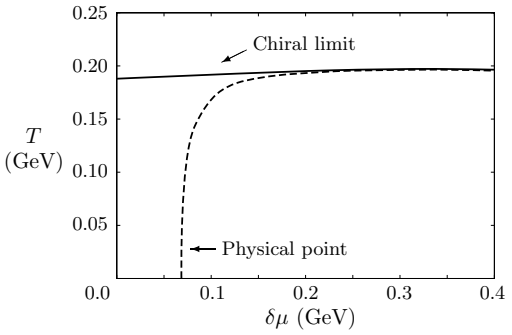

Figure 10. Phase diagram as a function of $\delta\mu$ and T for $\mu = 0$. The solid line is the chiral limit and the dashed line is at the physical point.

Since we are not considering colour superconducting phases, colour neutrality is automatically satisfied, while we have to impose electric charge neutrality.

In addition to charge neutrality, matter should also be in β equilibrium, that is, weak-interaction processes such as

$$\mathrm{u} \leftrightarrow \mathrm{d} + e^+ + \nu, \tag{45}$$

should go with the same rate in both directions. If we assume that the neutrinos can leave the system, their chemical potential μ_ν vanishes. In chemical equilibrium, equation (45) then implies

$$\mu_\mathrm{u} = \mu_\mathrm{d} - \mu_e. \tag{46}$$

The quark chemical potentials μ_u and μ_d, and the electron chemical potential μ_e can be written in terms of the quark chemical potential μ and the electric chemical potential μ_Q as

$$\mu_\mathrm{u} = \mu + \tfrac{2}{3}\mu_Q, \tag{47}$$

$$\mu_\mathrm{d} = \mu - \tfrac{1}{3}\mu_Q, \tag{48}$$

$$\mu_e = -\mu_Q, \tag{49}$$

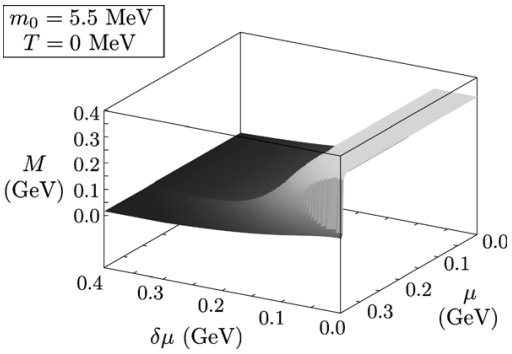

Figure 11. Chiral condensate as a function of quark chemical potential μ and $\delta\mu$ for zero temperature.

and so the system can be described in terms of the two independent chemical potentials μ and μ_Q. In order to impose the constraint of charge neutrality, we additionally require that

$$\frac{\partial\Omega}{\partial\mu_Q} = 0. \tag{50}$$

The constraint (50) implies that there is only one independent chemical potential, for example μ. Once we have picked a value for μ, the solutions to the gap equations (29) and (30) and the neutrality constraint (50) determine the chiral condensate M, the charged pion condensate ρ and the electric chemical potential μ_Q.

Note that the chemical potential appearing in equation (24) is half the sum of the quark chemical potentials μ_u and μ_d, and so according to equations (47) and (48), we need to make the substitution $\mu \to \tilde{\mu} = \mu + \mu_Q/6$. In the remainder, we also replace $\delta\mu$ by $\mu_Q/2$, which follows from equations (13), (47) and (48).

In the following, we describe the electrons by a noninteracting Fermi gas. We then add to the Lagrangian (9), the term

$$\mathcal{L}_{\text{electrons}} = \bar{\psi}_e(\gamma^\mu\partial_\mu + \gamma^0\mu_e e - m_e)\psi_e, \tag{51}$$

where ψ_e denotes the electron field, e is the electron charge and m_e is the mass of the electron. The thermodynamic potential for the electrons is

$$\Omega_{\text{electrons}} = -2\int\frac{\mathrm{d}^3p}{(2\pi)^3}\left\{E_p + T\ln\left[1+\mathrm{e}^{-\beta(E_p-\mu_Q)}\right] + T\ln\left[1+\mathrm{e}^{-\beta(E_p+\mu_Q)}\right]\right\}, \tag{52}$$

where $E_p = \sqrt{p^2+m_e^2}$. In the case of massless electrons, one can evaluate the integrals in equation (52) exactly and one finds

$$\Omega_{\text{electrons}} = -\frac{\mu_Q^4}{12\pi^2} - \frac{\mu_Q^2T^2}{6} - \frac{7\pi^2}{180}T^4. \tag{53}$$

In the remainder, we neglect the electron mass. Adding the electron contribution equation (53)

to (24) and differentiating with respect to μ_Q, we obtain

$$0 = \frac{\mu_Q^3}{3\pi^2} + \frac{1}{3}\mu_Q T^2 + \int \frac{\mathrm{d}^3 p}{(2\pi)^3}\left\{3\frac{E^+}{E_\rho^+} - 3\frac{E^-}{E_\rho^-}\right.$$
$$+ \left(1 - 3\frac{E^+}{E_\rho^+}\right)\frac{1}{\mathrm{e}^{\beta(E_\rho^+ - \tilde{\mu})}+1} - \left(1 + 3\frac{E^+}{E_\rho^+}\right)\frac{1}{\mathrm{e}^{\beta(E_\rho^+ + \tilde{\mu})}+1}$$
$$\left. + \left(1 + 3\frac{E^-}{E_\rho^-}\right)\frac{1}{\mathrm{e}^{\beta(E_\rho^- - \tilde{\mu})}+1} - \left(1 - 3\frac{E^-}{E_\rho^-}\right)\frac{1}{\mathrm{e}^{\beta(E_\rho^- + \tilde{\mu})}+1}\right\}. \tag{54}$$

In the zero-temperature limit, equation (54) reduces to that obtained by Ebert and Klimenko [39]:

$$0 = \frac{\mu_Q^3}{3\pi^2} + \int \frac{\mathrm{d}^3 p}{(2\pi)^3}\left\{\theta\big(\tilde{\mu} - E_\rho^+\big) + \theta\big(\tilde{\mu} - E_\rho^-\big) + 3\theta\big(E_\rho^+ - \tilde{\mu}\big)\frac{E^+}{E_\rho^+} - 3\theta\big(E_\rho^- - \tilde{\mu}\big)\frac{E^-}{E_\rho^-}\right\}. \tag{55}$$

5. Phase diagram revisited

In this section, we calculate the phase diagram of the two-flavour NJL model as a function of μ and T imposing the electric charge neutrality constraint (50). This equation and the gap equations (31) and (32) are then solved simultaneously to obtain the equilibrium values of M and ρ for the neutral system. We are using the same parameter values as in the previous section.

5.1. Chiral limit

Again the solutions to the gap equations are (a) $M = \rho = 0$, (b) $M \neq 0$, $\rho = 0$ and (c) $\rho \neq 0$, $M = 0$.

In figure 12, we show the pion condensate as a function of the quark chemical potential μ and temperature T for neutral matter. The results at $T = 0$ agree with those of Ebert and Klimenko [39]. Note the black wedge starting in the corner $\mu = T = 0$. In this area the electric chemical potential μ_Q vanishes, giving rise to a nonzero chiral condensate[5]. For $T = 0$, the chiral condensate vanishes for quark chemical potentials larger than the critical value of $\mu_{1\mathrm{c}} = 297$ MeV. For a quark chemical potential satisfying $\mu_{1\mathrm{c}} < \mu < \mu_{2\mathrm{c}}$, where $\mu_{2\mathrm{c}} = 329$ MeV, the pion condensate is nonvanishing. For chemical potentials larger than $\mu_{2\mathrm{c}}$, the system is in the normal phase, where both condensates vanish. The robustness of this result is discussed in section 6. Finally, we note that the transition from the pion-condensed phase to the symmetric phase is first order for $T = 0$. This first-order line ends at a critical point and the transition is second order all the way to $\mu = 0$.

5.2. Physical point

Again the two possible solutions of the gap equations are (1) $\rho = 0$ and (2) $\rho \neq 0$. It turns out that the only solution is $\rho = 0$, i.e. there is no charged pion condensate at the physical point. In other words, the isospin chemical potential $\mu_{\mathrm{I}} = \mu_Q$ is always smaller than the pion mass.

[5] Again the presence of the chiral condensate in the region where $\mu_Q = 0$ is due to the fact that the effective potential depends on $M^2 + \rho^2$ (Mexican-hat type potential) and we choose $M \neq 0$ so that parity is unbroken in the vacuum.

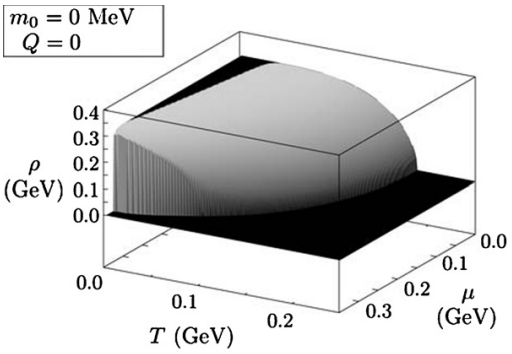

Figure 12. Pion condensate in the chiral limit for neutral matter as a function of quark chemical potential μ and temperature T.

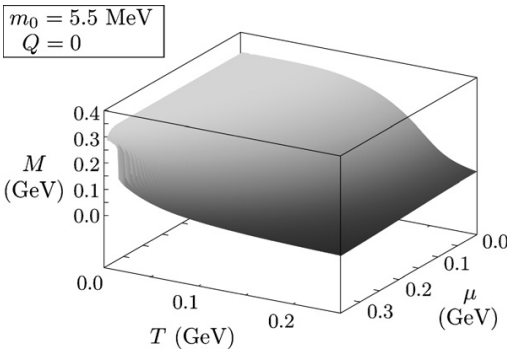

Figure 13. Chiral condensate at the physical point for neutral matter as a function of temperature T and quark chemical potential μ.

This is in accordance with the results of a recent study by Abuki *et al* [43], where they investigated pion condensation in neutral matter as a function of the pion mass from the chiral limit all the way to the physical value of 139 MeV. They found a tiny window of pion condensation for pion masses below approximately 10 keV. Thus, pion condensation is very sensitive to the explicit chiral symmetry breaking due to a finite quark mass m_0.

In figure 13, we show the chiral condensate for neutral matter as a function of temperature and quark chemical potential. The chiral condensate decreases with increasing μ and T, but never vanishes.

6. Summary

In this paper, we have calculated the phase diagram of the two-flavour NJL model as a function of the quark and the isospin chemical potential, and the temperature in the chiral limit and at the physical point. In the chiral limit, we have reproduced the results in [38, 39] at $T = 0$ and generalized them to finite temperature. At the physical point, we get similar results for

the phase structure as those obtained in [37]. The qualitative differences are due to different interaction terms in the Lagrangian and a different way of regulating the loop diagrams in the gap equations.

It is natural to ask what happens at larger values of the isospin chemical potential. We have extended our calculations of section 3 for $\mu = m_0 = 0$ up to $\delta\mu \approx 900$ MeV. These calculations seem to indicate that there is a phase transition from a pion condensed phase to a chirally symmetric phase. For zero temperature, this transition is located at $\delta\mu \sim 880$ MeV. However, this result should not be trusted since the UV cutoff is 651 MeV. In fact, there are reasons to believe that there is no phase transition as one increases $\delta\mu$. On general grounds, one can show that there is a nonzero condensate of the form $\langle \bar{\mathrm{d}}\gamma_5 u\rangle$ for larger values of μ_{I} [25]. Thus, one expects a BEC–BCS type of crossover as the quarks bound in the pions become weakly bound due to the fact that the QCD running coupling becomes weaker with increasing chemical potential μ_{I}.

Our main result comes from imposing the constraints of electric charge neutrality and weak equilibrium. In [39], the authors calculate the phases of neutral matter with another set of parameters at zero temperature. Using an ultraviolet cutoff of 600 MeV, a coupling constant $G = 6.82\ (\mathrm{GeV})^{-2}$, and a constituent quark mass of 400 MeV, their numerical analysis shows that the phase structure differs from the first set of parameters. At $T = 0$, there is in this case no phase with a pion condensate, but a phase transition directly from a phase of broken chiral symmetry to a chirally symmetric phase at a critical quark chemical potential of $\mu_{\mathrm{c}} = 386.2$ MeV. This seems to indicate that the window for pion condensation at $T = 0$ that can be seen in figure 12 is not a robust result.

We have seen that the charge neutrality constraint changes the phase diagram since it rules out charged pion condensation at the physical point. This is true for pion masses larger than approximately 10 keV [43]. However, in the presence of a dense neutrino gas, pion condensation again becomes a possibility even with realistic values of m_π, as shown in [46]. In nature this situation arises in supernova explosions and possibly at the early stages of the evolution of a neutron star. It does not arise in stable matter such as we have considered here, because the weakly interacting neutrinos will have had time to leave the system.

A natural next step would be to investigate the competition between pion and kaon condensation in neutral matter using a three-flavour NJL model at finite temperature and finite quark chemical potentials μ_{u}, μ_{d} and μ_s. Calculations without the neutrality constraint have already been done by Barducci *et al* [69].

Acknowledgments

The authors would like to thank T Brauner, D Boer and L E Leganger for useful discussions and suggestions.

References

[1] Wilczek F 1999 *Lectures given at 9th CRM Summer School: Theoretical Physics at the End of the 20th Century (Banff, Alberta, Canada, 27 Jun–10 Jul 1999)* **vol 567** (arXiv:hep-ph/0003183)
[2] Rajagopal K and Wilczek F 2000 *Festschrift in Honour of B L Ioffe: At the Frontier of Particle Physics/Handbook of QCD* vol 3 ed M Shifman (Singapore: World Scientific) pp 2061–151 (arXiv:hep-ph/0011333)
[3] Rischke D H 2004 *Prog. Part. Nucl. Phys.* **52** 197
[4] Stephanov M A 2006 PoS LAT2006 (024)
[5] McLerran L and Pisarski R D 2007 *Nucl. Phys.* A **796** 83
[6] Alford M G, Schmitt A and Rajagopal K 2008 *Rev. Mod. Phys.* **80** 1455
[7] Braun-Munzinger P and Wambach J 2009 *Rev. Mod. Phys.* **81** 1031

[8] Son D T and Stephanov M A 2000 *Phys. Rev.* D **61** 074012
Son D T and Stephanov M A 2000 *Phys. Rev.* D **62** 059902
[9] Bedaque P F and Schafer T 2002 *Nucl. Phys.* A **697** 802
[10] Kaplan D B and Reddy S 2002 *Phys. Rev.* D **65** 054042
[11] Schafer T 2002 *Phys. Rev.* D **65** 094033
[12] Buballa M 2005 *Phys. Lett.* B **609** 57
[13] Forbes M M 2005 *Phys. Rev.* D **72** 094032
[14] Ebert D and Klimenko K G 2007 *Phys. Rev.* D **75** 045005
[15] Ruggieri M 2007 *J. High Energy Phys.* JHEP07(2007)031
[16] Ebert D and Klimenko K G 2008 arXiv:0809.5254
[17] Kleinhaus V, Buballa M, Nickel D and Oertel M 2007 *Phys. Rev.* D **76** 074024
[18] Warringa H J 2006 arXiv:hep-ph/0606063
[19] Alford M G, Braby M and Schmitt A 2008 *J. Phys. G: Nucl. Part. Phys.* **35** 025002
[20] Ebert D, Klimenko K G and Yudichev V L 2008 *Eur. Phys. J.* C **53** 65
[21] Andersen J O and Leganger L E 2009 *Nucl. Phys.* A **828** 360
[22] Phat T H, Long N V, Anh N T and Hoa L V 2008 *Phys. Rev.* D **78** 105016
[23] Kogut J B and Sinclair D K 2002 *Phys. Rev.* D **64** 034508
Kogut J B and Sinclair D K 2002 *Phys. Rev.* D **66** 34505
Kogut J B and Sinclair D K 2004 *Phys. Rev.* D **70** 094501
[24] Gupta S 2002 arXiv:hep-lat/0202005
[25] de Forcrand P, Stephanov M A and Wenger U 2007 PoS LAT2007 (237)
[26] Son D T and Stephanov M 2001 *Phys. Rev. Lett.* **86** 592
[27] Splittorff K, Son D T and Stephanov M 2001 *Phys. Rev.* D **64** 016003
[28] Loewe M and Villavicencio C 2003 *Phys. Rev.* D **67** 074034
Loewe M and Villavicencio C 2004 *Phys. Rev.* D **70** 074005
Loewe M and Villavicencio C 2005 *Phys. Rev.* D **71** 094001
[29] Barducci A, Casalbuoni R, Pettini G and Ravagli L 2003 *Phys. Lett.* B **564** 217
[30] Jakovac A, Patkos A, Szep Zs and Szepfalusy P 2004 *Phys. Lett.* B **582** 179
[31] Kapusta J I 1981 *Phys. Rev.* D **24** 426
[32] Haber H E and Weldon H A 1982 *Phys. Rev.* D **25** 502
[33] He L, Jin M and Zhuang P 2005 *Phys. Rev.* D **71** 116001
[34] Andersen J O 2007 *Phys. Rev.* D **75** 065011
[35] Andersen J O and Brauner T 2008 *Phys. Rev.* D **78** 014030
[36] Shu S and Li J-R 2007 *J. Phys. G: Nucl. Part. Phys.* **34** 2727
[37] Barducci A, Casalbuoni R, Pettini G and Ravagli L 2004 *Phys. Rev.* D **69** 096004
[38] Ebert D and Klimenko K G 2006 *J. Phys. G: Nucl. Part. Phys.* **32** 599
[39] Ebert D and Klimenko K G 2006 *Eur. Phys. J.* C **46** 771
[40] Lawley S, Bentz W and Thomas A W 2006 *Phys. Lett.* B **632** 495
[41] He L, Jin M and Zhuang P 2005 *Phys. Rev.* D **71** 116001
[42] Hao X and Zhuang P 2007 *Phys. Lett.* B **652** 275
[43] Abuki H, Anglani R, Gatto R, Pellicoro M and Ruggieri M 2009 *Phys. Rev.* D **79** 034032
[44] Mukherjee S, Mustapha M G and Ray R 2006 *Phys Rev.* D **75** 094015
[45] Abuki H, Ciminale M, Gatto R, Ippolito N D, Nardulli G and Ruggieri M 2008 *Phys. Rev.* D **78** 014002
Ruggieri M 2008 *Prog. Theor. Phys. Suppl.* **174** 60
[46] Abuki H, Brauner T and Warringa H J 2009 *Eur. Phys. J.* C **64** 123
[47] Alford M and Rajagopal K 2002 *J. High Energy Phys.* JHEP06(2002)031
[48] Shovkovy I A 2005 *Found. Phys.* **35** 1309
[49] Dietrich D D and Rischke D H 2004 *Prog. Part. Nucl. Phys.* **53** 305
[50] Buballa M and Shovkovy I A 2005 *Phys. Rev.* D **72** 097501
[51] Blaschke D, Fredriksson S, Grigorian H, Oztas A M and Sandin F 2005 *Phys. Rev.* D **72** 065020
[52] Huang M and Shovkovy I A 2003 *Nucl. Phys.* A **729** 835
Huang M 2005 *Int. J. Mod. Phys.* E **14** 675
[53] Buballa M 2005 *Phys. Rep.* **407** 205
[54] 't Hooft G 1986 *Phys. Rep.* **142** 357
[55] Kobayashi M and Maskawa T 1970 *Prog. Theor. Phys.* **44** 1422
[56] 't Hooft G 1976 *Phys Rev. Lett.* **37** 8
[57] Dautry F and Nyman E M 1979 *Nucl. Phys.* A **319** 323
[58] Broniowski W and Kutschera M 1990 *Phys. Lett.* B **242** 133

[59] Sadzikowski M and Broniowski W 2000 *Phys. Lett.* B **488** 63
[60] Sadzikowski M 2003 *Phys. Lett.* B **553** 45
[61] Sadzikowski M 2006 *Phys. Lett.* B **642** 238
[62] Partyka T L and Sadzikowski M 2008 *J. Phys. G: Nucl. Part. Phys.* **36** 025004
[63] Miransky V A and Shovkovy I A 2002 *Phys. Rev. Lett.* **88** 111601
[64] Alford M and Wang Q 2005 *J. Phys. G: Nucl. Part. Phys.* **31** 719
[65] Alford M, Rajagopal K and Wilczek F 1998 *Phys. Lett.* B **422** 247
[66] Nielsen H B and Chadha S 1976 *Nucl. Phys.* B **105** 445
[67] Schäfer T, Son D T, Stephanov M A, Toublan D and Verbaarschot J J M 2001 *Phys. Lett.* B **522** 67
[68] Brauner T 2005 *Phys. Rev.* D **72** 076002
Brauner T 2006 *PhD Thesis* Nuclear Physics Institute, Prague (arXiv:hep-ph/0606300)
[69] Barducci A, Casalbuoni R, Pettini G and Ravagli L 2005 *Phys. Rev.* D **71** 016011

Paper IV

Jens O. Andersen, Lars T. Kyllingstad and Kim Splittorff:
"The sign problem across the QCD phase transition",
JHEP **1001** (2010), 055.

Is not included due to copyright